

INSTRUMENTED IMPACT TESTING
AND ITS APPLICATION TO THE STUDY OF
ACICULAR FERRITE STEELS

by

PAUL McCONNELL
B.S., Case Western Reserve University, 1970

A THESIS SUBMITTED IN PARTIAL FULFILLMENT OF
THE REQUIREMENTS FOR THE DEGREE OF
MASTER OF APPLIED SCIENCE

in

THE FACULTY OF GRADUATE STUDIES
Department of Metallurgy

We accept this thesis as conforming
to the required standard

The University of British Columbia

January, 1978

© Paul McConnell, 1978

In presenting this thesis in partial fulfilment of the requirements for an advanced degree at the University of British Columbia, I agree that the Library shall make it freely available for reference and study.

I further agree that permission for extensive copying of this thesis for scholarly purposes may be granted by the Head of my Department or by his representatives. It is understood that copying or publication of this thesis for financial gain shall not be allowed without my written permission.

Department of

Metallurgy

The University of British Columbia
2075 Wesbrook Place
Vancouver, Canada
V6T 1W5

Date

3 FEB 78

ABSTRACT

An instrumented impact test (IIT) machine was constructed and calibrated using static and dynamic loading. The theory and fundamentals of IIT have been reviewed.

Tests were performed to assess the proposed ASTM IIT validity criteria. The requirements that the fracture time be greater than 3 times the period of specimen oscillations and 1.1 times the electronic response time appear to be conservative. The data confirm that adoption of the criterion, $B > 2.5 (K_{Id}/\sigma_{yd})^2$, ensures plane strain fracture, whereas the acceptance of a linear load-to-failure condition (i.e., $P_{MAX} < P_{GY}$) may not be conservative enough.

For general yield failures, crack initiation was shown to occur prior to the attainment of maximum load. Thus, initiation energies calculated by assuming that crack initiation occurs at the maximum load are nonconservative.

The dynamic properties of two acicular ferrite pipeline steels were characterized by IIT. The information obtained, particularly the fracture toughness parameters and the initiation energies, revealed significant inadequacies in the toughness specifications and test methods presently used by the pipeline industry.

Tests performed to assess the significance of testing standard Charpy V-notch specimens versus full pipe wall thickness Charpys showed that lower upper shelf energies were obtained for the full wall specimens. However, the magnitude of the transition and lower shelf energies and the transition temperatures were similar.

Fatigue precracked standard Charpys specimens absorbed much lower energies and had higher transition temperatures than did the standard specimens.

Tests were also performed to assess the strain aging behaviour of the two acicular ferrite steels. Strain aging the semi-killed steel resulted in a decrease in the propagation energy, with no change in the magnitude of the initiation energy. For this steel, strain-aging does not increase the potential for crack initiation. Tests also revealed that sites near the seam weld of the pipe made with that semi-killed steel had experienced sufficient pipe-forming strain and thermal energy from the welding process to exhibit strain age effects. The fully killed acicular ferrite steel did not strain age; its strength and toughness were increased upon aging.

The instrumented impact test provided fracture toughness data that correlated very well with that obtained by more conventional

fracture toughness testing techniques. The total fracture energy from a standard Charpy test was shown to often mask the fracture toughness value of a material. The initiation energy obtained from testing a precracked Charpy specimen accurately indicated the relative magnitude of the fracture toughness, however.

TABLE OF CONTENTS

	<u>Page</u>
ABSTRACT	ii
TABLE OF CONTENTS	v
LIST OF FIGURES	xi
LIST OF TABLES	xvii
ACKNOWLEDGEMENTS	xix
DEDICATION	xx
 1. INTRODUCTION	 1
2. INSTRUMENTED IMPACT TESTING	3
2.1 Introduction	3
2.2 Instrumented Impact Test Machine	8
2.2.1 Machine Design	8
2.2.2 Instrumentation	11
2.2.3 Calibration	16
2.2.4 Test Variables	19
2.2.4.1 Drop Height	19
2.2.4.2 Temperature	22
2.2.4.3 Instrumentation Parameters	23
2.3 Interpretation of Load-Time Data	24
2.3.1 Validity Criteria for Load-Time Signals	24
2.3.1.1 Response Time	26
2.3.1.2 Signal Oscillations	28

	<u>Page</u>
2.3.1.3 Impact Energy	31
2.3.2 Data Reduction from Load-Time Curves	32
2.3.2.1 Energy	32
2.3.2.1.1 Velocity Reduction Correction	33
2.3.2.1.2 Compliance Correction for Initiation Energy	35
2.3.2.2 Deflection	38
2.3.2.3 Dynamic Yield Strength	38
2.3.2.4 Fracture Toughness Calculations	39
2.3.2.5 Computer Programs	40
2.3.2.6 Data Sheet	40
2.4 Effects of Test and Specimen Parameters	41
2.4.1 Significance of Test Validity Criteria	41
2.4.1.1 Inertial Loading Effect	41
2.4.1.2 Effects of Impact Velocity	44
2.4.1.3 Electronic Response Time	46
2.4.2 Specimen Parameters	50
2.4.2.1 Notch Radius	50
2.4.2.2 Notch Angle	54
2.4.2.3 Specimen Thickness	57
2.5 Crack Initiation	57
2.5.1 High Speed Movie Films	60
2.5.2 Electrical Resistance Study	62
2.5.3 Reduced Energy Tests	66

	Page
3. INSTRUMENTED IMPACT STUDY OF ACICULAR FERRITIC PIPELINE STEELS	70
3.1 Acicular Ferritic Steels	70
3.2 Pipeline Applications	73
3.3 Fracture Control in Pipelines	76
3.4 Test Program :	85
3.4.1 Steels/Pipelines	86
3.4.2 Metallography	87
3.4.3 Instrumented Impact Test Specimens	88
3.4.3.1 Specimen Preparation and Configuration..	88
3.4.3.2 Specimen Dimensions	95
3.4.3.2.1 Standard Charpy V-Notch Specimens ..	96
3.4.3.2.2 Precracked Charpy Specimens	96
3.4.3.2.3 Full Wall Charpy Specimens	97
3.5 Instrumented Impact Test Results	98
3.5.1 Absorbed Energy	111
3.5.1.1 Comparison of the Two AF Steels	111
3.5.1.1.1 Standard Charpy Data	111
3.5.1.1.1.1 Crack Parallel to Pipe Axis ..	111
3.5.1.1.1.2 Crack Parallel to Rolling Direction	120
3.5.1.1.1.3 Crack Transverse to Rolling Direction	124
3.5.1.1.1.4 Crack Transverse to Pipe Axis ..	126

	<u>Page</u>
3.5.1.1.2 Full Wall Charpys	128
3.5.1.1.2.1 Crack Parallel to Pipe Axis ..	128
3.5.1.1.2.2 Crack Parallel to Rolling Direction	130
3.5.1.1.2.3 Crack Transverse to Rolling Direction	132
3.5.1.1.3 Precracked Charpys	134
3.5.1.1.3.1 Crack Parallel to Pipe Axis ..	134
3.5.1.1.3.2 Crack Parallel to Rolling Direction	134
3.5.1.1.3.3 Crack Transverse to Rolling Direction	138
3.5.1.2 Significance of Specimen Size and Notch Acuity.	138
3.5.1.2.1 AF-1 Steel	138
3.5.1.2.1.1 Crack Parallel to Pipe Axis ..	138
3.5.1.2.1.2 Crack Parallel to Rolling Direction	143
3.5.1.2.1.3 Crack Transverse to Rolling Direction	144
3.5.1.2.2 AF-2 Steel	145
3.5.1.2.2.1 Crack Parallel to Pipe Axis ..	145
3.5.1.2.2.2 Crack Parallel to Rolling Direction	146
3.5.1.2.2.3 Crack Transverse to Rolling Direction	146
3.5.1.3 Conclusions of Absorbed Energy Study	147
3.5.1.4 Drop Weight Tear Test Correlations	149

	<u>Page</u>
3.5.2 Dynamic Yield Strengths	155
3.5.3 Load-Time Behaviour	157
3.5.4 Fractography	166
3.6 Strain Age Study	168
3.6.1 Effects of Straining and Strain Aging	169
3.6.2 Strain Aged Sites in AF-1 Pipe	176
4. DYNAMIC FRACTURE TOUGHNESS	183
4.1 Introduction	183
4.2 The Calculation of Fracture Toughness Parameters from IIT Data	187
4.2.1 Linear-Elastic Fractures	187
4.2.2 Elastic-Plastic Fractures	189
4.2.2.1 J-Integral	189
4.2.2.2 Crack Opening Displacement	193
4.2.2.3 Equivalent Energy Method	194
4.2.2.4 Critical Crack Sizes	195
4.3 Dynamic Fracture Toughness of Pipeline Steels	196
4.4 Correlations	207
4.4.1 Relationship Between Dynamic Stress Intensity Factor and Crack Initiation Energy	207
4.4.2 Comparisons Between K_{Id} and Statically Obtained K_{Ic}	213
4.4.3 Critical Flaw Sizes	219
4.4.4 Empirical Correlations Between K_{Id} and Other Material Properties	225

	<u>Page</u>
4.4.4.1 K_{Id} versus Charpy Energy	225
4.4.4.2 K_{Id} vs Yield Strength	228
5. CONCLUSION	231
5.1 Conclusions	231
5.2 Suggestions for Future Work	234
REFERENCES	237
APPENDIX A	246
APPENDIX B	247
APPENDIX C	251
APPENDIX D	256
APPENDIX E	257

LIST OF FIGURES

<u>Figure Number</u>		<u>Page</u>
2.1	Instrumented impact machine	9
2.2	(a) Diagram of tup showing position of strain gauges	12
	(b) Schematic of instrumented tup circuitry and IIT components	12
2.3	Closeup view of tup, anvils, centering device, and test specimen	13
2.4	Instrumented impact load-time photographs	25
	(a) elastic-plastic fracture	
	(b) linear-elastic fracture	
2.5	Effect of impact velocity, V_O , on load-time trace	45
	(a) $V_O = 5.46$ m/s	
	(b) $V_O = 3.46$ m/s	
2.6	Effect of electronic response time, T_R , on load- time trace	48
	(a) $T_R = 2.3$ ms	
	(b) $T_R = 0.719$ ms	
	(c) $T_R = 0.0729$ ms	
	(d) $T_R = 0.0007$ ms	
2.7	Electrical resistance study of crack growth	64
	(a) Load-time curve Scale: 500 lb/div. x 0.2 ms/div.	
	(b) Potential-time curve Scale: 1 mV/div. x 0.2 ms/div.	
3.1	AF-1 photomicrograph, 225X	89
	(a) unetched	
	(b) etched, 2% nital	
3.2	AF-2 photomicrographs, etched 2% nital, 363X ..	90
3.3	AF-1 SEM photomicrograph (3000X) and X-ray energy analysis of inclusions	91

<u>Figure Number</u>		<u>Page</u>
3.4	AF-2 SEM photomicrographs and X-ray energy analysis of inclusions (a) 480X (b) 1000X (c) 4000X	92-94
3.5	AF-1 steel load-time photographs, crack parallel to pipe axis	99
3.6	AF-2 steel load-time photographs, crack parallel to pipe axis	100
3.7	AF-1 steel load-time photographs, crack parallel to rolling direction	101
3.8	AF-2 steel load-time photographs, crack parallel to rolling direction	102
3.9	AF-1 steel load-time photographs, crack transverse to rolling direction	103
3.10	AF-2 steel load-time photographs, crack transverse to rolling direction	104
3.11	AF-1 steel fracture surfaces, crack parallel to pipe axis	105
3.12	AF-2 steel fracture surfaces, crack parallel to pipe axis	106
3.13	AF-1 steel fracture surfaces, crack parallel to rolling direction	107
3.14	AF-2 steel fracture surfaces, crack parallel to rolling direction	108
3.15	AF-1 steel fracture surfaces, crack transverse to rolling direction	109
3.16	AF-2 steel fracture surfaces, crack transverse to rolling direction	110
3.17	AF-1 IIT absorbed energies vs temperature, standard Charpys, crack parallel to pipe axis ..	116
3.18	AF-2 IIT absorbed energies vs temperature, standard Charpys, crack parallel to pipe axis ..	116

<u>Figure Number</u>		<u>Page</u>
3.19	AF-1/AF-2 IIT average absorbed energies vs temperature, standard Charpys, crack parallel to pipe axis	116
3.20	AF-1 IIT absorbed energies vs temperature, standard Charpys, crack parallel to rolling direction	121
3.21	AF-2 IIT absorbed energies vs temperature, standard Charpys, crack parallel to rolling direction	121
3.22	AF-1/AF-2 IIT average absorbed energies vs temperature, standard Charpys, crack parallel to rolling direction	121
3.23	AF-1 IIT absorbed energies vs temperature, standard Charpys, crack transverse to rolling direction	125
3.24	AF-2 IIT absorbed energies vs temperature, standard Charpys, crack transverse to rolling direction	125
3.25	AF-1/AF-2 IIT average absorbed energies vs temperature, standard Charpys, crack transverse to rolling direction	125
3.26	AF-1 IIT absorbed energies vs temperature, crack transverse to pipe axis	127
3.27	AF-1 IIT absorbed energies vs temperature, full wall/standard Charpys, crack parallel to pipe axis . . .	129
3.28	AF-2 IIT absorbed energies vs temperature, full wall/standard Charpys, crack parallel to pipe axis . . .	129
3.29	AF-1/AF-2 IIT average absorbed energies vs temperature, full wall Charpys, crack parallel to pipe axis	129
3.30	AF-1 IIT absorbed energies vs temperature, full wall/standard Charpys, crack parallel to rolling direction..	131
3.31	AF-2 IIT absorbed energies vs temperature, full wall/standard Charpys, crack parallel to rolling direction..	131

<u>Figure Number</u>		<u>Page</u>
3.32	AF-1/AF-2 IIT average absorbed energies vs temperature full wall Charpys, crack parallel to rolling direction	131
3.33	AF-1 IIT absorbed energies vs temperature, full wall/standard Charpys, crack transverse to rolling direction	133
3.34	AF-2 IIT absorbed energies vs temperature, full wall/standard Charpys, crack transverse to rolling direction	133
3.35	AF-1/AF-2 IIT average absorbed energies vs temperature, full wall Charpys, crack transverse to rolling direction	133
3.36	AF-1 IIT absorbed energies vs temperature, precracked/standard Charpys, crack parallel to pipe axis	135
3.37	AF-2 IIT absorbed energies vs temperature, precracked/standard Charpys, crack parallel to pipe axis	135
3.38	AF-1/AF-2 IIT average absorbed energies vs temperature, precracked Charpys, crack parallel to pipe axis	135
3.39	AF-1 IIT absorbed energies vs temperature, precracked/standard Charpys, crack parallel to rolling direction	136
3.40	AF-2 IIT absorbed energies vs temperature, precracked/standard Charpys, crack parallel to rolling direction	136
3.41	AF-1/AF-2 IIT average absorbed energies vs temperature, precracked Charpys, crack parallel to rolling direction	136
3.42	AF-1 IIT absorbed energies vs temperature, precracked/standard Charpys, crack transverse to rolling direction	139

<u>Figure Number</u>		<u>Page</u>
3.43	AF-2 IIT absorbed energies vs temperature, precracked/standard Charpys, crack transverse to rolling direction	139
3.44	AF-1/AF-2 IIT average absorbed energies vs temperature, precracked Charpys, crack transverse to rolling direction	139
3.45	AF-1 DWT percent shear and IIT full wall Charpy absorbed energies vs temperature, crack parallel to pipe axis	151
3.46	AF-1 DWT percent shear and IIT precracked Charpy absorbed energies vs temperature, crack parallel to pipe axis	151
3.47	AF-2 DWT percent shear and IIT full wall Charpy absorbed energies vs temperature, crack parallel to pipe axis	152
3.48	AF-2 DWT percent shear and IIT precracked Charpy absorbed energies vs temperature, crack parallel to pipe axis	152
3.49	AF-1/AF-2 IIT dynamic yield strengths vs temperature	156
3.50	AF-1 IIT maximum and general yield loads vs temperature, standard Charpys, crack parallel to pipe axis	158
3.51	AF-2 IIT maximum and general yield loads vs temperature, standard Charpys, crack parallel to pipe axis	158
3.52	AF-1 IIT maximum and general yield loads vs temperature, standard Charpys, crack parallel to rolling direction	158
3.53	AF-2 IIT maximum and general yield loads vs temperature, standard Charpys, crack parallel to rolling direction	158
3.54	AF-1 IIT maximum and general yield loads vs temperature, standard Charpys, crack transverse to rolling direction	159

<u>Figure Number</u>		<u>Page</u>
3.55	AF-2 IIT maximum and general yield loads vs temperature, standard Charpys, crack transverse to rolling direction	159
3.56	AF-1 IIT maximum and general yield loads vs temperature, standard Charpys, crack transverse to pipe axis	159
3.57	Schematic of variation in general yield load, fracture load, and absorbed energy with temperature for a Charpy specimen. Effect of notch on T_D	160
4.1	AF-1 IIT dynamic fracture toughness vs temperature, crack parallel to pipe axis	197
4.2	AF-2 IIT dynamic fracture toughness vs temperature, crack parallel to pipe axis	197
4.3	AF-1 IIT dynamic fracture toughness vs temperature, crack parallel to rolling direction	198
4.4	AF-2 IIT dynamic fracture toughness vs temperature, crack parallel to rolling direction	198
4.5	AF-1 IIT dynamic fracture toughness vs temperature, crack transverse to rolling direction	199
4.6	AF-2 IIT dynamic fracture toughness vs temperature, crack transverse to rolling direction	199
4.7	K_{Id}^2/E vs initiation energy for acicular ferrite steel IIT K_{Id} data meeting different validity requirements	211
4.8	AF-2 IIT dynamic J-Integral fracture toughness vs static J-Integral fracture toughness, crack parallel to rolling direction	216
4.9	Reduced pearlite steel IIT dynamic fracture toughness, crack parallel to rolling direction ..	216
4.10	Dynamic fracture toughness vs standard Charpy energy for acicular ferrite steels	227
4.11	Dynamic fracture toughness vs dynamic yield strength for acicular ferrite steels	227
E.1	Temperature gradient in Charpy specimens taken from near AF-1 seam weld for strain age study	259

LIST OF TABLES

<u>Table</u>		<u>Page</u>
2.1	Dynamic Calibration Results	18
2.2	Response Times	27
2.3	Validity Criteria	32
2.4	Comparison of Valid and Invalid Data as Determined by $t < 3\tau$	43
2.5	Comparison of Valid and Invalid Data as Determined by $t < 1.1 T_R$	49
2.6	Notch Radii Study	53
2.7	Notch Angle Study	56
2.8	High Speed Movie Film Results	61
2.9	Reduced Energy Test Results	68
3.1	Proposed Fracture Control Requirements for Arctic Pipelines	84
3.2	Steel Compositions	87
3.3	Standard Charpys - Average Absorbed Energies .. .	112
3.4	Full Wall Charpys - Average Absorbed Energies .. .	113
3.5	Precracked Charpys - Average Normalized Energies	114
3.6	Ductility Index - Steels AF-1 and AF-2	119
3.7	Effect of Notch Acuity	137
3.8	C_v 100 Temperatures	165
3.9	Strain Age Study	172
3.10	Strain Age Sites in Steel AF-1	181

<u>Table</u>		<u>Page</u>
4.1	Transition Temperatures	201
4.2	Fracture Toughness and Energy Data	203
4.3	K_{Id} Values for Different Validity Criteria	214
4.4	Critical Crack Sizes	222
E.1	Equivalent Aging Conditions	261

ACKNOWLEDGEMENTS

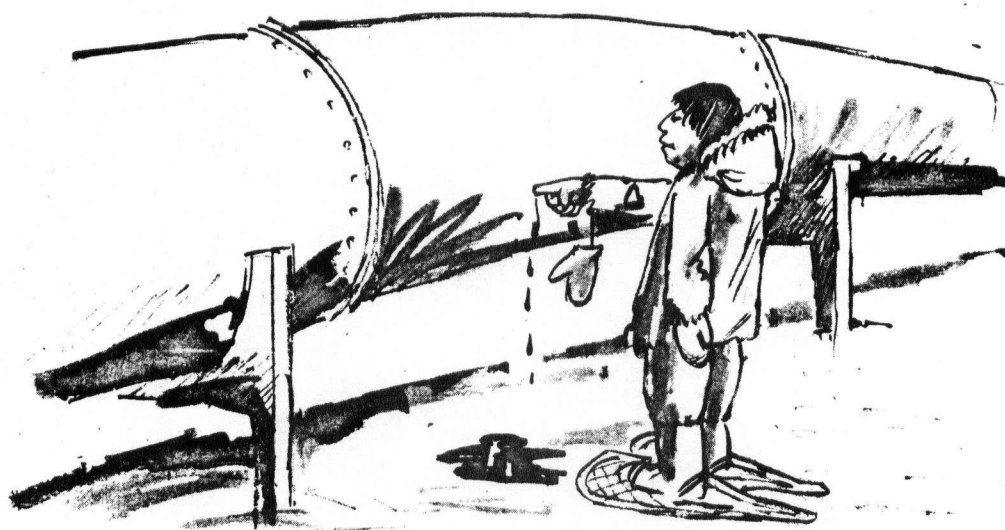
I wish to thank the staff and graduate students of the Department of Metallurgy who provided assistance throughout this research, including Jim Brezden, Yvonne Chung, Orman Leszek, Jim Walker, and in particular, my good friend V. Venkateswaran for his contributions in writing the computer programs. Bob Butters' and Ed Klassen's efforts in the design and construction of the test machine are commendable.

The support and advice of Mr. R.J. Cooke of the Alberta Gas Trunk Line Company, who provided much of the material tested in this program, and the Aluminum Company of Canada, who provided financial support, is gratefully appreciated.

The guidance of my supervisors, Drs. E.B. Hawbolt and N.R. Risebrough, is acknowledged. Bruce's constant interest in the project and his open-door policy are especially and sincerely appreciated.

To my wife, Janny, and my children, Heather and Grant, I express my utmost gratitude for their patience. Janny's considerable assistance during the test program and preparation of the manuscript was invaluable: she, after all, actually "broke" the specimens!

DEDICATION¹



Dedication

1. INTRODUCTION

This thesis is the culmination of a study of instrumented impact testing (IIT). Instrumented impact testing differs from the standard Charpy test in that the load-time response of a specimen is measured and recorded during the fracture event. The total absorbed energy, the area under the load-deflection curve, can be separated into two components, EI and EP. EI is the energy to initiate the crack, whereas EP is the crack propagation energy. In addition, the data provide a measure of the dynamic yield strength and the dynamic fracture toughness of a material.

The project objectives were:

1. To construct, calibrate, and render operational an instrumented impact machine.
2. To conduct a series of tests by which the proposed IIT validity criteria could be assessed.
3. To conduct tests to show the advantages of IIT as compared with standard Charpy testing. These tests included a study of the effects of specimen geometry and notch acuity.
4. To demonstrate the applicability of IIT by characterizing the directional dynamic properties of two X70 acicular ferrite pipeline steels. This study included an assessment of their potential for strain age embrittlement.

Considerable detail on the theory and applications of IIT has been included in this thesis to provide the necessary basis for future studies.

A comparison of the toughness properties of the current generation of Canadian X70 HSLA pipeline steels was included in this study since these steels are being proposed for use in Northern gas pipelines. The toughness characteristics of these steels are of prime importance, since one of the most important design problems is the prevention of pipe failure. The work has shown that IIT is particularly valuable in providing rapid, inexpensive, and detailed dynamic fracture toughness data. Valid fracture toughness values, particularly at high strain rates, are difficult to obtain by other test procedures.

It is hoped that this thesis will provide the necessary background for future studies using instrumented impact testing.

2. INSTRUMENTED IMPACT TESTING

2.1 Introduction

Instrumented impact testing (IIT) is becoming widely accepted as a means to rapidly and inexpensively generate data describing the dynamic response of materials^(eg., 2-13). The American Society for Testing and Materials recently devoted an entire Symposium to the subject⁽²⁾, and are currently preparing a tentative ASTM IIT specification to be included in the 1978 Annual Book of ASTM Standards (14-15).

A conventional impact testing machine (Charpy, dynamic tear, etc.) can be instrumented by locating calibrated load cells on the striking hammer (tup) near the contact points. A load-time or load-displacement signal is obtained in place of the conventional total energy to failure information. From such curves, determinations can be made of: 1) the differentiation between crack initiation and crack propagation energies; 2) the dynamic yield and fracture strengths; 3) dynamic fracture toughness values, and many other useful parameters. For Charpy-type tests, these parameters can be calculated by applying notch-bar three-point bending theories, with due regard for metallurgical principles. Although certain assumptions must be made to permit these calculations, meaningful, reproducible, and generally acceptable information can be generated.

The instrumented impact test also has all the advantages of the standard Charpy test: reveals temperature transitions, low cost, simple procedure, high strain rate, large sampling capability, established correlations with service performance.

Fracture and toughness tests generally measure either energy absorbed or critical loads from which design data, for example, stress intensity factors, may be derived. The IIT, when employing a pre-cracked Charpy specimen, yields both energy and fracture toughness data.

Several workers have made unique contributions to the development of IIT.

The earliest references to obtaining load-deflection curves representative of the dynamic response of materials appeared in the late 1920's, although the first uses of strain gages to record the loads were not reported until thirty years later⁽¹⁶⁻¹⁷⁾.

Augland was the first to correlate the energy results obtained from integrating the IIT load-time curve with the energy measured directly from the pendulum dial gauge of a standard Charpy machine⁽¹⁸⁾. He is also credited with deriving the expression which corrects the value of the area under the load-time trace to account for the

reduction in hammer velocity during impact.

Tardif and Marquis were apparently the first to suggest that the total energy of the impact event could be separated into the energy to initiate and the energy to propagate the crack⁽¹⁹⁾. They also proposed that the dynamic fracture toughness might be measured from IIT data.

Fearneough and Hoy used IIT data to calculate the dynamic yield strength⁽²⁰⁾. Their paper, and that of Kobayashi, et al⁽²¹⁾, described in detail the fracture process in terms of the load-time data obtained over a range of temperatures.

In the late 1960's, with the increasing interest in fracture and fracture mechanics, papers dealing with IIT became more numerous. Commercial IIT units became available. Many authors contributed by reporting the dynamic fracture toughness values obtained from IIT for a range of materials⁽²¹⁻²⁵⁾. Radon and Turner were the first to employ fatigue precracked Charpy specimens⁽²⁵⁾. Server and Tetelman published a comparison between the fracture toughness data generated from full size compact tension specimens, tested at various strain rates, and the fracture toughness data obtained using IIT and small precracked Charpy specimens. The data obtained from the much less expensive IIT (\approx \$500) compared favourably with that generated

from the standard compact tension tests (\approx \$2 million)⁽²⁶⁾.

Significant advances have been made since that time, particularly in assuring that the IIT data obtained is representative of the true mechanical response of the test specimen^(13,27-32). Approximately half the published literature on IIT in recent years has been concerned with refining the instrumentation, critically analyzing the nature and effect of inherent signal oscillations and/or establishing validity criteria by which all tests can be compared. In addition, a considerable amount of research has been directed to applying IIT to composites and non-metallics^(2,32-33).

Unfortunately, almost all the work published prior to the early 1970's must be considered suspect. Insufficient information regarding experimental parameters is included in these earlier papers to ensure that the now established validity criteria were met during testing⁽³⁴⁻³⁵⁾.

Data that can otherwise be obtained only at high costs (eg., fracture toughness test programs requiring full size specimens); or that cannot be obtained by other means (eg., dynamic data, per se, including high strain rate yield strengths and dynamic stress intensity factors) can easily be generated with IIT.

Precracking specimens, to simulate naturally occurring fatigue flaws, enhances the test and has been shown to provide sharper transition temperature curves and lower initiation energies. Precracking is considered essential to obtain fracture toughness data, it being required to ensure that the minimum fracture toughness parameters may be measured. IIT of precracked Charpys have been shown to give transition temperature curves which correspond closely to those of the 5/8-in dynamic tear tests^(4,7,36-38). Correlations with other tests, including the Battelle-Drop Weight Tear Test (used to determine full-thickness percent shear or the nil-ductility transition temperature), have also been attempted with some success^(7, 39-40).

Having the advantage of requiring simple, inexpensive specimen preparation while yielding valid energy, strength, and fracture toughness data, ensures that IIT will become more important in the future. Standardization of test techniques and the establishment of validity criteria will further the acceptance and growth of IIT, thereby extending its application from the research laboratory to industrial quality control programs⁽⁴¹⁾ and to the general area of materials selection and evaluation⁽⁴²⁾. Adoption of nonstandard test techniques should further extend the scope of instrumented impact testing⁽⁴³⁾.

2.2 Instrumented Impact Test Machine

The instrumented impact test machine used in this study was designed, constructed, and calibrated at the Department of Metallurgy, University of British Columbia, and is the only such unit in Western Canada. Credit for the design and instrumentation go primarily to Messrs. Robert Butters and Ed Klassen, respectively. Their efforts resulted in the construction of an extremely reliable unit at a savings of thousands of dollars. It is interesting to note that, at this writing, the unit qualifies as the only calibrated Charpy machine in British Columbia.

2.2.1 Machine Design

The IIT machine was designed and constructed to comply with the ASTM E 23⁽⁴⁴⁾ requirements for notched-bar impact testing, within, of course, the limits imposed due to the machine being of drop tower design, as opposed to pendulum loading. A photograph of the machine is shown in Figure 2.1.

The frame consists of a massive base plate, firmly secured to the concrete floor. Two 2.44 m (8 ft) vertical shafts extend up from the base plate. These shafts act as the runners for the striking edge (tup). At the top of the two shafts, a small variable speed electric motor is located which lifts or lowers the tup assembly. A "drop"

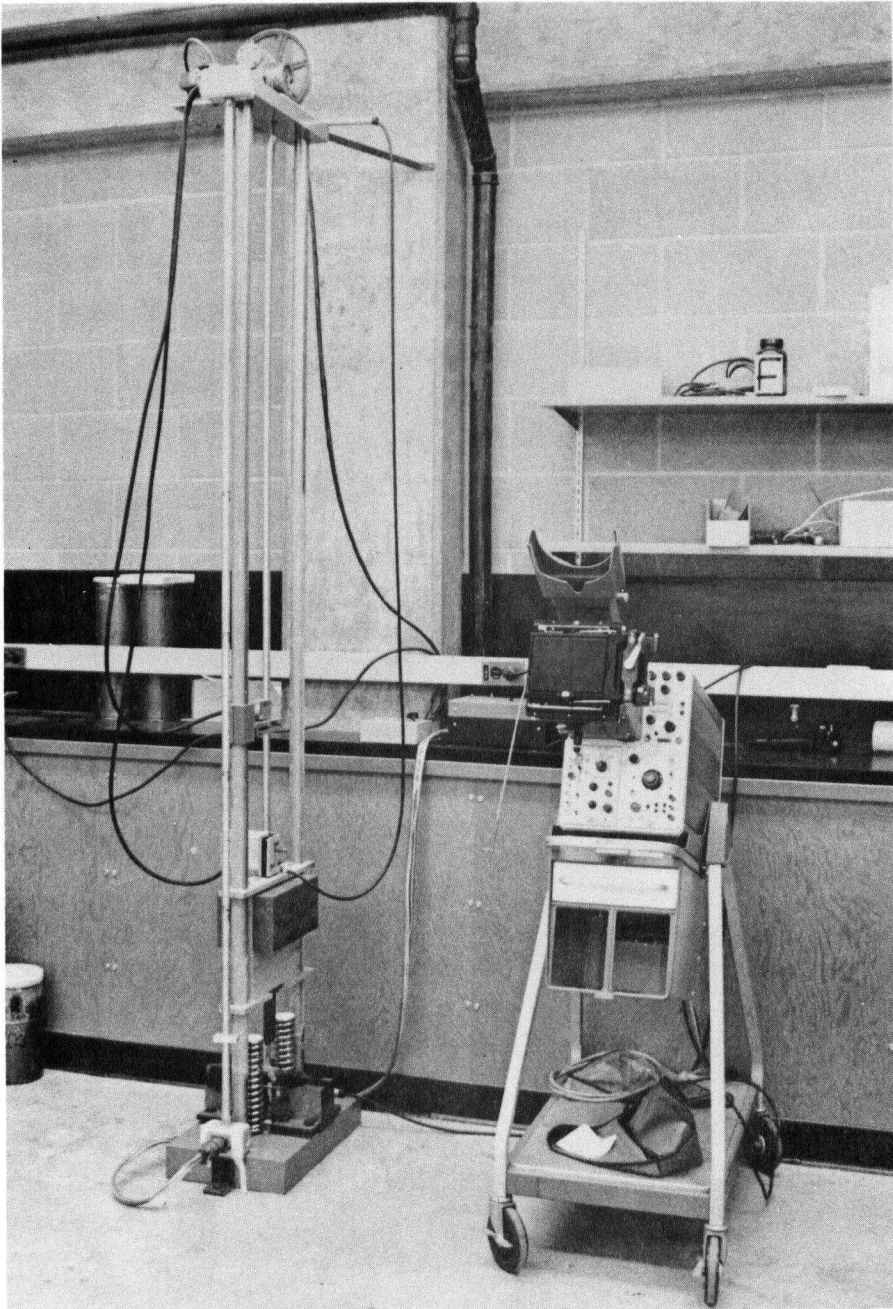


Figure 2.1 Instrumented impact machine.

button opens a solenoid clamp, dropping the tup and its associated mass onto a specimen. The fall of the tup assembly is assumed to follow the laws of gravity; the vertical shafts being well greased to minimize the effects of friction.

Attached to the base plate, are two shock absorbers which absorb the excess energy from the falling tup and thereby prevent the large mass from rebounding.

The tup assembly is that portion of the machine which provides the energy necessary to fracture a specimen. In order to achieve a large total impact energy, and yet a relatively low impact velocity (reasons for this shall be discussed in Section 2.3), the entire assembly has a mass of 45.76 kg (100.88 lb). This is a somewhat larger mass than a typical commercial pendulum Charpy machine. Variations in the mass of the striking tup can be obtained by bolting to or removing massive steel blocks from the sides of the tup frame.

The tup, being that portion of the machine which actually strikes the sample, is made of tool steel, fully hardened and drawn back to $R_c 55$. The tup is identical in dimension and design to that stipulated by the ASTM for the Charpy impact test, with one exception: it has recesses in its face to accommodate strain gauges which are essential to obtain load-time information. A diagram of the tup

is shown in Figure 2.2a.

The test specimens sit on hardened tool steel anvils ($R_c 55$), the size and shape of this support area also conforming to the ASTM specifications. These anvils can be removed to accommodate other specimen types or test methods. The anvils, in turn, rest on larger anvil supports. A close-up view of the tup, specimen, and anvils is shown in Figure 2.3.

Specimen guides were carefully aligned, perpendicular to the tup face, so that placing a specimen against these supports assured that the test piece was impacted by the tup at the exact midpoint of its striking edge. A small notch centering device, consisting of a "pointer" attached to a hinged bar, was installed to position the specimen so that the notch in the specimen would lie directly under the tup and midway between the anvil supports. No end stops were used in positioning the specimen. Correct positioning and centering of the test specimen is, of course, crucial and great care was exercised in assuring proper alignment of the specimen guides and the hinged notch centering device.

2.2.2 Instrumentation

The essential difference between the instrumented impact

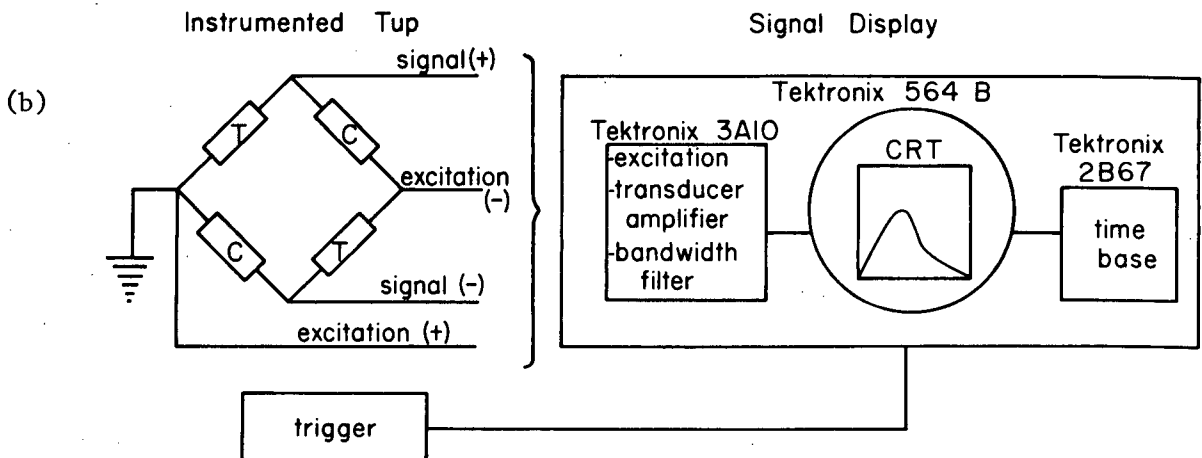
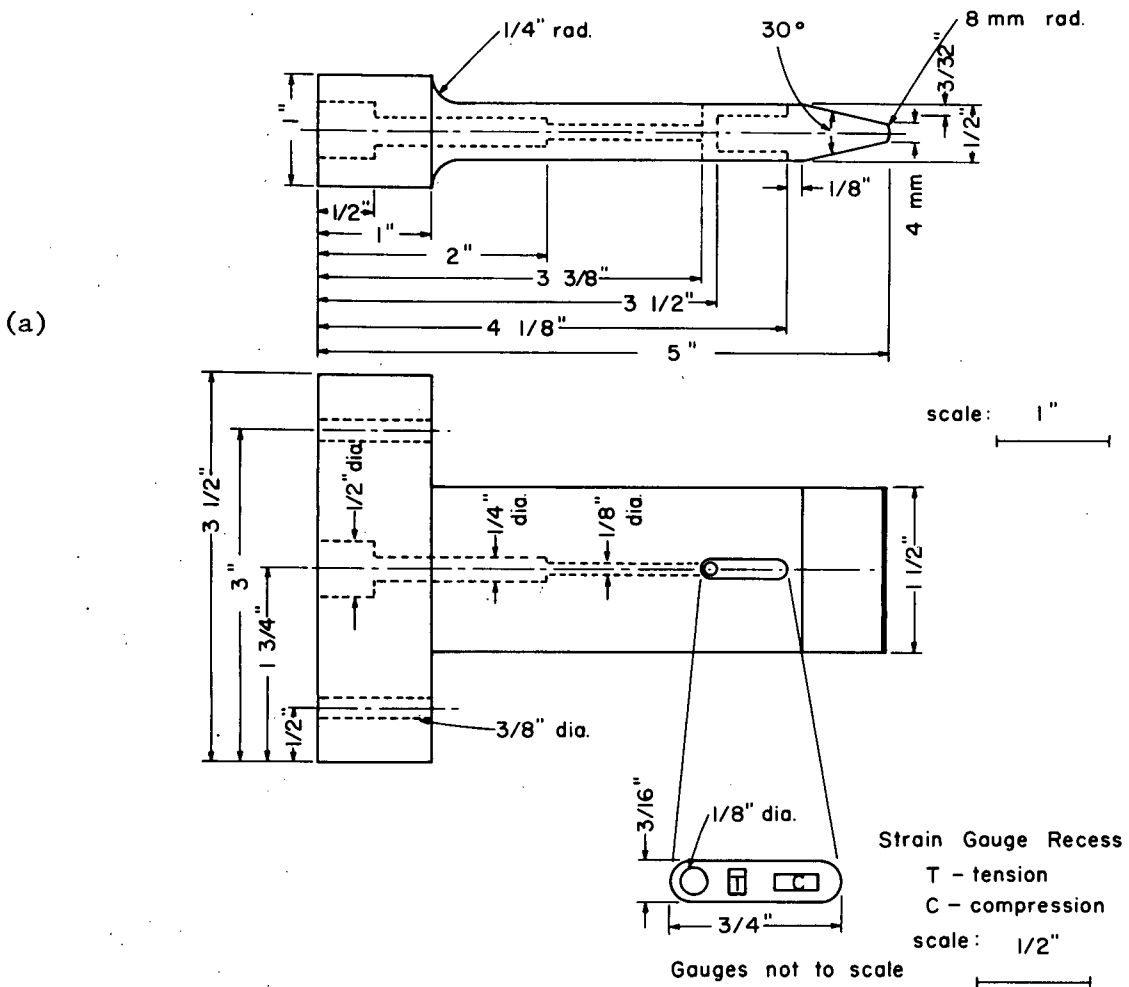


Figure 2.2 (a) Diagram of tup showing position of strain gauges.
 (b) Schematic of instrumented tup circuitry and IIT components.

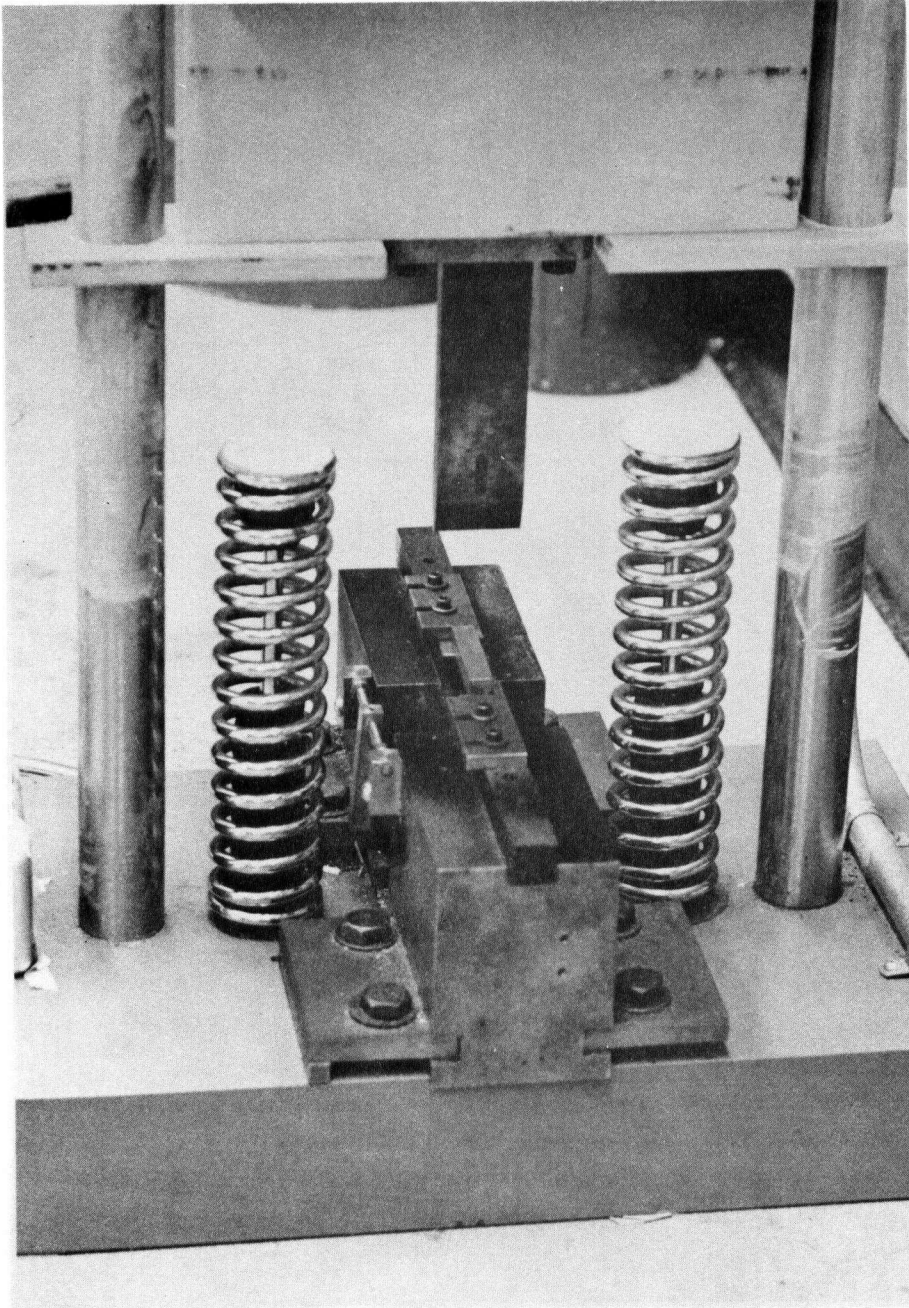


Figure 2.3 Closeup view of tup, anvils, centering device, and test specimen.

machine and a "standard" Charpy unit is the electronic instrumentation employed to yield an analog of the dynamic load-time response of a fracturing specimen.

The electronics package consisted of an instrumented tup (load cell), a power supply, a dynamic transducer amplifier, a signal recording and display system, and a system to trigger the signal just prior to the impact event.

The tup has been recessed on both faces for protective placement of the highly sensitive semi-conductor strain gauges. Figures 2.2a and 2.2b show the tup design with the position of the strain gauges, and a schematic of the instrumentation, respectively.

Semi-conductor strain gauges (Micro-sensor Type P01-05-120) were chosen due to their high gauge factor (+110), high signal/noise ratio, and small size (active gauge length of 1.27 mm). As shown in the circuitry diagram (Figure 2.2b), all four arms of the bridge are active gauges, which provide temperature compensating ability and higher sensitivity. This is an improvement over many other designs, including commercial units.

The gauges, once placed into the tup recesses, were covered with a protective epoxy. The gold gauge lead wires were soldered to heavier copper wires which led through a groove within the tup.

Upon impact, these strain gauges sense the compressive forces on the tup and provide the signal output voltage to the transducer amplifier.

A Tektronix 3A10 Transducer Amplifier Module provided the DC excitation for the strain gauges, and amplified and conditioned the output signal. A suitable upper frequency cutoff (generally 10 kHz) was utilized.

The signal was displayed on a Tektronix Type 564B oscilloscope with a 2B67 Time Base. Although the oscilloscope trace could be stored, for ease of data reduction and for permanent records, the sweep was usually photographed. A Tektronix C27 camera and Polaroid Type 57 High Speed film were used (f3). The camera shutter was manually opened prior to and independent of dropping the tup assembly.

The oscilloscope display was triggered just prior to the tup striking the test specimen. A small magnet attached to the falling tup assembly activated a reed switch. Closure of this switch triggered the oscilloscope sweep. The position of the reed switch was critical to ensure that the complete load-time signal was recorded on the screen of the oscilloscope. Small gauge marks were etched onto the drop tower frame for positioning of the trigger switch, the marks corresponding to a range of drop heights. (N.B. At this writing, an electronic triggering system has been constructed

which can trigger the oscilloscope sweep and the camera system simultaneously as the "drop" button is pushed.)

2.2.3 Calibration

The load cell was calibrated to determine the relationship between the strain gauge voltage output and the applied load.

Initially, a static calibration was made. The tup was pressed against a standard test specimen, the load being selectively increased by using a hydraulic jack mounted atop the tup assembly. A calibrated compression load cell attached to an Instron machine was located between the jack and a rigid restraining rod. By activating the jack, a force of calibrated magnitude could be applied to the tup and the specimen thereby correlating the compressive load and the strain gauge response of the tup.

The voltage output from the tup strain gauge was found to be linearly related to applied load from approximately 50 to 3000 lbs(222-13350 N). By adjusting the strain gauge transducer excitation voltage, a convenient output of 10 μ V per pound of applied load was obtained. (N.B. Actual loads in the test program commonly exceeded 3000 lb. However, the dynamic calibration extended the range of loads for which accurate calibration existed to over

8000 lb (35600 N). Additionally, this static calibration has since been redone. The voltage output was again linearly related to applied load, this time to 8500 lb (37825 N), and was within 4% of the original calibration⁽⁴⁵⁾).

The strain gauge signals, which are equated to load, are the results of elastic strains. Elastic properties are relatively strain-rate independent, and, so, static calibration should apply to dynamic loading as well⁽⁴⁶⁾. However, as Ireland suggests in his excellent review⁽⁴⁷⁾, dynamic calibration is nevertheless desirable since: 1) dynamic conditions are to be monitored; 2) strain gauges may have different response to dynamic loading, due to variations in the properties of the bonding medium; and, 3) the amplifier may have characteristics which vary with the rate at which the signal passes through the component. In addition, the ASTM E 23 impact test specification requires that a dynamic calibration be made periodically.

Thus, in order to determine if the microvolt-load relationship established from the static calibration would indeed apply to dynamic loading conditions, a set of standardized Charpy specimens, with guaranteed values of energy, were obtained from the U.S. Army Materials and Mechanics Research Center, Watertown, Massachusetts,

the only supplier of ASTM standard Charpy specimens.

Impact tests were performed at the specified temperature of - 40°C. The total energy to failure was determined as described in Section 2.3.2.1. The results are shown in Table 2.1 (a computer printout of the results of this calibration is given in Appendix A).

Table 2.1
DYNAMIC CALIBRATION RESULTS

Sample	IIT Total Energy (ft-lb)	Guaranteed Energy(ft-lb)
T1-0070	14.0	14.3 ± 1.0
T1-0296	13.9	14.3 ± 1.0
U3-0242	49.5	48.0 ± 2.4
U3-0786	46.9	48.0 ± 2.4
V7-0293	71.3	73.9 ± 3.7
V7-0963	72.3	73.9 ± 3.7

N.B. 1 ft-lb = 1.36 J

The IIT data compared favourably with the specified energies of the standard samples. Thus, the results indicated that the load cell was calibrated for dynamic conditions.

It should be emphasized that in calculating the total energy of these calibration samples, the static calibration factor (10 μ V/ 1 lb) was used. In addition, the V7-series of samples was impacted at a higher strain rate than were other two series, confirming that the IIT machine calibration was valid for a range of strain rates from "static" to impact loading.

Since it was shown that the static calibration was accurate under dynamic conditions, all subsequent checks of the calibration were done statically. The tup assembly has a known weight (100.88 lb), and, by allowing the entire assembly to rest on a test specimen, the tup assembly could be "weighed" by reading the strain gage voltage output on the oscilloscope and employing the relationship between output voltage and load. This was done periodically to verify that the machine was still calibrated. With well over 900 impact tests conducted, the machine never deviated from the original calibration.

The time base on the oscilloscope was calibrated with a Tektronix Type 184 TimeMark Generator and found to be within the manufacturer's specification.

2.2.4 Test Variables

2.2.4.1 Drop Height

The height from which the tup assembly drops determines

the total energy available to fracture a specimen, E_o , and the velocity at which the tup strikes the specimen, V_o .

For reasons to be discussed, E_o must, of course, be large enough to assure fracture, but V_o must be controlled to minimize effects due to:

- 1) the initial acceleration of the specimen
- 2) the amplitude of various oscillations
- and 3) the limited frequency response of the electronic system.

The drop tower design allows the tup assembly to be raised to any height from approximately 0.15 m to 1.525 m (0.5 - 5.0 ft).

The velocity of the tup at time of contact with the test specimen was calculated from:

$$V_o = (2gh_o)^{\frac{1}{2}} \quad (\text{Eq. 2.1})$$

where, V_o = impact velocity

g = gravitational acceleration constant

h_o = drop height

The corresponding total energy available upon impact was obtained from the relation:

$$E_o = \frac{1}{2}mV_o^2 \quad (\text{Eq. 2.2})$$

where, E_o = available impact energy

m = mass of tup assembly

Thus, the range of available impact velocities was 1.73 m/s to 5.47 m/s (5.67 - 17.94 ft/s). The ASTM requires that, for a valid Charpy test, the tup must impact the specimen at velocities between 3.05 m/s to 6.10 m/s (10 - 20 ft/s).

In some instances, however, the impact velocity of a test was less than that required by the ASTM. This lower impact velocity was sometimes necessary to decrease the amplitude of undesirable specimen oscillations and to extend the time for failure which avoided problems of limited electronic frequency response⁽⁴⁷⁾. These problems shall be discussed in more detail in Section 2.3.1.

Although the impact velocity was at times as low as 1.72 m/s (5.64 ft/s), this was not considered to be of major consequence when compared to the serious problems encountered in data reduction should the velocity be too high. Even strain rate sensitive steels require a factor of 10-100 change in strain rate to produce measurable changes in mechanical properties^(13,25). The lower velocity of 1.72 m/s still yields a strain rate more than 2×10^4 times that of a

conventional "static" tensile test rate of 0.5 cm/min (0.2 in/min) and therefore can certainly be described as being a "dynamic" test, although it does deviate slightly from the ASTM Charpy test specification. These nonstandard impact velocities were necessary only for very low toughness materials.

The drop height for a given sample at a given temperature was selected so that the total available energy from the falling tup assembly would be sufficient to fracture the specimen, and so that the initiation energy (energy to initiate a stable crack) would be less than a third of that total energy. This latter restriction was important, since in order to apply appropriate corrections to the data from the load-time records, the reduction in tup velocity must be minimized^(27,48). However, care was taken not to use impact velocities (i.e. drop heights and energies) much larger than necessary.

2.2.4.2 Temperature

Instrumented impact tests were carried out over a range of temperatures from -196°C to +100°C.

All low temperature test samples were brought to temperature by holding them in a liquid N₂-alcohol bath and were impacted within five seconds as prescribed in the ASTM Standard E 23⁽⁴⁴⁾. Incidentally,

Weiss, et al⁽⁴⁹⁾ have conducted tests in which thermocouples were implanted within the Charpy specimens and have shown that, even for samples cooled to as low as -60°C , 9 seconds out of the bath results in less than a 2°C rise in temperature.

High temperatures were achieved by placing the specimens in boiling H_2O .

2.2.4.3 Instrumentation Parameters

Trial and error dictated the Time/Division setting and Volts/Division setting for the strain gauge transducer. Generally, for high toughness materials ($> 70 \text{ J} = 52 \text{ ft-lb}$), the maximum applied load was on the order of 5000 lb (22250 N). Since the strain gauge voltage output was previously calibrated and found to be equivalent to $10 \mu\text{V/lb}$, a setting of 10 mV/division was used and was equivalent 1000 lb/division, thus ensuring that the total impact event could be recorded on the 10 division oscilloscope screen. Low toughness materials required a 5 mV/division setting.

The oscilloscope time scale for high toughness materials was set at 0.5 ms/division since the entire impact event took approximately 0.005 s. Usually, brittle samples fractured in less than 0.002 s, allowing a 0.2 ms/division scale to be used.

2.3 Interpretation of Load-Time Data

Upon testing a specimen, a photograph of the analog of the dynamic load-time response is obtained. Figure 2.4 is typical of that response for both an elastic-plastic failure (maximum load > general yield load) and a linear-elastic failure (maximum load < general yield load). The load-time information is similar to the load-deflection curves obtained from slow bend tests of notched specimens on an Instron machine.

2.3.1 Validity Criteria for Load-Time Signals

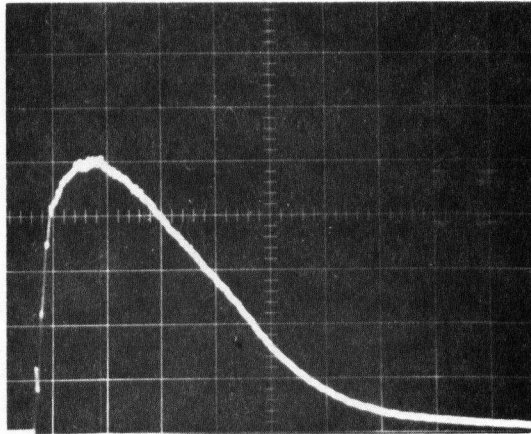
Ireland has reviewed the problems associated with obtaining valid instrumented impact data^(29,47). His works are based on programs which established test procedures to obtain consistent and valid IIT data for the determination of dynamic fracture toughness parameters from small specimens⁽³⁴⁻³⁵⁾.

Other than the obvious errors due to improper load cell calibration, the major sources of error in an instrumented impact test load-time signal are:

1. inadequate electronic frequency response
2. oscillations inherent in the tup signal
- and, 3. insufficient impact energy.

(a)

maximum load ———
general yield load ———



(b)

maximum load ———

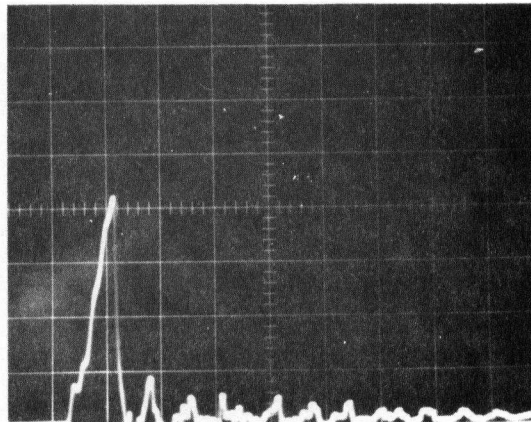


Figure 2.4 Instrumented impact load-time photographs:
(a) elastic-plastic fracture
(b) linear-elastic fracture.

2.3.1.1 Response Time

All electronic instrumentation has a limited frequency response, that is, the amplitude of a signal passing through the component may be attenuated. Most oscilloscope manufacturers define any acceptable frequency response as that at which the signal has been attenuated by 30% (3 dB). However, for instrumented impact tests, attenuation of at most 10% is considered acceptable⁽⁵⁰⁾, which corresponds to 0.915 dB attenuation, where

$$\text{dB} = 20 \log(\text{volts in/volts out}) \quad (\text{Eq. 2.3})$$

The frequency response is more easily represented by the frequency response time, T_R , which is that time required for a signal to rise to the desired amplitude (90% of the full amplitude in the case of IIT). Ireland⁽⁴⁷⁾ has pointed out that the relationship between signal frequency and T_R for a sine wave (which approximates an instrumented impact load-time curve) is:

$$T_R \approx 0.35/f_{.915\text{dB}} \quad (\text{Eq. 2.4})$$

This response time is experimentally determined by superimposing a constant amplitude sine wave on the output of the strain gauge circuit. The frequency of the sine wave is then increased until attenuation of ten percent is observed, giving $f_{.915\text{dB}}$. The

response time is then calculated from the above relationship. The 0.915dB frequency, and, hence, the response time, is a function of the upper frequency of the band width as set on the transducer amplifier.

This response time was determined for the system employed in this work and the values are given in Table 2.2.

Table 2.2
RESPONSE TIMES

3A10 Setting (kHz)	$f_{0.915dB}$ (kHz)	T_R (μ sec)
10	4.8	72.9
30	12	29.2
100	45	7.8
300	130	2.7
1000	500	0.7

The problem of errors due to the attenuation of the output signal can be avoided by adhering to tentative proposals of ASTM Committees^(15,51-52) and others^(27,29) which suggest that for a valid test

$$t \geq 1.1 T_R \quad (\text{Eq. 2.5})$$

where, t = any elapsed time to be used in
a data reduction calculation.

2.3.1.2 Signal Oscillations

The second major problem is the interpretation of the oscillations generated upon impacting a specimen. These oscillations have four primary sources⁽⁴⁷⁾:

1. the true mechanical response of the specimen
2. high frequency noise generated by the amplification system
3. inertial loading of the tup as a result of specimen acceleration
- and 4. low frequency oscillations caused by reflected stress waves and stored elastic energy.

The first is obviously the desired response.

The electronic noise is essentially eliminated by using the high gain (large signal/noise ratio) semiconductor strain gauges.

The third source of oscillations has been discussed in

depth, and from many points of view, by many authors^(13,18-19,25,29-31,47,53-56). It results from the specimen's resistance to sudden changes in its motion and is often described as being an "inertial loading" oscillation. It is identified as the first fluctuation on the load-time trace. The period of this oscillation is estimated to be on the order of 30 μ s for steel and aluminum specimens⁽²⁹⁾. However, it decays within approximately the first two oscillations, since, as the specimen accelerates the inertial load decreases^(29,47). Thus, the loads recorded during that initial period of time are dominated by this inertial loading phenomenon. The amplitude of this oscillation, which can cause serious problems in data analysis, is directly proportional to the impact velocity⁽⁵³⁾.

The last source of oscillations is said to be due to a combination of reflected stress waves and the damping of stored elastic energy^(13,31). The period of these oscillations can be reliably predicted through an empirical expression^(29,35):

$$\tau = 1.68S/C_0 (W/S)^{\frac{1}{2}} (EBC_s)^{\frac{1}{2}} \quad (\text{Eq. 2.6})$$

where, τ = period of specimen oscillations

S = support span

W = specimen width

B = specimen thickness

E = elastic modulus

C_o = speed of sound in specimen

C_s = specimen compliance

For steel and aluminum Charpy specimens, τ is on the order of 33 μ s (approximately the same period as the inertial oscillation). The amplitude of the stress waves is again a direct function of the impact velocity and can cause serious data analysis errors.

In order to avoid problems associated with the amplitude of all these various oscillations and the period for which the inertial oscillation masks the true signal, it has been proposed that any data to be used in a calculation meet the requirement (27,29):

$$t \geq 3\tau \quad (\text{Eq. 2.7})$$

This requirement is most easily met by decreasing the impact velocity, V_o , thereby extending the time for fracture. The period that the inertial load dominates is approximately 2τ , so the above restriction will assure that the true specimen response is not masked by contributions due to the inertial acceleration. A further advantage in decreasing the impact velocity is that the amplitudes of all the specimen oscillations are decreased, thus improving signal analysis. Furthermore, increasing the time to fracture, by decreasing the impact velocity, assures that the

electronic signal attenuation is much less than the acceptable 10% realized by meeting the requirement in Equation 2.5.

For some very low energy failures the fracture time can be quite short, so the impact velocity may have to be lowered to below that required by ASTM E 23 to meet the above stipulations. The effect of lowering V_0 to below the ASTM specification is not significant, as was discussed in Section 2.2.4.1. However, in most cases, the time to fracture obtained when using ASTM specified impact velocities satisfies the above restrictions.

2.3.1.3 Impact Energy

The third source of error is that associated with the energy supplied to fracture the specimen. Some calculations used to reduce the data obtained from an instrumented impact test rely on the assumption that the tup velocity is not reduced by more than approximately 20% so that the corresponding decrease in its velocity is considered to be essentially linear. To meet this requirement, a conservative stipulation is that the available impact energy, E_0 , be greater than three times that required to reach maximum load, and, of course, be sufficient to completely fracture the specimen. A compromise is necessary between intentionally reducing the velocity at impact, to limit the amplitude of specimen oscillations and extend the fracture time, and

keeping that velocity high enough to supply the energy to completely fracture the specimen with a linear decrease in velocity.

The tentative ASTM specifications shall require all of these restrictions to be met for a load-time signal response to be accepted as being indicative of the true specimen behaviour during impact. These requirements are summarized in Table 2.3.

Table 2.3

VALIDITY CRITERIA

Potential Source of Error	Criterion to Prevent Error
Inertial Loading Effects	$t > 3\tau$
Signal Attenuation	$t > 1.1 T_R$
Insufficient Energy;	$E_o > 3 E_{\text{Max Load}}$
Excessive Tup Deceleration	$E_o > E_{\text{Total}}$

2.3.2 Data Reduction from Load-Time Curves

2.3.2.1 Energy

The total energy obtained from a standard Charpy test is of limited value, even for comparing the relative toughness of

materials. A high strength, brittle material may have a high crack initiation energy though a low crack propagation energy. A low strength, ductile material, which may absorb the same total energy, can have a low initiation energy and a high propagation energy. The fracture characteristics must be examined in terms of the both energy to initiate and the energy to propagate a crack if fracture control is to be attempted.

2.3.2.1.1 Velocity Reduction Correction

The area under the load-time curve (which is actually the change in momentum or impulse) can be converted into the apparent energy for fracture:

$$E_a = V_o \int_0^t P dt \quad (\text{Eq. 2.8})$$

where, $\int_0^t P dt$ = area under load-time curve

t = elapsed time from initial contact
between tup and specimen

V_o = impact velocity

However, this is not the true energy absorbed by the specimen since the impact velocity decreases from V_o during the fracture event.

Assuming that the velocity decrease is linear, a correction for the apparent energy, which accounts for the decreasing velocity, can be derived^(18,57):

$$E_c = E_a (1 - E_a/4E_o) \quad (\text{Eq. 2.9})$$

where, E_c = corrected energy

E_o = available energy at impact

The derivation can be found in Appendix B. This correction factor often ranges as high as 10-12%.

That the velocity indeed decreases linearly (if the available energy, E_o , is more than twice that absorbed) and that the magnitude of the velocity change is usually small (on the order of 5%) have been experimentally demonstrated^(46,58). That this correction gives the same total energy as that conventionally observed from the dial-gauge on a standard Charpy machine has also been amply demonstrated^(18,20, 46-47,49,57-60). The dynamic calibration conducted for the present work verifies the correction as well.

The corrected energy up to the point of maximum load is generally considered to be the energy necessary to initiate a stable crack which propagates through the sample. For cleavage

failures, this assumption is widely accepted^(19,48,59,61-62). For fibrous fractures, at least for slow bend tests, the crack may initiate at a load less than maximum, and it may not begin to propagate rapidly through the specimen width until a time after maximum load has been reached^(20-21,63).

For consistency in data analysis, it was assumed that the crack initiation energy corresponds to the area under the load-time curve up to the point of maximum load. For cleavage failures this is no doubt true. For 100% shear failures this assumption, should it not be strictly valid, can cause nonconservative errors in the "initiation" energy calculations estimated to be on the order of 20%.

2.3.2.1.2 Compliance Correction for Initiation Energy

Ireland has suggested that when the tup strikes the specimen, the available energy, E_o , is reduced due to a variety of factors:

$$\Delta E_o = E_{ACC} + E_{SD} + E_B + E_{MV} + E_{ME} \quad (\text{Eq. 2.10})$$

where, ΔE_o = reduction in impact energy

E_{ACC} = energy required to accelerate the
specimen

- E_{SD} = energy required to bend and fracture
the specimen
- E_B = energy due to Brinell-type deformation
- E_{MV} = energy absorbed by impact machine through
vibrations
- E_{ME} = stored elastic energy absorbed by the
machine

The energy absorbed in deforming the specimen, E_{SD} , is the desired value. The values of E_B and E_{MV} are usually quite small. E_{ACC} can be disregarded when the oscilloscope response time is less than the specimen failure time ($t > 1.1 T_R$).

The stored elastic energy term, E_{ME} , is related to the machine compliance. An appreciable amount of the apparent initiation energy, E_I , as determined from Equation 2.9, can be a result of this energy, and so, this term must be eliminated from the "corrected" value of E_I . (N.B. The total energy need not be corrected for the machine compliance since the compliance is an elastic energy term).

It has been shown that this energy term can be given by⁽⁴⁷⁾:

$$E_{ME} = \frac{1}{2} P_{MAX}^2 C_M \quad (\text{Eq. 2.11})$$

where, P_{MAX} = maximum load on load-time trace
 C_M = machine compliance

The machine compliance can be calculated from⁽⁴⁸⁾:

$$C_T = C_M + C_s = d_{GY}/P_{GY} \approx V_o t_{GY}/P_{GY} \quad (\text{Eq. 2.12})$$

where, C_T = total compliance of the system
 d_{GY} = deflection at general yield (elastic limit)
 P_{GY} = load at general yield (elastic limit)
 t_{GY} = time at general yield (elastic limit)
 V_o = impact velocity
 C_s = specimen compliance

The non-dimensional specimen compliance, C_s , for a notched three-point beam with Charpy dimensions has also been established^(48,53). Thus, the machine compliance, and hence, the stored elastic energy of the machine can be conveniently determined.

Therefore, the true energy to initiate a crack (energy to maximum load) can be calculated by making corrections for both reduction in tup velocity and the effects of machine compliance:

$$EI = [EI_a (1 - EI_a/4E_o) - \frac{1}{2} P_{MAX}^2 C_M] \quad (\text{Eq. 2.13})$$

where, EI_a = initiation energy as calculated from
Equation 2.8.

2.3.2.2 Deflection

The corrections required for determining the specimen deflection at any time are similar to those employed in the energy calculations; the principles are discussed fully in References⁽⁴⁷⁻⁴⁸⁾. It can be shown, however, that:

$$d_t = tV_o(1 - E_a/4E_o) - P_t C_M \quad (\text{Eq. 2.14})$$

where, d_t = deflection at any time

t = elapsed time from initial impact

P_t = load at time of interest

E_a = energy as calculated from Equation 2.8

2.3.2.3 Dynamic Yield Strength

The point on the load-time trace corresponding to the load at which the curve first deviates from linearity is the general yield load. General yield is considered to occur when plastic yielding has spread across the entire cross-section of the specimen (for some steels, this corresponds to the lower yield load)^(20,64-65). Green and Hundy⁽⁶⁶⁾ have developed a relationship for determining the dynamic yield strength from the general yield load, which for three-point bending of notched specimens reduces to:

$$\sigma_{yd} = P_{GY} \frac{L}{B(W - a)^{2.21}} \quad (\text{Eq. 2.15})$$

where, P_{GY} = general yield load from IIT photo
 B = specimen thickness
 W = specimen width
 a = crack length
 L = support span

The equation has been validated for standard Charpy "V-notch" specimens by several investigators^(14,20,65). Employment of this equation, in conjunction with the data obtained from an instrumented impact test, is essentially the only means available for determining the yield strength of a strain rate sensitive material at very high strain rates (although the experimentally difficult Hopkinson-split bar technique has been used⁽⁶⁷⁾).

2.3.2.4 Fracture Toughness Calculations

The similarity between the instrumented impact load-time curve and the load-deflection curve used for fracture toughness determinations led to the application of fracture mechanics theory to IIT. The topic of dynamic fracture toughness is considered of such importance to be discussed separately in Chapter 4.

2.3.2.5 Computer Programs

To facilitate the many lengthy calculations necessary in analyzing the instrumented impact test data, two computer programs in FORTRAN language were written.

One, ENERGY, listed in Appendix C, must be supplied values for the area under the load-time curve for energy calculations. Measuring this area was most conveniently and accurately accomplished with a polar planimeter. Alternate methods of area measurement were investigated and included employing Simpson's Rule to integrate the curve, using a Quantimet, and, cutting and weighing the curve area. These tedious techniques were found to give inconsistent results, with errors greater than 10%, when compared with the accurate and reproducible results obtained by measuring the area under the load-time curves of the Army calibration samples with the planimeter.

The other program, IMPACT, uses digitized data of the load-time signal to fit a polynomial to the curve, and subsequently integrates that expression to determine the area under the curve.

2.3.2.6 Data Sheet

For each impact test, a number of data points were obtained

from the load-time trace for data reduction. An "Instrumented Impact Test Record" data sheet was printed to provide a permanent record of the parameters for each test and to facilitate computer analysis. Such a sheet is reproduced in Appendix D.

2.4 Effects of Test and Specimen Parameters

2.4.1 Significance of Test Validity Criteria

2.4.1.1 Inertial Loading Effect

As described in Section 2.3.1, ASTM tentative proposals suggest that to obtain consistent and universally acceptable IIT data, certain validity criteria must be met. A major problem in IIT is that the oscillation associated with the inertial loading of the specimen may overshadow the true specimen response if the time used in any data reduction calculation is less than the time for that inertial oscillation to decay. To avoid such problems, a validity criterion has been conservatively set for the times to be used in calculations:

$$t > 3\tau \quad (\text{Eq. 2.7})$$

The inertial oscillations decay in approximately 2τ .

To determine if errors in data calculations existed when this criterion was not met, samples were tested at velocities which inherently resulted in general yield and fracture times of less than the duration of the inertial loading event, 2τ (i.e., impact velocities were used that were higher than that necessary to simply achieve fracture and thereby decreased the time required for the fracture). Also, all data generated during this program which did not meet the $t \geq 3\tau$ criterion were examined. Representative results are shown in Table 2.4.

For those tests in which the fracture event occurred prior to 2τ , i.e., for tests in which the inertial load was considered to dominate the load-time curve, no significant nor consistent differences in any calculated property (e.g., absorbed energy, fracture toughness) were evident when compared with "valid" tests, under identical conditions, in which the failure times exceeded 3τ . All "invalid" results were within a reasonable scatter band.

For those tests in which the failure times were greater than the period of inertial loading (2τ), though less than the 3τ validity criterion, again no consistent deviation in properties was evident when compared with the "valid" data obtained from tests where $t \geq 3\tau$.

Although others have indicated that violating this criterion results in erroneous data (particularly fracture toughness values)^(29,68),

Table 2.4
COMPARISON OF VALID AND INVALID DATA
AS DETERMINED BY $t < 3\tau$

Specimen Code	Test Temperature (°C)	2τ (ms)	Time To General Yield (ms)	3τ (ms)	Total Energy (ft-lb/in ²)	Initiation Energy (ft-lb/in ²)	K_{Id} (ksi-in ^{1/2})
AF-1-STR-PC-07	- 40	.079 <	.133	> .118	116.7	4.7	61.6
AF-1-STR-PC-09	- 40	.085 <	.156	> .127	121.2	3.2	61.3
AF-1-STR-PC-08#	- 40	.104 >	.101	< .156	95.2	4.1	64.2
RP-PC-19	- 80	.085 <	.163	> .127	39.7	2.5	39.5
RP-PC-20*	- 80	.092 <	.103	< .138	32.8	2.5	41.2
RP-PC-21#	- 80	.092 >	.088	< .138	38.2	0.9	36.6
AF-2-STR-PC-5P	-100	.092 <	.143	> .138	46.0	3.3	43.0
AF-2-STR-PC-5Q	-100	.092 <	.141	> .138	51.1	4.1	45.2
AF-2-STR-PC-5L*	-100	.092 <	.104	< .138	50.8	3.5	47.4
AF-2-STR-PC-5N*	-100	.092 <	.106	< .138	43.9	5.0	47.1
AF-2-STR-PC-5O*	-100	.092 <	.127	< .138	42.4	3.0	45.4
AF-2-STR-PC-5M#	-100	.104 >	.101	< .156	57.9	4.6	50.4
AF-1-STR-PC-01	+ 20	.085 <	.137	> .127	120.7	7.6	68.3
AF-1-STR-PC-02	+ 20	.085 <	.155	> .127	146.8	4.9	68.1
AF-1-STR-PC-03*	+ 20	.101 <	.121	< .152	105.2	4.4	68.3
AF-1-STR-PC-11	- 60	.082 <	.126	> .123	74.8	3.6	47.1
AF-1-STR-PC-12	- 60	.085 <	.141	> .127	68.7	4.6	63.0
AF-1-STR-PC-10*	- 60	.092 <	.122	< .138	79.4	7.2	55.9
AF-2-STR-PC-3L	- 40	.085 <	.172	> .127	240.0	15.8	74.1
AF-2-STR-PC-3M	- 40	.092 <	.167	> .138	225.4	18.8	70.1
AF-2-STR-PC-3N*	- 40	.101 <	.143	< .153	237.5	21.2	76.0
AF-2-STR-PC-5J	- 80	.101 <	.155	> .152	89.3	0.4	53.4
AF-2-STR-PC-5K	- 80	.092 <	.163	> .138	102.9	6.6	54.1
AF-2-STR-PC-5I*	- 80	.092 <	.118	< .138	92.7	2.8	48.8

* Indicates invalid test: $t_{GY} < 3\tau$

Indicates inertial load dominated: $t_{GY} < 2\tau$

$$1 \text{ ft-lb/in}^2 = 0.21 \text{ J/cm}^2$$

$$1 \text{ ksi-in}^{1/2} = 1.1 \text{ MPa-m}^{1/2}$$

the present work does not bear this out. This is not to suggest, however, that the criterion is not useful; only that in this work, the inertial oscillations may have decayed in a time less than 2τ , and/or that the criterion may be quite conservative. Adherence to this criterion does not impose unreasonable restrictions in testing specimens; merely decreasing the impact velocity slightly is usually all that is required to meet specifications.

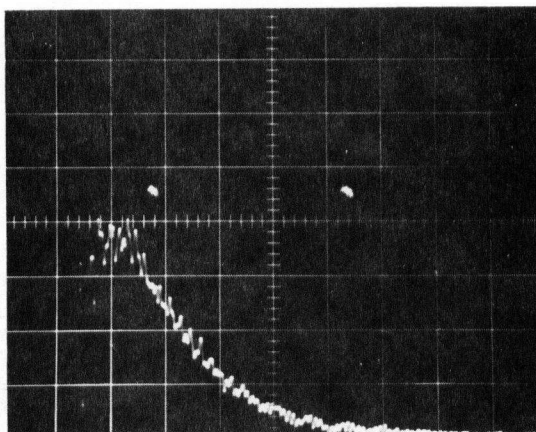
2.4.1.2 Effects of Impact Velocity

High impact velocities not only decrease the failure times, as just discussed, but, also increase the amplitudes of all the specimen oscillations. V_o should be controlled for this reason, as well.

To demonstrate this and the associated potential for error, samples were tested at both very high impact velocities and at velocities which minimized the amplitudes of the specimen oscillations.

Figure 2.5a shows the effect of impacting a specimen at 5.46 m/s (17.9 ft/s), which is within the standard Charpy test velocity range (10-20 ft/s), but relatively high for IIT. Another identical specimen was impacted at 3.46 m/s (11.34 ft/s), also within the standard test velocity range (Figure 2.5b).

(a)



(b)

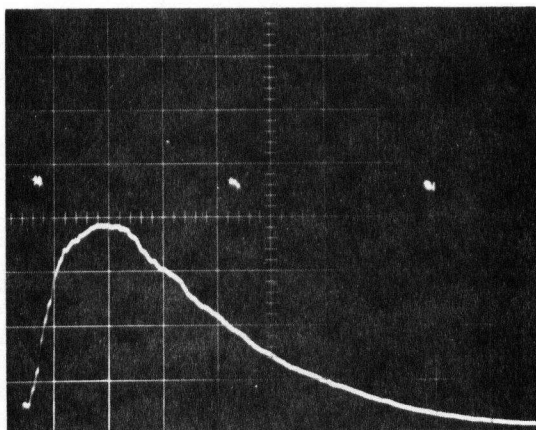


Figure 2.5 Effect of impact velocity, v_0 , on load-time trace:

(a) $v_0 = 5.46 \text{ m/s}$

(b) $v_0 = 3.46 \text{ m/s}$

The time to general yield, t_{GY} , was only 0.078 ms for the specimen impacted at the higher velocity (Figure 2.5a), which is less than the 3τ (0.099 ms) criterion used to assure that the initial portion of the load-time trace is not overshadowed by the inertial oscillation. Also, this test did not meet the requirement that the signal not be unduly attenuated, since t_{GY} was less than $1.1 T_R$ (Equation 2.5). This high velocity test must therefore be considered invalid on these two counts.

This example shows that 1) interpretation of the load-time trace can be made much more difficult due to oscillations (compare Figures 2.5a and 2.5b); 2) thus potential for error in data reduction is consequently increased; and, 3) a test can be rendered invalid by using an excessively high impact velocity.

For these reasons, all tests were performed at velocities which minimized the amplitudes of the oscillations and extended the fracture time.

2.4.1.3 Electronic Response Time

The response time of the electronic system (a function of the upper band width frequency) must be such that a signal is displayed which has not been excessively attenuated.

Tests were performed to determine if attenuated data would give erroneous results. Steel specimens known to give very reproducible results were tested under identical conditions, except that the setting of the upper band width frequency was varied. The response time, T_R , was correspondingly increased (refer to Table 2.2). Therefore, the fracture event, in some cases, occurred in a time much less than the response time of the electronic system, and the signal was attenuated by more than 10% (i.e. $t < 1.1 T_R$). (N.B. The same results may have been obtained if the impact velocity were unduly increased and the response time kept constant. However, the attendant increase in the amplitudes of the oscillations would confuse the comparisons of the effects of varying the response time relative to the fracture time).

Results of this series of tests are given in Table 2.5. The corresponding impact photographs are shown in Figures 2.6a - d.

The data show that inadequate system response times result in signals that have been grossly attenuated and thus yield inaccurate results. The accurate values are those of the totally unfiltered test with the 1MHz setting and corresponding 0.0007 ms response time (Figure 2.6d). The 0.3 kHz and 1 kHz band width settings, which give response times of 2.3 ms and 0.714 ms, respectively, yielded data with greatly extended fracture times (time to maximum load),

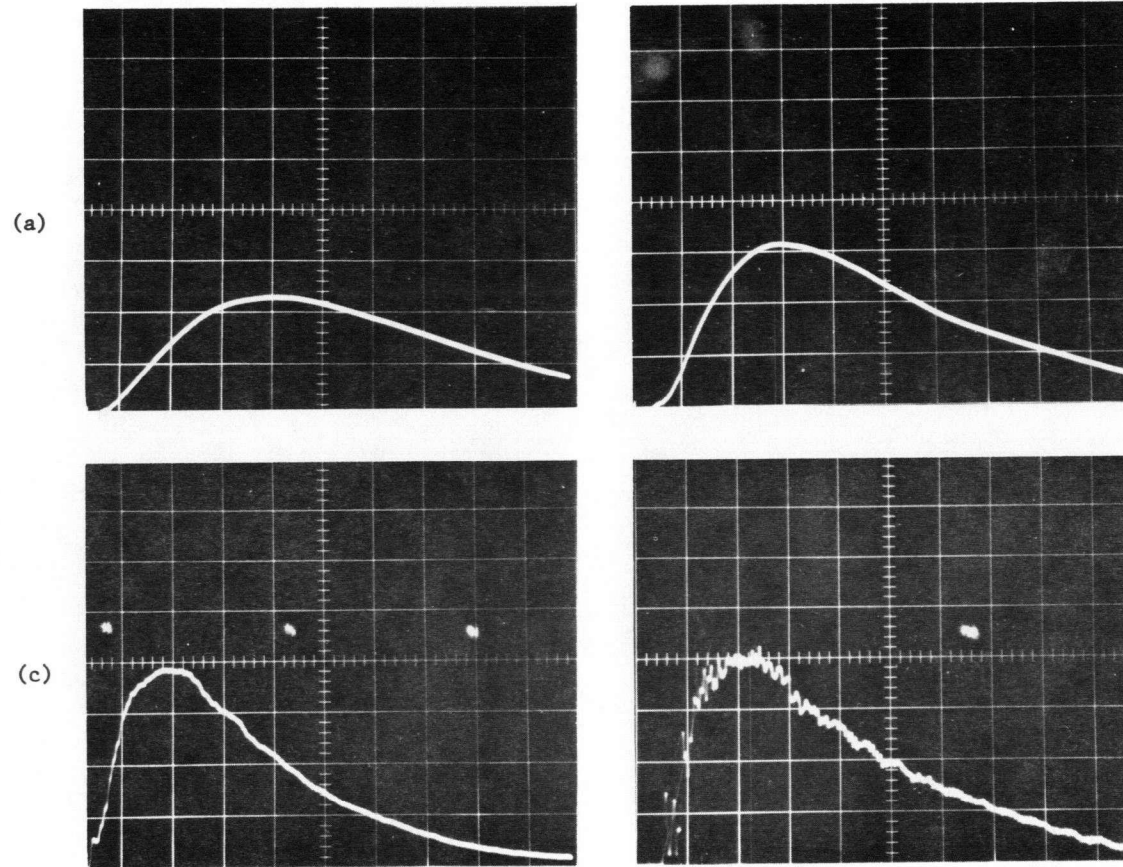


Figure 2.6 Effect of electronic response time, T_R , on load-time trace:

(a) $T_R = 2.3$ ms
 (b) $T_R = 0.714$ ms

(c) $T_R = 0.0729$ ms
 (d) $T_R = 0.0007$ ms

Table 2.5

COMPARISON OF VALID AND INVALID DATA

AS DETERMINED BY $t < 1.1 T_R$

	Response Time (ms)	Time To General Yield (ms)	Time To Maximum Load (ms)	General Yield Load (lb)	Maximum Load (lb)	Total Energy (ft-lb)	Stress-Intensity Factor (ksi - inch ^{1/2})
AF-1-SLP-TR1*	2.3	.334	.661	1761	2287	22.2	104.9
AF-1-SLP-TR2*	.714	.231	.435	2481	3134	26.0	109.0
AF-1-SLP-TR3	.0729	.169	.328	3388	3821	24.5	138.0
AF-1-SLP-TR5	.0007	.160	.345	3507	3955	25.0	141.7

* Indicates Invalid Test

For a Valid Test $T_{GY}/T_R > 1.1$

though attenuated loads (Figure 2.6a, b). The fracture toughness parameters were also seriously attenuated. It is interesting to note that the total absorbed energy was not affected by attenuation, however.

These results are in agreement with those of Hoover who studied Borsic-aluminum composites⁽⁵⁰⁾.

Note that filtering the signal somewhat by using a 10 kHz setting (Figure 2.6c) results in valid, accurate data with the advantage that the amplitudes of the superfluous specimen oscillations are greatly suppressed.

2.4.2 Specimen Parameters

2.4.2.1 Notch Radius

It was found to be extremely difficult to cut large numbers of Charpy notches with the accurate $0.25 \text{ mm} \pm 0.025 \text{ mm}$ standard notch radii⁽⁴⁴⁾. Specimens received from outside sources and samples produced within the Department commonly deviated from this standard radius.

The effect of any notch is 1) to raise the effective strain rate below the notch root, which implies for bcc materials,

that the yield stress increases; 2) to concentrate plastic strain and raise the yield strength additionally by strain hardening; and 3) to introduce a triaxial stress state at the notch root. The result is to raise tensile stress levels below the notch and to raise the ductile-brittle transition temperature^(64,69). Decreasing the notch root radius, as in precracking accentuates those effects by increasing the plastic stress concentration factor; decreasing the stress level required to achieve the maximum degree of stress intensification; and, by decreasing the plastic zone size required to maximize the degree of triaxiality⁽⁵⁾.

A series of preliminary tests were performed on Charpy specimens with nonstandard notches to determine the effect of this test variable on IIT results.

Steel specimens with notch radii from 0.16 mm to 0.33 mm were tested. Charpy samples having fatigue cracks at the notch root were also tested. All other specimen dimensions conformed to the ASTM E 23 requirements.

The results of the study are presented in Table 2.6. The data show that the propagation energy was not affected by variations in the notch radius. However, the results of the tests conducted at +20°C indicate that the initiation energy was affected by decreases

in the radius. The fatigue precracked notches, having a very sharp radius, yielded extremely low initiation energy values. For notches with radii in the range from 0.25 mm to 0.16 mm, there is little difference in the initiation energy. The relatively blunt 0.33 mm notches gave the highest initiation energies.

The results obtained at temperatures of -20°C and below (transition region) show that specimens with the 0.18 mm radius notch have a higher initiation energy than those with the standard 0.25 mm radius notch. Ciampi and coworkers⁽⁷⁰⁾ also found that specimens with a 0.12 mm radius notch often had higher initiation energies than those with the 0.25 mm notch in this temperature range. This is unexpected on a theoretical basis⁽⁵⁾. Apparently, the variations in the notch toughness due to changes in the notch radius (at least for this steel in the limited range of from 0.25 mm to 0.18 mm) are not so great as to overshadow either the inherent scatter found in toughness data or the bimodal behaviour of Charpy data in the transition region^(69,71).

Results of the critical crack opening displacement, COD, data are also indicated in Table 2.6. The critical COD can be defined as the amount of inelastic stretching of the material immediately ahead of the crack tip at the moment of crack initiation⁽⁷²⁾. Discussion on the calculation of this parameter from IIT

Table 2.6

NOTCH RADII STUDY

T(°C)	0.33 mm			0.25 mm			0.18 mm			0.16 mm			0 mm		
	EP/A	EI/A	COD	EP/A	EI/A	COD	EP/A	EI/A	COD	EP/A	EI/A	COD	EP/A	EI/A	COD
+ 20	123	52	6.6	124	40	5.6	125	38	5.4	123	35	4.8	125	7	1.3
- 20				124	29	4.1	123	43	5.3				112	7	1.4
- 40				107	21	3.1	107	33	4.2				107	4	1.4
- 50				93	17	2.8							85	5	1.2
- 60				74	14	2.0	72	33	4.3				67	4	1.1
- 70	44	19	3.1				48	15	2.2	44	15	2.4	60	4	1.0

All values are averages of several tests

EP/A = Propagation Energy/Unit Area (ft-lb/in²)

EI/A = Initiation Energy/Unit Area (ft-lb/in²)

COD = Critical Crack Opening Displacement (in x 10³)

All tests performed on Steel AF-1 with crack running parallel to rolling direction.

data is deferred until Chapter 4.

The trends are very similar to those noted for the initiation energy. In comparing COD data for the fatigue precracked versus the notched samples tested at +20°C, it is evident that the crack opening deflection decreases with decreasing notch radius. The relatively blunt 0.33 mm notch resulted in the highest displacements prior to fracture initiation. The specimens with the 0.25 mm, 0.18 mm, and 0.16 mm notch radii did not show significant differences in COD.

Again, in the transition temperature range, the 0.18 mm notch radius specimens experienced more deflection prior to crack initiation than did the standard specimens.

The ASTM E 23 specification for the Charpy notch radius is $0.25 \text{ mm} \pm 0.025 \text{ mm}$. The results of this preliminary study have shown that though it is difficult to machine specimens to such a tolerance, specimens with notch radii which deviate only slightly from the standard still yield data within the expected scatter band of the material.

2.4.2.2 Notch Angle

Charpy specimens having a 60° notch angle as opposed to

the specified $45^\circ \pm 1^\circ$ standard were tested, all other specimen dimensions adhering to the ASTM standard. The results of the study are shown in Table 2.7.

The observed increases in both the initiation and the propagation energies of the 60° notched materials (versus the 45° notch) conform to the theoretical expectations.

On a theoretical basis, increasing the notch angle (as with increasing the root radius) should have the effect of decreasing the maximum value of the plastic stress intensification factor. The plastic stress intensification factor is defined as the ratio of the maximum tensile stress existing below a notch to the tensile yield stress of an unnotched specimen⁽⁵⁾. Lowering the maximum value of this factor decreases the magnitude of the tensile stresses in the plastic zone ahead of a notch for a given applied stress and thereby increases the measured ductility and toughness manifested by increases in both the propagation and initiation energies. Thus, the greater the notch angle, the less the constraint at the notch root, and the greater the notch toughness of the specimen. The maximum possible value of the stress concentration factor below the notch is 2.82 for a 0° notch and 1.0 for an unnotched bar⁽⁵⁾. The values for 45° and 60° notches are 2.18 and 2.05, respectively, which are not significantly different. Nevertheless, measurable increases in toughness

Table 2.7

NOTCH ANGLE STUDY

T(°C)	AF-1-Crack Parallel RD 60° Notch		AF-1-Crack Parallel RD 45° Notch	
	Initiation Energy*	Propagation Energy*	Initiation Energy*	Propagation Energy*
+ 100	6.0	18.0	5.6	15.9
+ 20	5.8	17.9	4.6	15.6
0	5.6	19.2	5.7	18.5
- 20	5.3	17.2	4.4	15.3
- 40	4.2	17.2	3.2	13.8
- 60	3.5	12.9	3.2	11.5
- 80	1.3	4.7	1.1	4.9

T(°C)	AF-1-Crack Transverse RD 60° Notch		AF-1-Crack Transverse RD 45° Notch	
	Initiation Energy*	Propagation Energy*	Initiation Energy*	Propagation Energy*
+ 100	34.3	69.3	30.8	64.9
+ 20	37.3	71.7	30.0	72.3
0	30.9	85.3	22.3	82.4
- 20	26.1	92.9	21.4	84.4
- 40	20.1	74.2	18.9	69.0
- 60	18.3	59.5	14.5	55.8
- 80	1.2	8.4	1.2	9.1

* in ft-lb

All values are averages of several tests

1 ft-lb = 1.36 J

were observed for the 60° notched specimens.

The results of this study are important in that 1) they show the usefulness of instrumenting an impact test for revealing differences in the dynamic response of different types of specimens, and 2) they underline the importance of adhering to the notch angle requirement in the ASTM E 23 specification.

2.4.2.3 Specimen Thickness

Tests were performed to determine the effect of specimen thickness on the IIT results. Since pipeline steels were employed in this study, these results are included in Chapter 3.

2.5 Crack Initiation

An important assumption in the analysis of the load-time data from an instrumented impact test is that the area under the curve to the point of maximum load is a direct measure of the energy required to initiate the crack. This initiation energy parameter, EI, is not only used to describe the crack initiation event, but also is used to calculate fracture toughness parameters, such as the J-integral and its associated stress-intensity factor, K_J . In addition, the assumed relationship between the peak load

and crack initiation is used in establishing critical deflections for crack opening displacement calculations and critical loads for other fracture toughness values.

It has been reported^(19,63,73-74) that for work hardenable notched three-point bend specimens, tested under slow strain rate conditions, the idealized crack initiation/propagation behaviour is as follows: Several microscopic cracks initially appear, essentially simultaneously, at mid-width, on the tension side of the specimen being loaded. Edge effects and unconstrained plasticity in the center of the specimen account for this. These small subcritical cracks eventually join together into a much wider and deeper crack, resulting in a "thumbnail" appearance on the fracture surface. This is known to occur at a point on the load-deflection trace beyond general yield but prior to maximum load, the exact location on that curve being a function of specimen size, composition, and strain rate. The depth of the initiating crack at this stage remains essentially constant up to the point of maximum load; whereas, its width extends laterally, as the regions near the edges of the specimen begin to form micro-cracks which combine with the central crack. The crack eventually reaches the sides of the test specimen at the point of maximum load. Beyond maximum load the crack propagates through the width of the specimen with an attendant loss in load. The mode of propagation at this stage, whether it be cleavage, fibrous, or a combination of

the two, determines the magnitude of the propagation energy.

Iyer and Miclot⁽⁷⁵⁾ reported that for non-work hardening materials, however, no subcritical crack growth occurs in the post yield region prior to reaching maximum load. Crack extension was always accompanied by a drop in load.

For those specimens which fracture prior to general yield (i.e. linear-elastic failures) or which fracture entirely by cleavage, crack initiation is believed to occur at the maximum load as the crack front "pops in" straight across the entire specimen thickness^(20-21,62).

These descriptions of the cracking process have been drawn from studies done under slow bend conditions. It is reasonable to assume that the general crack formation process is the same under impact loading conditions⁽¹⁹⁻²⁰⁾; the only difference being the precise position between general yield and maximum load at which the crack initiates - the crack should still reach full specimen thickness at maximum load.

Various instrumented impact tests were performed to determine

1) if, in fact, during fibrous or mixed mode fracture the crack extends to full specimen thickness at the maximum load; and, 2) if the precise point on the load-time curve at which a crack initiates

could be established under impact loading conditions.

These tests, to study the relationship between peak load and fracture, included: 1) High speed movie films to record the surface evidence of the fracture event; 2) an electrical resistance technique; and, 3) "reduced energy" tests.

2.5.1 High Speed Movie Films

The high speed film technique employed a Hycam movie camera, capable of up to 10,000 frames per second, to examine the surface of the test specimen during impact. Comparison of the specimen surface on each frame of the high speed film with the corresponding IIT load-time trace was used to determine the actual load at which a surface crack appears.

Due to the restraints imposed by the high intensity lighting required for high speed filming and the coordination required in triggering the impact machine and the high speed camera, tests were possible only at ambient temperatures (30° - 35°C). Thus, only fibrous failures could be studied.

Charpy specimens of an acicular ferrite steel were notched so that the crack would propagate transverse to the rolling direction.

This particular steel (designated AF-1) exhibits relatively high impact energies when cracking occurs in this direction.

Table 2.8 summarizes the results of this study.

Table 2.8

HIGH SPEED MOVIE FILM RESULTS

Specimen Code	Film Speed At Impact	Time to Maximum Load From IIT Photo	Time of First Observation of Surface Crack on High Speed Movie Film
AF-1-49	4625 ft/s	0.633 ms	$0.649 < t < 0.845$ ms
AF-1-47	5250 ft/s	0.727 ms	$0.762 < t < 0.952$ ms

These results indicate that under impact loading conditions the crack does indeed appear on the surface at a time that is approximately equivalent to that required to attain the maximum load, in agreement with slow bend test results. The time uncertainty shown in the tabulated data is associated with the time elapsed between individual frames of the movie film. These times determined from the high speed films do fall on the maximum load "plateau" of the load-time trace. The difference in initiation energy between that

obtained using the maximum load from the load-time trace versus that corresponding to the median time obtained from the high speed film tests is equivalent to approximately 6-7 J; the magnitude of this difference is similar to other errors inherent in analyzing the load-time data.

2.5.2 Electrical Resistance Study

McIntyre and Priest⁽⁷⁶⁾ have described the application of the electrical resistance technique to study crack growth. A constant current is passed through a notched specimen, a certain potential difference existing between the current leads placed at the ends of the specimen. As a crack initiates and extends from the notch during loading, this potential difference will suddenly increase due to the increase in the path of resistance. This change in the potential drop across the sample can be monitored using an oscilloscope. By comparing the time at which the potential difference initially increases with the time for attaining the peak load on the load-time trace, the relationship between peak load and crack initiation can be assessed. This method offers the advantage that the crack formation process can be monitored throughout the entire impact event.

Stranded copper wire current leads were spot welded to the

ends of standard Charpy specimens (the material was identical to that employed in the high speed movie study). A constant current of 20 amps was supplied across the test specimen. Great care was taken to insulate the entire system, particularly by separating the specimen from the anvils with a thin sheet of insulating material.

Typical results are shown in Figure 2.7. The potential difference across the specimen generally increased rapidly, and unexplainably, at the instant of impact, then dropped to a value below that of the initial potential in a time span within the elastic region on the corresponding load-time trace. The potential difference then, usually, rose rapidly in the time range between that associated with general yielding and the maximum load. The rapid rise in potential apparent after yielding was thought to be associated with the crack initiation and consequent increase in the path of electrical resistance. Late stages of the fracture event generally correlated well with a rapid increase in the potential across the specimen.

However, in some tests the potential difference decreased rather than increased as the specimen fractured. In other tests, the initial increase in potential difference corresponded to a point beyond the maximum load. Such inconsistencies cast doubt as to the reliability of the technique.

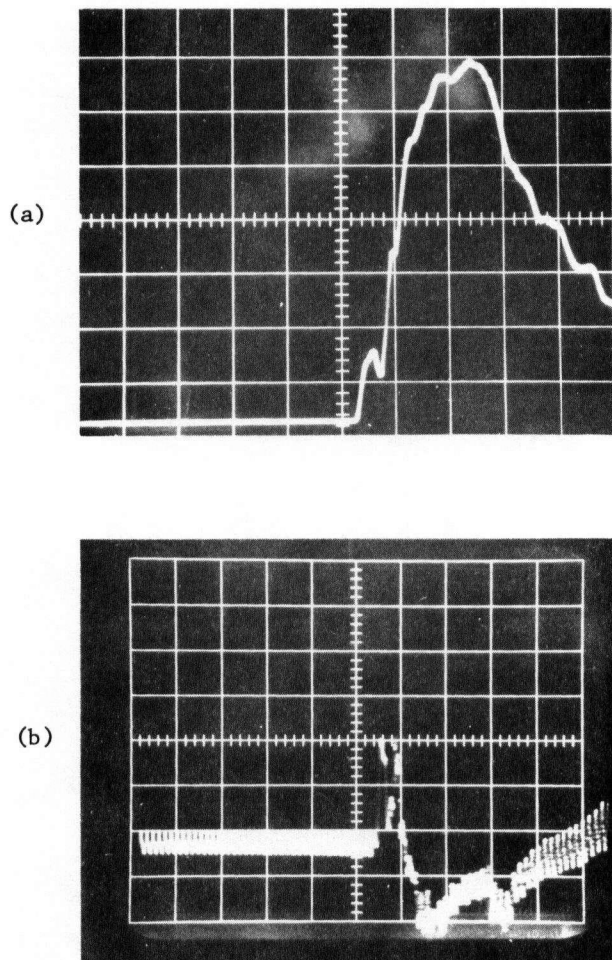


Figure 2.7 Electrical resistance study of crack growth.
(a) load-time curve. Scale: 500 lb/div x 0.2ms/div
(b) potential-time curve. Scale: 1 mV/div
x 0.2ms/div.

The following are possible reasons for these test problems:

1. Although McIntyre and Priest were successful in monitoring crack growth in Charpy specimens, they employed a well insulated system and slow bend tests. The present work, under impact loading conditions, necessarily involved the falling tup assembly, a massive block of steel. Thus, this moving magnetic field may have generated electric fields which drastically influenced the test results.

2. The initial crack front of these specimens is curved. The resistance method produces an output which is proportional to the average crack length between the mid-section and the edges of the sample. Thus, the resistance change in the initial stages of crack formation are small and may have been overshadowed by the factors described in 1.

3. During the initial stages of cracking, prior to extensive bending of the specimen, rough surfaces on the opposing fracture faces may have interconnected and caused short circuiting, thereby reducing the magnitude of the potential drop or giving erroneous results altogether.

If the system could be better insulated, this technique could be useful in monitoring crack growth under impact loading

conditions to establish the exact point on the load-time curve at which fracture initiates.

2.5.3 Reduced Energy Tests

A series of steel specimens were subjected to a range of impact energies varying from a magnitude in excess of that required to initiate the crack to energies less than that required for initiation. This "initiation" energy (energy to maximum load) was determined from previous tests of the same material and found to be 50.6 ± 4.1 J (37.3 ± 3.0 ft-lb).

Specifically, specimens in this study were impacted at one of the following levels of available energy, E_0 : 1) An impact energy of less than the lowest value of the initiation energy, including scatter; i.e., less than 46.5 J (34.3 ft-lb); 2) an impact energy within the initiation range, i.e. 46.5 to 54.7 J (34.4 - 40.3 ft-lb); or, 3) an E_0 value greater than the highest known value of the initiation energy (> 54.7 J).

After the reduced energy was imparted to each specimen, the specimens were heat tinted to oxidize any resulting crack surfaces and subsequently fractured to reveal the extent of crack propagation.

The results of these tests, presented in Table 2.9, supported, at least qualitatively, the description of crack formation previously discussed: crack initiation apparently occurs near mid-center of the specimen, prior to maximum load; the crack extends laterally to full specimen thickness at maximum load; and, thereafter, the full width crack propagates through the specimen.

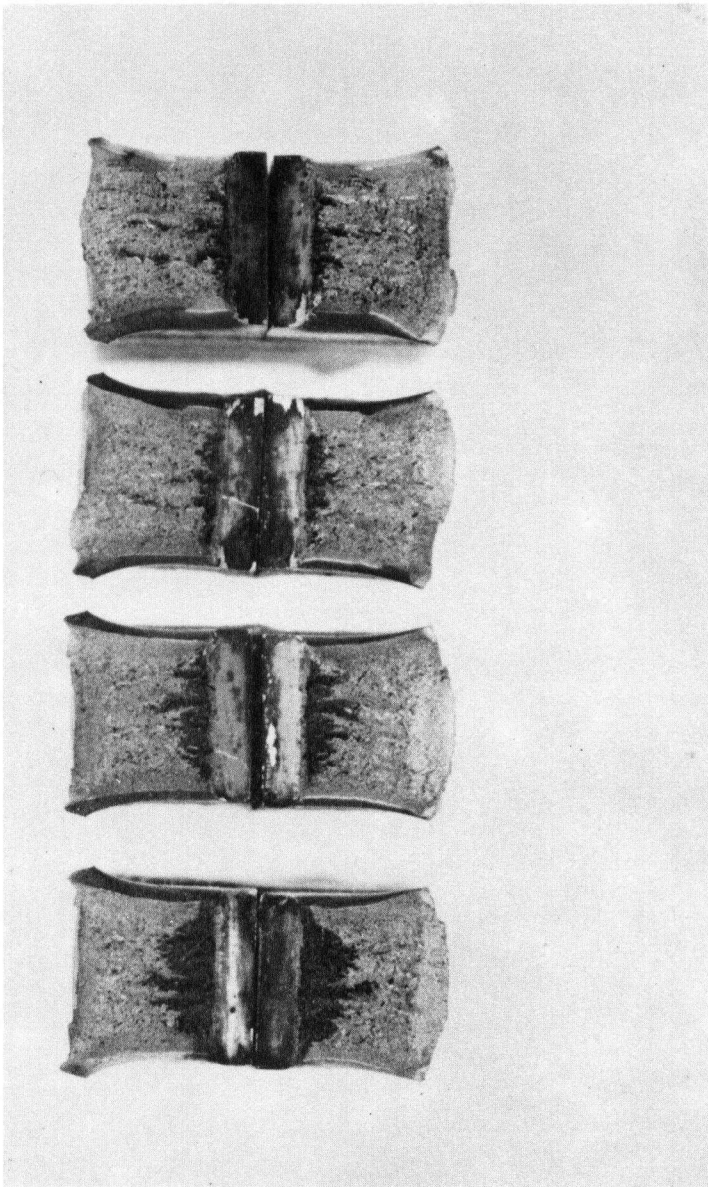
Specimens 1 and 2, impacted with available energies of less than 46.5 J, both showed very slight evidence of crack initiation. These cracks were extremely short (< 1 mm) and did not extend across the samples.

Specimen 4, impacted at an energy of 51.2 J (within the "initiation" range) exhibited a crack which had extended to the sides of the specimen and showed some full width propagation. Whereas, specimen 3, impacted at 45.6 J, just less than the "initiation" energy, displayed a crack which had not quite extended across the test sample.

The behaviour shown in specimen 4 is comparable to that found using slow bend testing⁽⁷³⁻⁷⁴⁾ and agrees with the results of the high speed movie films which showed that the crack first extends to the sides of the specimen at maximum load.

Table 2.9

REDUCED ENERGY TEST RESULTS

Specimen	Impact Energy (J)	Photograph
1	34.2	
2	39.9	
3	45.6	
4	51.2	
5	62.6	
6	68.3	

Energy to maximum load ("initiation" energy)

Predetermined to be 50.6 ± 4.1 J (37.3 ± 3.0 ft-lb).

All specimens AF-1 steel notched transverse to rolling direction
Tests all at +20°C.

Specimens 5 and 6, impacted with energies exceeding the initiation energy, exhibited cracks which had extended across the sample and then propagated approximately halfway through the remaining ligament.

In summary then, these tests show that for shear type failures resulting from impact loading: 1) crack initiation occurs prior to maximum load, and 2) that the crack extends to the sides of the sample at the point of maximum load. Calculations of initiation energy, among others, depend upon the assumption that crack initiation starts at maximum load. Since no reliable technique exists to establish the precise point of crack initiation under high strain rate conditions, all calculations in this study were made assuming that the maximum load is equivalent to the point of crack initiation. It is recognized that some values determined employing this assumption may be non-conservative (unless fracture was entirely cleavage or occurred before general yielding). This remains one of the major areas in the field of instrumented impact testing requiring further work^(14,34,72,75).

3. INSTRUMENTED IMPACT STUDY OF ACICULAR

FERRITIC PIPELINE STEELS

3.1 Acicular Ferritic Steels

The relatively new high strength, low alloy (HSLA) acicular ferritic steels have become an important class of structural materials due to their low cost per unit of strength, high toughness, and good formability and weldability. Material having a yield strength of 70 to 80 ksi (480-550 MPa), a Charpy upper shelf energy of well over 115 ft-lb (155 J), and a Drop Weight Tear Test 50% shear fracture appearance temperature of about -45°C is now available.

The innovative production techniques employed to produce this new generation of steels have been reviewed in several publications (77-86).

Acicular ferrite (AF) is defined as a highly substructured, non-equiaxed ferrite that forms on continuous cooling by a transformation involving both diffusion and shear. The transformation temperature is slightly higher than that of upper bainite. AF is also distinguished from bainite in that only a very small amount of carbide is present due to the limited amount of carbon available in such steels⁽⁷⁸⁾.

Strengthening is achieved through several independent mechanisms. The AF is inherently fine grained (ASTM 12-14)⁽⁸⁶⁾ and has a high dislocation density. The niobium addition (0.04 - 0.07 w/o) provides additional strengthening by precipitating as a niobium carbonitride.

The very low carbon additions (less than 0.07 w/o) and the exceptionally fine grain size of AF contribute to its high toughness, a property not generally associated with high strength materials. Higher carbon levels and the consequent formation of carbides result in higher transition temperatures and lower shelf energies. The low carbon level has the added advantage that both weldability and formability are markedly improved. A minimum carbon level of 0.01 - 0.02 w/o is desirable to facilitate precipitation strengthening⁽⁷⁸⁾.

The addition of molybdenum (0.25 - 0.50 w/o), manganese (1.50 - 2.25 w/o), and to a lesser extent, niobium, suppresses the austenite-ferrite transformation temperature to below 700°C which increases the nucleation time required to form polygonal ferrite; the alternative acicular ferrite microstructure is thereby allowed to form upon cooling⁽⁷⁹⁾.

That the AF transformation occurs at a relatively low temperature is significant, in that: 1) the decreased solubility

of Nb in ferrite promotes the formation of Nb(C,N) at a slower rate and therefore produces a finer, more homogeneous precipitate; the steel ages only slightly⁽⁷⁸⁾; and, 2) the low transformation temperature also contributes to the formation of the very fine ferrite grain sizes. Both effects improve strength and toughness⁽⁸¹⁾.

Strict process control during the hot rolling of these HSLA steels is essential to achieve the very fine ferritic grain size and the desired balance of toughness and strength necessary for critical applications such as pipelines.

A reduced slab reheating temperature (approximately 1150°C) ensures that the austenite is fine grained prior to hot rolling. During the initial rolling stages ($\approx 1150^\circ - 980^\circ\text{C}$) the steel is heavily deformed and it recrystallizes repeatedly, further refining the γ -grain size⁽⁸⁶⁾. There is some Nb(C,N) precipitation in the austenite at these temperatures which tends to retard austenite recrystallization and grain growth^(78,81,85-86); this is another beneficial effect of the niobium addition (Al, V, and Ti, for instance, retard grain growth but not recrystallization)⁽⁸²⁾.

Below 980°C, where recrystallization of the austenite ceases, finish rolling takes place (980°-800°C). At the lower end of this temperature range, heavy deformation of the fine grained γ imparts a

heavily dislocated structure and elongates the grains, thereby providing more sites for the subsequent nucleation and growth of a fine grained ferrite. The heavy deformation of the γ -phase also suppresses the γ - α transformation temperature⁽⁸⁰⁾. The minimum rolling temperature is controlled to ensure that no deformation of the ferrite phase occurs, as this would be detrimental to the toughness of the final product.

In general, decreasing the slab reheat and finish rolling temperature (to limit γ recrystallization and grain growth) and increasing the degree of deformation in the late rolling stages (to enhance substructure strengthening and to provide more ferrite nucleation sites) results in more refined ferrite grains thereby improving the strength and toughness of the steel^(81-82,86).

Very low sulfur levels and/or additions of rare earths, for sulfide inclusion shape control, are desirable to assure adequate toughness and to reduce the anisotropy of the toughness and ductility properties^(78,85).

Acicular ferrite steels are often killed, sometimes with aluminum since silicon can impair impact resistance⁽⁷⁸⁾.

3.2 Pipeline Applications

Vast resources of recoverable oil and gas exist; nearly

20% of the gas fields are believed to be situated in the distant offshore Arctic regions of Alaska and Canada and perhaps another 50% in Siberia alone⁽⁸⁷⁾.

The social and economic pressures to retrieve these resources are enormous. The Alyeska trans-Alaska oil pipeline and the proposed Alcan/Foothills gas line are notable engineering projects which extend the limits of pipeline technology.

Such pipelines are being built at incredible costs through an extremely hostile, yet fragile, environment - the Alyeska pipeline was recently completed at a cost of over \$9 billion. Thus, to ensure the integrity of these lines, imperative for economic and ecological reasons, stringent demands must be made on the materials of construction, fabrication techniques, and test procedures⁽⁸⁸⁾.

From a design standpoint, economics dictate larger diameter lines operating at higher pressures to maximize throughput and thereby lower the operating costs over the life of the line⁽⁸⁹⁾. These factors necessitate the employment of higher strength materials and/or greater wall thicknesses since the maximum hoop stresses, σ_H , in a pipeline can be determined from⁽⁹⁰⁾:

$$\sigma_H = Pd/2t \quad (\text{Eq. 3.1})$$

where, P = operating pressure

d = pipe diameter

t = pipe wall thickness

There are limits, however, to the pipe wall thickness due to:

1) restrictions imposed by mill facilities, 2) the toughness requirement of a pipeline (which is also a function of thickness), 3) difficulties in retaining high strength and toughness in very thick plate, and 4) additional difficulties in welding and field inspection.

The new generation of Arctic pipelines have been or are proposed to be constructed using HSLA acicular ferrite steels. Their higher strengths per unit of cost and weight allow reduction in pipe wall thickness and total pipeline weight and consequent savings in initial cost, transportation, and field handling, while permitting the use of higher operating pressures. Important, too, is the fact that these steels have very high toughness thereby significantly reducing the potential for failures in the pipelines.

Additional advantages of the AF steel to the pipeline industry is the fact that they do not exhibit discontinuous yielding and they have higher work hardening rates than conventional ferrite-pearlite pipeline steels. Thus, they offset the yield strength losses, observed when testing flattened tensile specimens or when forming pipe,

known to result from the Bauschinger effect^(80,84,86,91). This is particularly important for spiral welded pipe which is not cold expanded after forming. (N.B. A Canadian producer plans to cold expand its spiral welded pipe in the near future - a unique innovation - to take advantage of this feature of AF steels. They shall realize a net increase in the strength of the pipe, relative to that of the controlled rolled plate)⁽⁹²⁾.

The Canadian metallurgical community has pioneered and continues to be a leader in the production and use of AF steels for pipeline applications. The first commercial application of such steel was a 130 km section of 107 cm (42 in) diameter, 9.4 mm (0.370 in) wall thickness spiral welded gas pipeline produced by The Inter-provincial Steel and Pipe Corporation, Ltd., Regina, Saskatchewan (IPSCO) in the late 1960's. The Steel Company of Canada (Stelco) has recently begun to market HSLA acicular ferrite steels suitable for Arctic pipeline applications. Pipeline manufactured by both companies will likely be used in the Alcan/Foothills gas pipeline project.

3.3 Fracture Control in Pipelines

Gas pipeline failures pose a particularly serious problem because the velocity of a propagating crack may be greater than the decompression rate of the gas. Thus, the crack front would remain in

a high pressure region, a condition which could lead to long catastrophic failures: one of up to 12 km has been documented⁽⁸⁸⁾. The crack initiation and propagation resistance of the pipeline steel is therefore of importance in designing gas lines.

In oil pipelines, decompression is rapid, and cracks do not propagate great distances. However, the environmental damage resulting from a cracked oil line and the high costs involved in repairing such a leak in remote locations requires that great importance be placed on preventing crack initiation.

Studies by the Battelle Memorial Institute, sponsored by the American Gas Association, have been ongoing for the past twenty years to delineate the causes and criteria for the prevention and arrest of brittle and ductile pipeline failures. Conclusions from this program have been incorporated into most pipeline strength and toughness specifications throughout the world, including those of the Canadian National Energy Board, the Canadian Standards Association (Z 245.1), the American Petroleum Institute specifications (API 5LX and 5LS), and virtually every pipeline company.⁽⁹²⁻⁹³⁾

The basic fracture control philosophy inherent to all of these standards is: 1) to prevent brittle failures by assuring that the pipeline operates above the material's ductile-to-brittle transition temperature; 2) to prevent ductile crack initiation by specifying

a minimum toughness for a pipe operating at a specific stress level; and 3) to control ductile crack propagation by specifying some average toughness that will assure self-arrest^(88,93-95). These criteria must be met at some specified minimum design temperature. For the Alcan/Foothills gas line the most severe design temperature is - 18°C⁽⁹²⁾.

That the full scale pipe fracture behaviour shall be ductile and, therefore, that brittle fracture shall be prevented is ensured, according to the Battelle studies⁽⁹⁶⁾, if the fracture appearance of a Battelle-Drop Weight Tear Test specimen⁽³⁹⁾ exhibits 85% or more shear when tested at the minimum operating temperature. Typical pipeline specifications therefore require that of all the material tested (i.e., 50% of the heats per every 10 miles of pipe shipped), the average percent shear exhibited by the DWTT specimens be greater than 85%. However, any given heat can be accepted if 60% shear is obtained in the DWTT⁽⁹²⁾.

The Battelle studies also generated an empirical formula which relates Charpy upper shelf energies to the critical defect size necessary for ductile crack initiation under static loading conditions. This equation is geometry dependent⁽⁹⁵⁻⁹⁷⁾.

$$\frac{K^2 \pi}{8c \sigma_F} 2 = \ln[\sec (\pi M \sigma_p / 2 \sigma_F)] \quad (\text{Eq. 3.2})$$

where, $K^2 = 12C_v E/A$

C_v = Charpy upper shelf energy (ft-lb) = ET

A = Area of Charpy specimen ligament ($\approx 0.124 \text{ in}^2$)

$2c$ = Length of sharp through-wall flaw (in)

σ_F = Flow stress (\approx yield stress + 10 ksi) (psi)

M = "Folias correction" ($= f(\text{pipe radius and wall thickness})$)

E = Elastic Modulus (psi)

σ_p = Failure stress (psi)

This equation is widely used in the pipeline industry to predict allowable defect sizes for the prevention of ductile crack initiation (94-95). However, it should be noted that this equation is applicable only for the range of temperatures over which the Charpy upper shelf energy exists. Furthermore, it does not account for initiation resulting from dynamic loading or as a result of unusual stress states and/or geometries. These latter conditions could be created by impacts from machinery or seismic action, or from bending stresses and buckling due to frost heave and differential settlement which could cause plastic instability (92).

At very high levels of toughness a material becomes essentially "flow stress dependent", that is the failure stress predicted from Equation 3.2 becomes dependent only upon crack length, yield strength, and pipe geometry (96).

For design purposes, pipeline companies typically calculate the size of the toughness independent critical crack and then determine, from Equation 3.2, the minimum Charpy upper shelf energy necessary to prevent the initiation of a crack 95% the size of that flow stress dependent defect⁽⁹²⁾.

This critical defect size must be large enough to be observed as a leak during hydraulic proof testing, or to be detectable by nondestructive test techniques⁽⁹⁵⁾. Proof testing of the pipeline is generally conducted at 1.05 times the specified minimum yield stress (SMYS) to assure that no critical size defects exist⁽⁹²⁾.

Equation 3.2 predicts for a 42-in (107 cm) diameter, 0.540-in (13.7 mm) wall, X70 pipeline, operating at a design factor of 0.8, that a minimum Charpy energy of 51 ft-lb (69 J) is needed to prevent the initiation of the 95% flow stress dependent critical size defect of 5.8-in (15 cm). This toughness level is being specified as the all heat minimum value for the Alcan/Foothills pipeline⁽⁹²⁾. However, current proposals for that project call for X70 pipe of either 48-in (122 cm) or 54-in (137 cm) outside diameter, 0.540-in wall thickness. Such pipe would require 55 ft-lb (75 J) and 60 ft-lb (81 J) minimum Charpy toughness to assure initiation prevention of the 95% flow stress dependent defect. Current pipeline specifications remain at 50 ft-lb minimum, however.

Another empirical relationship generated by Battelle from full scale burst tests simulating actual pipeline operating conditions has established the toughness required of a steel to arrest a fast-running ductile crack. For certain grades of steel, pipe geometries yield strengths, and stress levels, an empirical formula has been derived which predicts the minimum Charpy energy, C_v , required for ductile fracture arrest⁽⁹⁶⁾:

$$C_v = 0.0873 \sigma_H^2 (Rt)^{1/3} A \text{ (ft-lb)} \quad (\text{Eq. 3.3})$$

where, σ_H = operating stress (ksi)
 R = pipe radius (in)
 t = pipe wall thickness (in)
 A = area of Charpy specimen ligament
($\approx 0.124 \text{ in}^2$)

The operating stress level, σ_H , is typically 0.8 SMYS.

Although the final dimensions of the Alcan/Foothills pipeline has not been set, a current proposal is for a 48-in (122 cm) diameter, 0.540-in (13.7 mm) wall thickness pipe operated at a design factor of 0.8 of the SMYS of 70 ksi (483 MPa). For this material and the operating conditions chosen, Equation 3.3 requires that the pipeline steel have 79 ft-lb (107 J) Charpy upper shelf energy at the minimum operating temperature. An energy level of 80 ft-lb (108 J) is, in fact, often used in pipeline steel specifications as

an all heat average toughness value. This "average" toughness philosophy is based upon the hypothesis that although all sections of the pipeline may not have sufficient toughness to arrest a propagating crack, the crack would eventually run into a section with high toughness and would thereby be arrested.

Unfortunately, the empirical relationship has not always correlated well with results from larger diameter (over 42-in), higher strength (over X65 grade), and heavier wall pipe^(94-96,98). In fact, for the newer, controlled-rolled AF steels "it is impossible [from this relationship] to accurately specify the toughness requirements" for ductile fracture arrest⁽⁹⁶⁾. Until relationships similar to that given in Equation 3.3 are established for the AF steels and/or the larger pipelines (through full-scale burst testing), employment of empirical correlations should be used with caution. Nevertheless, pipeline companies continue to apply such correlations to establish minimum toughness levels for crack arrest in line pipe materials^(92, 94-95).

Pipeline manufacturers when testing pipeline material to determine if it meets the toughness specifications, test specimens in which the fracture path is representative of the longitudinal axis of the pipe; the maximum operating stresses in a pipeline are the

hoop stresses, σ_H , which tend to open cracks along the pipe axis.*

The Battelle-Drop Weight Tear Test and the standard Charpy impact test are specified for specimens oriented for fracture along the pipe axis direction.

Pipeline steels, particularly if not treated with rare earths and/or desulfurized, are known to exhibit anisotropy in mechanical properties, especially toughness. Thus, although a steel may be spiral welded and thereby exhibit a maximum toughness along the pipe axis, the properties of the pipe at small angles to the pipe axis may be significantly below the specified minimums; yet the pipe stresses would still be a significant fraction of the maximum hoop stress. However, as yet no specifications require tests or minimum toughnesses for directions other than the pipe axis.

The fracture control philosophy used in the pipeline industry is one which strives for prevention of both fracture initiation and propagation. Table 3.1 summarizes the current fracture control proposals for Arctic pipelines.

* Weld zones are also tested, but this area of investigation is not a topic of discussion in this work.

Table 3.1

PROPOSED FRACTURE CONTROL REQUIREMENTS
FOR ARCTIC PIPELINES

PIPE DIAMETER	WALL THICKNESS	MINIMUM YIELD STRENGTH	OPERATING PRESSURE	CURRENT REQUIREMENTS		BASIS FOR REQUIREMENTS		
				Pipe Toughness (ft-lb)	DWT % Shear	95% Flow Stress Dependent*		C _v for Crack Arrest** (ft-lb)
						Critical Flaw Size (in)	C _v for Initiation Prevention (ft-lb)	
42	0.540	70	1440	50 ft-lb	60%	5.8	51	76
48	0.540	70	1260	<u>minimum</u>	<u>minimum</u>	6.2	55	79
54	0.540	70	1120	any heat	85%	6.6	60	82
48	0.720	70	1680	80 ft-lb				
				<u>average</u>	<u>average</u>	7.2	65	88
				all heats				

Tests done only in pipe axis orientation

Minimum design temperature, -18°C

Maximum operating stress, 56 ksi

* From Equation 3.2

** From Equation 3.3

To prevent brittle fracture, an average of 85% shear is required on the DWTT conducted at the minimum design temperature. However, this test is primarily a measure of the propagation mode as revealed by the associated percent shear on the fracture surfaces. Ductile failures are controlled only through empirical equations which are based upon the Charpy upper shelf energy. The standard Charpy test, in itself, reveals nothing of the crack initiation process. Both it and the B-DWTT employ blunt notches and are not, therefore, representative of the most severe defect, for example, a weld or fatigue crack.

3.4 Test Program

In this series of tests the response of two acicular ferrite HSLA pipeline steels to dynamic loading by IIT was determined. The comparison study is important for the following reasons:

1. Both steels are to be employed in the proposed Alcan/Foothills gas pipeline and, therefore, the dynamic response of the steels must be characterized to assess the effect of in service loading.

2. For pipelines, fracture control is a high priority concern. At present only two tests are routinely conducted on pipeline materials to assess their fracture resistance - the Drop Weight Tear Test and the standard Charpy impact test. Neither test

provides a measure of crack initiation nor distinguishes between crack initiation and crack propagation. To ensure adequate fracture resistance, pipeline companies employ empirical correlations established for lower strength, nonacicular pipeline steels, the relationships being valid only at temperatures corresponding to the Charpy upper shelf energy.

3) An IIT study will provide initiation and propagation energy data which can then be used to establish more fundamental fracture toughness correlations. The IIT lacks general acceptance because it is a relatively new test and correlations are still required for full scale behaviour. Analysis of the IIT data may contribute to a more meaningful and sophisticated basis for fracture control and/or point out the applicability of IIT as a rapid, inexpensive test for quality assurance purposes.

3.4.1 Steels/Pipelines

Sections of pipe from production heats were supplied by two Canadian producers for the test program. Both pipe products were 42-in (107 cm) outside diameter, with a 0.540-in (13.7 mm) wall thickness, and were rated as X70 grade steel (minimum yield strength of 70 ksi). These HSLA steels had been controlled rolled to achieve a fine grained acicular ferrite microstructure. Both pipe sections had been spiral welded.

The chemical compositions of these steels are given in Table 3.2.

Table 3.2
STEEL COMPOSITIONS

	C	Mn	Mo	Nb	Si	Al	S	P	Cu	Ni	Cr	Sn	Ti	Ce
AF-1	.05	1.93	.26	.063	.03	-	.023	.012	.24	.10	.04	.02	-	-
AF-2	.06	1.82	.45	.05	.26	.045	.006	.006	.037	.027	.068	.005	.002	.034

All values in weight percent

From Table 3.2 it can be seen that the steel designated AF-2 was fully killed and rare earth treated. This was not the case for the steel AF-1. The sulfur content of the AF-1 steel was also comparatively high.

3.4.2 Metallography

The structure of both steels was examined to determine the sulphide inclusion shape and the grain size.

Both steels had a very fine non-equiaxed ferritic grain structure, their low carbon contents precluding the possibility of

visible carbide formation. This microstructure is typical of that of acicular ferrite. The grain sizes, determined using the Heyn-Intercept method⁽⁹⁹⁾, were ASTM 13.25 for steel AF-2, and ASTM 12.7 for the AF-1 material.

The high sulfur AF-1 steel had not been rare earth treated for inclusion shape control and therefore exhibited numerous long sulfide "stringers". Figure 3.1 shows the directional inclusions and very fine grained AF microstructure of this steel.

The structure of the AF-2 steel is shown in Figure 3.2, only globular nondirectional inclusions being visible.

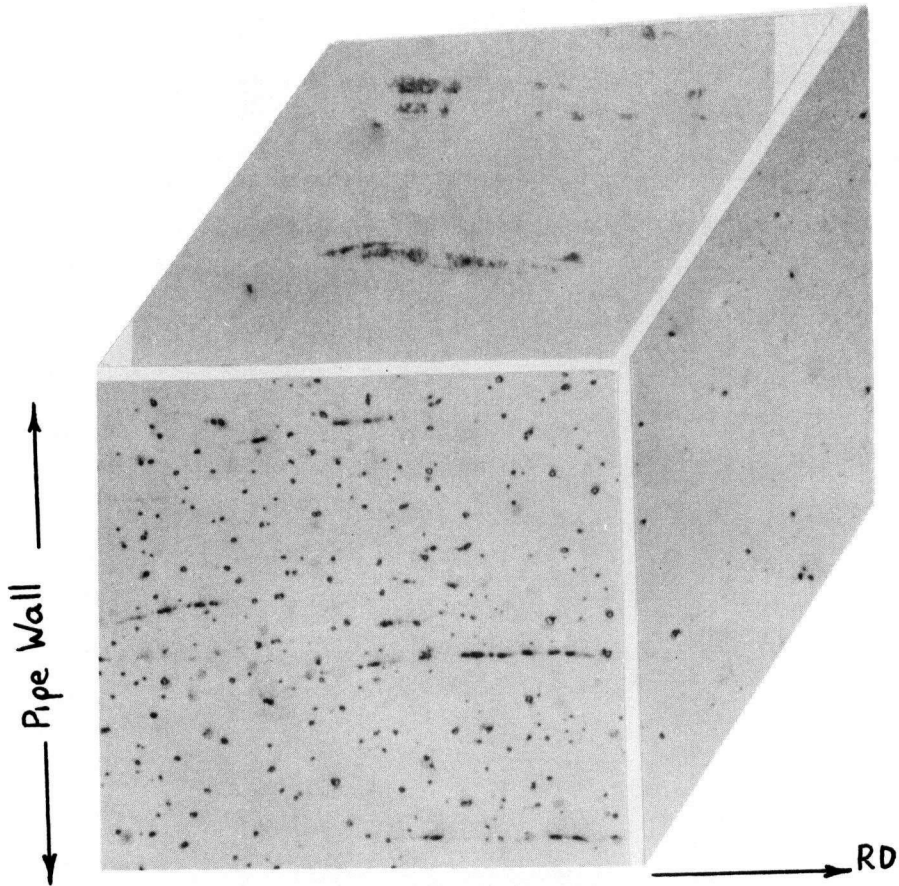
The inclusions in both AF steels were examined using the analytical capability of the scanning electron microscope. The results showed that the AF-1 steel contained only MnS inclusions, as shown in Figure 3.3, whereas the AF-2 steel contained inclusions of several different compositions, not all of which were sulfides (Figures 3.4a - c).

3.4.3 Instrumented Impact Test Specimens

3.4.3.1 Specimen Preparation and Configuration

Large sections were initially flame cut from the pipe. Test specimens were then saw cut such that the notch in each test

(a)



(b)

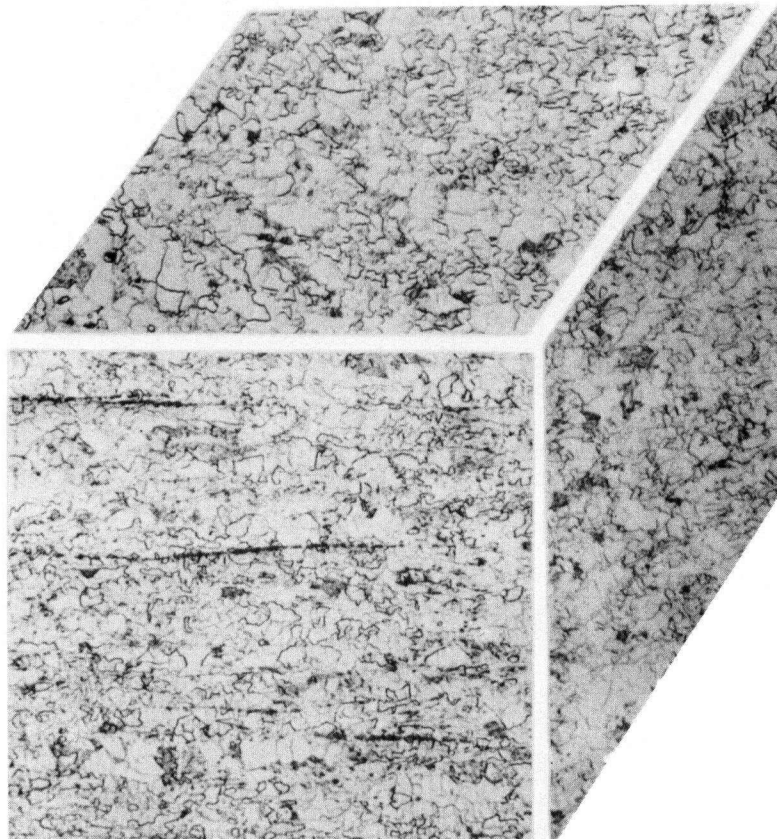


Figure 3.1 AF-1 photomicrographs, 225X
(a) unetched
(b) etched, 2% nital

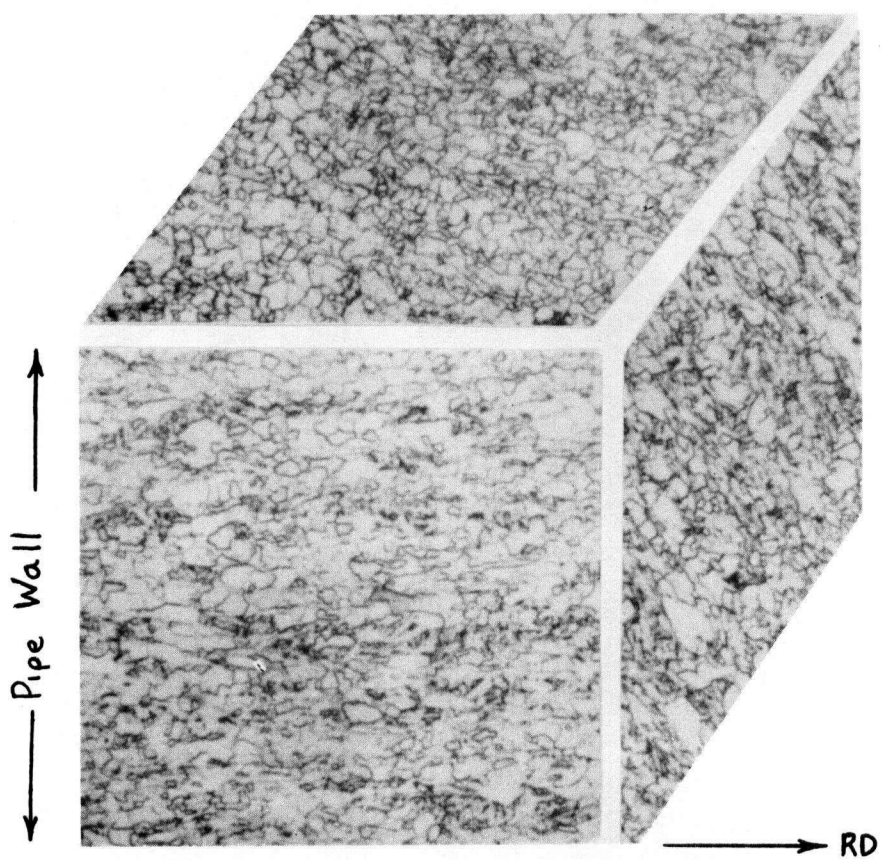


Figure 3.2 AF-2 photomicrographs, etched 2% nital, 363X.

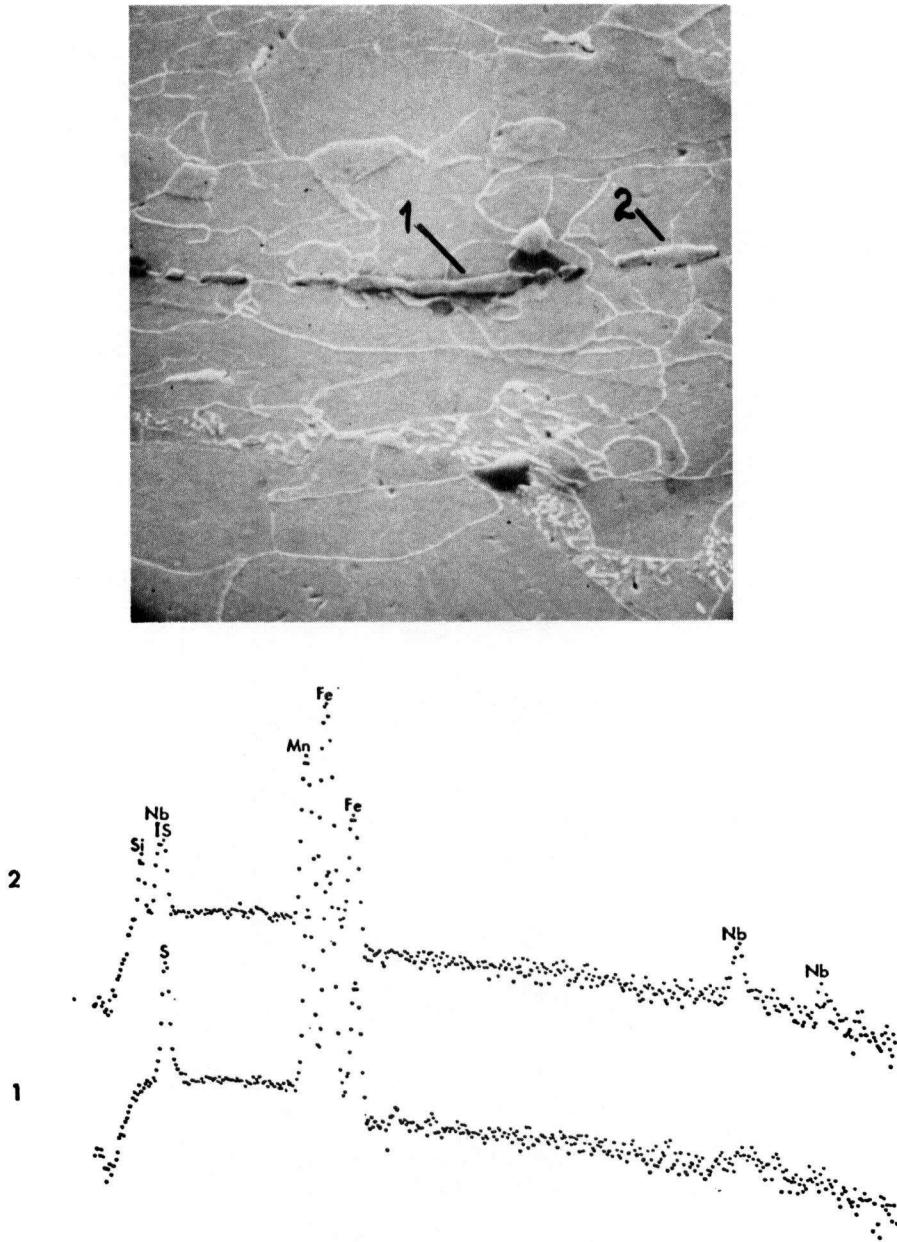


Figure 3.3 AF-1 SEM photomicrograph (3000X) and X-ray energy analysis of inclusions.

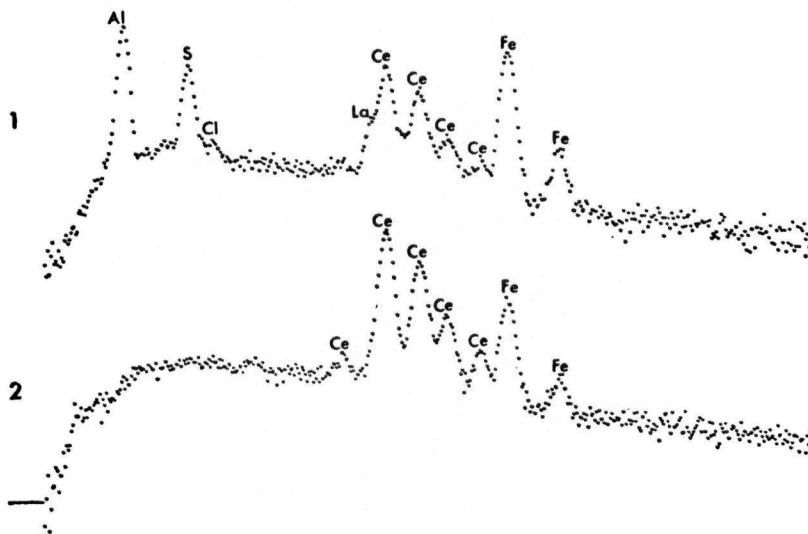
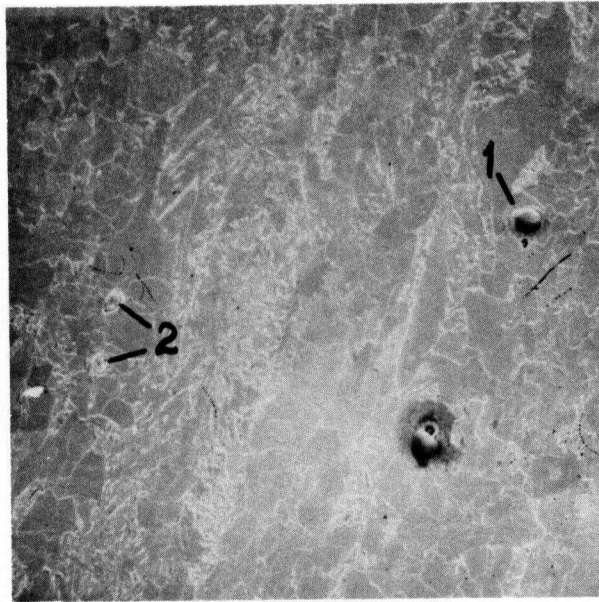


Figure 3.4a AF-2 SEM photomicrograph (480X) and X-ray energy analysis of inclusions.

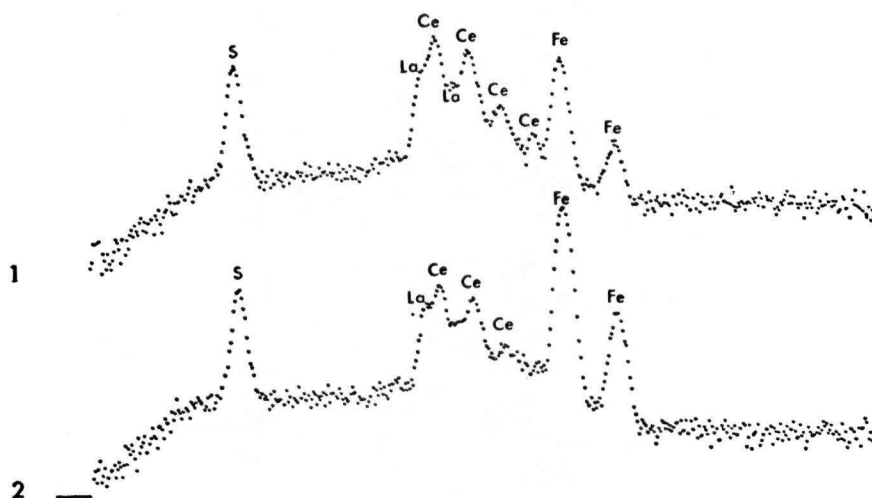
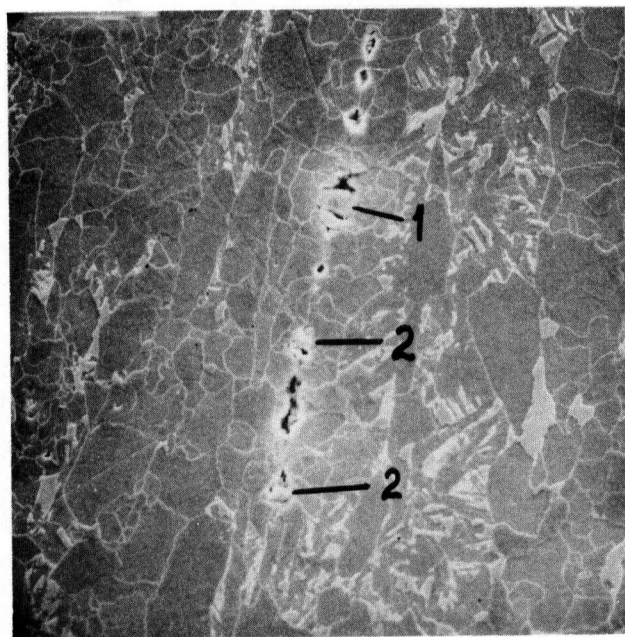


Figure 3.4b AF-2 SEM photomicrograph (1000X) and X-ray energy analysis of inclusions.

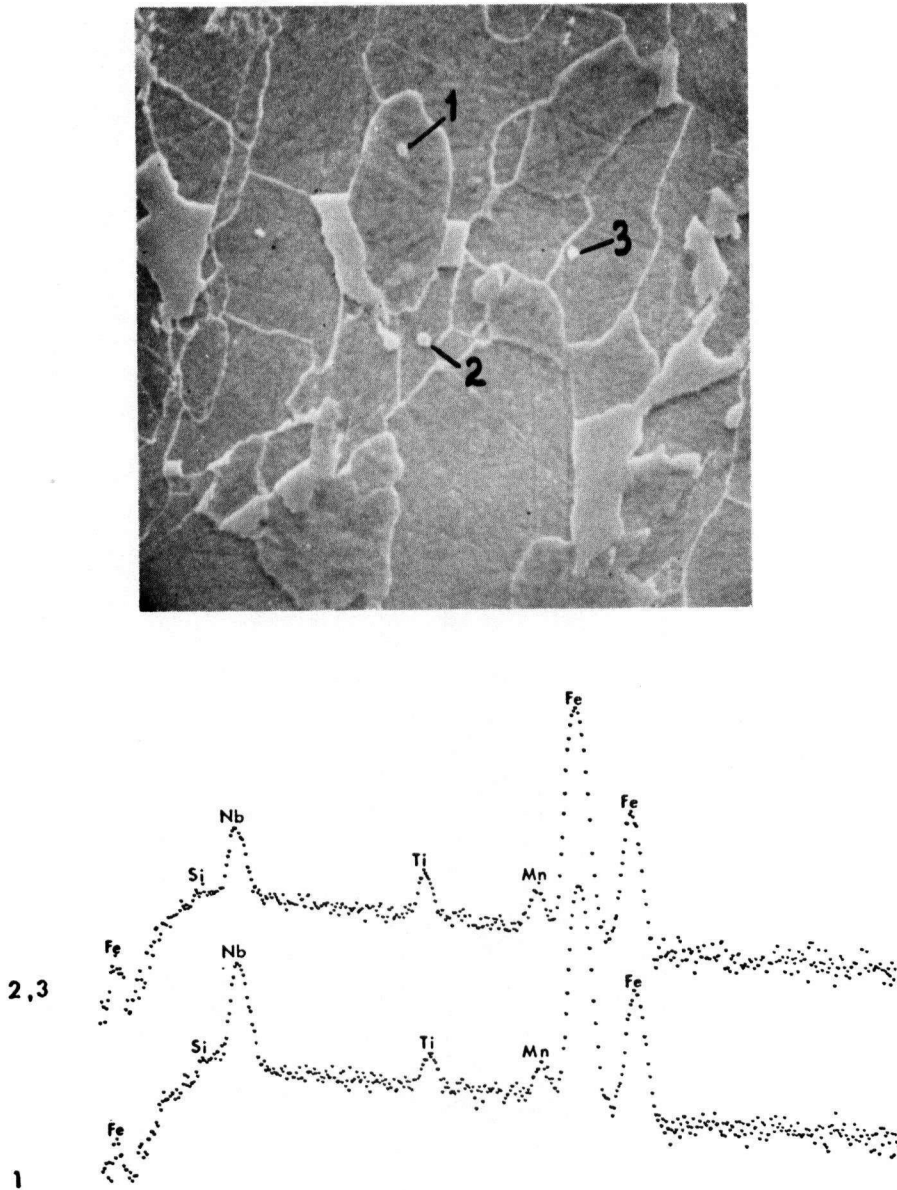


Figure 3.4c AF-2 SEM photomicrograph (4000X) and X-ray energy analysis of inclusions.

specimen was a minimum of 15 cm from any weld or flame cut edge.

The specimens were notched through the pipe wall thickness and cut so that the cracks would follow a path: 1) parallel to the pipe axis; 2) parallel to the rolling direction; and, 3) transverse to the rolling direction. The rolling direction was at an angle of 63° to the pipe axis for the AF-1 pipe and 45° to the pipe axis for the AF-2 pipe.

3.4.3.2 Specimen Dimensions

Three types of specimens were tested in order to assess the behaviour of different defects and thicknesses. This broader range of test conditions allowed better characterization of the dynamic properties of the steels. For each of the orientations discussed in the previous Section, standard Charpy V-notch specimens, precracked Charpy specimens, and "full wall" Charpys were prepared. Thus, for each steel, a minimum of nine series of ductile-to-brittle transition curves were established using the instrumented impact test equipment. A minimum of three tests were performed at each temperature. In addition, for the AF-1 steel only, standard Charpy specimens with notches cut transverse to the pipe axis were also tested.

3.4.3.2.1 Standard Charpy V-Notch Specimens

Standard Charpy V-notch specimens were considered the reference samples. The Charpy test is widely used in the pipeline industry, fracture control being based upon correlations and relationships which employ Charpy test data. The standard Charpy specimen is 10 mm x 10 mm x 55 mm, with a 2 mm deep 45° V-notch with a root radius of 0.25 mm⁽⁴⁴⁾.

3.4.3.2.2 Precracked Charpy Specimens

Standard Charpy V-notch specimens were fatigue precracked prior to testing. The sharp fatigue crack provides the most severe notch acuity and is better adapted for fracture toughness measurements.

Samples were precracked using a Dynatup Precracker following tentative ASTM specifications for precracking small specimens⁽¹⁵⁾. Both surfaces perpendicular to the V-notch were polished prior to fatigue precracking so that crack growth could be observed. The ASTM requirements are that the crack front be relatively straight (i.e., not a "thumbnail"); that the plane of symmetry between the notch and the precrack be less than 10°; that the cracks have a minimum length (1.3 mm) to avoid the plastic

region ahead of the machined notch; that the total crack length (notch plus precrack) to sample width ratio (a/w) lie between 0.35 and 0.55; and, that the stress intensity factor associated with the fatigue precracking, K_f , be strictly controlled and sufficiently small to avoid plastic deformation at the crack tip (in general, K_f must not exceed 60 percent of the stress-intensity value determined in subsequent testing). For the AF steels, K_f was necessarily kept below $25 \text{ ksi-in}^{\frac{1}{2}}$ ($27.5 \text{ MPa-m}^{\frac{1}{2}}$) and the specimens were precracked in approximately 15-20,000 cycles. All these precracking criteria are essentially the same as those required for large fracture toughness specimens⁽¹⁰⁰⁾.

After each instrumented impact test the fracture surface was examined with a travelling microscope to determine the precrack length and to assure that the fatigue crack characteristics met the ASTM requirements.

3.4.3.2.3 Full Wall Charpy Specimens

It is well established that sub-size specimens can have transition temperatures, toughness, and fracture modes which differ from those of a full size component⁽¹⁰¹⁻¹⁰²⁾. As the thickness of a specimen increases, the degree of constraint also increases until plane-strain conditions exist⁽⁵⁾. This increasing constraint results

in a decrease in both the fracture stress and toughness, to a limiting plane-strain value. The extent to which variations in thickness affect crack initiation energy or fracture toughness is, of course, of great interest. To ensure that toughness and fracture data is conservative for design applications, it is necessary that the test specimens duplicate the thicknesses of the actual service components to maximize constraint and thereby minimize the toughness behaviour.

To test full pipe wall thickness specimens, Charpy-style samples were prepared in which the thickness (dimension across the notch) was that of the pipe wall (nominally 13.7 mm). The other dimensions, including the notch size and acuity, were identical to the standard Charpy specimen.

3.5 Instrumented Impact Test Results

Figures 3.5 - 3.10 show representative load-time traces, over a range of temperatures, for the AF-1 and AF-2 steels, and for each specimen type and sample orientation. Corresponding fracture surfaces of the test specimens are shown in Figures 3.11 - 3.16.

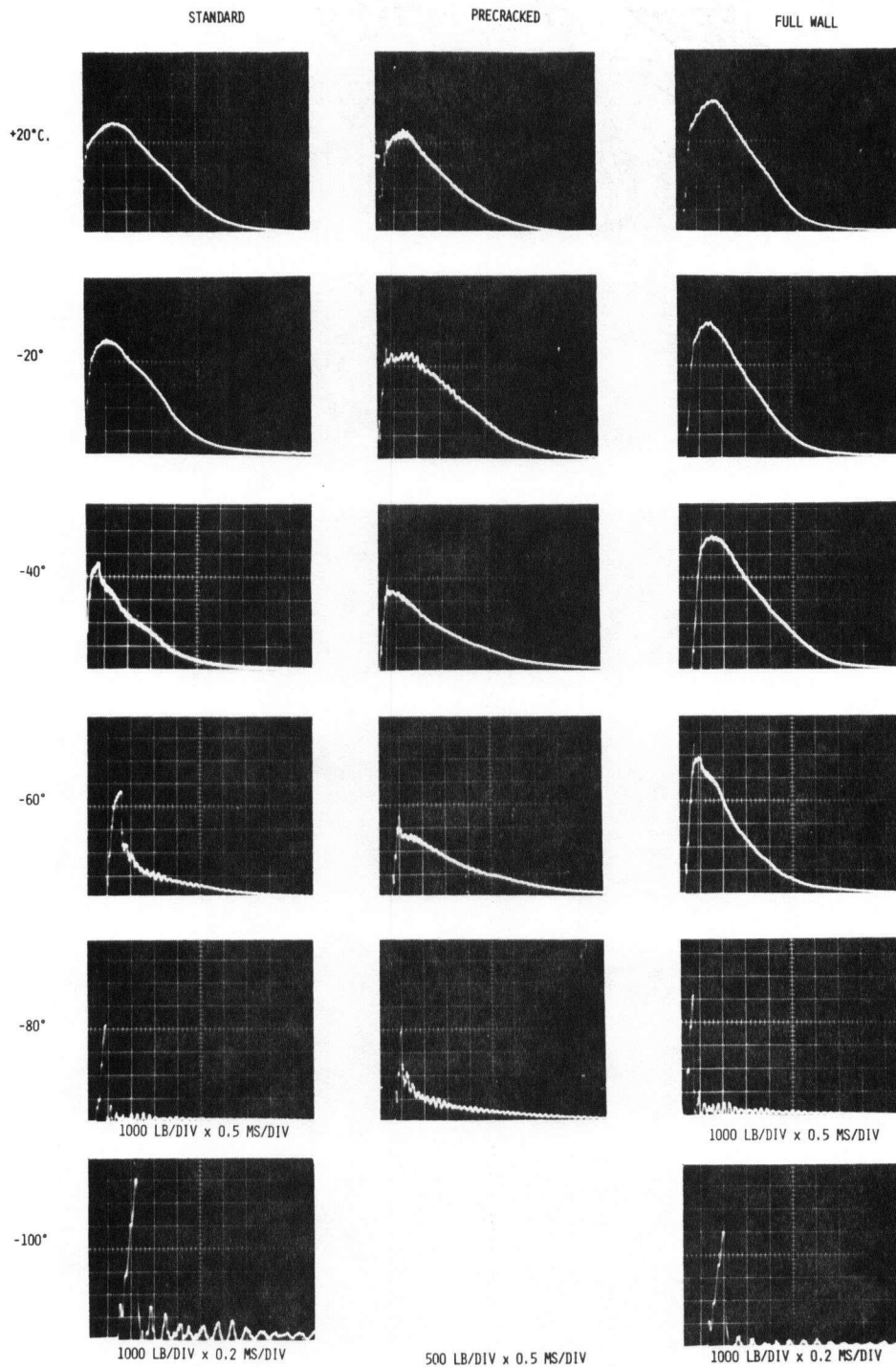


Figure 3.5 AF-1 steel load-time curves, crack parallel to pipe axis.

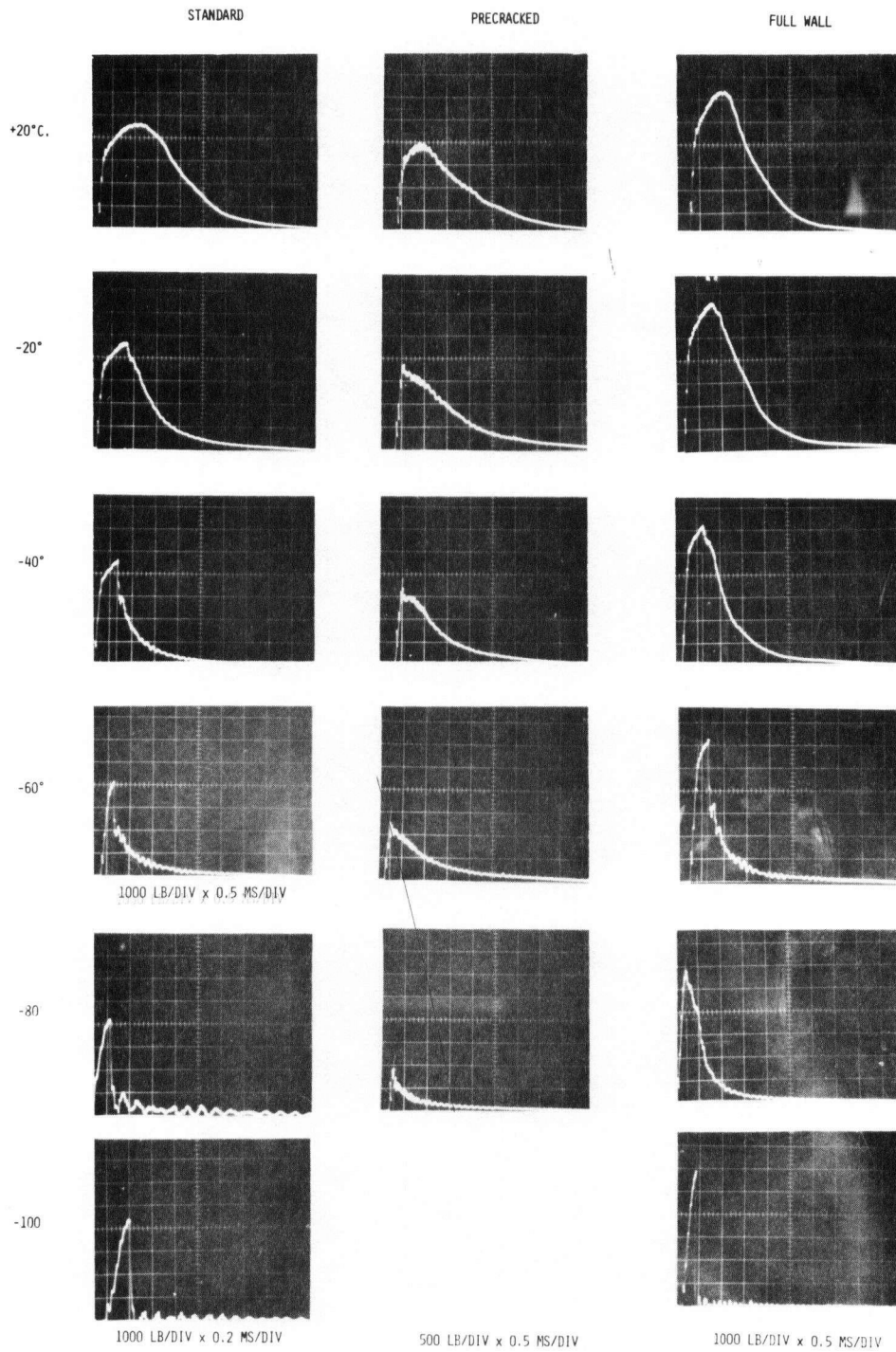


Figure 3.6 AF-2 steel load-time curves, crack parallel to pipe axis.

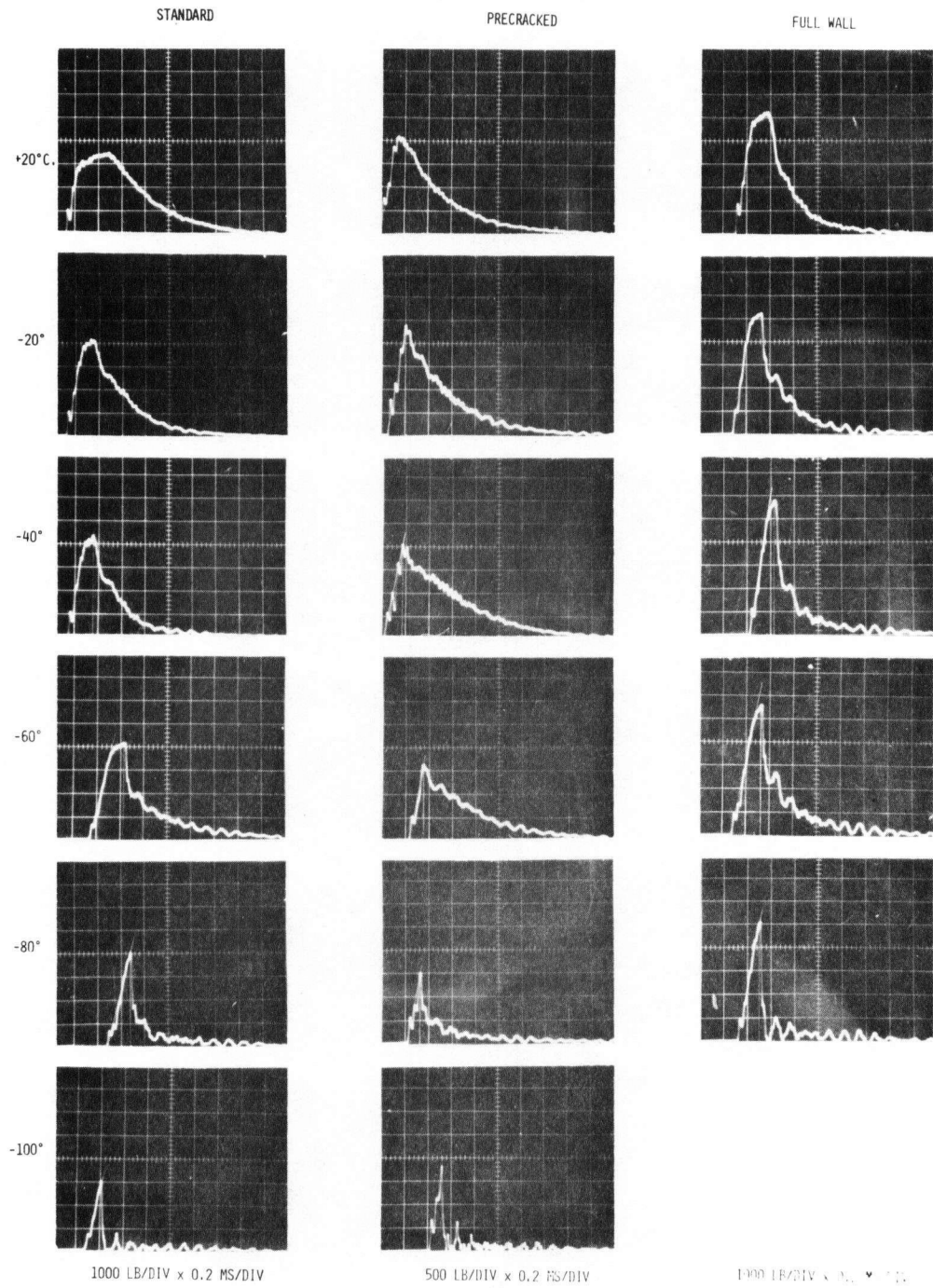


Figure 3.7 AF-1 steel load-time curves, crack parallel to rolling direction.

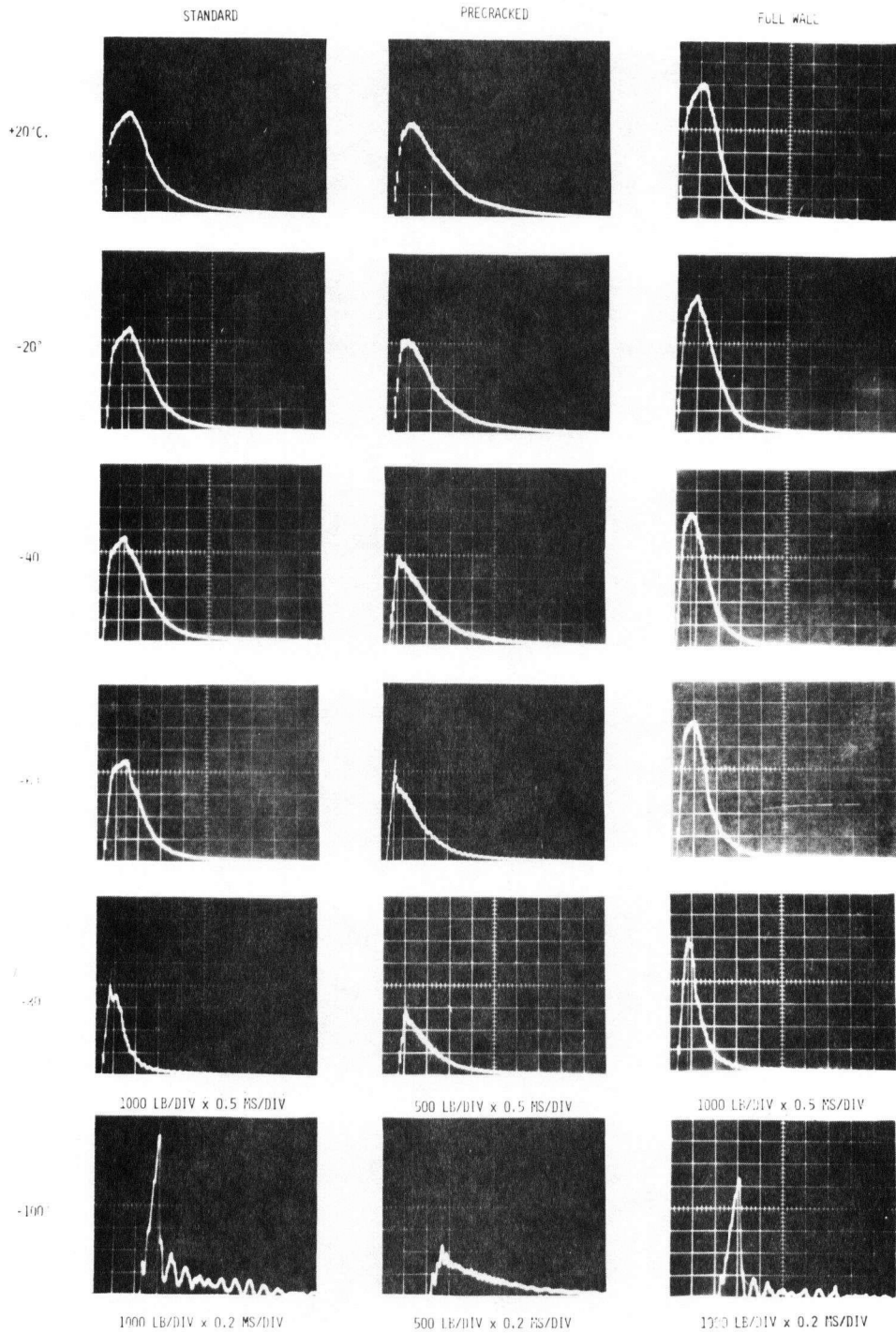


Figure 3.8 AF-2 steel load-time curves, crack parallel to rolling direction.

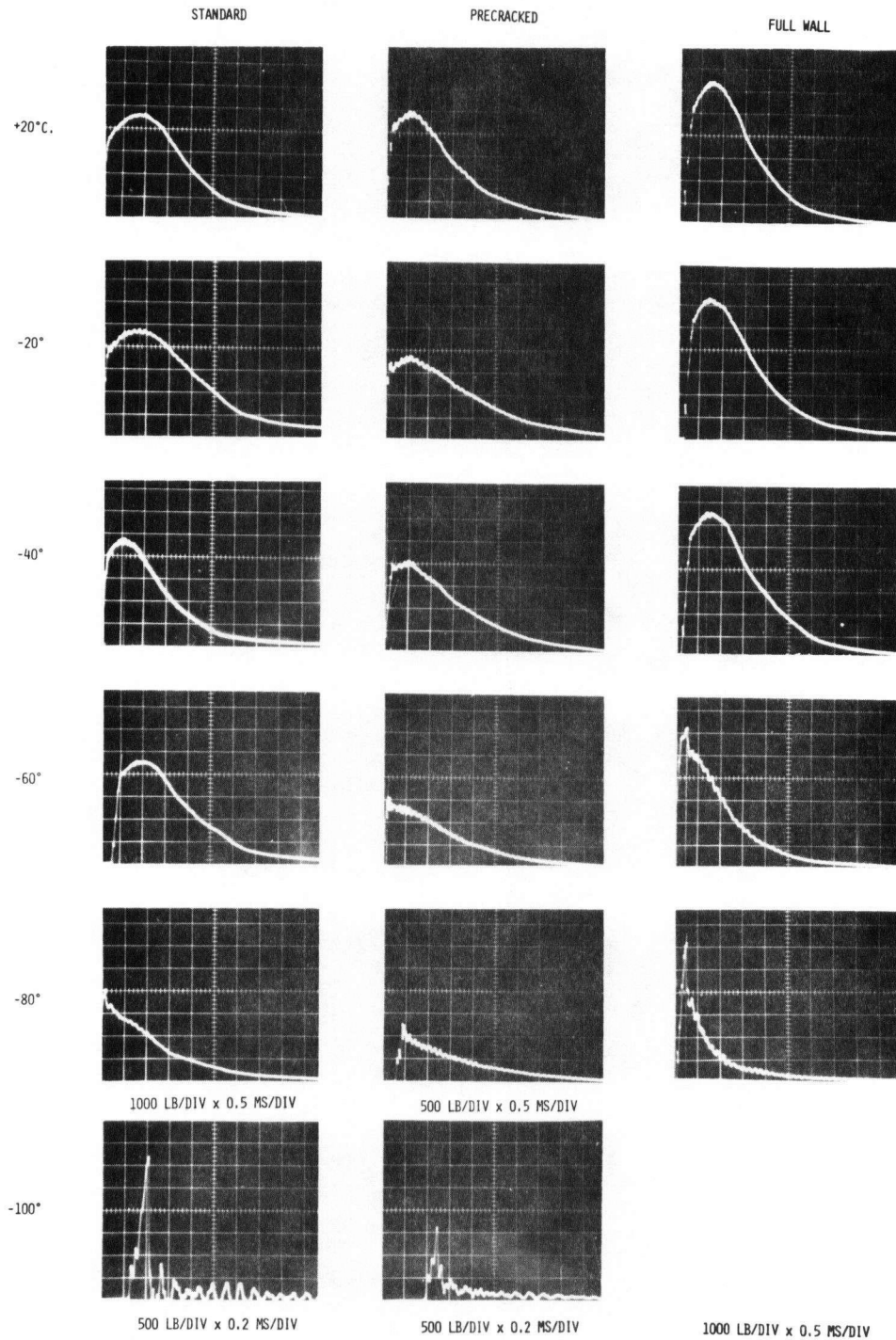


Figure 3.9 AF-1 steel load-time curves, crack transverse to rolling direction.

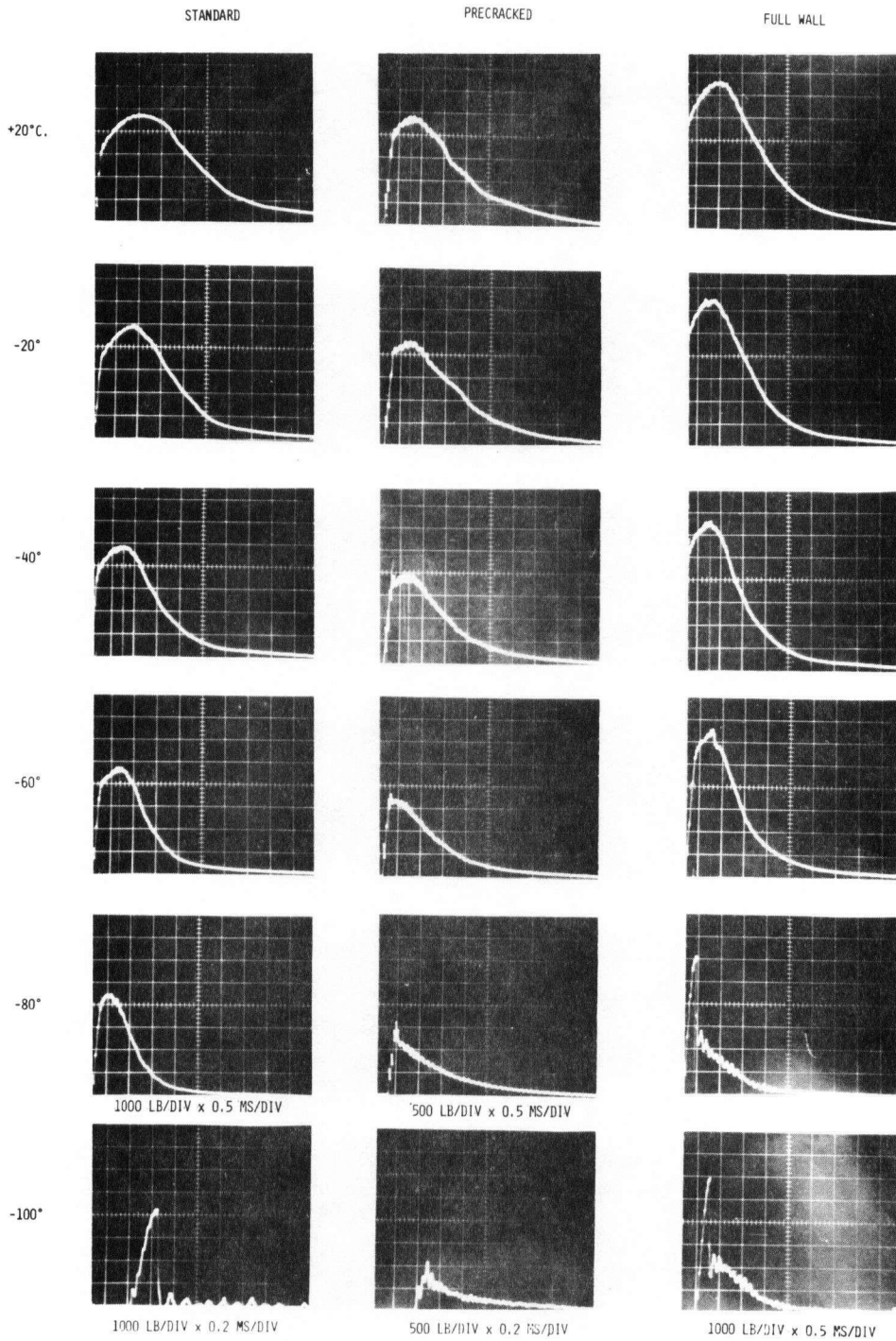


Figure 3.10 AF-2 steel load-time curves, crack transverse to rolling direction.

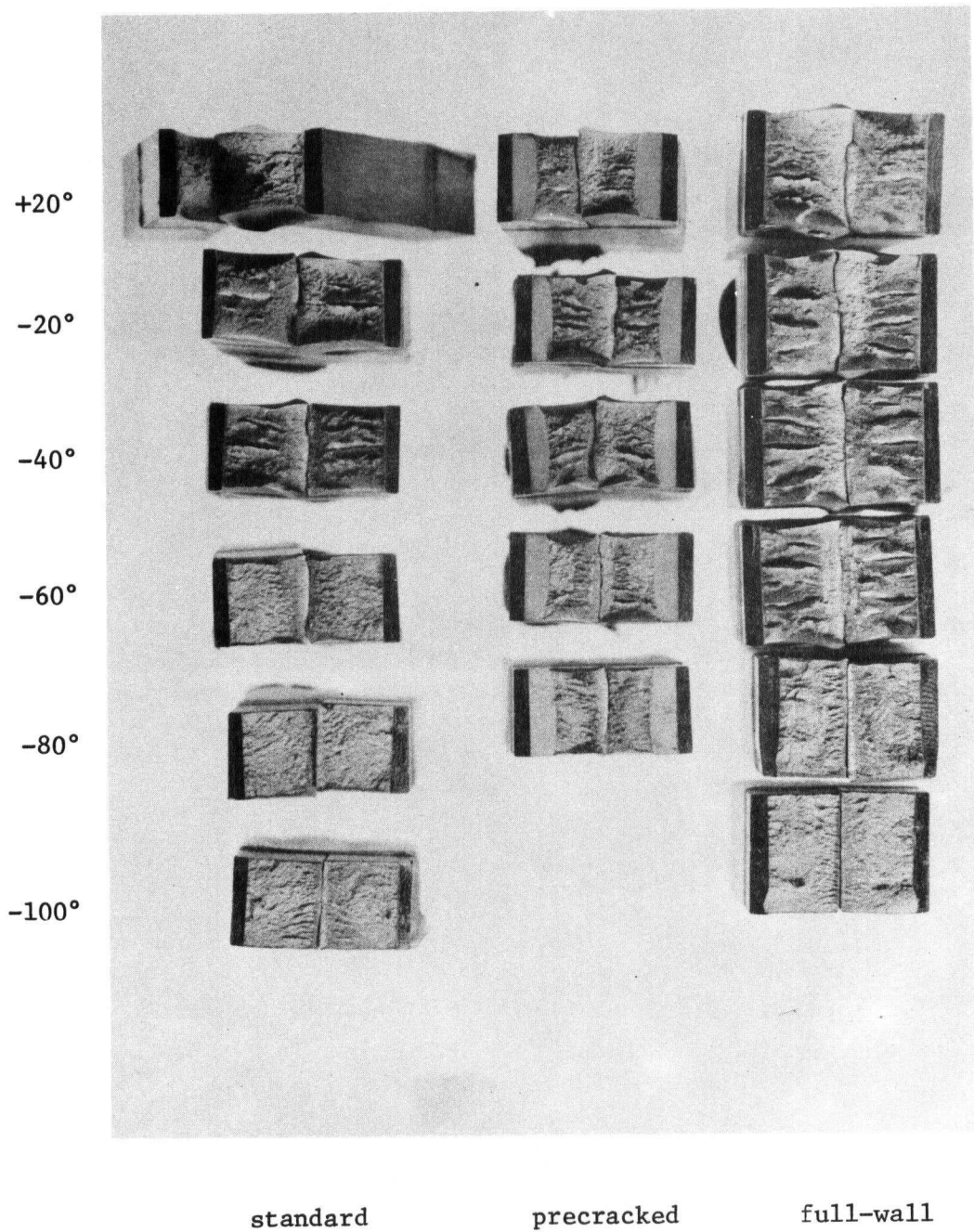


Figure 3.11 AF-1 steel fracture surfaces, crack parallel to pipe axis.

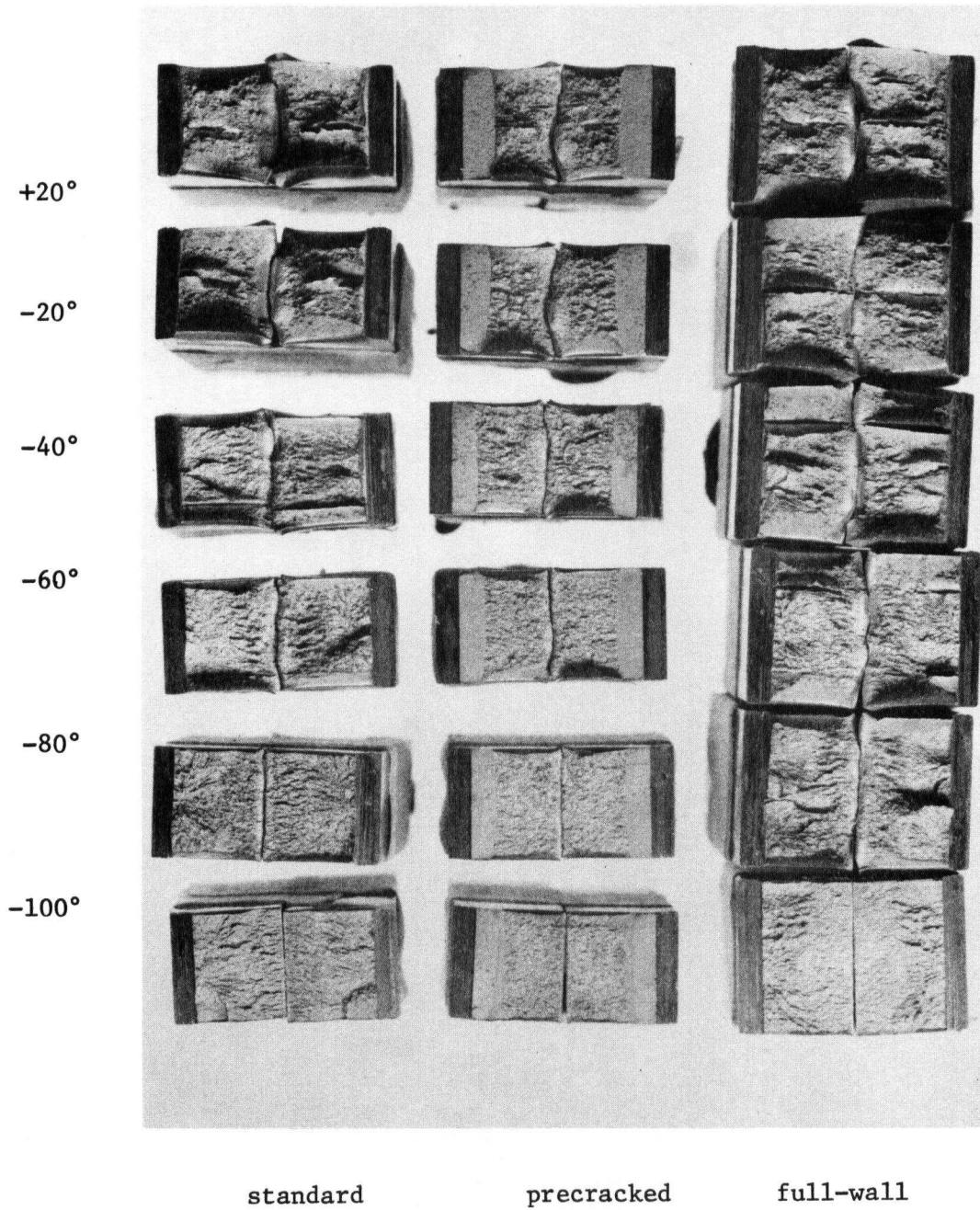


Figure 3.12 AF-2 steel fracture surfaces, crack parallel to pipe axis.

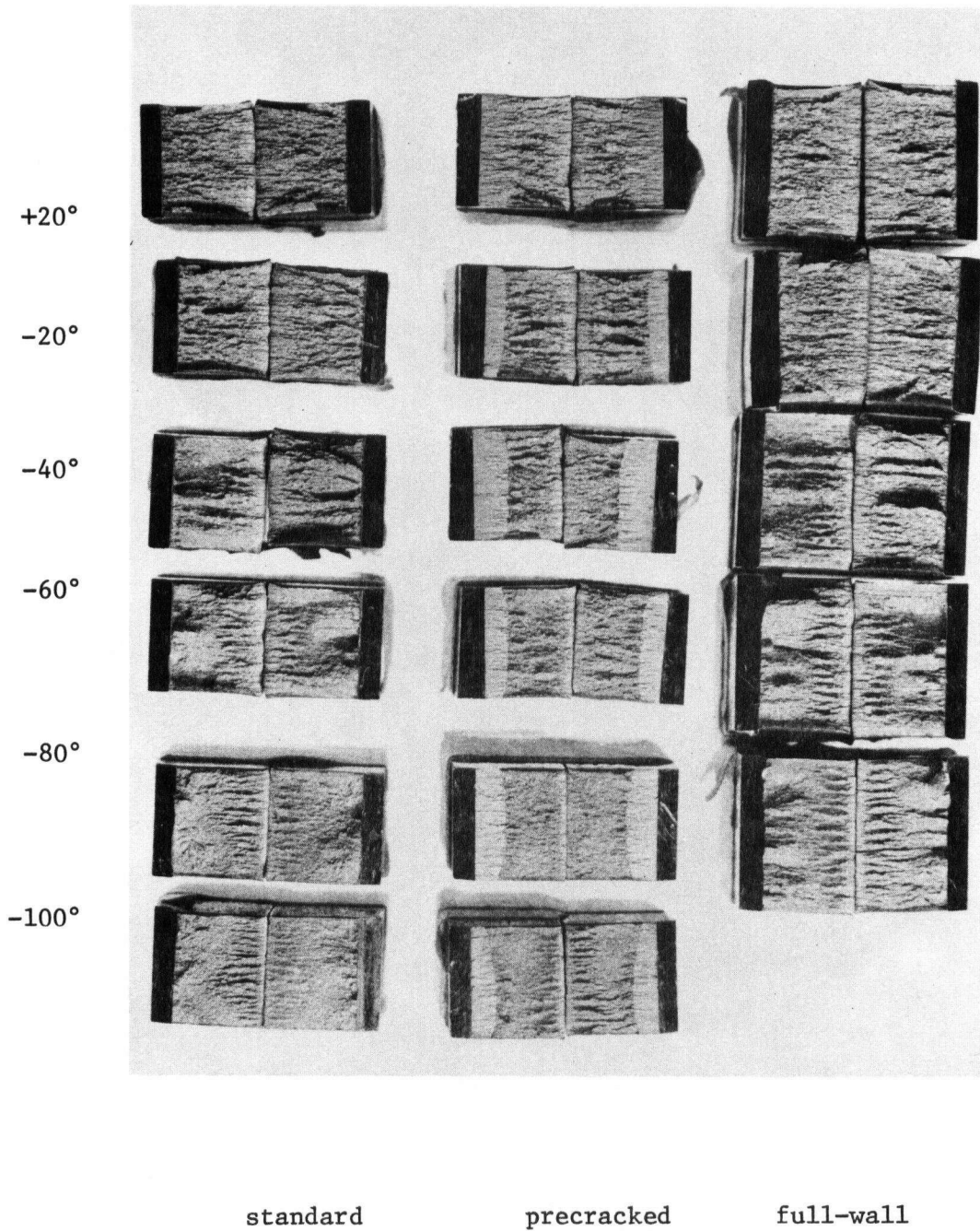


Figure 3.13 AF-1 steel fracture surfaces, crack parallel to rolling direction.

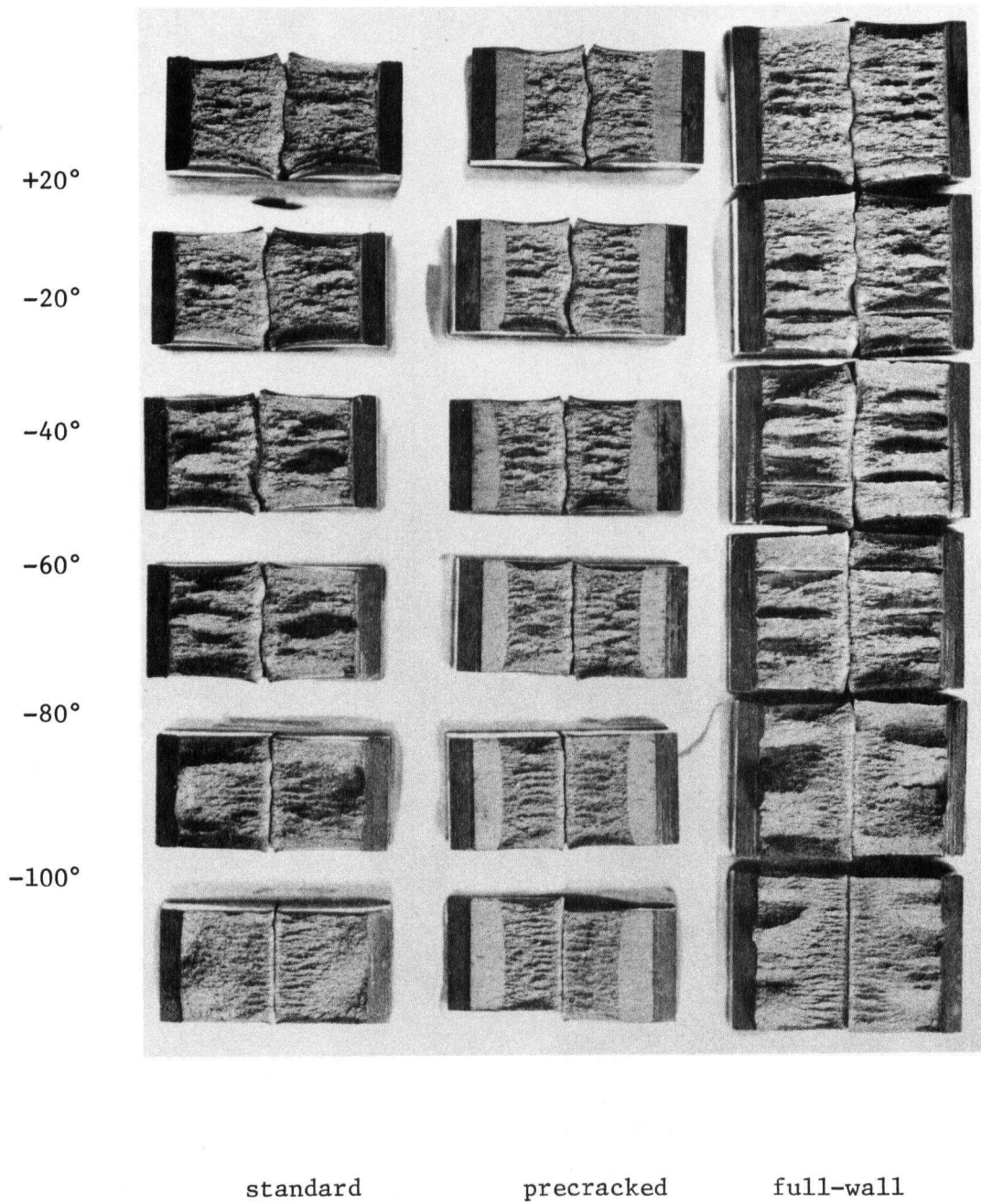


Figure 3.14 AF-2 steel fracture surfaces, crack parallel to rolling direction.

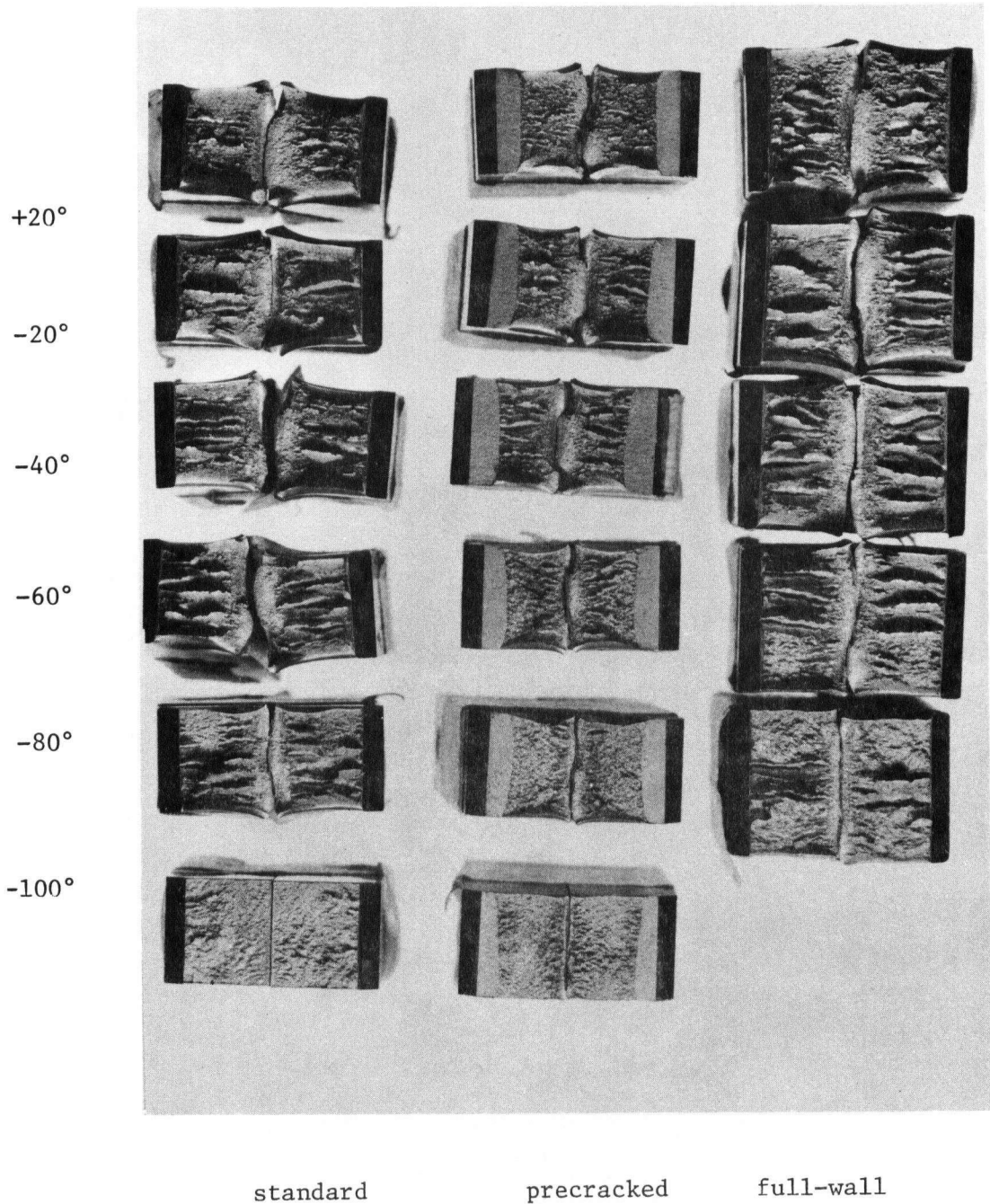
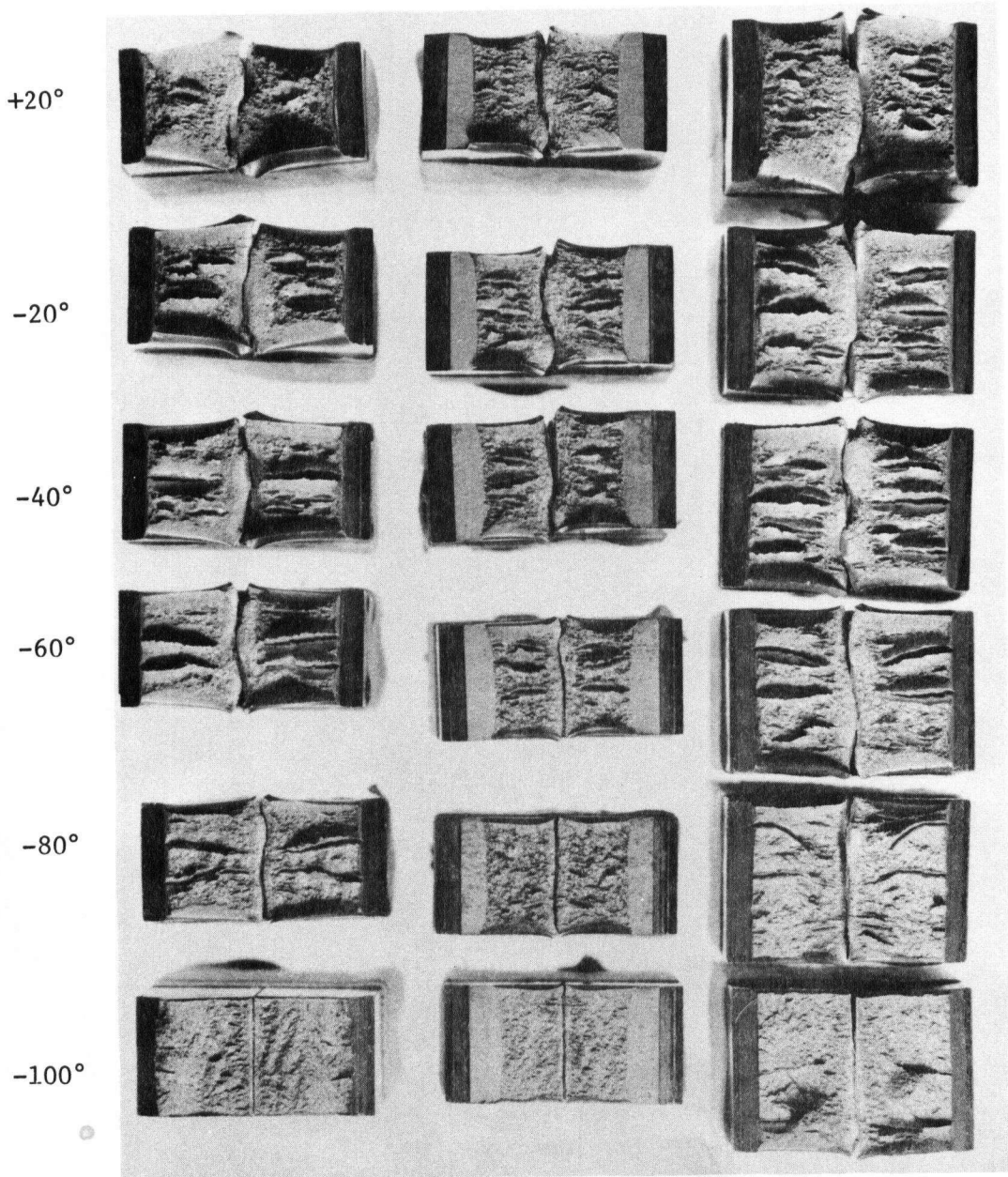


Figure 3.15 AF-1 steel fracture surfaces, crack transverse to rolling direction.



standard precracked full wall

Figure 3.16 AF-2 steel fracture surfaces, crack transverse to rolling direction.

3.5.1 Absorbed Energy

The total energy absorbed by each specimen has been differentiated into two components, the crack initiation energy (energy to maximum load) and the crack propagation energy (post-maximum load energy). Energy values are listed in Tables 3.3 - 3.5 for each specimen type; these values represent the averages of many tests. The absorbed energy data are presented graphically in Figures 3.17 - 3.44. For the full wall and precracked Charpy data, the energy values have been normalized by dividing the measured absorbed energy values by the ligament area of the specimen prior to impact. The average absorbed energy values of the corresponding standard Charpys have been included to facilitate comparisons.

3.5.1.1 Comparison of the Two AF Steels

3.5.1.1.1 Standard Charpy Data

3.5.1.1.1.1 Crack Parallel to Pipe Axis

The standard Charpy tests with the fracture path parallel to the pipe axis is identical to that required by the pipeline specifications. This is considered the most important orientation

Table 3.3

STANDARD CHARPYS - AVERAGE

ABSORBED ENERGIES (EI + EP = ET)

T(°C)	Parallel to Pipe Axis		Parallel to Rolling Direction		Transverse to Rolling Direction		Transverse to Pipe Axis
	AF-1	AF-2	AF-1	AF-2	AF-1	AF-2	AF-1
+100	-	-	7+20=27	-	31+65=95	-	6+17=23
+ 20	33+89=121	32+56=88	5+15=20	24+37=61	30+72=102	36+83=119	5+20=25
0	30+98=128	34+50=84	6+19=24	22+36=58	22+83=105	-	6+25=30
- 10	25+78=102	-	-	-	-	-	-
-20	19+77=96	21+41=62	4+16=20	17+34=50	28+84=112	39+63=102	6+19=25
-30	20+75=95	20+37=58	4+11=17	-	20+73=93	33+61=94	-
-40	13+64=76	15+26=42	4+13=17	14+32=45	19+69=88	30+55=85	3+13=16
-50	19+56=75	10+21=31	2+12=14	13+26=39	-	22+53=75	-
-60	10+38=48	5+13=18	3+11=14	9+24=34	13+53=66	23+44=67	3+8=11
-70	2+7=9	2+8=10	2+5=7	7+21=27	9+46=55	19+44=63	-
-80	2+5=7	2+5=7	1+5=6	1+15=16	1+12=13	12+29=41	1+6=7
-100	1+3=4	2+3=5	1+3=4	1+5=6	1+4=5	5+3=8	1+3=4
-196	0+1=1	-	0+1=1	-	0+1=1	-	0+1=1

All values given in ft-lb

1 ft-lb = 1.4 J

Table 3.4

FULL WALL CHARPYS - AVERAGE

ABSORBED ENERGIES (EI + EP = ET)

T(°C)	Parallel to Pipe Axis		Parallel to Rolling Direction		Transverse to Rolling Direction	
	AF-1	AF-2	AF-1	AF-2	AF-1	AF-2
+ 20	26+85=111	39+75=114	8+16=24	21+42=63	36+91=127	46+86=132
0	-	30+71=102	-	22+43=65	-	36+81=117
- 20	24+87=111	29+69=98	6+15=21	16+44=60	24+97=121	30+79=109
- 30	-	28+50=78	-	-	-	-
- 40	20+91=110	23+47=70	6+13=19	18+38=56	23+102=125	32+73=105
- 50	20+79=99	10+28=39	-	15+35=50	19+81=93	26+69=95
- 60	13+68=81	8+35=43	3+11=14	10+33=43	12+81=93	25+61=86
- 70	7+53=60	5+25=30	2+10=12	3+23=26	15+68=83	19+58=77
- 80	2+9=12	3+26=28	2+6=8	4+23=27	5+29=34	12+42=54
-100	2+3=5	1+4=5	-	2+6=8	-	5+38=43

All values given in ft-lb

1 ft-lb = 1.4 J

Table 3.5

PRECRACKED CHARPYS - AVERAGE

NORMALIZED ENERGIES (EI - ET)

T(°C)	Parallel to Pipe Axis		Parallel to Rolling Direction		Transverse to Rolling Direction	
	AF-1	AF-2	AF-1	AF-2	AF-1	AF-2
+ 20	82 - 442	92 - 408	7 - 128	55 - 287	94 - 483	106 - 490
0	-	76 - 367	-	39 - 276	-	97 - 429
- 20	100 - 472	45 - 311	7 - 114	26 - 254	100 - 478	82 - 406
- 30	71 - 420	45 - 305	-	-	99 - 502	-
- 40	47 - 343	12 - 221	4 - 119	17 - 234	50 - 423	76 - 328
- 50	9 - 311	9 - 183	5 - 91	13 - 191	22 - 383	37 - 329
- 60	11 - 232	8 - 125	4 - 72	5 - 142	7 - 245	14 - 248
- 70	-	5 - 120	4 - 59	7 - 114	5 - 178	9 - 208
- 80	4 - 120	4 - 78	6 - 43	4 - 95	2 - 132	6 - 136
-100	-	5 - 22	4 - 22	4 - 49	3 - 24	3 - 46

All values given in ft-lb/in²

For a standard Charpy specimen

1 ft-lb represents \approx 8 ft-lb/in²

8 ft-lb/in² = 1.7 J/cm²

because full scale tests indicate that failures do propagate along the pipe axis. The maximum operating stress in pipelines is the hoop stress which tends to open such cracks.

The differences in the impact resistance of the two AF steels are striking, as shown in Figures 3.17-3.19. In terms of their meeting the suggested standards outlined in Table 3.1 at the -18°C specification temperature, the AF-2 steel does not meet the 80 ft-lb (108 J) average energy criterion, having only 62.3 ft-lb (84 J) at -20°C (Figure 3.18). Similar results from the pipe manufacturer confirm this lack of toughness for this heat. (N.B. This does not imply that all such pipe will not meet the 80 ft-lb specification. The proposed specification requires only that the average value for all heats be 80 ft-lb; on this basis the AF-2 steel has been shown to thus qualify as Arctic grade pipe)⁽⁹²⁾.

The AF-1 steel easily met the 80 ft-lb requirement, having an average toughness of 95.7 ft-lb (130 J) at -20°C (Figure 3.17). However, the data did exhibit considerable scatter. The standard deviations for the total absorbed energy ranged from a maximum of 39.4 ft-lb (53 J) in the transition region, to 22.7 ft-lb (31 J) at the upper shelf temperatures. Scatter in the transition region, however, is often observed in Charpy testing.

Figure 3.17

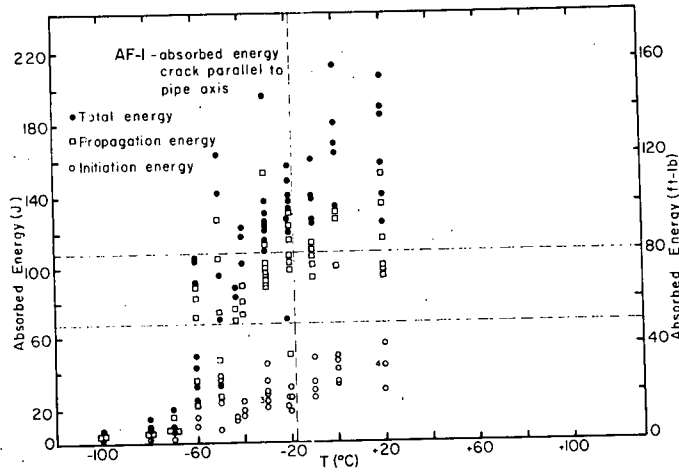


Figure 3.18

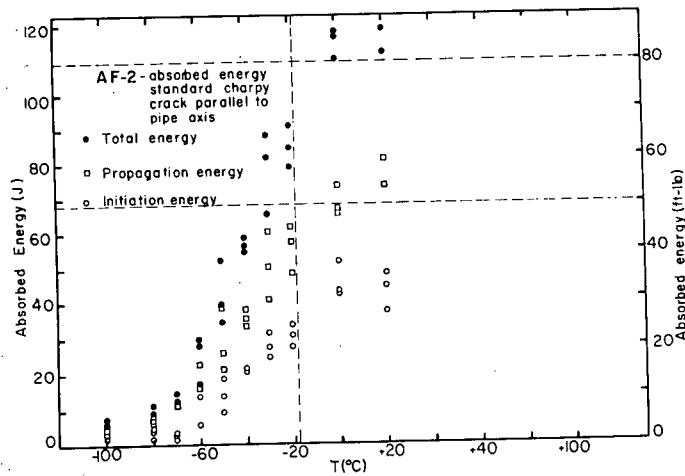
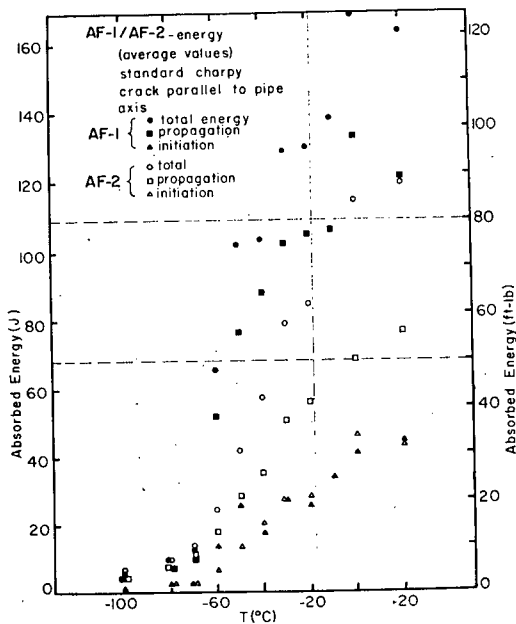


Figure 3.19



In a classic paper, Crussard and coworkers⁽⁷¹⁾ have shown that this is due to an effect termed "bimodal behaviour". In the transition region, two mechanisms of fracture (cleavage and fibrous) may be operative at the same temperature. The magnitude of the absorbed energies therefore fall into two distinct groups: one of high energy, void formation and coalescence being the dominant fracture mechanism; or a low energy group characteristic of cleavage dominating the fracture event. This bimodal behaviour in the transition region was often observed in the AF-1 steel, though not in the AF-2 material.

It should be emphasized that the AF-1 steel revealed a high degree of scatter at all temperatures, not just in the transition region. This may be due to the greater number of inclusions present (0.023 w/o S in AF-1; 0.006 w/o S in AF-2) which are well known to be deleterious to impact resistance.

Although the AF-1 steel exhibited higher total energies than did the AF-2 steel (to -70°C), the AF-2 steel had essentially equivalent initiation energies (refer to Table 3.3 and Figure 3.19). Thus, the AF-2 steel requires an equivalent energy to initiate a crack while crack propagation is much more difficult in the AF-1 steel. This implies that the matrix of AF-1 had a higher work hardening rate and hence void coalescence was more difficult^(5,103).

The higher work hardening rate must counteract the possibility of a lower energy due to fibrous fracture associated with the higher inclusion content of the AF-1. However, elongated inclusions aligned normal to the crack tip require a larger plastic zone size to "envelop" them before the fracture strain can be attained. Thus, the rate of void growth from such inclusions is lower than from inclusions aligned parallel to the crack tip⁽¹⁰³⁾. In addition, the advancing crack can propagate in the transverse direction in AF-1 upon reaching a band of inclusions, and thereby effectively blunt the crack tip^(5,9). The fracture surface of the AF-1 standard Charpy specimen at +20°C (Figure 3.11) is indicative of such behaviour.

The relative ductilities of the two steels can be compared by examining the "ductility index", DI. This is the ratio of propagation energy to initiation energy⁽¹⁰⁴⁾:

$$DI = EP/EI \quad (\text{Eq. 3.4})$$

Low indices imply a "brittle" material behaviour since most of the energy is absorbed elastically. Typical values range from 0.4 for E-glass to 61.5 for laminate composites, with steels having values generally between 2 to 20, depending on temperature, microstructure, etc.^(33,48,104).

Table 3.6 lists ductility indices for both steels for each specimen geometry tested, at selected temperatures. For the AF-1 steel, independent of crack orientation, the propagation energy is, in general, a significantly higher proportion of the total energy

Table 3.6

DUCTILITY INDEX - STEEL AF-1

T(°C)	Parallel to Pipe Axis			Parallel to Rolling Direction			Transverse to Rolling Direction		
	Standard	Full Wall	Precracked	Standard	Full Wall	Precracked	Standard	Full Wall	Precracked
+20	2.7	3.2	4.4	3.3	2.2	17.2	2.4	2.7	4.2
-20	4.0	3.7	3.7	3.5	2.3	14.9	3.1	4.0	3.8
-40	5.0	4.5	6.4	3.8	2.2	29.1	3.6	4.4	7.4
-60	3.8	5.4	20.9	3.3	3.2	16.5	3.9	6.6	33.5
-80	3.2	8.0	23.3	4.6	3.6	6.4	9.9	6.4	38.1
DUCTILITY INDEX - STEEL AF-2									
+20	1.8	1.9	3.4	1.6	2.0	4.3	2.3	1.9	3.6
-20	1.9	2.3	6.0	2.0	2.7	8.8	1.6	2.6	3.8
-40	1.7	2.0	17.2	2.3	2.1	12.5	1.8	2.2	3.3
-60	2.5	4.1	14.4	2.6	3.2	26.5	1.9	3.0	17.0
-80	2.2	9.4	19.4	2.2	6.2	26.1	1.6	3.6	19.8

to failure as compared to the AF-2 steel.

The 50 ft-lb (68 J) transition temperature for the AF-1 steel was -59°C versus -37°C for AF-2 (Figure 3.19). It should be noted that the AF-1 material retained a 50 ft-lb propagation energy down to -55°C .

Below -70°C the absorbed energy values of the two steels were essentially equivalent.

3.5.1.1.1.2 Crack Parallel To Rolling Direction

The absorbed energies of specimens of both steels oriented with the crack path in the rolling direction are shown in Figures 3.20 - 3.22.

In terms of the potential Arctic gas pipeline specifications outlined in Table 3.1 neither steel meets the 80 ft-lb (108 J) average total energy criterion at -18°C , nor does the AF-1 material meet the 50 ft-lb (68 J) minimum (at -20°C , the AF-2 steel had 50.4 ft-lb (68 J) average; AF-1 only 20.2 ft-lb (27 J)). However, at this time, toughness specifications require testing only in the pipe axis orientation.

This raises disturbing questions regarding pipeline toughness specifications and their usefulness in preventing failures. The specifications are written to ensure high toughness along the pipe

Figure 3.20

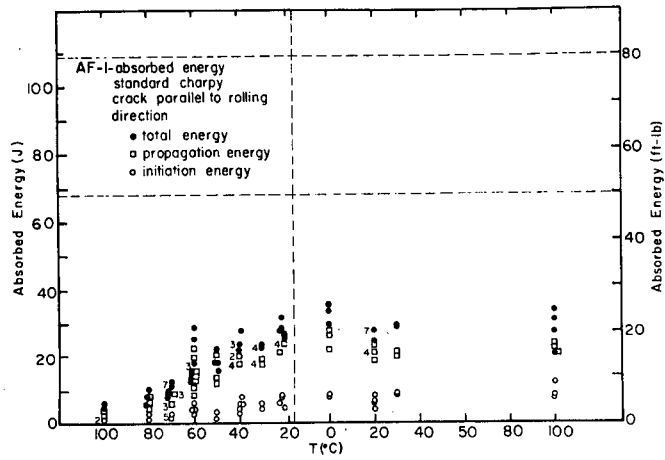


Figure 3.21

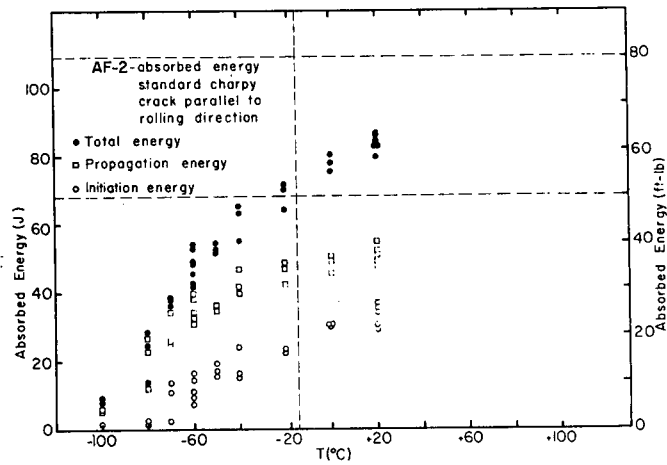
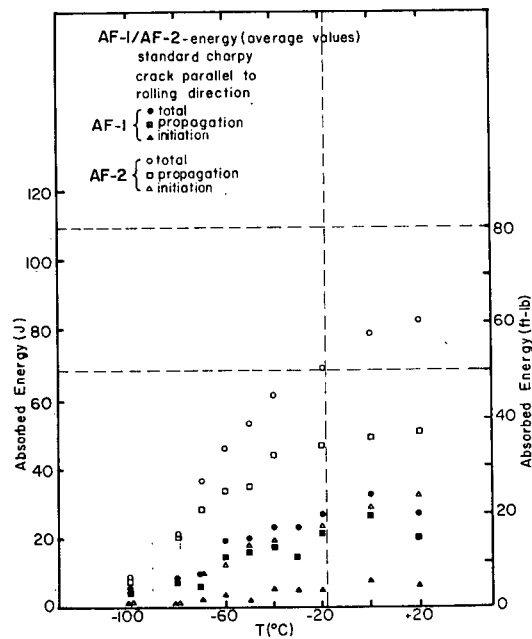


Figure 3.22



axis since the maximum crack opening hoop stress is operative in that direction. However, the magnitude of the minimum operating stresses in a pipeline are only 1/3 that maximum hoop stress. The AF-1 steel exhibits a fivefold decrease in toughness at -20°C on changing the test direction from the crack parallel to the pipe axis to the crack parallel to the rolling direction (i.e., 95.7 ft-lb (130 J) to 20.2 ft-lb (27 J)). The rolling direction in the AF-1 pipe is 63° from the pipe axis and hence the operating stresses are greater than the minimum. This casts serious doubt upon the effectiveness of preventing crack initiation when the weakest direction is not included in the toughness test specifications.

In addition, the AF-1, when tested with the crack parallel to the rolling direction, exhibits an extremely low crack initiation energy of approximately 5 ft-lb (7 J) for the entire test temperature range from $+100^{\circ}\text{C}$ to -60°C (refer to Table 3.3 and Figure 3.20). This suggests that a defect having even a relatively blunt notch radius may easily initiate in this lower toughness direction due to any sudden damage from pipe-laying equipment or buckling as a result of frost heave. High residual stresses could contribute to initiation, also. It seems quite possible that a critical size crack may then be created which could propagate in this low energy direction. Even if the crack was not sufficient to cause a long running failure, it still represents a localized crack requiring repair.

The pipeline industry should address itself to those possibilities by: 1) requiring minimum toughness values in all orientations; and, 2) establishing specifications based upon initiation energies for crack initiation prevention.

In the rolling direction, the AF-2 steel was significantly superior to the AF-1 material, both in initiation and propagation energy. No doubt the numerous elongated MnS "stringers" in the AF-1 steel provided low energy crack initiation and propagation paths in the rolling direction (Figures 3.1 and 3.3), which could explain the lack of scatter in the test data for the AF-1 material in this orientation.

However, the AF-2 steel also exhibited its lowest energies in this direction. Since this is a low sulfur rare earth treated steel, the reduced energy is probably due to the rolling texture and alignment of grain boundaries developed during controlled rolling (5). In addition, as Figure 3.4b indicates, the spherical inclusions present in AF-2 were aligned along the rolling direction. Crack propagation, through the mechanism of void coalescence, is therefore easier for the AF-2 steel in the rolling direction (compare +20°C data for AF-2 in Table 3.3).

In comparing the general shape of the transition curves

for both steels, the AF-2 steel, for all orientations, showed a continuous decrease in initiation and propagation energy with decreasing temperature. The AF-1 steel exhibited a more sudden change from a high energy upper shelf region to the low energy values.

3.5.1.1.1.3 Crack Transverse to Rolling Direction

The data obtained from testing both steels with the crack running transverse to the rolling direction are shown in Figures 3.23 - 3.25.

The two steels showed similar total energy values over the total range of test temperatures. The AF-2 initiation energy was considerably higher than the EI of the AF-1 material, whereas the propagation energy of AF-1 was higher than that of AF-2 (refer to Table 3.3).

As noted in the previously discussed data, the AF-1 steel displayed more scatter and showed a "classic" upper shelf and sharp energy transition temperature at -80°C (Figure 3.23). The AF-2 steel showed less scatter and a continuous decrease in energy with decreasing temperature (Figure 3.24).

Figure 3.23

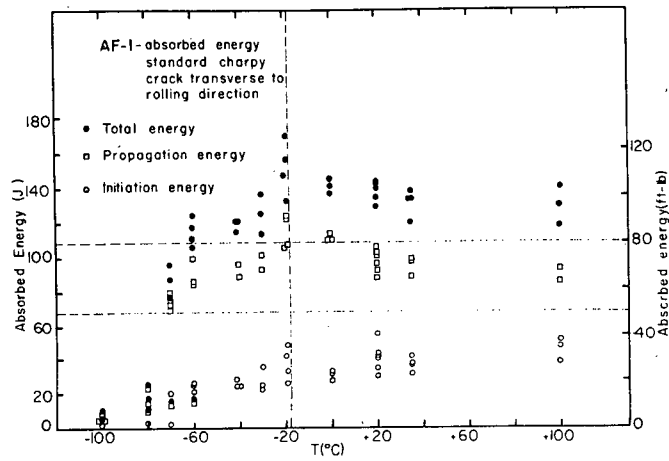


Figure 3.24

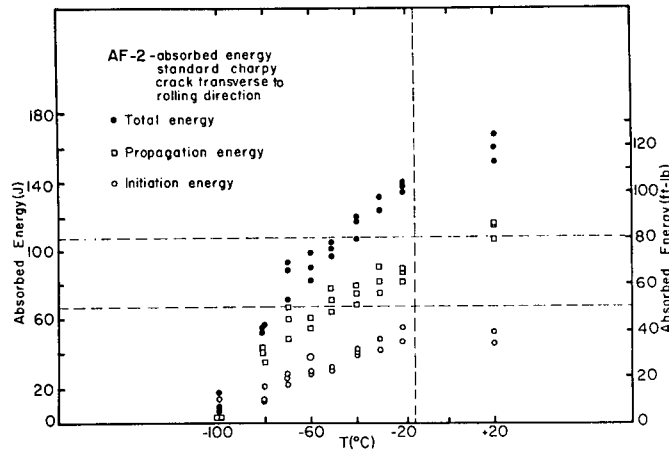
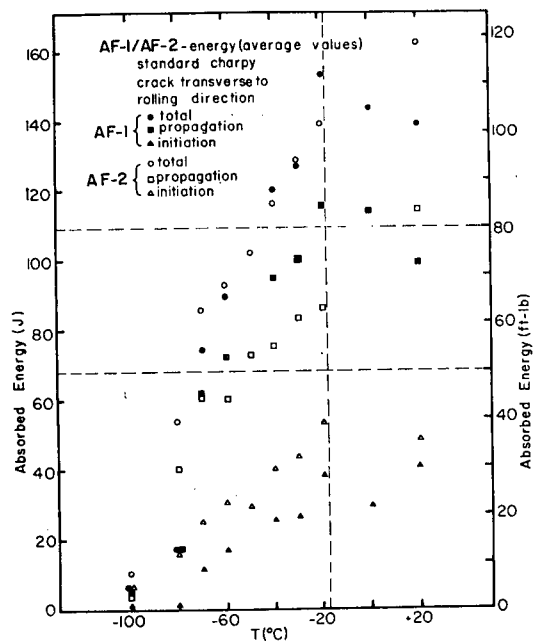


Figure 3.25



Both steels met the 80 ft-lb (108 J) average/50 ft-lb (68 J) minimum -18°C criteria; AF-2 had 102.0 ft-lb (138 J) and AF-1 112.1 ft-lb (152 J) average total energies at -20°C . The 50 ft-lb transition temperatures were similar for both steels: -73°C for AF-1; -77°C for AF-2.

3.5.1.1.1.4 Crack Transverse to Pipe Axis

Only the AF-1 steel was examined in this direction, the results being shown in Figure 3.26.

Very low energies, 25.3 ft-lb (34 J) at -20°C , were obtained. This orientation is only 27° from the rolling direction which is also the direction in which the sulfide inclusions lie. The observed low energies are thought to be due to cracks following the path of these "low energy stringers". The high energy orientations observed for the AF-1 steel were oriented at 63° (crack parallel to the pipe axis) and 90° (crack transverse to the rolling direction) to the rolling direction, both orientations lying at a high angle from the path of the sulfide stringers.

The toughness of the AF-1 steel in this direction and in the rolling direction was very poor, exhibiting low values of propagation energy and extremely low values of initiation energy. Since the pipe

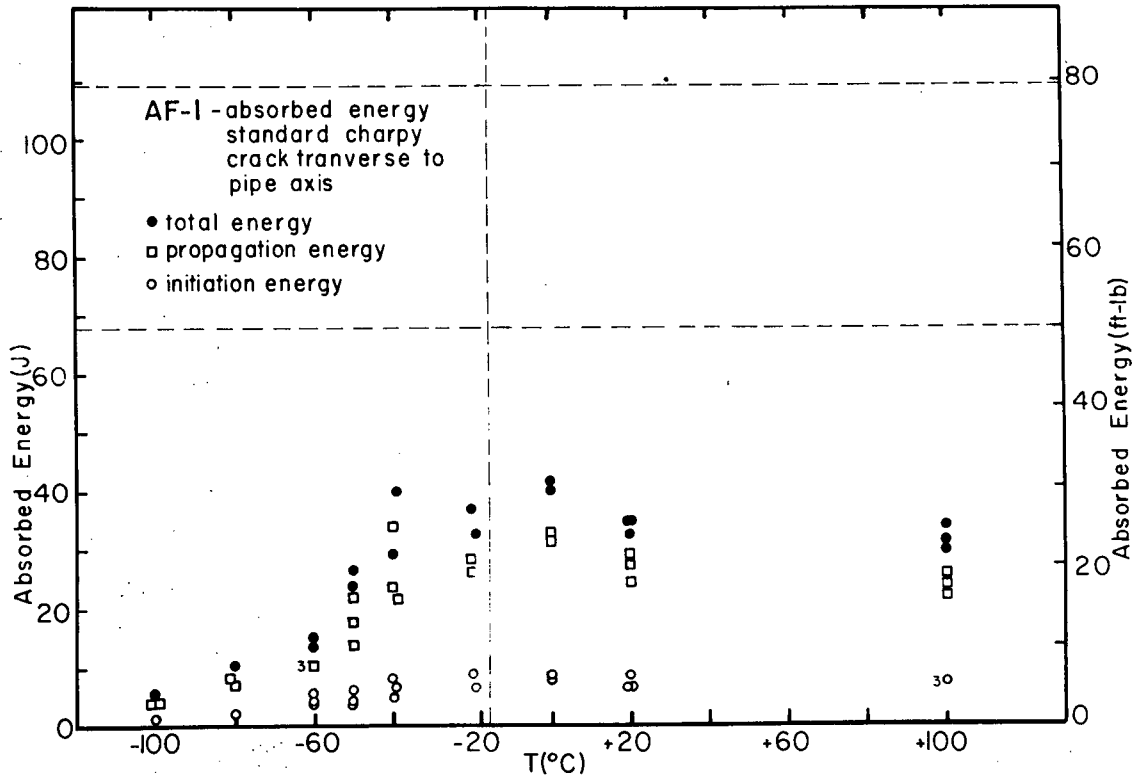


Figure 3.26 AF-1 absorbed energies, standard Charpy, crack transverse to pipe axis.

operating stresses in these directions are significant fractions of the maximum operating hoop stress ($> 0.33 \sigma_H$) some toughness requirement should be established.

3.5.1.1.2 Full Wall Charpys

A valid criticism of the standard Charpy specimen is that it cannot predict the toughness of thicker materials. More important, though, the standard Charpy test is nonconservative, since toughness decreases with increasing thickness⁽¹⁰¹⁻¹⁰²⁾. Full pipe wall Charpys would better represent the full-scale behaviour of a pipeline because the constraint across the notch simulates the service conditions. By testing such specimens for pipeline applications, it was hoped that correlations between the full wall Charpy data and the full wall Battelle-Drop Weight Tear Test could be generated, and that the adequacy of the standard Charpy specimen to represent full-size behaviour could be ascertained.

3.5.1.1.2.1 Crack Parallel to Pipe Axis

The standard Charpy test samples showed that the AF-1 material had a much higher total absorbed energy with the initiation energy being comparable for both steels.

Figure 3.27

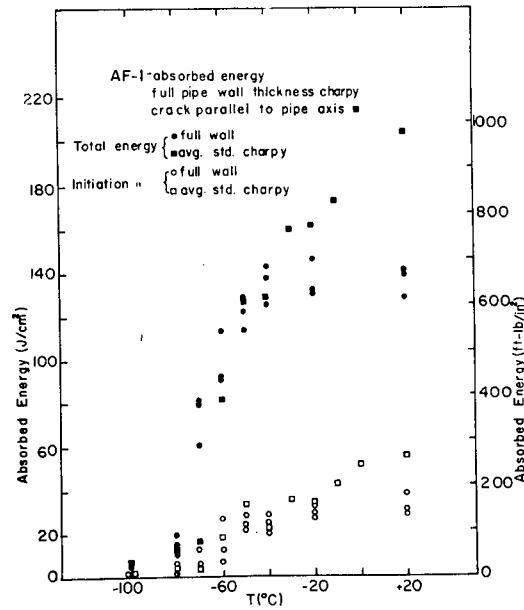


Figure 3.28

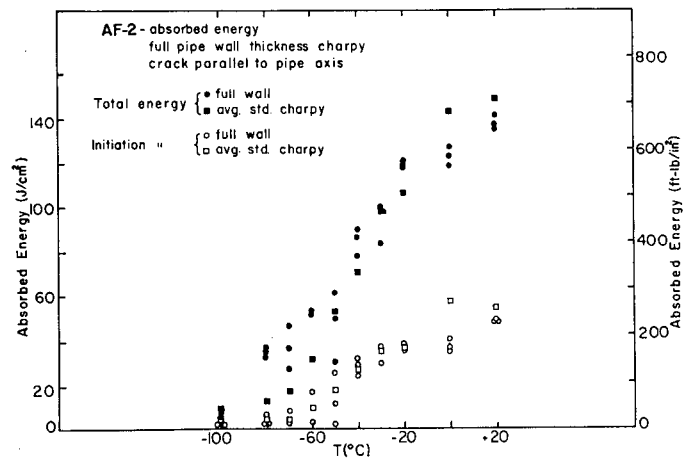
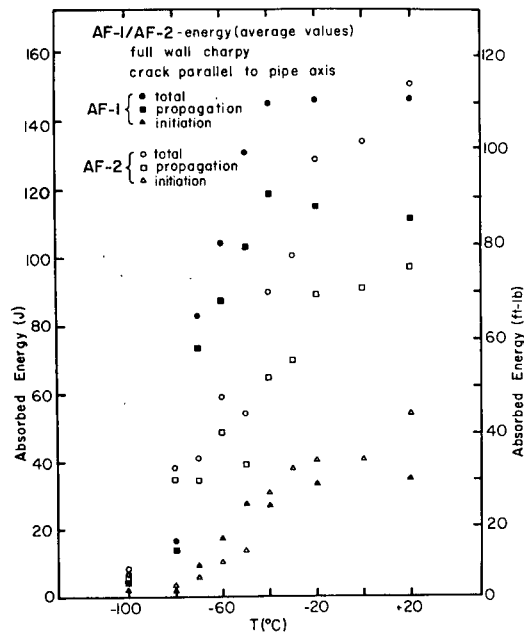


Figure 3.29



The full wall data shows similar behaviour. However, at +20°C, the total energies were essentially equal (Figures 3.29), the AF-1 steel had 111 ft-lb (150 J) and AF-2 had 114 ft-lb (155 J); and the AF-2 material exhibited a higher initiation energy (39 ft-lb (53 J)) as compared to 26 ft-lb (35 J) for AF-1. Since the AF-2 steel did not exhibit an upper shelf, as did the AF-1 steel which retained upper shelf energies to -40°C, the AF-2 total energy decreased progressively to values less than that of AF-1 to -70°C. The higher toughness of the AF-1 was related to its higher propagation energy.

There was little scatter in the data for either steel, nor was bimodal behaviour observed (Figures 3.27 - 3.28).

3.5.1.1.2.2 Crack Parallel to Rolling Direction

As with the standard Charpy comparison, the full wall AF-2 specimens were tougher, requiring considerably more energy than those of the AF-1 steel (Figures 3.30 - 3.32). At no temperature was the toughness of the AF-1 steel comparable to that of the AF-2.

The upper shelf initiation energy of the AF-1 steel was constant at 6 ft-lb (8 J) down to -40°C, compared with approximately 20 ft-lb (27 J) EI for AF-2 to -40°C. The total absorbed energy for the full wall AF-1 Charpy was only 21.4 ft-lb (29 J) at -20°C; the

Figure 3.30

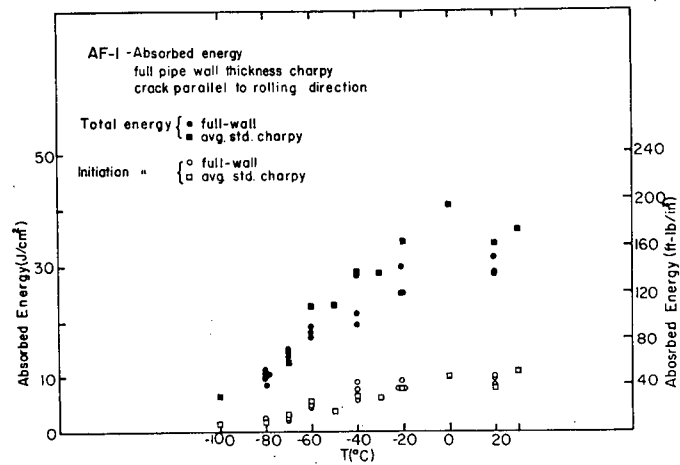


Figure 3.31

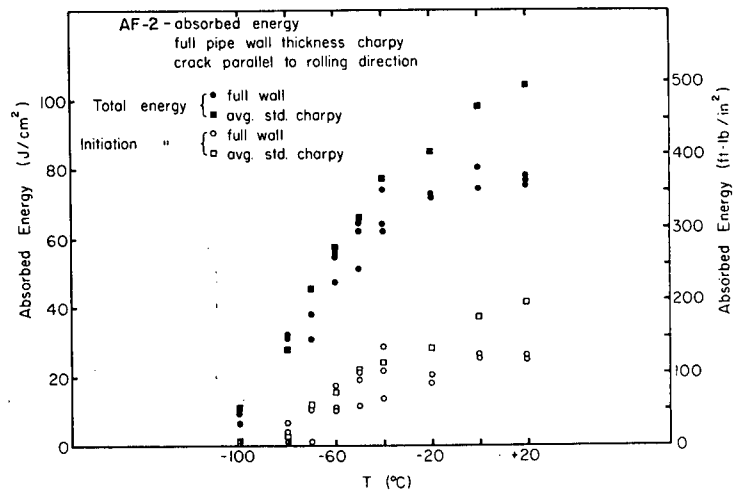
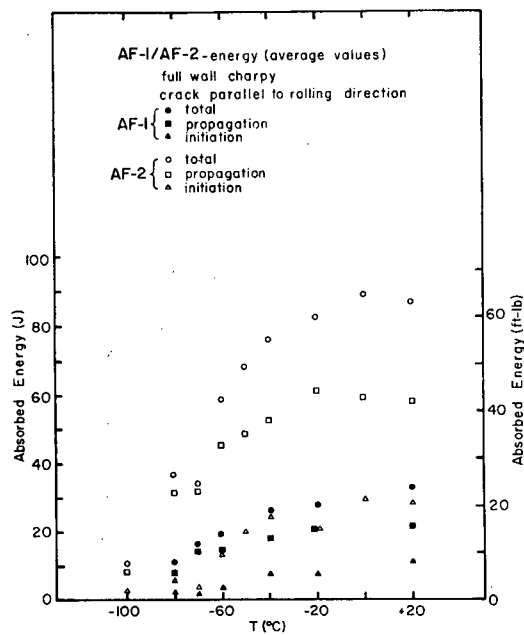


Figure 3.32



average total energy for the AF-2 specimens was 60.0 ft-lb (81 J) (refer to Table 3.4).

Little scatter and no bimodal behaviour was evident in either steel.

3.5.1.1.2.3 Crack Transverse to Rolling Direction

The total energy of the two steels was similar over the entire temperature range (Figures 3.33 - 3.35). The AF-2 steel exhibited only a marginally higher energy than the AF-1 material at +20°C, but was less at lower temperatures.

As noted with the standard Charpy specimens, the initiation energies of the AF-2 steel were comparable to, but slightly higher than those of the AF-1 steel; whereas, the propagation energies of the AF-1 were higher. These differences were most noticeable at -40°C, where the AF-1 and AF-2 propagation energies were 102 ft-lb (138 J) and 73 ft-lb (99 J), respectively; but the initiation energy values were 23 ft-lb (31 J) for the AF-1 and 32 ft-lb (43 J) for AF-2.

The AF-1 steel exhibited bimodal behaviour from -50° through -80°C in this orientation (Figure 3.33).

Figure 3.33

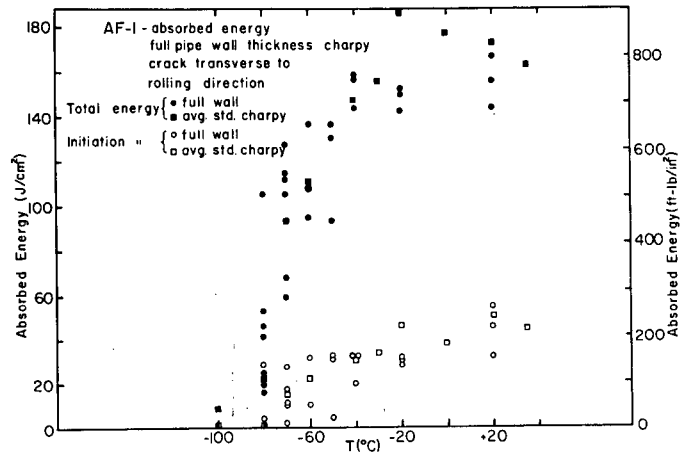


Figure 3.34

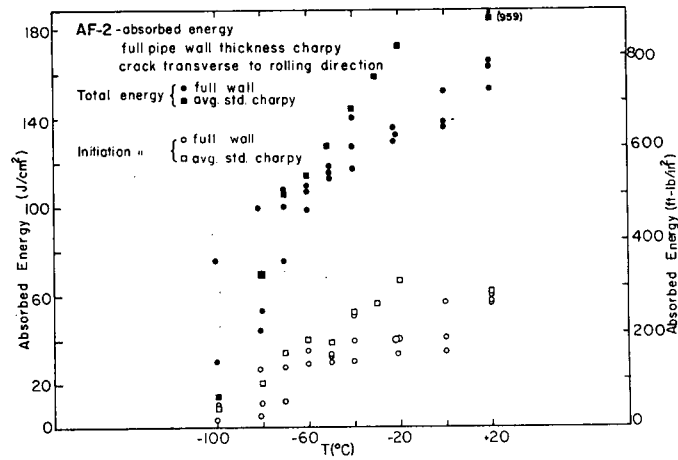
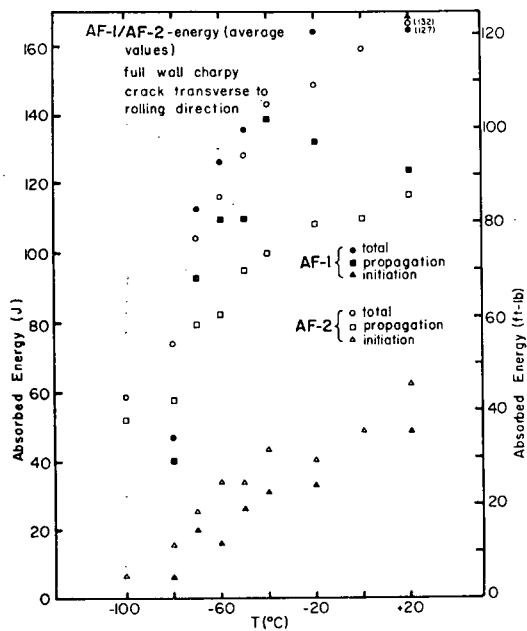


Figure 3.35



3.5.1.1.3 Precracked Charpys

3.5.1.1.3.1 Crack Parallel to Pipe Axis

The AF-1 steel shows higher total energies at all test temperatures (Figures 3.36 - 3.38) and superior initiation energies for the temperature range of -20° to -40°C . For the full wall and standard Charpys, the initiation energy of the AF-2 steel was generally equivalent or higher than that of the AF-1 material over the entire temperature range studied (compare Table 3.3 - 3.5). This indicates that the AF-2 steel may be more susceptible to crack initiation as the notch acuity increases.

At -40°C , both steels exhibit sharp initiation energy transitions and lower shelf energies of $5\text{-}10 \text{ ft-lb/in}^2$ ($1\text{-}2 \text{ J/cm}^2$).

There was very little data scatter nor was bimodal behaviour observed.

3.5.1.1.3.2 Crack Parallel to Rolling Direction

The AF-2 steel required more energy for fracture than the AF-1 steel in this direction (Figures 3.39 - 3.41). This same effect was observed for the standard and full wall specimens.

Fatigue precracking the samples significantly reduced the

Figure 3.36

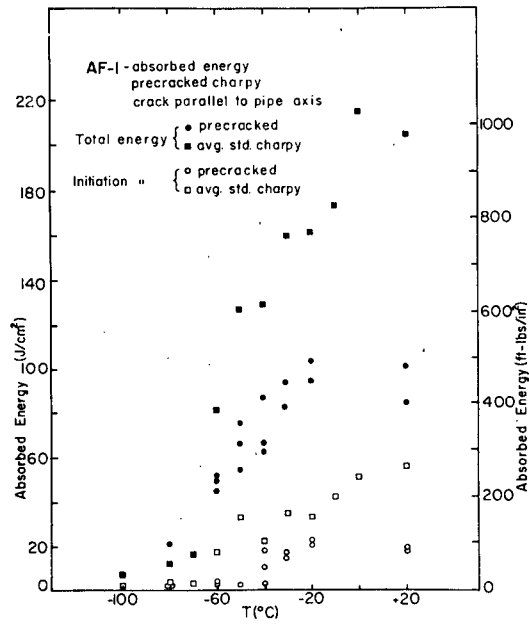


Figure 3.37

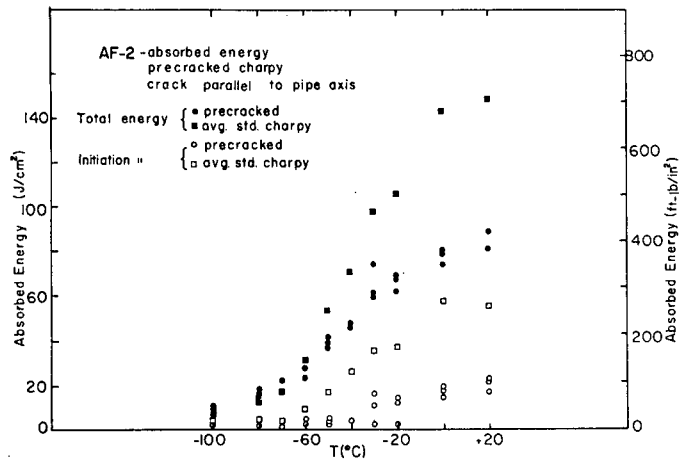


Figure 3.38

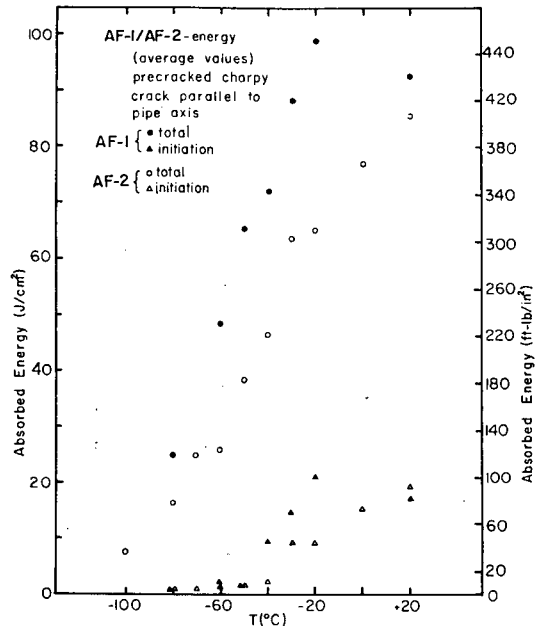


Figure 3.39

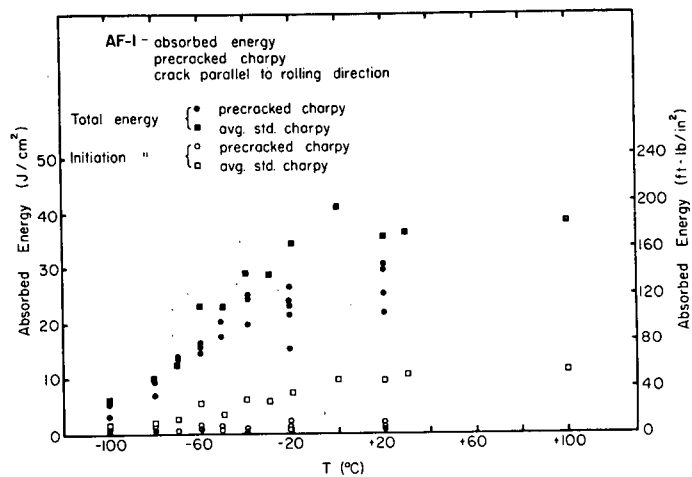


Figure 3.40

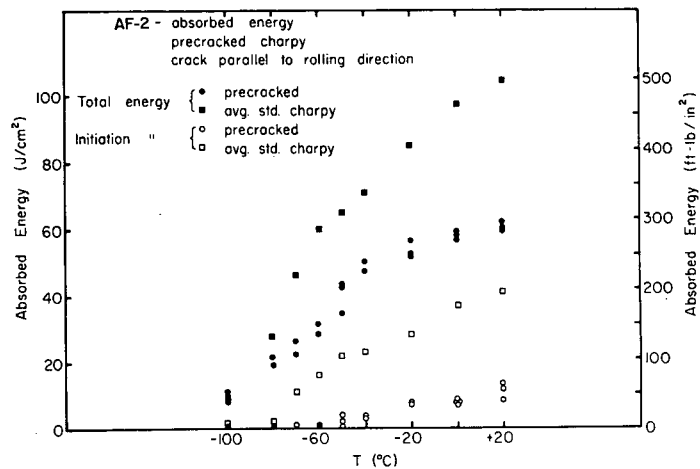
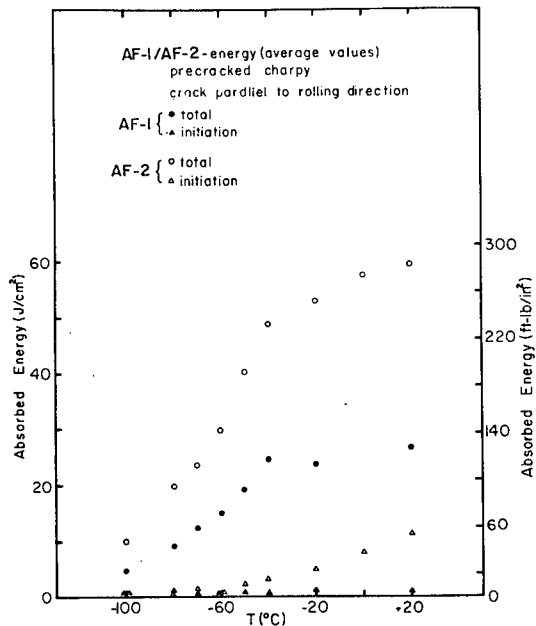


Figure 3.41



initiation energies: the AF-1 specimens, at all temperatures, exhibited an initiation energy of less than 1 ft-lb (1.4 J); whereas at -20°C, the AF-2 precracked Charpys required only 3 ft-lb (4 J) for crack initiation.

The effect of notch acuity in this direction can be seen by examining Table 3.7. The initiation energy of AF-2 is more

Table 3.7

EFFECT OF NOTCH ACUITY

		Standard Notch		Fatigue Precracked Notch	
		AF-1	AF-2	AF-1	AF-2
+20°C	ET	20	61	16	36
	EI	5	24	0.9	7
-20°C	ET	20	50	14	32
	EI	4	17	0.9	3

All values in ft-lb

Precracked values determined by multiplying normalized energies by area of standard Charpy ligament.

sensitive to the increased notch acuity. The initiation energy of the AF-1 is very low for both notch conditions at all temperatures.

3.5.1.1.3.3 Crack Transverse to Rolling Direction

The two steels in this orientation, for all specimen types, yielded similar test results. For the precracked Charpys, the total energies were approximately equal for both steels, although the AF-1 steel maintained an upper shelf energy to below -20°C and exhibited a sharp transition at -60°C. The energy of the AF-2 steel gradually decreased with decreasing temperature (Figure 3.43).

The initiation energy of the AF-2 steel was more sensitive to the presence of the sharper fatigue crack than was AF-1 (compare initiation energies on Figures 3.42 and 3.43).

3.5.1.2 Significance of Specimen Size and Notch Acuity

3.5.1.2.1 AF-1 Steel

3.5.1.2.1.1 Crack Parallel to Pipe Axis

Figures 3.27 and 3.36 show the IIT absorbed energy results obtained from the full wall and precracked specimens versus the standard Charpys, respectively, for the AF-1 steel.

Figure 3.42

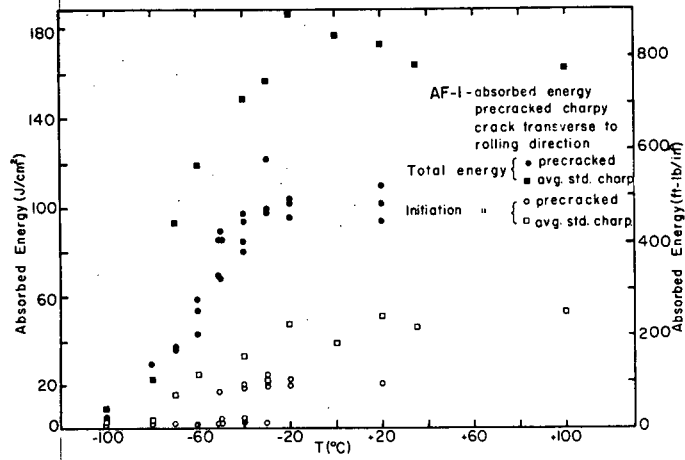


Figure 3.43

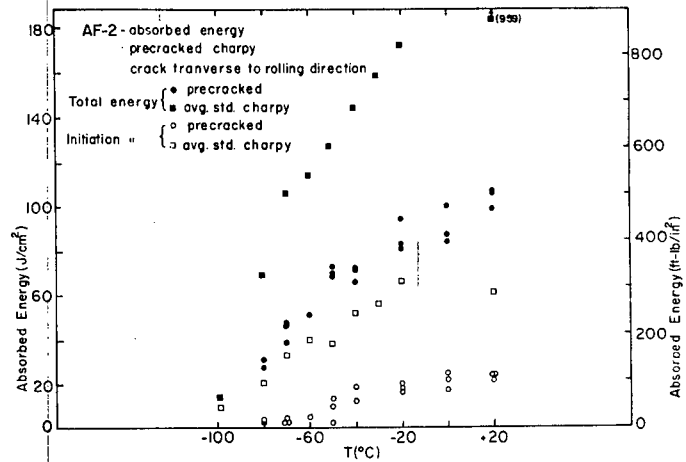
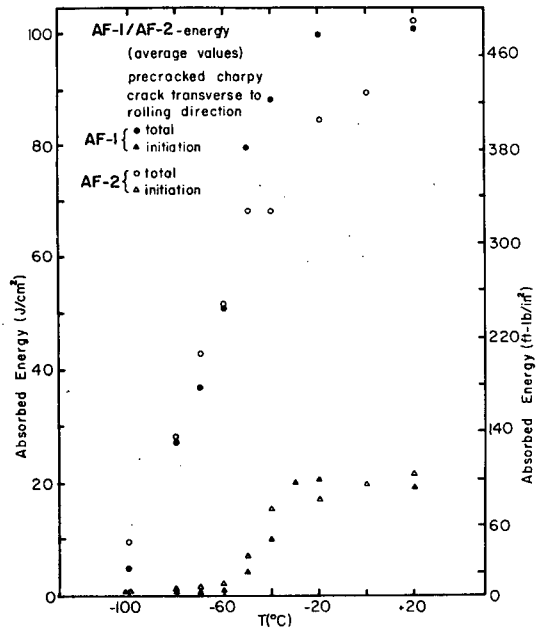


Figure 3.44



It should be remembered that the data from the AF-1 steel exhibited significant scatter; the average values also exhibit similar scatter (refer to Figure 3.17). The minimum standard deviation was approximately 20 ft-lb (27 J) or more. Bimodal behaviour was also observed in the transition region for the standard specimens, but not for the precracked or full wall Charpys.

In comparing the full wall and standard specimens (Figure 3.27), the standard Charpys show a much higher total absorbed energy (977 ft-lb/in² (205 J/cm²) for the standard specimen, 651 ft-lb/in² (137 J/cm²) for the full wall at +20°C). This behaviour can be explained in that the greater thickness of the full wall specimen provides greater constraint across the notch, thereby lowering the toughness. However, as the temperature decreased to below -40°C, the absorbed energies of the two specimen types became essentially equivalent.

The initiation energies were nearly equal at -20°C and below.

The full wall Charpys exhibited a sharp energy transition at about -80°C, whereas the standard size specimens had a total energy transition 10°C higher. Others⁽¹⁰²⁾ have observed that increasing the thickness of a Charpy specimen increases the transition temperature, however.

Thus, for the AF-1 steel in this orientation, the standard Charpy specimen is not representative of the full size behaviour, except at very low temperatures; the standard Charpy data is non-conservative. For pipeline applications, adoption of a full size specimen would provide more meaningful data and would be easier to prepare.

A comparison of the precracked and standard Charpy specimen data is shown in Figure 3.36. As expected, the introduction of a fatigue precrack significantly reduces the crack initiation energy.

It is interesting to note the effect that notch acuity has on the fracture process and the corresponding total absorbed energy. By multiplying the -20°C precracked specimen normalized energy (absorbed energy per unit area) by the area of a standard Charpy ligament (0.124 in^2), a value of 58.6 ft-lb (79 J) total energy and 12.4 ft-lb (17 J) initiation energy would be obtained. The standard Charpys, at that same temperature, absorbed 96 ft-lb (130 J) total and 19 ft-lb (26 J) initiation. Thus, the presence of the sharp fatigue crack significantly reduces the energy to initiate and the energy to propagate a crack, as shown in Figure 3.36.

The effect of the precrack can be further demonstrated by comparing the relative amount of energy absorbed in fracture propagation and initiation through an examination of the ductility indices

(DI) in Table 3.6. That Table shows that for the AF-1 steel, tested with the crack parallel to the pipe axis at temperatures from +20°C to -40°C, the DI for the precracked specimens is only slightly higher than that of the standard blunt notched Charpys. Thus, although the fatigue flaw requires a much lower crack initiation energy than the standard Charpy notch, the propagation energy is also greatly reduced (though not to the same extent). As a notch lengthens and sharpens during the fracture event, the strain concentrated near its tip increases and the point of maximum stress intensification moves back towards the crack tip. The stress level immediately ahead of the crack consequently increases and the crack accelerates. Therefore, the presence of a sharper notch in the sample will facilitate the crack initiation and subsequently the propagation process by causing crack acceleration and subsequent strain hardening earlier in the fracture event⁽⁵⁾.

At temperatures of -60°C and -80°C, the AF-1 precracked specimens exhibited very high ductility indices (> 20) indicating that the propagation energy was a significant proportion of the total energy absorbed in the crack process; i.e., very little energy was required for crack initiation.

The transition behaviour of the total energy for the precracked specimens was better defined than that of the standard Charpys.

The precracked Charpy initiation energy also showed a marked transition between -40° and -50°C , decreasing from an upper shelf initiation energy of approximately 10 ft-lb (14 J) to a lower shelf value of less than 1 ft-lb (1.4 J). The transition in the standard Charpy initiation curve was not so sharp, exhibited bimodal behaviour, and did not reach the lower shelf until -70°C (Figure 3.36). This observed behaviour illustrates the classic effect of a sharp flaw in a structure: the transition temperature curve is shifted to higher temperatures and the magnitude of the upper shelf energy is significantly reduced.

3.5.1.2.1.2 Crack Parallel to Rolling Direction

The results from the standard, full wall, and fatigue precracked Charpy specimens were not significantly different, probably due to the low magnitudes of the energies involved in cracking along the brittle MnS inclusions (Figures 3.30 and 3.39).

Although the standard Charpy specimens did have marginally higher total energies, the differences between the standard and full wall specimens were small, being approximately 3-4 ft-lb (4-5 J) at $+20^{\circ}\text{C}$. The initiation energies of those specimen types were virtually equal at all temperatures. Thus, for this orientation, a standard Charpy adequately represents the full thickness impact behaviour.

All three specimens of the AF-1 steel, when tested with the crack running parallel to the rolling direction, showed almost no initiation energy transition; values of EI ranged from 8 ft-lb (11 J) to 2 ft-lb (3 J) for the full wall Charpys, whereas the precracked Charpys had only a constant low magnitude initiation energy of less than 1 ft-lb (1.4 J) over the entire temperature range studied. These extremely low values of the initiation energy for the AF-1 steel in this orientation must be emphasized.

The precracked ductility indices were quite high (Table 3.6), indicating that crack initiation was an insignificant component of the total absorbed energy. In fact, the normalized propagation energies for the precracked specimens were essentially equivalent to that of the standard Charpys for this orientation (Figure 3.39).

3.5.1.2.1.3 Crack Transverse to Rolling Direction

The full wall and standard specimens in this orientation gave similar total and initiation energy results (Figure 3.33). Both specimens exhibited bimodal behaviour in the -60° to -80°C range. A significant decrease in the total and initiation energies occurred for both specimens between -70° and -80°C .

As with the previous orientations, the standard Charpy specimens with the crack running transverse to the rolling direction had much higher energies than the precracked samples (Figure 3.42). Only at -80°C did the two energy curves coincide. The precracked initiation energy curve exhibited a sharp transition between -50° and -60°C , the energy decreasing to less than 1 ft-lb (1.4 J). The corresponding transition for the standard specimens was not as distinct, and occurred over a lower temperature range of -60° to -80°C .

3.5.1.2.2 AF-2 Steel

3.5.1.2.2.1 Crack Parallel to Pipe Axis

The results of the AF-2 full wall thickness Charpy tests are compared with those of the standard Charpys in Figure 3.28. The increased constraint at the root of the notch in the full wall specimens caused a reduction in the toughness of the AF-1 samples (Figure 3.27), but did not decrease the energy of the AF-2 specimens in this direction. The full wall Charpys showed similar normalized total and initiation energies to those obtained from standard Charpys down to -60°C . At lower temperatures, the propagation energy, and hence the total energy of the full wall specimens was greater. The transition behaviour showed no thickness effect. Thus, the standard

Charpy adequately describes the full wall impact behaviour of the AF-2 steel. This is in direct contrast to the comparison of results made on the AF-1 steel.

The data in Figure 3.37 shows that precracking greatly reduced the initiation energy and increased the transition temperature by approximately 30°C.

3.5.1.2.2.2 Crack Parallel to Rolling Direction

The standard and full wall Charpy results are compared in Figure 3.31. It can be seen that for the AF-2 steel, the standard Charpys adequately describe the full size behaviour for temperatures below -20°C.

The precracked AF-2 specimens exhibited a continuously decreasing initiation energy with decreasing temperature, with less than 10 ft-lb (14 J) required below -40°C (Figure 3.40).

3.5.1.2.2.3 Crack Transverse to Rolling Direction

The differences between the standard Charpy and the full wall Charpy are more distinct in this orientation for the AF-2 material (Figure 3.34). The normalized total energies of the standard specimen are higher for temperatures down to -70°C. The

initiation energies of the standard Charpys were higher at all temperatures. The full wall Charpys exhibited bimodal behaviour between -80° and -100°C , unusual for the full wall specimens in this study.

The differences between the standard and the precracked specimens were also more pronounced than for the other orientations (Figure 3.43). The normalized initiation energy of the standard Charpys was approximately equal to the total normalized energy of the precracked specimens. This points out the importance of basing fracture control specifications on the worst possible defect and on the initiation energy, rather than total energy, since the transition temperatures and energy levels of the two are quite different.

3.5.1.3 Conclusions of Absorbed Energy Study

The AF-1 steel exhibited a higher degree of anisotropy than did the AF-2 material. Very low toughness was observed for the AF-1 in the orientations for which the crack followed the rolling direction or was transverse to the pipe axis. The AF-1 initiation energies in these directions were extremely low, even for the relatively blunt notched standard Charpy specimens.

The initiation energy of the AF-2 steel was a greater portion of the total energy than was the EI for the AF-1 material, in all directions, as shown by the ductility indices in Table 3.6. Although the AF-1 steel often showed higher total energies than AF-2, it also exhibited lower initiation energies.

It is suggested that pipeline specifications require testing and minimum toughnesses in all directions of the pipe. Further tests are required to establish a specification for an acceptable initiation energy to better ensure protection against crack initiation.

The AF-1 steel had more scatter in the data and often exhibited bimodal behaviour in the transition region.

The energy transition curves for AF-1 showed a classic upper and lower shelf connected by relatively sharp transition regions. The energy of the AF-2 steel decreased continuously with decreasing temperature.

The shape of the curves for the propagation and initiation energy components of the total energy also showed this transition behaviour. This suggests that the initiation energy may have significance in terms of a transition temperature approach.

Both steels met the 80/50 ft-lb (108/68 J) energy criteria at -18°C for the standard specimens in which the crack followed the pipe axis. However, due to the very low toughnesses of the AF-1 steel in other orientations, the adequacy of this fracture control specification is questioned.

Fatigue precracked specimens greatly reduced the absorbed energies and yielded higher transition temperatures than for the standard Charpys. Full wall Charpys generally displayed lower upper shelf energies, although the energy values of the standard and full wall specimens were similar in the transition and lower shelf regions. The standard Charpy specimen often gave nonconservative results at the pipeline specification temperature of -18°C ; it is suggested that a full wall Charpy be adopted for routine testing of pipeline steel.

3.5.1.4 Drop Weight Tear Test Correlations

The pipeline industry employs two tests to ensure the toughness of the steels used in pipelines: the standard Charpy impact test and the Battelle-Drop Weight Tear Test⁽³⁹⁾.

The DWTT is used to define the percent shear on the fracture surfaces of a full-thickness test specimen. Absorbed energy data is also obtained, although it is not employed in pipeline specifications.

The specimen is provided a pressed notch, the flank angle and root radius being identical with that of the standard Charpy specimen. The DWTT specimen differs from that of the Charpy test in that: 1) it is a full plate thickness specimen to ensure maximum constraint; 2) the pressed notch provides a brittle crack initiation site; and 3) the dimensions are such that the propagation stage dominates the fracture event (76 x 305 mm).

The two nonstandard specimens in this study have features in common with the DWTT specimen: the full wall Charpy specimens have the same thickness (dimension across the notch); and the precracked Charpys require a low initiation energy making the propagation stage the major component of the fracture process.

In addition, the instrumented impact test provides information regarding the crack propagation stage which may be associated with the percent shear.

Both pipe manufacturers provided DWTT data for the steels used in this study. Only data for the crack path following the longitudinal axis of the pipe could be obtained since that is the only specified test direction.

Figures 3.45-3.48 compare the data from the DWTT with that obtained from the IIT of the full wall and precracked Charpys of the

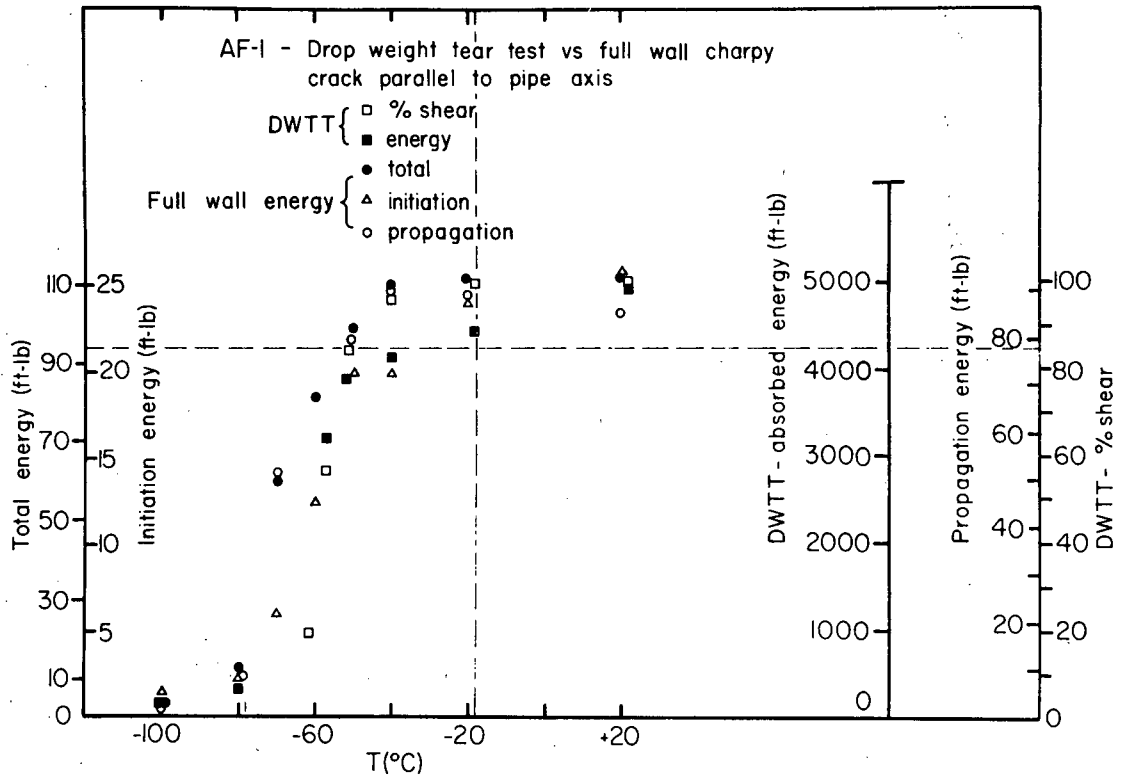


Figure 3.45

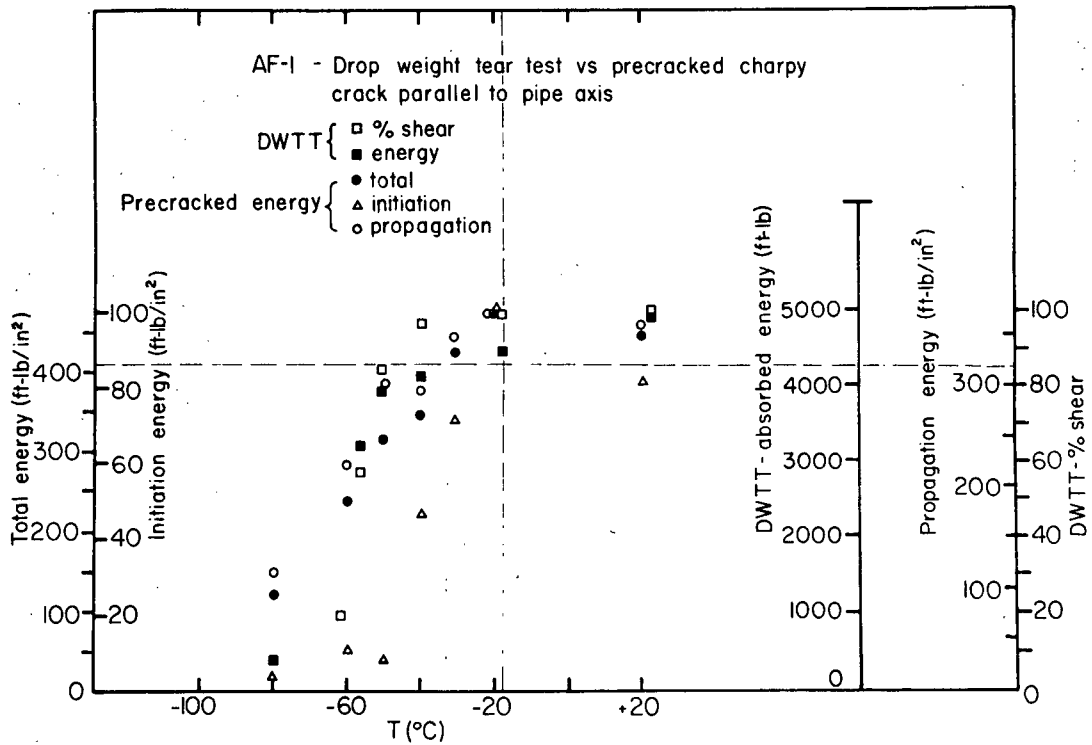


Figure 3.46

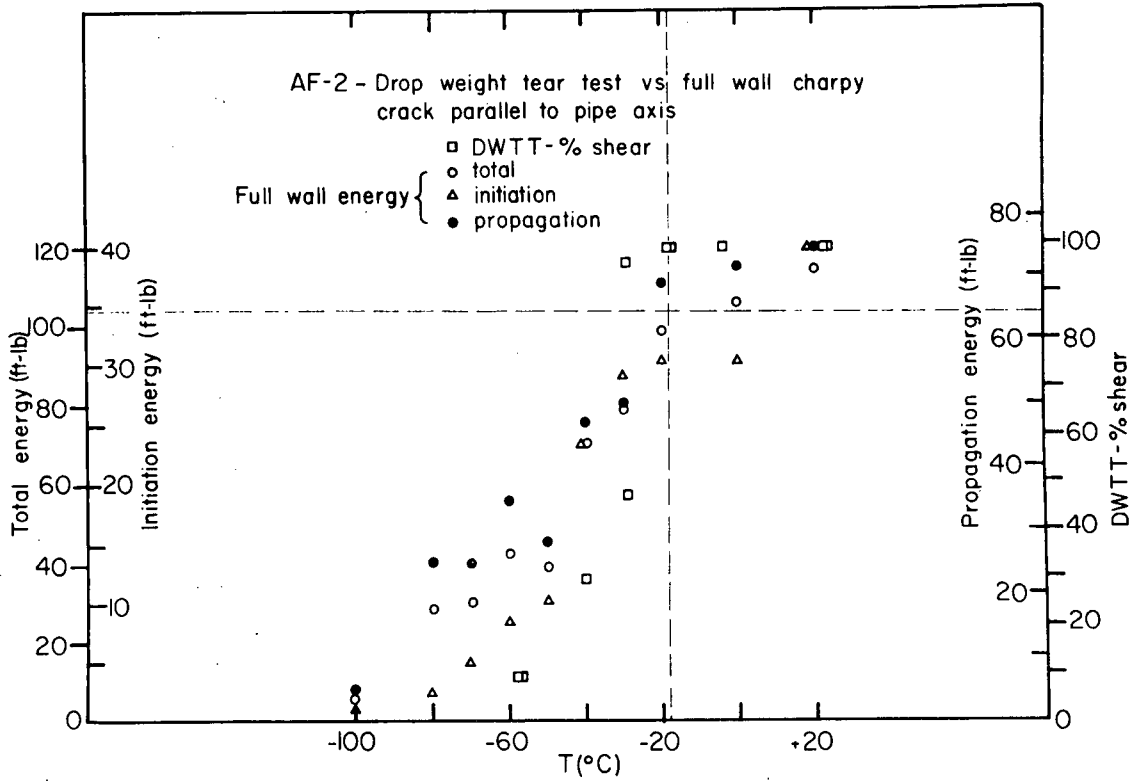


Figure 3.47

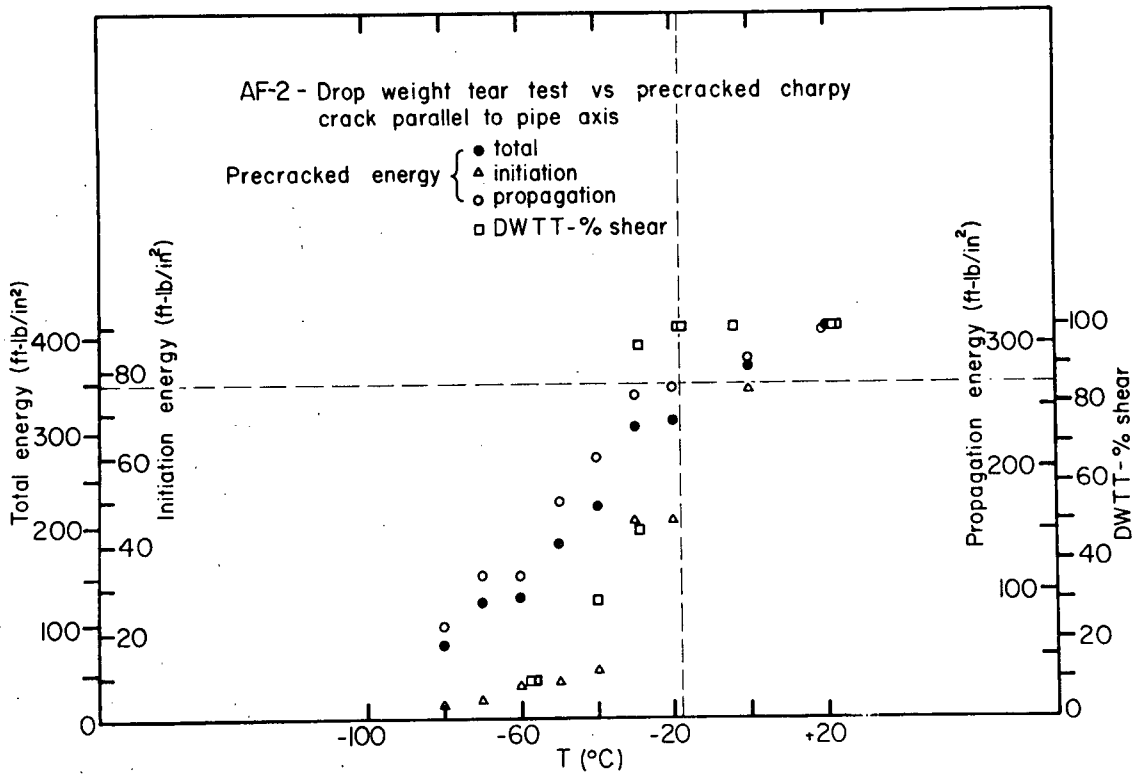


Figure 3.48

AF-1 and AF-2 steels, respectively.

Distinct similarities exist between the IIT and the DWTT data for the AF-1 steel. For the full wall specimens, at the -18°C specification temperature, where the specification requires an average of 85% shear, all the energy components, total, initiation, and propagation, were at upper shelf conditions as was the percent shear from the DWTT (Figure 3.45). Furthermore, the shapes of the IIT energy transition curves and their initial deviation from upper shelf values closely matched that of the percent shear transition curve of the DWTT, although the DWTT data exhibited a sharper transition.

The DWTT absorbed energy data exhibited a similar energy transition to those of the full wall Charpy specimens. However, it did not maintain a constant upper shelf energy even though approximately 100% shear was reported for temperatures down to -40°C .

The precracked Charpy data also showed close similarities with that of the AF-1 DWTT (Figure 3.46). In comparing the precracked Charpy data with the B-DWTT data, all three energy components of the precracked specimens were at the upper shelf or peak energy condition at the -18°C specification temperature. Both the total energy and the propagation energy decreased from their upper shelf values at

approximately the same temperature as did the DWTT percent shear, although their transitions were not as steep. The precracked initiation energy transition was sharp but the transition temperature was higher than the DWTT transition by approximately 15°C.

Although more data correlations are certainly necessary, this work does indicate that an empirical relationship may exist for the AF-1 steel between a full wall Charpy or a precracked full wall Charpy and the Drop Weight Tear Test. It is possible that the full wall Charpy test could provide the industry with a single instrumented impact test that would measure the propagation behaviour in terms of percent shear and absorbed energy while still providing a measure of the initiation energy. Such a test would have time and cost saving advantages for quality assurance purposes.

No simple correlations existed between the DWTT results and the full wall and precracked Charpy data of the AF-2 steel (Figures 3.47 - 3.48). The AF-2 steel energy decreased continuously with decreasing temperature, whereas the DWTT percent shear curve did have an upper shelf which remained constant with decreasing temperature to approximately -30°C where it exhibited a very sharp ductile-brittle transition.

3.5.2 Dynamic Yield Strengths

Dynamic yield strengths were obtained for all specimens from the load-time traces as described in the preceeding Chapter. Fig. 3.49 shows the average values of the dynamic yield strengths versus temperature for each steel in each orientation, as determined from the standard Charpy tests. This property was very reproducible.

The yield strength of a bcc material increases with:

1. decreasing temperature since the Peierl's stress is a strong inverse function of temperature; and
2. with increasing strain rate since the density and velocity of moving dislocations is proportional to strain rate⁽⁵⁾.

The strain rate effect can be seen in this study by examining the data at +20°C. The dynamic yield strengths of the steels, for the orientations examined, ranged from 100-120 ksi (690 - 828 MPa), whereas the "static" yield strengths of these steels, at this same temperature and for the same orientations ranged from 72-79 ksi (497 - 545 MPa).

The strain rates imparted by the IIT were approximately the same at all temperatures. Thus, the increase in dynamic yield strengths with decreasing temperature, observed on Figure 3.49, can be attributed primarily to the temperature dependence of the yield stress. At the

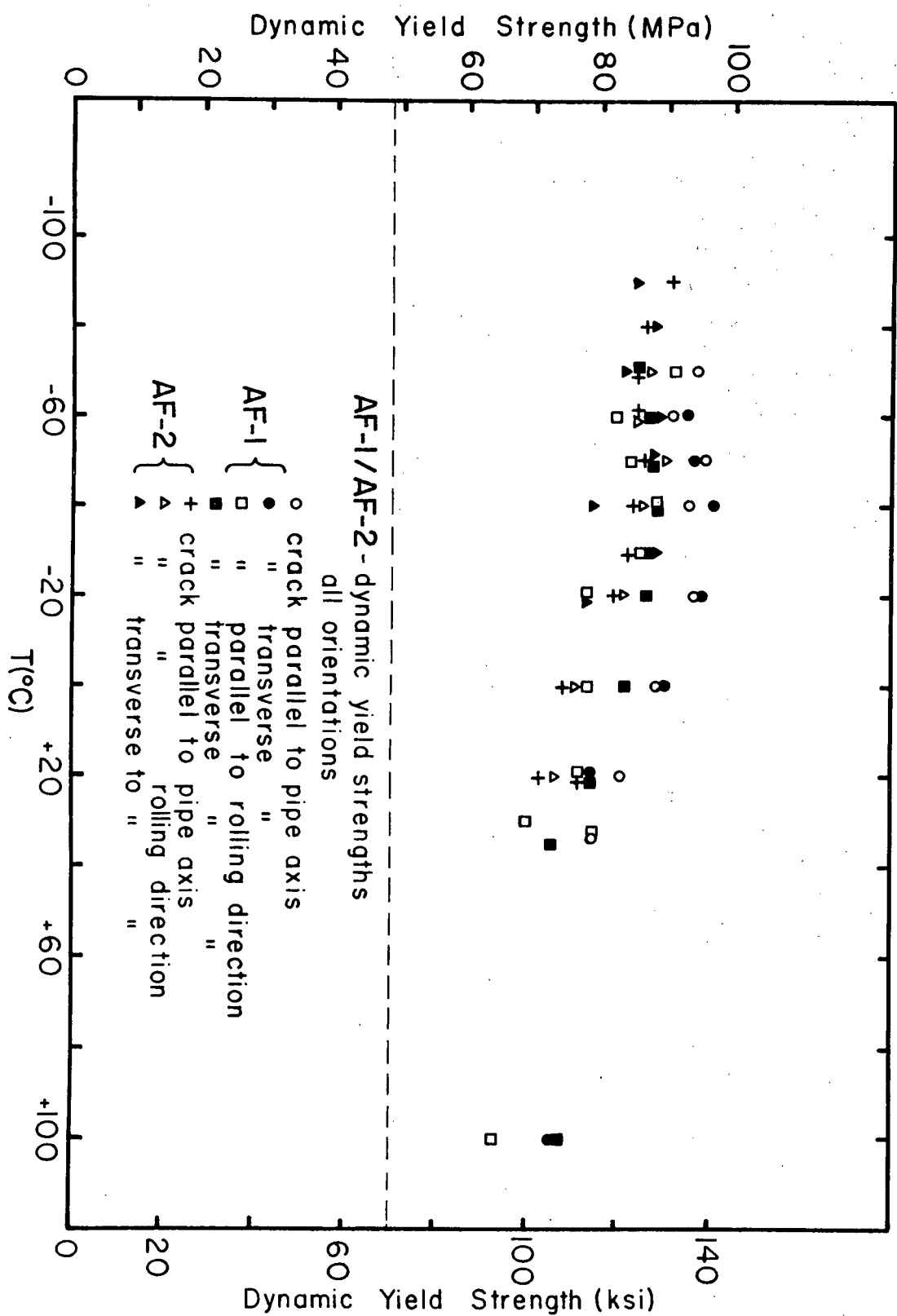


Figure 3.49 AF-1/AF-2 dynamic yield strengths.

lower temperatures, the yield strengths increased to 140 ksi (966 MPa).

The dynamic yield strength data was employed in calculations used to verify dynamic fracture toughness validity and should be used to estimate the yield strength of pipe sections subjected to dynamic loading.

3.5.3 Load-Time Behaviour

Figures 3.50 to 3.56 show the maximum and general yield loads and the time to realize the maximum load ("crack initiation") for each orientation of the two steels as a function of temperature. These data were obtained from standard Charpy specimen tests; the load-time traces are shown in Figures 3.5 - 3.10.

Several investigators have proposed theories which permit detailed analyses of such load-temperature diagrams in terms of the mechanisms of deformation and fracture behaviour^(5,20-21,64,105). Diesburg⁽⁷⁾ has described the load/time behaviour of acicular ferritic steels.

At low temperatures, cleavage fracture takes place at a load less than that required for general yielding - linear-elastic failures occur.

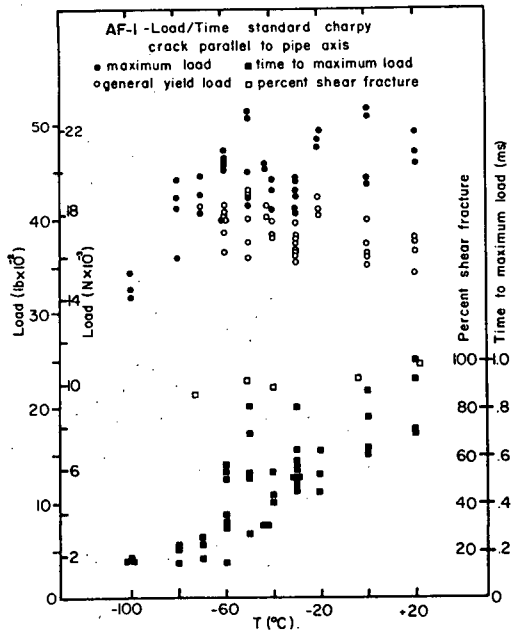


Figure 3.50

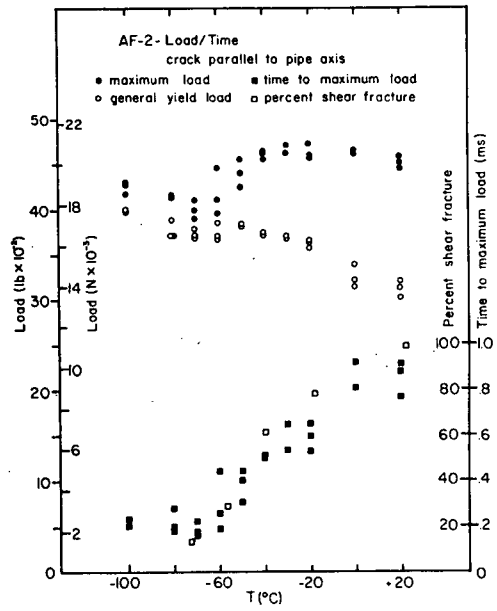


Figure 3.51

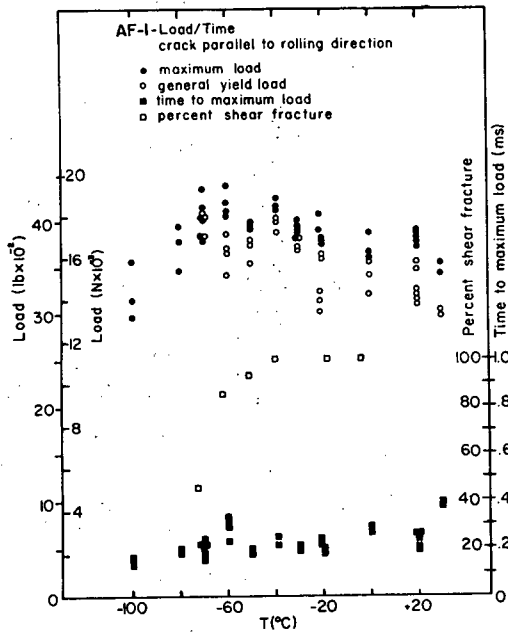


Figure 3.52

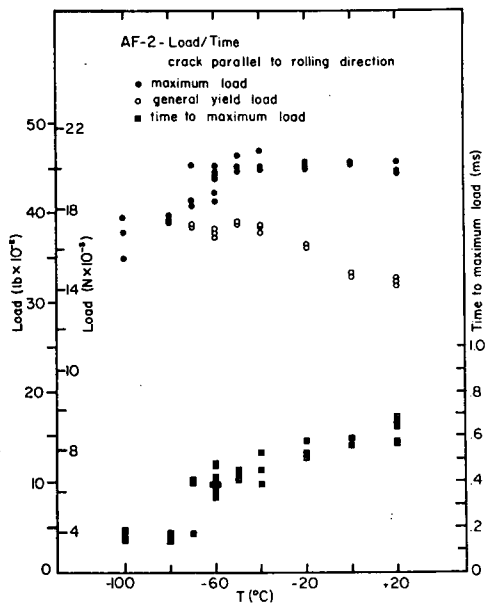


Figure 3.53

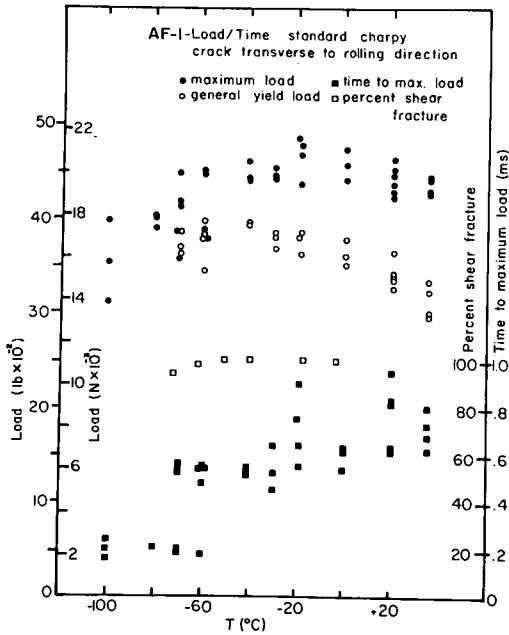


Figure 3.54

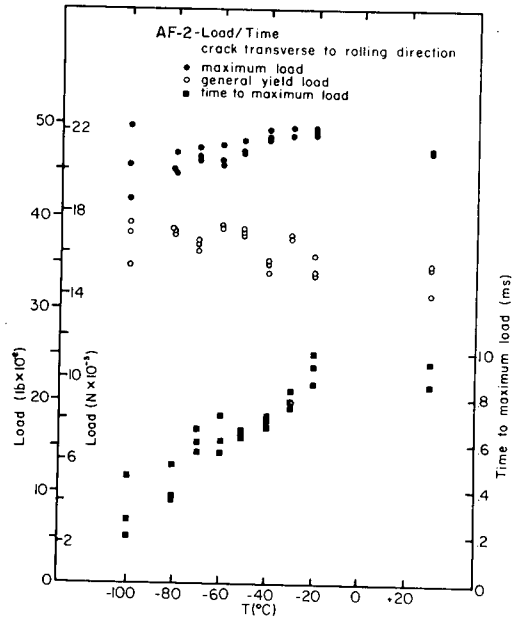


Figure 3.55

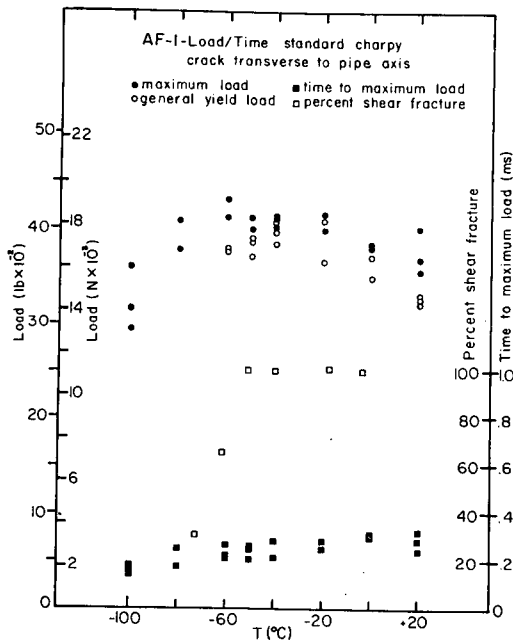


Figure 3.56

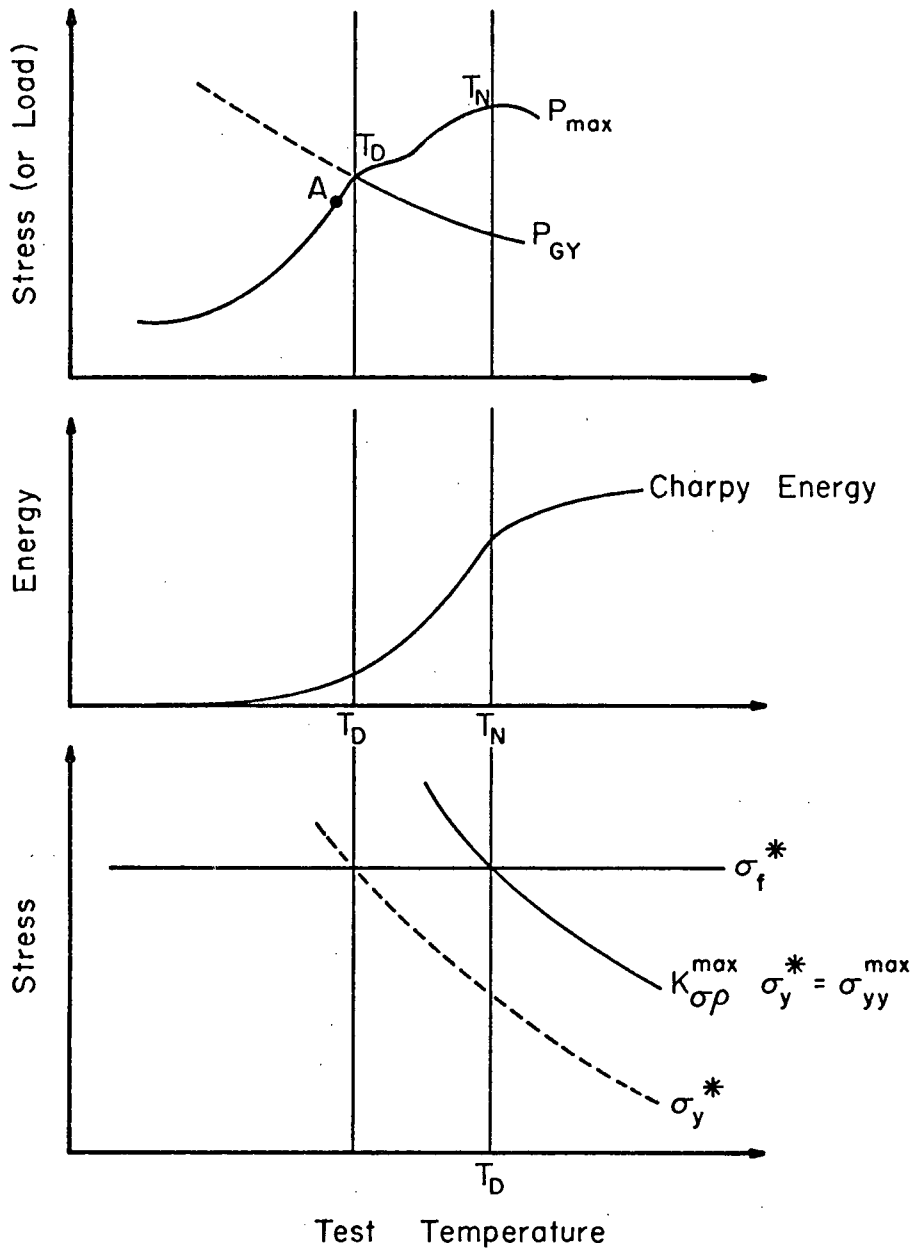


Figure 3.57 Schematic of variation of general yield load, fracture load, and absorbed energy with temperature. Effect of notch on T_D

Since the effective yield strength of notched steel specimens is an inverse function of temperature, the extent of plastic deformation required to raise the tensile stress at the root of the notch to that required for cleavage fracture increases with temperature⁽⁶⁴⁾:

$$\sigma_{yy}^{\max} \quad (= K_{\sigma\rho} \sigma_y^*) = \sigma_f^* \quad \begin{array}{l} \text{for cleavage} \\ \text{fracture} \end{array} \quad (\text{Eq. 3.5})$$

where, σ_{yy}^{\max} = maximum tensile stress below notch
 σ_f^* = cleavage fracture stress (\approx constant)
 σ_y^* = yield strength below notch
 $K_{\sigma\rho}$ = $\sigma_{yy}^{\max} / \sigma_y^*$ (by definition) = plastic
stress concentration factor

The loads required for cleavage failure therefore also increase with increasing temperature since:

$$\sigma_y^* = f(1/T) \quad (\text{Eq. 3.6})$$

so, as $\uparrow T$, $\uparrow K_{\sigma\rho}$ for $\sigma_{yy}^{\max} = \sigma_f^*$

but, $K_{\sigma\rho} = f(\text{plastic zone size}) = f(\text{applied load})$

In this study, incidentally, at temperatures as low as -100°C , considerable plastic deformation at the crack tip was evidently required for the cleavage failures observed, since the load required for failure (and, hence, the plastic zone size required) was found to be much less in tests conducted at -196°C (approximately 2000 lb (8900 N) at -196°C versus loads on the order of 3500 lb (15575 N) at -100°C).

In Charpy specimens, the stress concentration factor, $K_{\sigma\rho}$, reaches a maximum, $K_{\sigma\rho}^{\max}$ ($= 2.18$), at some temperature less than T_D (point A Figure 3.57). This temperature has been experimentally determined to be that at which the applied load, P , equals $0.8 P_{GY}^{(106)}$. At this point, work hardening is required to raise the tensile stresses below the notch to equal the cleavage stress ($K_{\sigma\rho}^{\max} \sigma_y^* < \sigma_f^*$).

Above the temperature at which the general yield load and maximum (fracture) load are equal, called the brittleness transition temperature, T_D , the fracture mode becomes a combination of fibrous tearing (ductile) and cleavage fracture⁽⁷⁾.

The fracture load necessarily increases with temperature beyond T_D due to a relaxation of the triaxial stress state ($K_{\sigma\rho}^{\max}$): the strain needed to produce the work hardening required to raise σ_{yy}^{\max} to σ_f^* is so large that the plastic constraint is decreased - plane stress conditions are approached.

A peak in the maximum load curve is eventually reached at some temperature above T_D . This peak temperature, T_N , is termed the ductility transition temperature. It corresponds to the point where the strain (and thus the load) required to initiate cleavage fracture is so large that it exceeds that required for the initiation of fibrous tearing. Beyond that temperature, the fracture load decreases with increasing temperature.

This "knee" in the load-temperature curve (T_N) is associated with the temperature at which fracture is initiated solely by fibrous tearing^(5,64). Other researchers have identified this point, for acicular ferritic steels, as corresponding to the " C_v 100" temperature^(7,107). This temperature is defined as the lowest temperature at which the fracture surfaces of a Charpy specimen exhibit 100% shear, i.e., the lowest temperature at which fracture initiates and propagates in an entirely ductile manner, and is often used in pipeline specifications.

For nonacicular steels, fibrous cracks do initiate at the ductility transition temperature, T_N , the temperature associated with the peak load on the load-temperature diagram⁽²⁰⁾. However, at high rates of strain, the stress field ahead of the advancing ductile crack can cause large increases in the dislocation density. This may result in cleavage fracture initiating ahead of the advancing ductile crack tip and a mixed mode failure would be apparent on the fracture surface even at temperatures above T_N . This has been observed for polygonal ferritic structures^(20,64). Such behaviour is manifested on the load-time trace by a sudden drop in the load at some point beyond that of the maximum load.

An acicular ferrite steel is already highly dislocated and consequently the dislocation build up ahead of an advancing crack will

not be significant and thus no change in fracture mode is observed. The fracture resistance at the onset of crack initiation is therefore the same as the fracture resistance ahead of the propagating crack. The implication is that if cleavage fracture does not occur early in the fracture process in AF steels, it will not occur during the propagation stage. Therefore, for the AF steels, the peak load temperature, T_N , is also associated with $C_v 100^{(7)}$.

This suggests that the temperature at which the initiation energy first deviates from its upper shelf value may also be associated with the $C_v 100$ temperature, since that initial decrease in EI may signify the transition from fibrous to cleavage initiation. If this is true, then that initiation energy transition temperature may be used to protect against cleavage failures.

The percent shear on the fracture surfaces of standard Charpy specimens of the steels tested in this work was supplied by the steel manufacturers. These data have also been plotted on Figures 3.50-3.52, 3.54, and 3.56.

Table 3.8 presents the $C_v 100$ temperatures as determined from the fracture surfaces and from the peak in the IIT load-temperature curves. In addition, the initiation energy transition temperature (initial deviation from upper shelf value) for the corresponding standard Charpys is given.

Table 3.8

C_v 100 TEMPERATURES

	Peak on Load-Temperature Curve, T _N	Fracture Appearance	EI Transition	DWTT 85% Shear
AF-1-Crack Parallel to PA	-21°C	>+22°C	+20°C	-51°C
AF-1-Crack Parallel to RD	-40°C	-40°C	-40°C	-
AF-1-Crack Transverse to PA	-60°C	-51°C	-60°C	-
AF-1-Crack Transverse to RD	-20°C	-51°C	-20°C	-
AF-2-Crack Parallel to PA	-30°C	>+22°C	0°C	-30°C

The correlations between the temperatures presented in Table 3.8 are inconsistent. For those specimens which did not exhibit "splitting" on the fracture surfaces (to be discussed in the next Section), all three temperatures were in agreement (AF-1 specimens with cracks parallel to rolling direction and transverse to pipe axis). However, when splitting was observed (see Figures 3.11 -3.16) no correlations could be made. It is extremely difficult to determine the percent shear on the fracture surfaces of heavily control-rolled AF steels which exhibit splitting by direct-examination; the reliability

of such measurements is in question⁽⁹²⁾. However, the peak load, $T_N (C_v 100)$ on the load-temperature curves (Figures 3.50 - 3.56) was not always well defined either. More correlating data is required.

In addition, it has been suggested that the B-DWTT 85% shear temperature should lie between the peak temperature, T_N , and the brittleness transition temperature, $T_D (P_{max} = P_{GY})$ ⁽⁴⁰⁾. As long as T_N is less than the pipeline specification temperature for 85% shear (-18°C), a Drop Weight Tear Test may not be required should IIT be employed to evaluate pipeline materials. However, the validity of this suggestion could not be established, as Table 3.8 indicates.

3.5.4 Fractography

Although no fractography study was made in this thesis, several unique characteristics of the fracture surfaces were noted.

The fracture surfaces of both the acicular ferrite steels exhibited irregularities known as "splits". These appear as sharp, deep, quasi-cleavage fractures normal to the fracture face and parallel to the plane of the plate (see Figures 3.11 - 3.16). Splitting is commonly observed on the fracture surfaces of full-scale tests of pipe made of AF steels and on impact specimens tested in the upper

shelf and transition temperature range. The effect of splitting on the absorbed energy is not fully established^(7,108-110).

Some workers have claimed that rolling AF steels below the Ar_3 temperature is a necessary prerequisite for splitting⁽¹⁰⁸⁾. However, the AF-1 steel was finish rolled at approximately 800°C, whereas AF-2 was finish rolled at about 760°C, both temperatures being above the 700°C Ar_3 temperature^(86,108). Others have suggested that even though HSLA AF steels are rolled above Ar_3 , at very low finish rolling temperatures where essentially no γ -recrystallization can occur, the elongation of the γ -grains is severe. The mechanical anisotropy thereby introduced may be the cause of splitting⁽¹⁰⁹⁾. This anisotropy is increased with decreased rolling temperatures.

The presence of Nb(C,N), which retards the γ -recrystallization, effects the degree of that splitting⁽¹⁰⁸⁻¹¹⁰⁾. The AF-1 steel contained 0.063 w/o Nb; AF-2 contained 0.05 w/o.

Killed steels have been said to have a greater tendency to split than do semi-killed steels⁽¹⁰⁸⁾. However, this was not observed in this study: the semi-killed AF-1 steel (0.03 w/o Si) had a slightly greater tendency to split than did the killed AF-2 material (0.26 w/o Si, 0.045 w/o Al).

Diesburg⁽⁷⁾ suggests that no distinct upper shelf energy plateau exists in that temperature range where splitting occurs, even though the fracture remains 100% ductile. Instead, the ductile fracture energy decreases with decreasing temperature and a sloping shelf is observed. Indeed, sloping energy curves were observed for the AF-2 steel. However, the AF-1 steel, which had the slightly greater tendency to split, had a distinct upper shelf plateau (compare Figures 3.23 - 3.24 and 3.15 - 3.16).

The splitting phenomena evidently is a result of a complex interaction of composition and processing variables. A complete understanding of the causes and effects of splitting in AF pipeline steels is still to be resolved.

3.6 Strain Age Study

Pipeline steel specifications call for high strengths and toughnesses in the as-rolled and the as-formed product. Pipe and fittings are subjected to plastic straining, after specification testing, particularly during field bending. Subsequent girth welding then provides the potential for strain aging. The potential for strain aging also exists in areas adjacent to seam welds since the initial cold pipe forming operations impart prior strain to the steel.

An IIT study was conducted to determine the effects of straining and the subsequent aging on the dynamic properties of the AF-1 and AF-2 pipeline steels.

This study was conducted in two parts. First, a characterization of the effects of straining and strain aging of the two steels was made. Second, for the AF-1 steel, impact specimens taken from near the seam weld were tested to determine if strain aging had occurred within the pipe.

3.6.1 Effects of Straining and Strain Aging

The effects of straining and subsequent aging on the IIT properties were examined in the AF-1 steel in two orientations:

1) for cracks running parallel to the pipe axis; and 2) for cracks running parallel to the rolling direction. The AF-2 steel, which had shown much less anisotropy, was tested only with cracks running parallel to the pipe axis.

To introduce a constant amount of strain into the test materials, large tensile bars were cut from the pipe. The reduced section of these bars was approximately 28 cm long and at least 55 mm wide to permit the cutting of a standard Charpy specimen. The tensile bars were cut from the pipe so that the straining direction was parallel to the Charpy crack

path. The grip areas were pressed flat, although the gauge length retained the original pipe curvature. Gauge marks were carefully scribed every 13 mm along the reduced section to allow determination of the actual strain after testing.

The bars were plastically strained 3-5% in uniaxial tension on a 100,000 kg tensile machine. This strain level approximates the combined maximum strain involved in fabrication and installation of pipe^(92,111-112). It should be emphasized, however, that this operation provided strain in excess of that already introduced due to the pipe forming operations.

After straining, the bars were stored in dry ice until Charpy specimens could be cut from the gauge section. Upon cutting the Charpy blanks from the strained bars, half the specimens were placed in stainless steel bags and aged in an air furnace for one hour at 275°C. This time and temperature was chosen to optimize the expected effects of strain aging⁽¹¹³⁾. Charpy specimens were then machined from the blanks, notched through the pipe thickness, and stored in dry ice until tested.

In all cases, control specimens taken from the pipe adjacent to the position from which the tensile bar was cut were first tested to establish the properties of the cold formed pipe. An

instrumented impact test temperature equivalent to the transition temperature of the as received pipe was chosen; if straining and strain aging produced any measurable change in dynamic properties, the magnitude of those changes would therefore be expected to be large.

The results of these tests are presented in Table 3.9. A measure of the ductility of the specimens was made by: 1) calculating the ductility index, DI; and 2) taking the difference between the time to maximum load, t_{MAX} , and the time to general yield load (elastic limit), t_{GY} , from the IIT load-time traces. This time should be directly related to the amount of strain occurring prior to plastic instability.

The shift in transition temperature was estimated by assuming that the strain and strain aging did not change the shape of the energy transition curves. A measured energy could then be associated with a specific temperature on the control specimen energy curve; the difference between this temperature and the test temperature was considered to be the shift in the transition temperature.

In general, the data show that the toughness and ductility of the AF-1 steel was reduced by straining and strain aging as its

Table 3.9

STRAIN AGE STUDY

Material	T (°C)	ET	EI	EP	DI	σ_{yd} (ksi)	$t_{MAX} - t_{GY}$ (ms)	TT Shift (°C)	R_B
		(ft - lb)							
AF-2-TR-CN	-60°	35.0	10.0	24.2	2.4	127.1	.247	-	94.2
AF-2-TR-S	-60°	46.4	13.5	32.9	2.4	137.3	.309	-30°	92.7
AF-2-TR-SA	-60°	64.2	16.6	47.7	2.9	145.7	.353	-91°	95.6
AF-1-TR-CN	-60°	10.9	1.7	9.2	5.4	>120.1	.117	-	91.2
AF-1-TR-S	-60°	11.1	2.1	9.0	4.3	109.8	.055	0°	93.8
AF-1 TR-SA	-60°	8.4	1.3	7.1	5.5	>120.7	.008	+ 4	94.0
AF-1-TP-CN	-30°	94.4	18.3	76.1	4.2	122.2	.434	-	92.4
AF-1-TP-S	-30°	89.1	19.0	70.1	3.7	135.1	.336	+ 5°	94.5
AF-1-TP-SA	-30°	81.0	17.3	63.7	3.7	139.0	.333	+12°	96.5
AF-1-TP-CN	-40°	84.5	14.4	70.1	4.9	129.0	.277	-	92.4
AF-1-TP-S	-40°	76.9	15.0	61.9	4.1	132.9	.264	+ 7°	94.5
AF-1-TP-SA	-40°	65.7	13.6	52.1	3.8	>138.2	.210	+14°	96.5

TR: Crack parallel to rolling direction

TP: Crack parallel to pipe axis

CN: Control specimens from pipe

S: 3-5% plastic strain

SA: strained and 1 hour at 275°C

All values are averages of several tests.

strength and hardness increased. It is significant to note that the strength, toughness, and ductility of the AF-2 steel all increased upon straining and subsequent aging.

Straining of the AF-1 steel produced the classic effects expected of a cold worked material: hardness and yield strength increased and the ductility decreased (as indicated by the observed decrease in $t_{MAX} - t_{GY}$ and decrease in DI) as the dislocation density increased⁽⁶⁹⁾. Consequently, the impact resistance was reduced as manifested by a decrease in the absorbed energy and a shift in the transition temperature to a higher temperature.

Subsequent strain aging of the AF-1 steel produced a further increase in strength and hardness, and a decrease in the ductility and the impact resistance. Others have observed a similar increase in the transition temperature in semi-killed AF steels, but without the loss of absorbed energy^(85,111).

It was not surprising that the AF-1 steel showed these effects. This steel was semi-killed (0.03 w/o Si), contained few nitride formers other than Nb, and thus, no doubt contained a high free nitrogen content⁽¹¹⁴⁾. It is well established that strain aging results from free interstitials, particularly carbon and nitrogen, diffusing to dislocations and locking them; acicular

ferrite steels are no exception^(111,113,115-116).

One significant observation from the AF-1 data, however, was that the decrease in total absorbed energy resulting from straining and strain aging was due primarily to a decrease in the crack propagation energy. The initiation energy was only marginally affected by either straining or strain aging. This observation is significant to the pipeline industry in particular. Although the total toughness of the AF-1 steel is adversely affected by straining (as could occur from field bending or frost heave) and strain aging (as could result from welding prestrained pipe), the initiation energy of the steel is not reduced. Therefore, though the AF-1 steel is susceptible to strain age embrittlement, it does not increase the potential for crack initiation.

One possible explanation for this important observation is that at the temperatures at which the AF-1 steel was tested (-30° and -40°C), the primary fracture mode for cracking parallel to the pipe axis was ductile. Figure 3.50 indicates that significant plastic flow was associated with the fracture event. The initiation of ductile failure is known to occur by void formation at inclusions or precipitates, either by interface separation or particle cracking^(5,117). The ductile crack propagates through the matrix as these voids coalesce between particles. The initiation

step in the fibrous crack process is therefore a function of the strength of the inclusions and/or the strength of the inclusion/matrix interface. The propagation stage of ductile fracture is dependent upon the matrix properties (strength, ductility). Straining and strain aging of the AF-1 steel was shown to increase the yield strength and decrease the ductility, the combination of which results in lower toughness. It is suggested that the matrix properties are primarily affected by these factors; the properties of the inclusions remaining relatively unaffected. This would explain why the crack initiation energy was unaffected, whereas the crack propagation energy was reduced with straining and strain aging.

The AF-2 steel gave much different results (Table 3.9). Not only did the strength increase with straining and aging, but so did the ductility. As this is a highly killed steel containing several nitride formers (Nb, Al, Ti, and La), a minimum concentration of free interstitials should be available to lock dislocations and therefore no strain aging effects would be expected⁽¹¹³⁻¹¹⁴⁾. However, the magnitude of the improvement in impact resistance with straining and aging was significant, the total energy increasing from 35 ft-lb to 64 ft-lb (47 - 87 J) with a 91°C improvement in transition temperature.

The AF-2 steel was probably underaged in the as rolled condition⁽⁷⁹⁾ and aging may have enhanced the Nb(C,N) precipitation⁽¹¹¹⁾. This increased precipitation could increase the ductility by retarding the dislocation motion and thus increasing the work hardening rate. The prior strain could have optimized the effective precipitate size as dislocation loops formed around the fine under-aged precipitates. This factor, plus the increased dislocation density, may have caused a significant increase in the work hardening rate, and hence, forced necking to occur at a higher plastic strain thereby increasing the observed ductilities.

In summary, the behaviour of the AF-1 and AF-2 steels with straining and aging was markedly different. The AF-1 steel exhibited the classic effects of cold work and strain aging, while the ductility and toughness properties of the AF-2 steel were significantly improved by straining and aging.

3.6.2 Strain Aged Sites in AF-1 Pipe

Having established that the AF-1 steel was susceptible to strain aging and recognizing the fact that the pipe forming operation imparts a degree of strain to the material (approximately 2-3%)^(111,118), a series of tests were performed to assess the presence of strain aged

embrittlement in the AF-1 pipe. The obvious location for a strain aged structure would be adjacent to the seam weld; this material would have been strained during the pipe forming operation and subsequently aged from the heat associated with the seam welding process. Although the properties of the weld bead and the heat-affected-zone (HAZ) have been documented^(85,119), no published work has been done to identify the strain aged site outside the HAZ in welded AF pipe, though the need for such a study has been recognized^(92,95).

Using welding parameters supplied by the pipe manufacturer, the peak temperatures versus distance from the HAZ were established (the pertinent calculations are included in Appendix E). At a position approximately 15 mm (0.6-in) from the weld fusion boundary a peak temperature of approximately 337°C was realized. Using cooling rate equations, it was further determined that this region of the pipe should experience temperatures optimum for strain aging for approximately 30 seconds (337° to 285°C)⁽¹¹³⁾ during the two-pass spiral welding process.

To check the reliability of a reported activation energy equation for strain aging HSLA steels⁽¹²⁰⁾, Charpy blanks were cut from a region well away from the seam weld. Using the relationship between time and temperature, several equivalent strain aging times

and temperatures were established. The Charpy blanks were aged at specific times and temperatures chosen to simulate the strain aging conditions predicted for the position 15 mm from the edge of the weld fusion boundary.

It should be noted that Rashid's equation:

$$\log t_1/t_2 = 7500 [1/T_1 - 1/T_2] \quad T_1 < T_2 \quad (\text{Eq. 3.7})$$

indicates that the HSLA steels will not strain age at room temperatures.*

After aging the blanks, standard Charpy specimens were prepared and notched so that the crack would propagate parallel to the pipe axis. Charpy control specimens with no aging treatment, only pipe forming strain, were also prepared.

In addition, Charpy specimens were also cut so that the structure below the notch was approximately 15 mm from the weld fusion boundary of the seam weld and had experienced the 337°C - 30 second

* An optimum strain age condition is 1 hour at 275°C = 548°K; the equivalent strain age time at room temperature (298°K) is:

$$\log t_1/1 = 7500[1/298 - 1/548]$$

$$t_1 \approx 3 \times 10^{11} \text{ hours !}$$

aging treatment. In actual fact, the structure below the notch had experienced a temperature gradient ranging from 285°C directly below the notch (19 mm from the weld fusion boundary) to 421°C at the opposite face (11 mm from the weld fusion boundary). Calculations are given in Appendix E. It was recognized that these Charpy specimens taken from near the seam weld actually experienced a range of aging conditions which could only be approximated by the artificially aged specimens. Nevertheless, should:

1. the artificially aged Charpys yield similar results upon impact testing - these results having different values from the IIT data of the nonaged control samples; and,

2. should the results compare reasonably well with those obtained from the "seam weld" specimens, then it could be concluded that the area near the seam weld had indeed experienced strain aging and that Equation 3.7 is applicable to the acicular ferrite steels studied.

Instrumented impact tests were conducted at -30°C, this being a temperature near the upper shelf transition region of the control specimens. Table 3.10 gives the results of this study.

The data shows:

1. that those samples artificially aged showed definite signs of strain aging - their yield strengths and hardness values

increased and their absorbed energies decreased relative to the values observed for the control specimens. A simple aging or stress relieving treatment, i.e., one for which no prior strain had been imparted to the specimens, should not have reduced the impact resistance^(85,111). This indicates that the pipe forming strains were sufficient to cause strain aging.

2. As in the previous phase of the strain age study, only the propagation energy was affected by strain aging; the initiation energies reported in Table 3.10 are constant for each aging condition.

3. Equation 3.7 was shown to be accurate in determining equivalent time/temperature strain aging conditions. The fact that the specimens aged 1 minute at 337°C gave a somewhat higher yield strength can be rationalized in that Rashid's equation actually predicts that 1 minute at 316°C or 1/2 minute at 330°C would give the equivalent strain age effects as the other three aging conditions.

4. The samples removed from adjacent to the seam weld showed a marked decrease in absorbed energy and an increase in yield strength and hardness; both are definite indications that the region had been strain aged. In fact, the properties near the seam weld indicated that the area had been strain aged to a greater extent than that estimated from the peak temperature and cooling rate calculations. However, those calculations were considered conservative.

Table 3.10

STRAIN AGE SITES IN STEEL AF-1

Age Treatment	ET	EI	EP	R_B	σ_{yd} (ksi)	Grain Size ASTM
	(ft - lb)					
As Formed Pipe	94.4	18.3	76.1	92.4	122.2	12.7
1 hr @ 244°C	85.5	18.2	67.2	93.3	127.9	
15 min.@ 266°C	84.5	18.1	66.4	93.2	127.6	
5 min. @ 289°C	84.0	19.0	65.0	95.0	129.2	
1 min. @ 337°C	83.4	19.2	64.2	93.9	134.0	
15 mm from seam weld	78.5	18.1	60.4	97.3	134.4	12.4

All notches parallel to pipe axis

All tests at -30°C

All values are averages of many tests.

A microstructural examination of the specimens taken from adjacent to the seam weld of the pipe indicated that no apparent structural modification could be associated with the observed change in properties, the microstructure and grain size being identical to that found in the control specimens.

It is important to note that the potential for crack initiation (EI) was not increased by strain aging, even near the weld. Thus, although sites do exist which have been strain aged in the AF-1 pipe, the effect of the strain aging is relatively small, the total energy still meeting the toughness specifications (78.5 ft-lb (106 J) at -30°C).

4. DYNAMIC FRACTURE TOUGHNESS

4.1 Introduction

A fundamental principle of fracture mechanics is that the stress field ahead of a crack can be characterized by a single parameter, K , the stress intensity factor. The magnitude of K is directly related to the crack size:

$$K \propto \sigma (\pi a)^{\frac{1}{2}} \quad (\text{Eq. 4.1})$$

where, σ = applied stress

a = sharp flaw size

thus providing the design engineer with a means of relating the defect size and allowable stress.

For a particular combination of stress and defect size, the stress intensity factor reaches a critical value, K_c , where unstable crack growth occurs. This critical value is described as the "fracture toughness" and is a basic property of a material.

This relationship is significant in that it allows considerable flexibility in design for fracture control. Trade-offs in material selection (K_c), design stress (σ), and allowable

flaw sizes (a), as determined by NDT flaw detection capability, can be made in a quantitative manner.

The critical stress intensity factor decreases to a minimum value as the thickness of a plate increases to a condition of maximum constraint where triaxial stresses exist at the tip of the notch. A condition of plane strain then exists since plastic deformation in the direction parallel to the crack front (through-thickness) is restricted. When tensile stresses are applied across the notch, fracture occurs by the crack surfaces being displaced normal to themselves (Mode I). This minimum plane strain value for Mode I type fracture is designated K_{Ic} .

Most structural steels exhibit such a high fracture toughness that for the available structural thicknesses, the K_{Ic} value cannot be measured. The linear-elastic analysis used to calculate $K_{Ic}^{(100)}$ is invalidated when insufficient specimen thickness results in general yielding and the formation of large plastic zones ahead of the crack tip. Elastic-plastic analyses have extended the fracture mechanics concepts to account for such behaviour⁽¹²¹⁾.

The value of K_{Ic} is determined for quasi-static conditions, that is, at strain rates of approximately 10^{-5} /s; this

is equivalent to a stress intensity rate, \dot{K} , of approximately 10 ksi-in^{1/2}/s, where \dot{K} is the ratio of K_{Ic} to the time required for fracture. For strain-rate sensitive materials, increasing the loading rate to that corresponding to an impact test, i.e., approximately 10/s ($\dot{K} \approx 10^5$ ksi-in^{1/2}/s), causes a decrease in the plane strain fracture toughness to a minimum value⁽¹²²⁻¹²³⁾. This value is called the dynamic fracture toughness, K_{Id} , and is generally the most conservative value of a material's fracture toughness at a given temperature.

For structural steels, at temperatures where cleavage failures occur, the static and dynamic values of the plane strain fracture toughness are approximately equivalent⁽¹²⁴⁻¹²⁵⁾.

The strain rate sensitivity of fracture toughness is explained by the increase in the yield strength with increasing loading rate (as with decreasing temperature). Increases in the yield stress imply a higher level of tensile stress in the plastic zone ahead of the crack and hence both a higher density of voids and easier void coalescence. The energy required for the ductile crack process is thereby lowered. Consequently, with increasing strain rate, the fracture toughness decreases⁽⁵⁾. For cleavage fracture initiation, however, since the cleavage strength is relatively insensitive to changes in the strain rate or temperature,

$$K_{Ic} \approx K_{Id} \quad (126).$$

Interestingly, it has been established that for some high strength titanium alloys and high strength steels ($\sigma_y > 145$ ksi), increasing the strain rate increases both the yield strength and the fracture toughness (i.e., $K_{Id} > K_{Ic}$). Although the reasons are not fully understood, the effect is thought to be due to adiabatic heating in front of the crack tip; the localized heating increases the energy required to deform the associated plastic zone by causing a relative decrease in the tensile properties⁽¹²⁵⁾.

The dynamic fracture toughness is useful for design purposes when: 1) conservative estimates of the fracture toughness are desired - as is the case in the nuclear power industry, or 2) dynamic loading conditions are expected in service.

Since large size specimens may be required to achieve plane strain conditions, the cost of machining the specimens and the intricate test procedures required have kept fracture toughness testing from being used in other than laboratory settings.

Instrumented impact testing using precracked Charpy specimens is currently receiving considerable attention as a relatively simple means of generating valid fracture toughness values

from fracture occurring in both the linear-elastic and elastic-plastic regimes. IIT has the advantage of being a rapid, inexpensive technique that employs small, easily machined test specimens. The impending standardization of IIT and the use of precracked Charpy specimens^(15,51-52,127) should encourage a wider acceptance of this test approach for obtaining fracture mechanics data.

4.2 The Calculation of Fracture Toughness Parameters from IIT Data

4.2.1 Linear-Elastic Fractures

For precracked Charpy specimens in which the fracture initiates prior to general yielding, i.e., when the maximum load, P_{MAX} , is less than the general yield load, P_{GY} , as in Figure 2.4b, the stress intensity factor can be calculated from⁽¹²⁸⁾:

$$K_{Id} = \frac{6 Y M a^{\frac{1}{2}}}{B W^2} \quad (\text{Eq. 4.2})$$

where, B = specimen thickness

W = specimen width

a = crack length (notch plus precrack)

M = applied moment at fracture

Y = $f(L/W, a/w)$

For three-point bend specimens (eg., Charpy specimens):

$$M = P_{MAX} L/4 \quad (\text{Eq. 4.3})$$

where, L = specimen support span

and:

$$Y = 1.93 - 3.07(a/w) + 14.53(a/w)^2 - 25.11(a/w)^3 + 25.8(a/w)^4 \quad (\text{Eq. 4.4})$$

For the calculated value of K_{Id} to be "valid", that is, for the value to represent plane strain conditions, the ASTM E 399 standard⁽¹⁰⁰⁾ stipulates that:

$$B, a, (W - a) \geq 2.5(K_{Ic}/\sigma_y)^2 \quad (\text{Eq. 4.5})$$

where, σ_y = yield strength at the test
temperature and loading rate

However, Tetelman, et al⁽¹²⁹⁾, have indicated that the central 90 percent of the Charpy specimen thickness is in plane strain so long as:

$$B \geq 1.6(K_{Ic}/\sigma_y)^2 \quad (\text{Eq. 4.6})$$

However, both Equations 4.5 and 4.6 were established for statically obtained fracture toughness parameters. The expressions from which K_{Ic} is derived may not be strictly valid for dynamic loading conditions⁽⁷²⁾.

Ireland has reported⁽¹⁴⁾ that the only validity requirement for K_{Id} in the tentative ASTM standard for instrumented impact testing shall be that fracture occur before general yielding, i.e.:

$$P_{MAX} < P_{GY} \quad (\text{Eq. 4.7})$$

The size requirements of Equations 4.5 and 4.6 have been reported to be too conservative for dynamic loading conditions^(27,35,130). (Of course, certain other criteria must be met in precracking the Charpy specimens⁽¹⁵⁾).

The criterion outlined in Equation 4.7 was employed in this work in assessing the validity of the K_{Id} measurements.

4.2.2 Elastic-Plastic Fractures

4.2.2.1 J-Integral

The J-Integral approach to general yielding fracture

mechanics⁽¹³¹⁻¹³⁴⁾ characterizes the stress-strain conditions existing near the crack tip in an elastic-plastic solid. The J-Integral is calculated by taking the load-displacement records from the same material for two different crack lengths and determining the change in potential energy for an incremental crack length change^(9,132), i.e.:

$$J = \frac{\partial (U/B)}{\partial a} \quad (\text{Eq. 4.8})$$

The J-Integral is also described as being the crack extension force per unit length of crack front, or the general fracture energy release rate per unit area. For elastic conditions, $J = G$, the elastic strain energy release rate⁽⁷²⁾.

The ASTM is presently preparing a proposed standard for J-Integral testing which is to supersede the plane strain fracture toughness standard, ASTM E 399⁽⁷²⁾. The main advantage in employing elastic-plastic toughness parameters for design is that valid test specimens can be one tenth to one hundredth the size of those required by E 399. Such a test shall have application for both linear-elastic and elastic-plastic failure conditions.

In practice, the calculation of the critical J-Integral value is dependent upon making the appropriate measurements to the point of crack initiation and calculating J_{Ic} from the expression⁽¹³³⁾:

$$J_{Ic} = \frac{2A}{B(W - a)} \quad (\text{Eq. 4.9})$$

where, A = area under the load-deflection
curve to the point of crack
initiation

Several techniques are used to determine the point of crack initiation in slow bend J-Integral tests, including ultrasonics and electrical resistance. The common, though tedious method is to load several specimens to various deflections and to determine the extent of crack growth in each specimen by heat tinting. A plot of the applied J-Integral versus the extent of cracking is made and the data is extrapolated back to the crack initiation condition to give J_{Ic} ⁽⁷²⁾.

For IIT, crack initiation is assumed to occur at the point of maximum load. Thus, the critical dynamic J-Integral, J_{Id} , is determined by substituting the initiation energy, EI, for A in Equation 4.9. From this expression, the elastic-plastic stress intensity factor can then be calculated:

$$K_J = (EJ_{Id})^{\frac{1}{2}} \quad (\text{Eq. 4.10})$$

where, E = elastic modulus

This calculation is necessarily nonconservative when crack initiation precedes the point of maximum load. Elaborate test techniques for more accurately determining the point of initial crack extension in a Charpy specimen during instrumented impact testing are being developed⁽¹³⁵⁾. Such procedures have been shown to provide a better estimate of the J-Integral when considerable yielding transpires prior to maximum load. However, even when assuming that P_{MAX} indicates the point of crack initiation, good correlations between the J-Integral stress intensity factor determined from IIT and valid K_{Id} values for steels have been obtained⁽⁷⁵⁾.

The ASTM Committee concerned with standardizing this technique for IIT⁽¹²⁷⁾ has suggested that for fibrous crack initiation, the specimen thickness requirement be⁽²⁷⁾:

$$B > \frac{25 J_{Id}}{\sigma_F} \quad (\text{Eq.4.11})$$

where, σ_F = flow stress = average of yield stress
and ultimate stress $\approx \sigma_y + 10$ ksi

and, for cleavage initiation:

$$B > 50 J_{Id}/\sigma_F \quad (\text{Eq.4.12})$$

4.2.2.2 Crack Opening Displacement

This method of determining the elastic-plastic fracture toughness relies on a knowledge of the strains at the crack tip at point of failure⁽¹³⁶⁾. In applying instrumented impact test information to determine a COD value it is again assumed that crack initiation occurs at the point of maximum load. The specimen deflection at the point of crack initiation, d_i , can then be calculated as described in Section 2.3.2.2.

Once the initiation deflection has been established, a calculation of the crack opening displacement, COD, may be made, which for the Charpy-geometry can be expressed as⁽⁴⁸⁾:

$$\text{COD} = 2.54[r(W - a)]d_i \quad (\text{Eq. 4.13})$$

where, r = rotational ratio

There is still controversy over the computational methods for establishing a COD value⁽⁷²⁾. In particular, the value to be assigned to the rotational ratio, which is a measure of the hinge distance below the crack tip, remains to be settled. Values for r ranging from 0.20 to 0.50 have been cited for IIT^(23,48,105,137-139). In this work, for sake of computational consistency, a commonly

accepted value of 0.33 was selected for the rotational ratio.

Once the COD has been calculated, the strain energy release rate, G_d , may be determined⁽¹⁴⁰⁾:

$$G_d = (COD)(\sigma_{yd}) \quad (\text{Eq. 4.14})$$

from which⁽⁹⁾:

$$K_{COD} = (G_d E)^{\frac{1}{2}} \quad (\text{Eq. 4.15})$$

It should be noted that when fracture occurs prior to general yield, the dynamic yield strength cannot be determined from IIT. Therefore, the COD stress intensity factor can be calculated only for elastic - plastic fractures.

Vitek and Chell⁽¹⁴¹⁾ report that post yield fracture toughness calculations for fast fracture are best based upon the J-Integral criterion, whereas for time dependent failure (slow crack growth) the COD method is more suitable.

4.2.2.3 Equivalent Energy Method

The equivalent energy method for calculating the stress intensity factor assumes that had a sufficiently large sample been

employed, fracture would have occurred prior to general yield, under plane strain conditions, at any energy corresponding to that of the initiation energy of the smaller test specimen⁽¹⁴²⁾. The load at which the larger specimen would have fractured is established by extrapolating the linear slope of the elastic region of the smaller specimen's load-time curve so that the area under this extrapolated curve equals that corresponding to the energy to maximum load for the small specimen. This "equivalent energy" load is then used to calculate the stress intensity factor, K_{EE} , as per the equation for linear-elastic fracture (Equation 4.2).

Although Robinson and Tetelman⁽¹⁴³⁾ have criticized this method as being far too nonconservative, others claim that the values obtained for K_{EE} from IIT correlate better with large specimen K_{Ic} values than do the IIT K_J parameters⁽¹⁴⁾.

4.2.2.4 Critical Crack Sizes

Many functions relating the fracture toughness, applied stress, and flaw size have been determined for a variety of specimen configurations⁽¹⁴⁴⁻¹⁴⁶⁾.

For pipeline applications, a through-wall flaw is considered to be the most severe defect. The critical length of such

a flaw, i.e., the length at which unstable crack propagation occurs, can be determined from:

$$K_{Ic} = \sigma_f (\pi a)^{\frac{1}{2}} \quad (\text{Eq. 4.16})$$

where, σ_f = applied stress to initiate unstable
crack growth

$2a$ = sharp flaw length

4.3 Dynamic Fracture Toughness of Pipeline Steels

The fracture toughness parameters described in the previous Section were calculated using data obtained from the precracked Charpy IIT load-time traces. These data are graphically presented in Figures 4.1 to 4.6 for each orientation of the AF-1 and AF-2 steels. The J-Integral validity requirements were applied to the data and those values of K_J not meeting these criteria have been separated with a dashed line in each Figure.

It can be seen that for both steels there was a sharp temperature transition in the J-Integral dynamic fracture toughness in all test directions except in the rolling direction; the transition was much sharper than the corresponding energy transitions for the same precracked specimens. At the bottom shelf of these transition curves, K_{Id} data correlated well with the K_J values. The COD stress

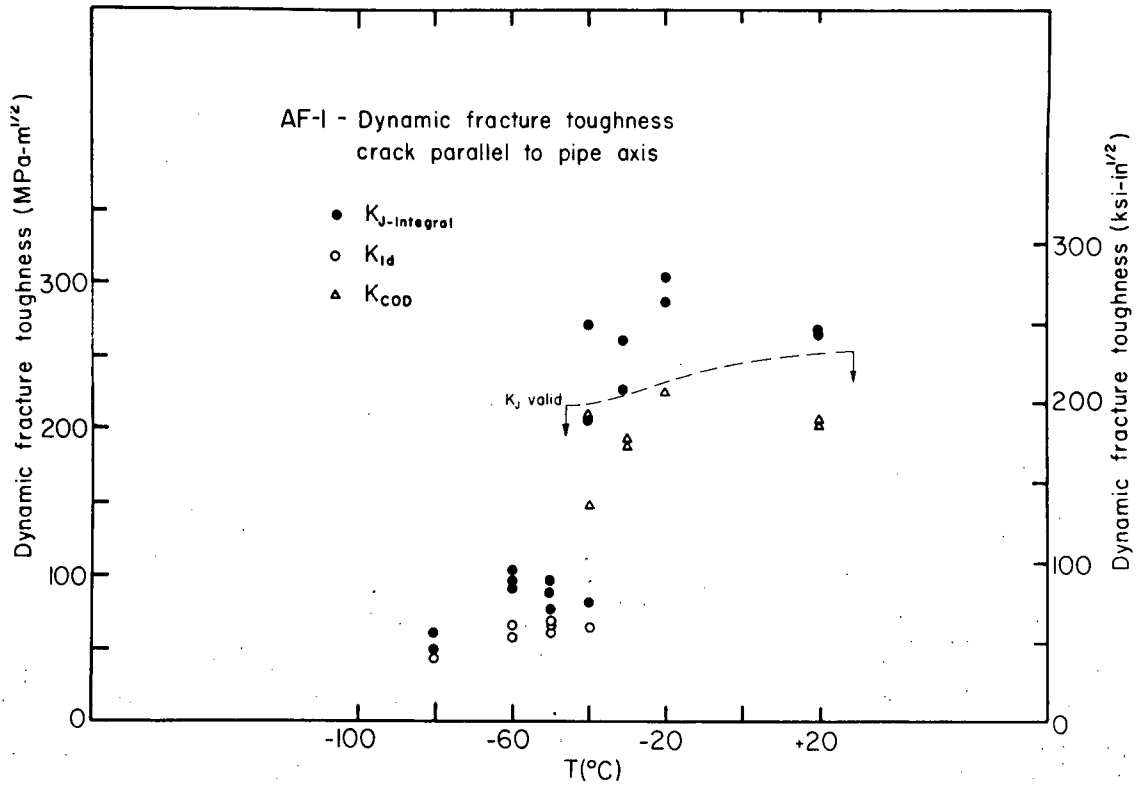


Figure 4.1

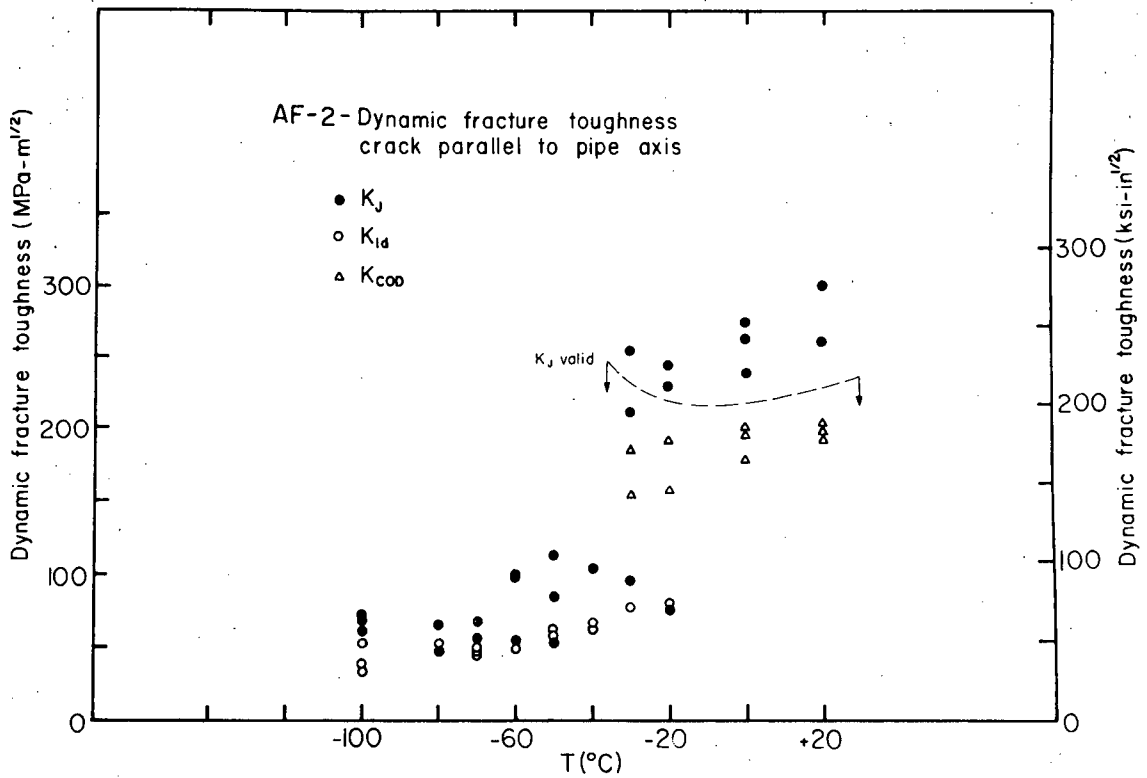


Figure 4.2

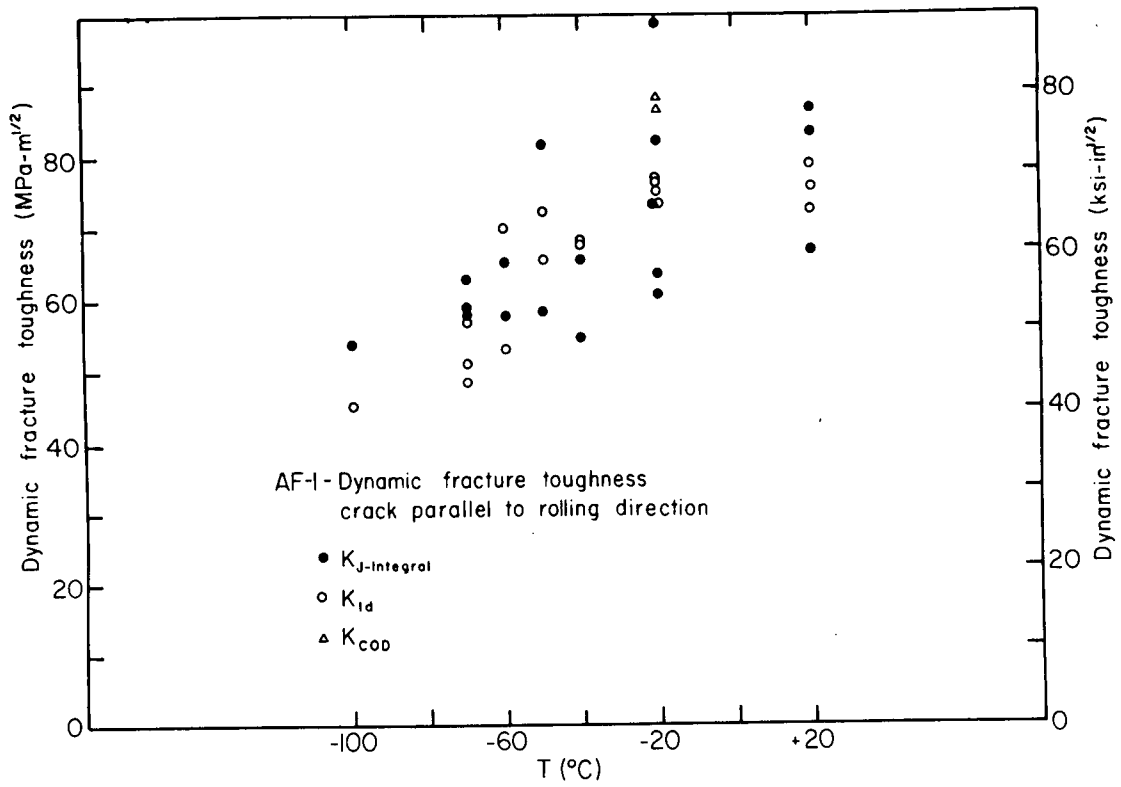


Figure 4.3

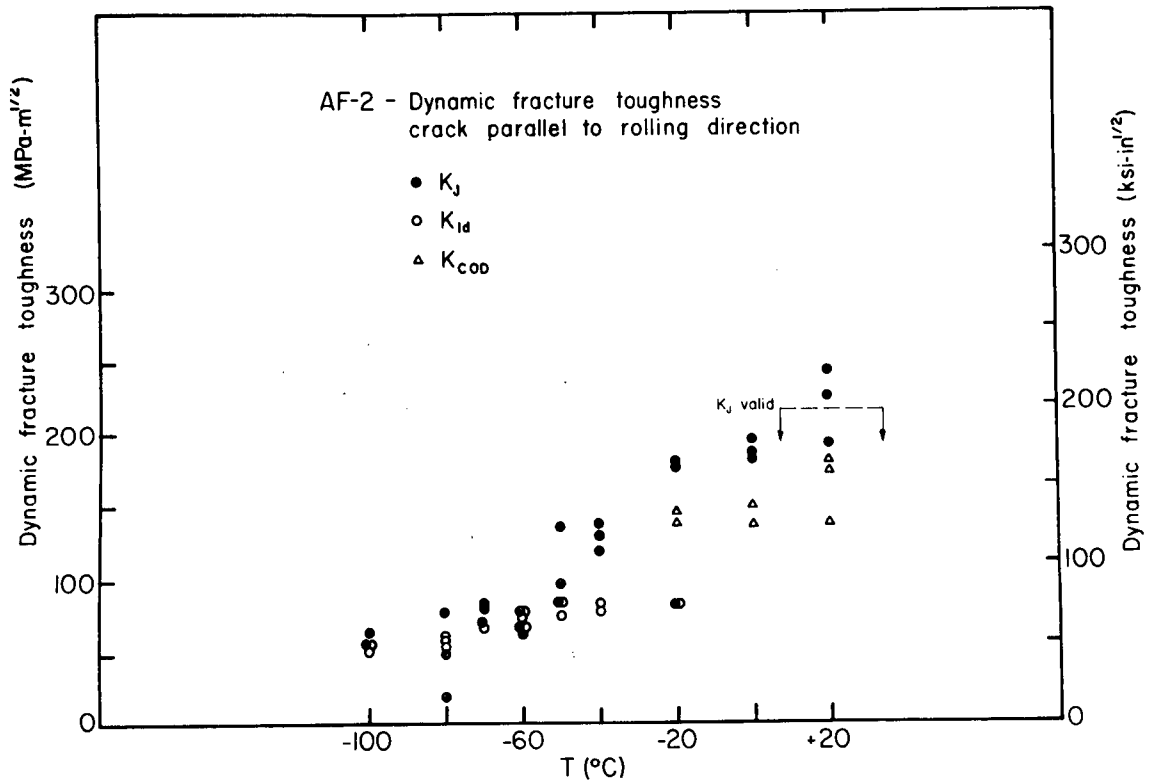


Figure 4.4

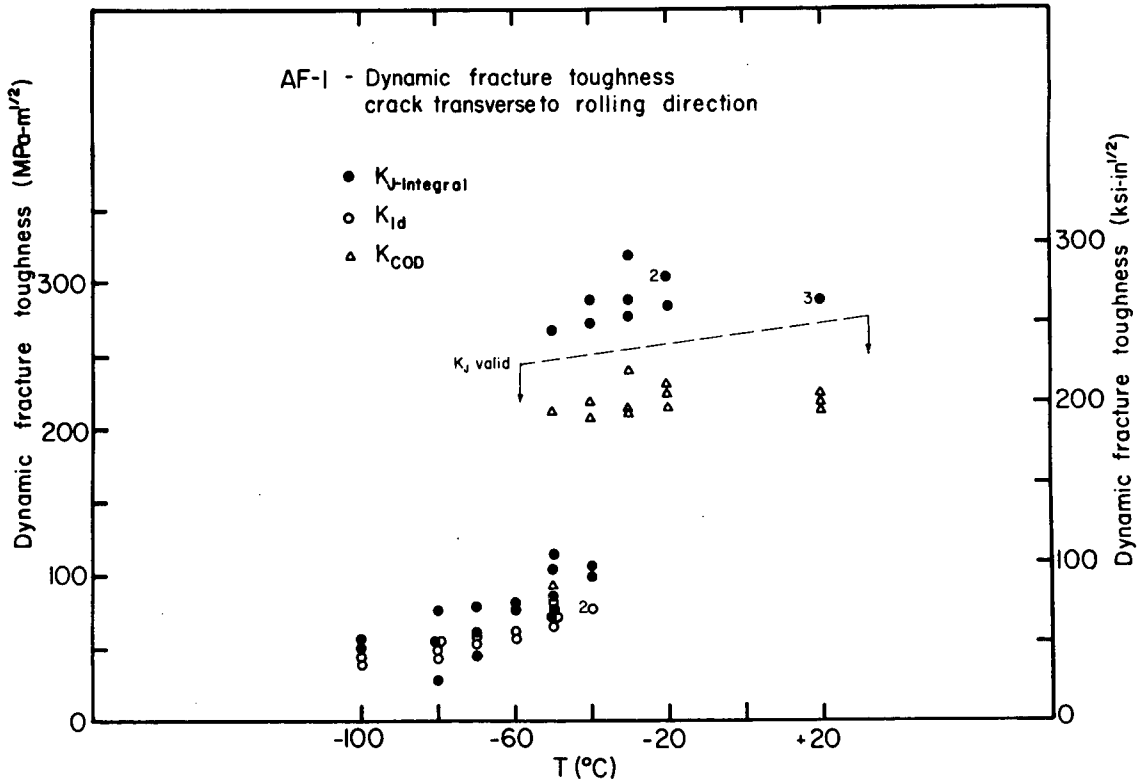


Figure 4.5

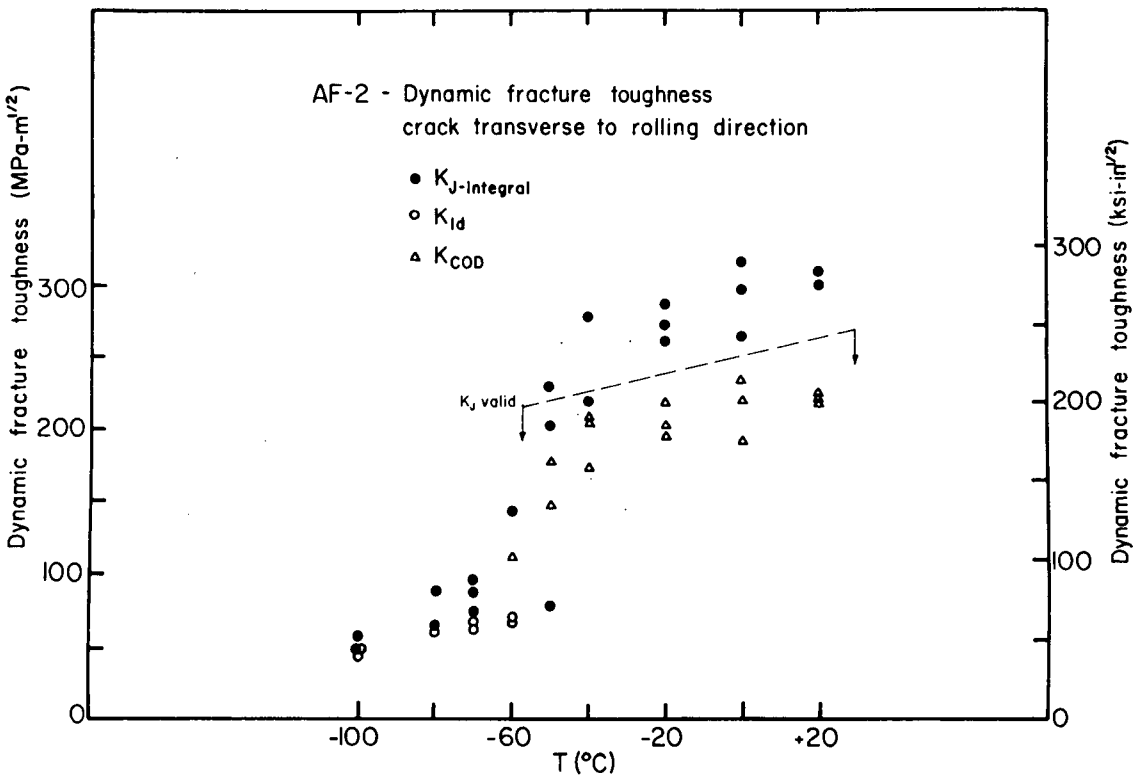


Figure 4.6

intensity factors lay along the upper shelf. This fracture toughness transition coincided with the onset of fracture prior to general yielding; it is assumed that plane strain conditions existed across much of the specimen thickness and cleavage fracture was the dominant mode of fracture^(7,124).

Table 4.1 lists the transition temperatures for the fracture toughness curves (from Figures 4.1 - 4.6), the precracked Charpy initiation energy curves (from Figures 3.36 - 3.44), the Drop Weight Tear Test percent shear (Figures 3.45 and 3.47), and the standard Charpy total energy curves (Figures 3.17 - 3.25). It is significant that the transition temperatures are equivalent for all but the standard Charpy total energy curves. The transition for those curves occurred over a wide range of temperatures and at a lower temperature than the sharp transitions of the fracture toughness, precracked initiation energy, and DWTT percent shear.

Barsom and Rolfe⁽¹⁴⁷⁾ have shown that at the low end of the fracture toughness transition temperature curve, the mode of initial crack extension is cleavage. At the upper end, the initiation mode is ductile tearing. In the transition region, both modes occur. Since the critical fracture toughness describes a crack initiation event, it is not surprising that the precracked Charpy initiation energy curve has the same general shape and transition temperature as the fracture

Table 4.1

TRANSITION TEMPERATURES

	Crack Parallel to Pipe Axis				Crack Parallel to Rolling Direction			Crack Transverse Rolling Direction		
	K	EI _{pc}	DWTT	ET _{std}	K	EI _{pc}	ET _{std}	K	EI _{pc}	ET _{std}
AF-1	-40	-40	-45	-60	lower shelf	lower shelf	-60	-50	-50	-70
AF-2	-30	-30	-30	*	-50	-50	-85	-55	-50	-80

All temperatures in °C

* No sharp transition.

toughness.

It is interesting, however, that the fracture toughness transitions for the material tested in the pipe axis orientation coincided well with the Battelle-Drop Weight Tear Test percent shear transition (Table 4.1). The fracture toughness transition is believed to be due to a change in the microscopic initiation mode; the DWTT is primarily a measure of the propagation mode.

In general, the values of K_J were greater than those of K_{COD} . The calculation of both parameters is based upon the assumption that the crack initiates at the peak load. Thus, when considerable general yielding occurs prior to the attainment of maximum load, these values tend to be nonconservative. However, the K_J calculation employs the area under the load-time curve to the point of maximum load, whereas that of K_{COD} requires only the deflection to maximum load. Thus, K_{COD} is a more conservative measure of a material's dynamic elastic-plastic fracture toughness than is K_J .

In general, the reproducibility of all the fracture toughness data was excellent; standard deviations of less than 10% were obtained, which is within the expected scatter band for static K_{Ic} data⁽¹⁴³⁾.

The AF-1 and AF-2 steel exhibited comparable dynamic fracture toughness when tested with the crack running parallel to the pipe axis (Figures 4.1 - 4.2). However, the AF-2 steel showed a marked transition at -30°C , 10°C higher than that of the AF-1 material.

Data from Tables 3.3 and 3.5 have been included in Table 4.2 and indicate that for the pipe axis orientation, the AF-1 steel absorbed far more energy in a standard Charpy test than did the AF-2 steel, in the temperature range from -40° to -60°C . However, as shown in Table 4.2, their fracture toughness values are virtually equivalent. Notice also, though, that the precracked Charpy

Table 4.2

FRACTURE TOUGHNESS AND ENERGY DATA

Material	Orientation	ET_{std}	K_{Id}	EI_{pc}
AF-1	Parallel Pipe Axis	75 ft-lb	$60 \text{ ksi-in}^{\frac{1}{2}}$	9 ft-lb/in^2
AF-2	Parallel Pipe Axis	31 ft-lb	$55 \text{ ksi-in}^{\frac{1}{2}}$	9 ft-lb/in^2
AF-1	Parallel Rolling Direction	14 ft-lb	$62 \text{ ksi-in}^{\frac{1}{2}}$	5 ft-lb/in^2

All data for -50°C

initiation energies were equal for both steels in this orientation. Since the critical fracture toughness describes a crack initiation event, it would be expected that the two materials have similar K_{Id} values if their crack initiation energies were similar. A standard Charpy test would mask such vital information, however. Although overall the AF-1 steel had greater total absorbed Charpy energies than did the AF-2 steel, precracked initiation energies of the two materials were generally similar. This equivalence of crack initiation energy was manifested in the very similar fracture toughnesses of the two steels.

It should be noted that the AF-2 steel precracked Charpy data showed some linear-elastic fractures at -20°C . At that temperature, that steel's average K_{COD} was $162 \text{ ksi-in}^{\frac{1}{2}}$ ($178 \text{ MPa-in}^{\frac{1}{2}}$), though the mean K_{COD} for the AF-1 steel was $207 \text{ ksi-in}^{\frac{1}{2}}$ ($228 \text{ MPa-in}^{\frac{1}{2}}$). Using Equation 4.16, this represents a variance in the critical through-wall flaw size of over 3 inches (7.6 cm) for a pipeline operating at a stress of 56 ksi (386 MPa) (5.3 in [13.5 cm] for AF-2; 8.7 in [22.1 cm] for the AF-1 steel). Both flaw sizes are quite large, however, and could be detected as leaks prior to unstable crack propagation⁽⁹⁾.

The biggest differences between the fracture toughness values of the two steels were observed for tests in which the crack

was parallel to the rolling direction (Figures 4.3 and 4.4). Although neither steel showed a sharp transition, the AF-2 steel exhibited a higher fracture toughness; valid K_J values for temperatures from +20°C to -100°C were 175 to 57 ksi-in^{1/2} (193-62 MPa-in^{1/2}). The K_J values for the AF-1 steel in that same temperature range were only 72 to 54 ksi-in^{1/2} (79-59 MPa-m^{1/2}).

The absorbed Charpy energy of the AF-1 steel in this direction, particularly the initiation energy, was essentially at lower shelf over the complete temperature range. It is likely that the MnS inclusions, aligned along the rolling direction during hot rolling, are responsible for the relatively low fracture toughness values observed. The AF-2 steel, treated with rare earths, maintained a high toughness even in the rolling direction. This detrimental effect of elongated inclusions on fracture toughness has been observed by others⁽¹⁴⁸⁾.

At -20°C, assuming a failure stress of 56 ksi (386 MPa) and an average K_{COD} of 128.5 ksi-in^{1/2} (141 MPa-in^{1/2}), the AF-2 steel in the rolling direction had a critical through-wall defect size of 3.4-in (8.5 cm). The AF-1 steel, using a mean K_{Id} value of 68 ksi-in^{1/2} (75 MPa-in^{1/2}) had a critical flaw size of only 0.9-in (2.3 cm).

It is known that strain age embrittlement can occur near the welds in pipelines and that this could reduce the fracture toughness. In addition, residual stresses in these regions can attain a stress level equal to that of the yield strength of 70 ksi (483 MPa). Under such conditions, the critical flaw size for the AF-1 pipe in the rolling direction would be less than 0.6-in (1.5 cm); this estimate does not account for the loss in fracture toughness that might be associated with the strain age embrittlement.

Specifying a minimum toughness of 50 ft-lb (68 J) in the pipe axis orientation is equivalent to ensuring a minimum critical flaw size of approximately 6-in (15.2 cm) in this direction (Table 3.1)⁽⁹⁵⁾. Since the critical flaw size is approximately 1/10 of this value for a crack running parallel to the rolling direction, this direction must be included in any pipeline specification imposed to restrict fracture initiation.

It should be noted that for the AF-1 steel, a significantly higher total absorbed energy is required in the pipe axis orientation as compared to parallel to the rolling direction. However, the fracture toughness data is similar in both directions from - 50°C and below, as shown in Table 4.2 (also refer to Table 3.3 and Figures 4.1 and 4.3). The initiation energies for the precracked Charpy specimens for these two orientations are equivalent, in this

temperature range, thus explaining this apparent discrepancy (Tables 4.2 and 3.5).

Both steels showed equivalent fracture toughness in specimens oriented with the crack transverse to the rolling direction (Figures 4.5 and 4.6). The absorbed Charpy energy values were also quite similar (Table 3.3). The AF-1 steel showed a transition from -40° to -50°C , whereas the AF-2 material's fracture toughness transition was more gradual, occurring over the range from -40°C to -60°C . Within these transition ranges both linear-elastic and elastic-plastic failures were observed.

At -20°C , employing K_{COD} values of $188 \text{ ksi-in}^{\frac{1}{2}}$ for AF-2 and $206 \text{ ksi-in}^{\frac{1}{2}}$ for AF-1 (207 and $227 \text{ MPa-in}^{\frac{1}{2}}$) and an applied stress of 56 ksi (386 MPa), the critical through-wall flaw sizes would be 7.2-in (18.3 cm) and 8.6-in (21.8 cm), respectively, both quite large.

4.4 Correlations

4.4.1 Relationship Between Dynamic Stress Intensity Factor and Crack Initiation Energy

A fundamental relationship for plane strain fracture is (5,9):

$$K_{Ic} = [EG_{Ic}/(1 - \nu^2)]^{1/2} \quad (\text{Eq. 4.17})$$

The term G_{Ic} is defined as the critical elastic energy release rate and can be described as being the work required to initiate unstable fracture at the tip of a flaw. Through Equation 4.17 it can be seen that the stress intensity and energy approaches to fracture toughness are equivalent.

In instrumented impact testing, when fracture occurs prior to general yielding, unstable crack growth begins at the point of maximum load⁽²⁷⁾. The parameter G_{Id} can therefore be associated with the energy to maximum load, i.e., the crack initiation energy, EI per unit area. Thus, should plane strain conditions exist, Equation 4.17 can be modified such that:

$$K_{Id}^2/E = \frac{1}{(1 - \nu^2)} \cdot \frac{EI}{A} \quad (\text{Eq. 4.18})$$

where, E = elastic modulus

A = ligament area of Charpy specimen

Koppenaar⁽⁵⁹⁾ in an IIT study showed a correlation between

K_{Id} and the crack initiation energy where, of course, both terms were measured under equivalent strain rates. Others^(60,72-73,149) have attempted similar correlations, with and without IIT, by assuming the total energy absorbed by the precracked specimens could be related to K_{Ic} (or K_{Id}) through the relationship:

$$K_{Ic}^2/E = \frac{1}{2(1 - \nu^2)} \frac{ET}{A} \quad (\text{Eq. 4.19})$$

These correlations were not based on sound principles for one or more of the following reasons:

1. K_{Ic} is defined by conditions existing at point of crack initiation, whereas the measurement of ET/A involves the total fracture process;
2. the factor of $1/2$ in Equation 4.19 was explained by Ronald⁽¹⁴⁹⁾ on the basis of two surfaces being created at fracture, although that fact was accounted for in the basic definition of G_{Ic} ; that Ronald⁽¹⁴⁹⁾ and others⁽⁶⁰⁾ showed a correlation between K_{Ic} and $ET/2A$ was fortuitous, since it was later shown⁽⁵⁹⁾ that for the materials they studied (high strength Ti-alloys) $ET/2A \approx EI/A$;
3. in some instances, K_{Ic} was measured under slow bend conditions but the data for ET/A was obtained at an impact loading rate; no correlation should be expected for strain-rate sensitive materials.

All the K_{Id} data for which fracture occurred prior to general yielding has been plotted against the corresponding precracked Charpy crack initiation energies in Figure 4.7.

Not all of the K_{Id} values calculated in this study could be considered valid according to the ASTM E 399 criterion⁽¹⁰⁰⁾ which requires a minimum thickness for plane strain conditions (Equation 4.5), nor for the more liberal restriction cited in Equation 4.6. Those data that did meet those respective plane strain criteria have been so distinguished in Figure 4.7.

It is significant that for the data obeying the most conservative validity criterion, $B > 2.5 (K_{Id}/\sigma_y)^2$, excellent agreement exist between the theoretical and the measured relationship between EI and (K_{Id}^2/E) . The initiation energy thus appears to be a reasonable estimate of G_{Id} for those tests adhering to that requirement.

The specimens meeting the stipulation that their thickness be greater than $1.6 (K_{Id}/\sigma_y)^2$ displayed somewhat more scatter, but their data still agreed well with the theoretical line.

However, those specimens meeting only the $P_{MAX} < P_{GY}$ criterion, which is to be employed in the tentative ASTM IIT

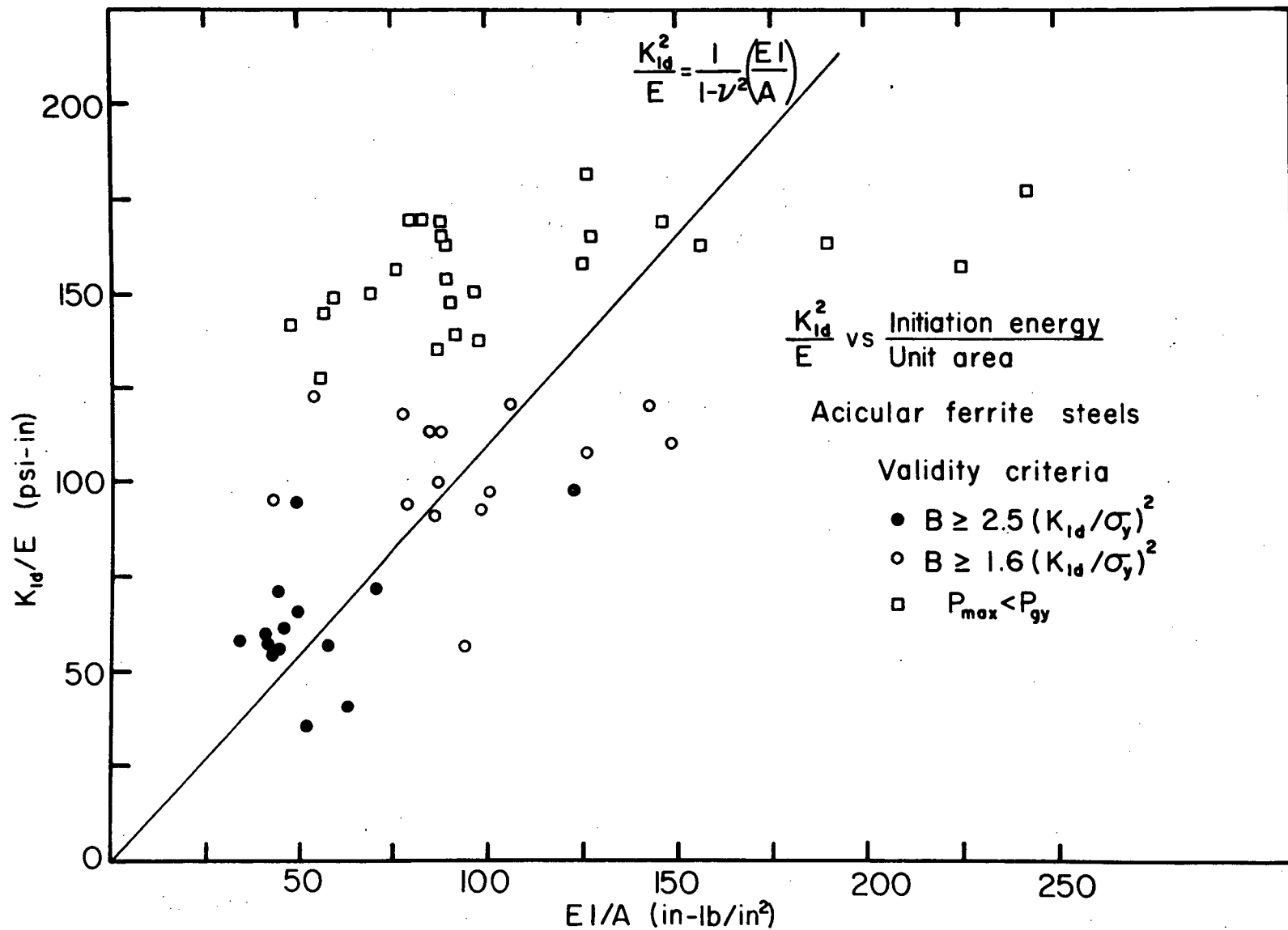


Figure 4.7 K_{Id}^2/E vs initiation energy for acicular ferrite IIT
 K_{Id} data meeting different validity requirements.

standard, show the greatest scatter, and little, if any, relationship to the theoretical line. This means that $P_{MAX} < P_{GY}$ is an insufficient criteria for ensuring plane strain conditions.

Apparently for such specimens, the initiation energy as measured from the IIT load-time trace includes factors other than those strictly associated with G_{Id} . Possibly, energy losses due to subcritical crack growth (doubtful for cleavage fractures occurring prior to general yielding) or plastic indentation at the contact points during impact (Brinell energy, E_B , in Section 2.3.2.1.2) are significant. It is also possible that the limited ligament depth below the crack in a Charpy-size specimen may preclude a true measurement of a material's fracture resistance. The ASTM E 399 validity criterion (Equation 4.5) stipulates a minimum crack size(a) and ligament depth ($W-a$), in addition to thickness (B), so that the stress field ahead of the crack approximates that in a linear-elastic body⁽⁷²⁾. This crack length and ligament depth requirement is not met by the small Charpy specimens.

It should also be emphasized that the definition of G_{Id} is the change in strain energy, U , with a change in crack length (dU/da)⁽⁹⁾. The initiation energy, however, has been normalized by dividing by the total precracked Charpy ligament area, i.e., EI/A , since no accurate measure of the ligament depth associated with the initial crack extension is possible. The initiation energy EI may indeed be

equivalent to U , but the precracked Charpy ligament area, A , is definitely not equal to da . Thus EI/A would be expected to be a conservative estimate of $G_{Id}^{(22)}$.

The data also indicate that the ASTM E 399 thickness requirement provides a more conservative K_{Id} value, as shown in Table 4.3.

4.4.2 Comparisons Between K_{Id} and Statically Obtained K_{Ic}

Due to the relatively high fracture toughness of acicular ferrite steel and the limited thickness of the controlled rolled plates used to produce the line pipe, valid K_{Ic} data is impossible to obtain except perhaps at very low temperatures. Indeed, no references to the linear-elastic plane strain fracture toughness of AF pipeline steels could be found in the literature.

Diesburg⁽¹⁵⁰⁾ has reported the results of a J-Integral study of an acicular ferrite, aluminum killed, rare earth treated steel very similar in composition to the AF-2 steel examined in the present work. Using compact tension specimens and the procedure described by Landes and Begley⁽¹³⁴⁾, the quasi-static J-Integral plane strain fracture toughness was determined.

Table 4.3

K_{Id} VALUES FOR DIFFERENT VALIDITY CRITERIA

Material Code	T(°C)	σ_{yd} (ksi)	$K_{Id}(\text{ksi-in}^{\frac{1}{2}})$ $B > 2.5(K_{Id}/\sigma_{yd})^2$	$K_{Id}(\text{ksi-in}^{\frac{1}{2}})$ $B > 1.6(K_{Id}/\sigma_{yd})^2$	$K_{Id}(\text{ksi-in}^{\frac{1}{2}})$ $P_{MAX} < P_{GY}$
AF-1-TR	-50	122.7	-	59.0	65.0
AF-1-TR	-60	119.1	47.1	55.9	63.0
AF-2-TR	-60	126.6	-	61.7	68.6
AF-1-TP	-50	139.0	55.4	62.8	-
AF-1-LR	-50	126.5	-	61.9	70.4

A comparison of Diesburg's results with the dynamic J-Integral fracture toughness obtained from the IIT approach is shown in Figure 4.8. An excellent correlation exists, the fracture toughness values being nearly equivalent at all temperatures.

Dynamic fracture toughness data is generally expected to be slightly more conservative than statically obtained values. This was observed above -20°C , although only small differences are apparent. However, no consistent deviation is evident below that temperature. Diesburg reported that the cleavage fracture transition temperature was -18°C . Hahn and coworkers⁽¹⁵¹⁾ have shown that the rate sensitivity of K_{Ic} decreases with increasing yield strength and decreasing temperature. In addition, for low and medium strength structural steels there appears to be little strain rate sensitivity in the plane strain fracture toughness where cleavage fracture dominates (124-125,152). It appears that the fracture toughness of this AF steel is not sensitive to increasing strain rate where cleavage fracture occurs.

In a separate study, Akhtar⁽¹⁵³⁾ measured the fracture toughness (ASTM E399) of a section of a X70 pipe nominally 42-in (106.7 cm) O.D., 0.425-in (10.8 mm) wall thickness. This steel had a reduced-pearlite (RP) microstructure and contained 0.15 w/o C, 1.6 w/o Mn, 0.05 w/o Nb, and 0.12 w/o Cr. The pipe had been formed

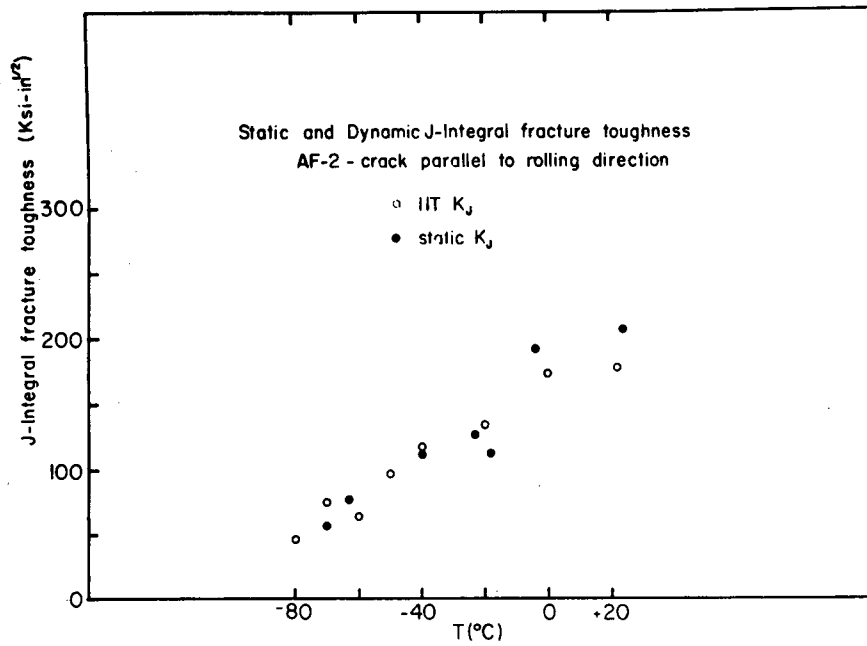


Figure 4.8

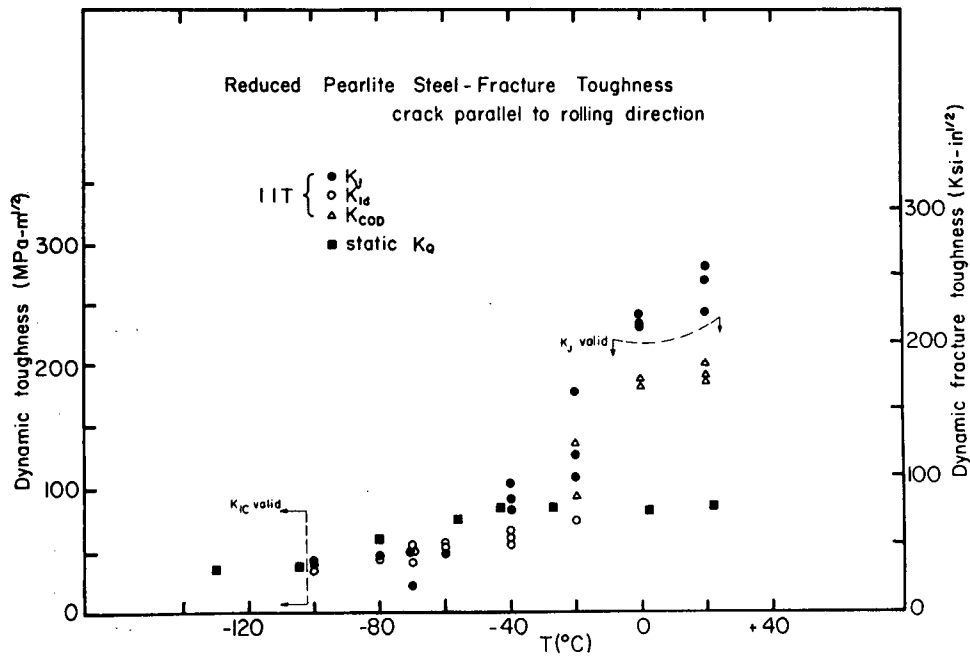


Figure 4.9

by the U.O.E. process and therefore the longitudinal pipe axis was the same as the rolling direction.

However, due to the thickness limitation, Akhtar's data was estimated to be valid (plane strain) only at temperatures below -105°C !

Instrumented impact tests with the crack following the pipe axis (rolling direction) were conducted on this same material.* Both the static and dynamic fracture toughness results are shown in Figure 4.9.

For temperatures at which the static K_{Ic} value was valid (approximately -105°C and below), Figure 4.9 shows that the IIT values, K_J and K_{Id} , yield equivalent results.

It thus appears that where fracture occurs by cleavage, $K_{Ic} \approx K_{Id}$ for both acicular ferrite and reduced pearlite steels.

Barsom⁽¹⁵²⁾ has shown that the fracture toughness transition temperature for impact loading tests ($\dot{\epsilon} \approx 10/\text{s}$) is shifted to higher

* Supplied by The British Columbia Hydro and Power Authority, Materials Research Center, Vancouver, B.C.

temperatures than that obtained by static loading ($\dot{\epsilon} \approx 10^{-5}/s$). He presents an equation which predicts the magnitude of this shift:

$$T_{\text{shift}} = 119 - 0.12\sigma_{ys} \quad (\text{Eq. 4.20})$$

$$\text{for, } 250 \text{ MPa} < \sigma_{ys} < 965 \text{ MPa}$$

where, T_{shift} = magnitude of shift in fracture
toughness transition temperature
between slow and impact loading
conditions, °C

σ_{ys} = room temperature yield strength, MPa

For this reduced pearlite steel ($\sigma_{ys} \approx 483 \text{ MPa}$) the static K_{Ic} transition was at approximately -80°C . The IIT K_{Id} transition occurred at approximately -20°C (Figure 4.9), a shift of 60°C . This is in excellent agreement with Equation 4.20 which predicts a shift of 61°C !

The static versus dynamic fracture toughness correlations shown in Figures 4.8 and 4.9 are among the few reported for pipeline steels, and in both cases they indicate that the IIT technique produces fracture toughness data which is in excellent agreement with the "accepted" statically measured values.

4.4.3 Critical Flaw Sizes

The Battelle ductile fracture initiation equation:

$$\frac{K^2 \pi}{8c \sigma_F^2} = \ln[\sec(\pi M \sigma_p / 2 \sigma_F)] \quad (\text{Eq. 3.2})$$

was employed to calculate the critical crack lengths for a sharp through-wall flaw for the RP and for the AF materials. The Folias correction, M, in Equation 3.2 is a function of the crack length ($\approx (1 + 1.255 c^2/Rt)^{1/2}$), so a graphical procedure was used to solve for "c". For comparison purposes, critical crack sizes were also calculated from the IIT fracture toughness data using Equation 4.16.

The Battelle calculation employs the standard Charpy upper shelf energy as a measure of the fracture toughness and is therefore empirical. This Charpy energy is related to the fracture toughness by the equation⁽⁹⁶⁾:

$$K = (12C_v E/A_c)^{1/2} \quad (\text{Eq. 4.21})$$

where, C_v = upper shelf energy (ft-lb) = ET

A_c = area of Charpy ligament ($\approx 0.124\text{-in}^2$)

= B(w-a)

E = elastic modulus

Incidentally, this Equation is equivalent to that used to calculate K_J (see Equations 4.9 and 4.10) if the initiation energy EI is set equal to $\frac{1}{2} C_V$. However, this equivalence is not well supported by the energy data presented in the previous Chapter (Tables 3.3 and 3.5), EI being much less than $\frac{1}{2} C_V$. Equation 4.21 is therefore empirical.

Since the Charpy upper shelf temperature is employed in the Battelle equation, it is strictly valid only at upper shelf temperatures. The equation has merit, however, in that the Folias correction accounts for bulging which occurs around defects in pressurized cylinders (pipelines). This bulging can cause increases in the stress at the crack tip and therefore can result in smaller critical crack sizes than required for a similar flaw in a flat plate⁽⁹⁷⁾. Furthermore, the Battelle relationship has been shown to accurately predict the critical flaw sizes in full scale burst tests for certain grades of pipeline steels⁽⁹⁴⁾.

Equation 4.16 ($K_{Id} = \sigma_f (\pi a)^{\frac{1}{2}}$), on the other hand, utilizes a true material property (K_{Id}) instead of an empirical estimate of the fracture toughness (Equation 4.21). Its application is limited, however, as the equation assumes a through-wall crack in an infinitely wide plate⁽¹⁴⁴⁾ and is therefore nonconservative for pipeline geometries.

Table 4.4 lists the critical crack lengths for the two AF steels and the RP steel as determined from the empirical Battelle equation and from the three IIT fracture toughness parameters, K_J , K_{COD} , and K_{Id} . Two failure stress levels were employed in the calculations: the specified minimum yield strength (SMYS), 70 ksi (483 MPa), and the typical design pressure (hoop stress) for a X70 gas pipeline, 56 ksi (= 0.8 SMYS). For the AF-1 steel, a reduced stress level of 28 ksi (193 MPa) was also employed for determining the critical crack length for a crack parallel to the rolling direction.

At +20°C, i.e., in the region of elastic-plastic fracture for the pipe axis orientations, the IIT K_{COD} critical crack lengths were in good agreement with those predicted from the Battelle equation. The K_J crack sizes are, however, much larger. This is probably due to the non-conservative nature of K_J at temperatures where crack initiation occurs prior to maximum load.

The Battelle critical crack lengths are quite different from those predicted by the IIT data for the AF-1 steel in its lowest toughness rolling direction. The Battelle relationship predicts critical crack sizes that would easily be located as leaks prior to unstable crack growth. Indeed, the IIT fracture toughness calculations predict relatively large critical crack lengths for operating stresses of 28 ksi (193 MPa).

Table 4.4
CRITICAL CRACK SIZES

Material & Orientation	Failure Stress (psi)	Critical Crack Size(in)				C _v Upper Shelf (ft-lb)	T (°C)
		Battelle	K _J	K _{COD}	K _{Id}		
AF-2	70000	4.0	9.0	4.4	-	88	+20
pipe axis	56000	6.7	14.0	6.9	-		
AF-1	70000	3.5	7.9	4.6	-	121	+20
pipe axis	56000	6.3	12.4	7.2	-		
AF-1	70000	3.2	0.7	-	0.6	20	+20
rolling direction	56000	5.1	1.1	-	0.9		
	28000	8.8	4.2	-	3.8		
RP	70000	3.4	7.7	4.1	-	94	+20
pipe axis	56000	5.5	12.0	6.4	-		
AF-2	70000	4.0	3.7	3.4	-	62	-20
pipe axis	56000	6.7	5.8	5.3	-		
AF-1	70000	3.5	9.7	5.6	-	96	-20
pipe axis	56000	6.3	15.2	8.7	-		
AF-1	70000	3.2	0.7	0.8	0.6	20	-20
rolling direction	56000	5.1	1.0	1.3	0.9		
	28000	8.8	4.2	5.0	3.8		
RP	70000	3.4	2.1	1.5	0.6	41	-20
pipe axis	56000	5.5	3.2	2.3	0.9		

However, it should be pointed out that the critical crack sizes predicted by the Battelle equation for the AF-1 steel in the rolling direction are considerably larger than those predicted from the IIT parameters. The Battelle equation is therefore not conservative.

The critical crack lengths predicted from the IIT data for the AF-1 steel in the rolling direction are less than one inch for stresses above 56 ksi! If one introduces the real possibility of strain age embrittlement, tensile residual stresses, frost heave and subsequent buckling, or dynamic loading from machinery, the IIT fracture toughness data suggest that the AF-1 is highly susceptible to unstable crack propagation in the rolling direction. The Battelle equation does not suggest this, however, and this discrepancy warrants further investigation.

Furthermore, the Battelle equation is insensitive to material properties; similar crack sizes are predicted for Charpy upper shelf values from approximately 30 to 80 ft-lb (41-108 J)⁽⁹⁵⁾! The fracture toughness values for materials of such widely different Charpy energies should not be equivalent and therefore the critical crack sizes should be different. It is unlikely that the AF-1 steel in the rolling direction would have the same critical crack length as it would have along the pipe axis since the Charpy upper shelf values for the two orientations

are 20 ft-lb and 121 ft-lb, respectively (27 and 167 J), and the fracture toughnesses are $68 \text{ ksi-in}^{\frac{1}{2}}$ and $189 \text{ ksi-in}^{\frac{1}{2}}$ (K_{COD}).

Nevertheless, the Battelle relationship predicts very similar crack sizes of 3.2-in and 3.5-in for a 70 ksi hoop stress. The IIT data, however, predicts critical crack sizes of 0.6-in in the rolling direction and 4.6-in along the pipe axis.

Table 4.4 also lists the critical crack sizes at -20°C . The pipeline industry assumes that the Battelle ductile fracture initiation equation (Equation 3.2) is valid at all temperatures above the 85% shear transition temperature (as defined by the DWTT) since that transition specifies the regime of ductile fracture. However, Equation 3.2 employs the Charpy upper shelf energy (through Equation 4.21), a value which may not apply at the minimum design temperature of -18°C , even though ductile failures may be expected at that temperature (85% shear obtained in the DWTT). The critical flaw sizes from the Battelle equation at -20°C are therefore equal to those at $+20^{\circ}\text{C}$, although, as Table 4.4 shows, there were significant decreases in the Charpy energy of the steels between those temperatures. However, using fracture toughness data obtained at -20°C , different, smaller flaw sizes are obtained. The use of fracture toughness parameters determined by IIT to determine critical crack sizes is therefore more objective, less dependent upon empirical assumptions, and more responsive to fracture toughness temperature transitions.

The use of fracture toughness data in the pipeline industry is virtually nonexistent, however.

4.4.4 Empirical Correlations Between K_{Ic} and Other Material Properties

4.4.4.1 K_{Ic} versus Charpy Energy

The difficulty in obtaining fracture toughness data and the wide popularity of the simple Charpy impact test have prompted many workers to attempt correlations between K_{Ic} and the total absorbed energy obtained from a Charpy test, C_v (=ET). Such correlations are necessarily empirical since comparisons are being made between tests which have significant differences. The Charpy test is conducted under impact loading, whereas K_{Ic} data is obtained under slow strain rate conditions; the Charpy specimen has a relatively blunt notch, the fracture toughness specimens require fatigue precracks; and, the energy absorbed in a Charpy test is a measure of the entire fracture event, whereas K_{Ic} is related to the initiation of a crack. For these reasons, empirical relationships between C_v and K_{Ic} can at best have limited application. Nevertheless, many such correlations can be found in the literature^(4,72) and their use in the absence of fracture toughness data is often suggested⁽¹⁵⁴⁾.

Sailors and Corten⁽¹⁵⁵⁾ have correlated the dynamic fracture toughness with the corresponding Charpy energy obtained at the same temperature (transition and lower shelf range). This correlation is noteworthy because it was derived from data from eleven low alloy structural steels and two pressure vessel steels, and since similar strain rates were used in obtaining the correlating data. Their relationship is:

$$K_{Id} = 15.873(C_v)^{0.375} \quad (\text{Eq. 4.22})$$

where, K_{Id} expressed in ksi-in^{1/2}

C_v in ft-lb

Those workers obtained a surprisingly good linear regression correlation coefficient of +0.94 in their study which employed data from the thirteen different steels and both precracked and standard Charpy specimens!

The K_{Id} data obtained in this study (which also comes from the transition and lower shelf temperatures) has been plotted against the corresponding standard Charpy total energy in Figure 4.10. Equation 4.22 does not fit this data. An empirical correlation was fitted to the acicular ferrite pipeline steel data by linear regression and is of the form:

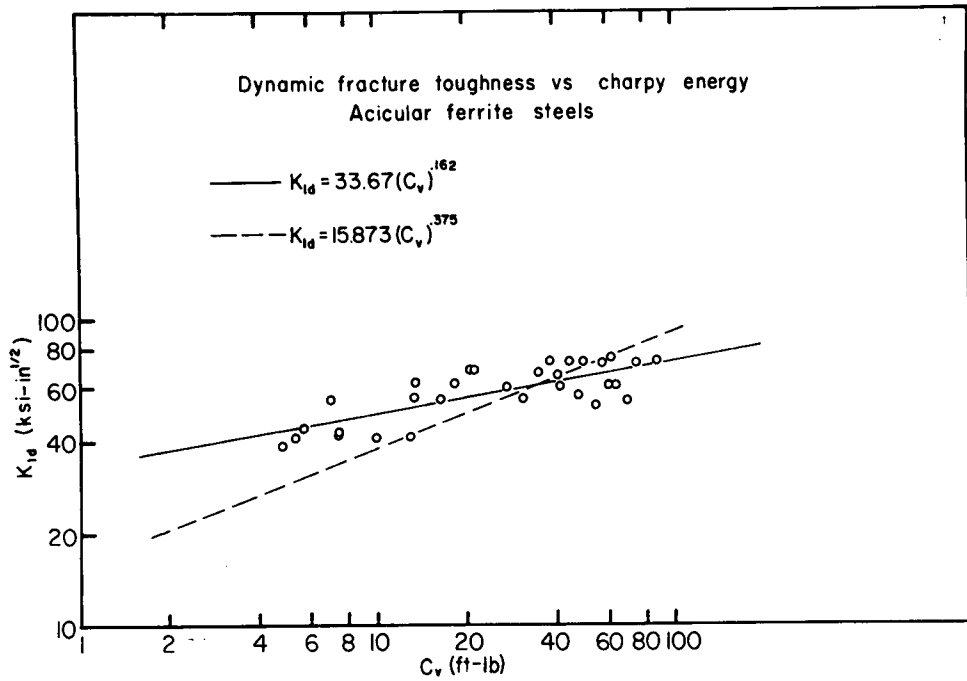


Figure 4.10

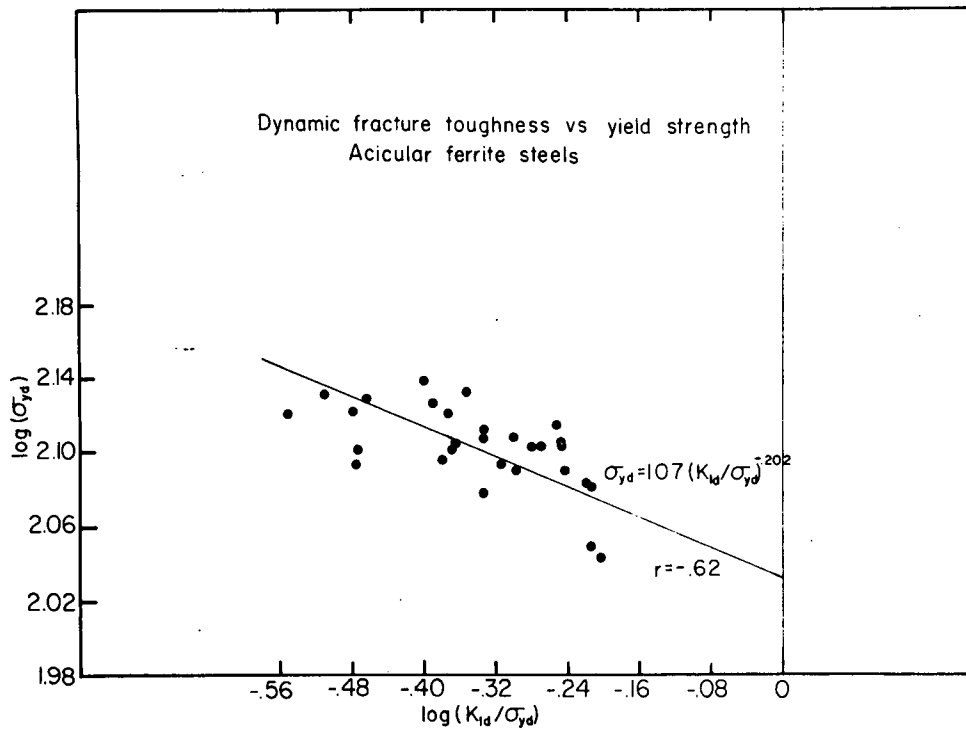


Figure 4.11

$$K_{Id} = 33.67(C_v)^{0.162} \quad (\text{Eq. 4.23})$$

The correlation coefficient was +0.74.

4.4.4.2 K_{Id} vs Yield Strength

Fracture toughness values are also often correlated with the yield strength. The yield stress is believed to be the single most important mechanical property governing the fracture toughness of a material⁽¹²⁵⁾. The ratio (K_{Ic}/σ_y) is often used as a fracture control criterion since it is a direct measure of both the plastic zone size ahead of a crack tip and the critical flaw size for unstable crack extension⁽¹⁰⁾.

For cleavage fractures, many of these correlations have been reduced to the form⁽¹⁵¹⁾:

$$\sigma_f^*/\sigma_y = \alpha(K_{Ic}/\sigma_y)^\beta \quad (\text{Eq. 4.24})$$

where, σ_f^* = cleavage fracture stress

σ_y = yield stress

α, β = empirical material constants

The cleavage fracture stress is independent of temperature and strain rate⁽¹²⁶⁾, so Equation 4.24 can be rearranged to give:

$$\sigma_y = C(K_{Ic}/\sigma_y)^{-\beta} \quad (\text{Eq. 4.25})$$

where, $C = \sigma_f^*/\alpha$

For the wide range of materials examined by Hahn, et al⁽¹⁵¹⁾, Equation 4.25 was shown to reduce to:

$$\sigma_y = \sigma_f^*/2.35(K_{Ic}/\sigma_y)^{-.333} \quad (\text{Eq. 4.26})$$

The K_{Id} data obtained in this study was similarly correlated with the dynamic yield strength and the resulting graphical representation of Equation 4.25 is shown in Figure 4.11. The equation representative of this data is:

$$\sigma_{yd} = 107(K_{Id}/\sigma_{yd})^{-.202} \quad (\text{Eq. 4.27})$$

The correlation coefficient was only - 0.62.

Note from Equation 4.25 that the constant 107 in Equation 4.27 is equal to σ_f^*/α . Using a value of 2.35 for α ⁽¹⁵¹⁾, the cleavage strength of the acicular ferrite pipeline steels is estimated to be on the order of 251 ksi (1734 MPa). An independent estimate of the cleavage fracture stress, σ_f^* , for these steels can be made from IIT data⁽¹⁵⁶⁾:

$$\sigma_f^* \text{ (ksi)} = 72.5 P_{GY} \text{ (lbs)} \quad (\text{Eq. 4.28})$$

$$\text{when, } P_{MAX}/P_{GY} = 0.8$$

From this equation, assuming $P_{MAX}/P_{GY} = 0.8$ at approximately -100°C and that the dynamic yield strength for the acicular ferrite steels is approximately 130 ksi (897 MPa) at that temperature, the cleavage fracture stress is estimated to be 283 ksi (1952 MPa).

The conclusion to be drawn from these correlations between K_{Id} and other material properties are that they are empirical and unreliable (poor correlation coefficients). Although such correlations may be useful for crudely measuring the relative fracture toughness of materials, they are not necessary with an instrumented Charpy machine since the fracture toughness, yield strength, and absorbed energy values may be obtained simultaneously.

5. CONCLUSION

5.1 Conclusions

An instrumented impact test machine with a drop tower design was statically and dynamically calibrated to accurately measure the energy absorbed by a Charpy specimen.

The importance of adhering to proposed ASTM IIT validity criteria was assessed. When the fracture time, t_f , is less than the electronic system response time, T_R , the measured results can be seriously inaccurate: measured loads and fracture toughness parameters are attenuated and fracture times increased. The validity criterion, $t_f > 3\tau$ (τ = period of inherent specimen oscillations) appears to be quite conservative.

An unnecessarily high impact velocity, v_o , is the single most detrimental test parameter. The effect is to decrease the fracture time such that $t_f < T_R$ and/or $t_f < 3\tau$, thus invalidating the test results. High amplitude specimen oscillations are also generated which hinder data analysis.

It appears that the proposed plane strain fracture toughness validity requirement, $P_{MAX} < P_{GY}$, may not be restrictive enough to

ensure plane strain conditions and the measurement of the most conservative fracture toughness parameters. The specimen thickness requirement, $B > 1.6 (K_{Id}/\sigma_{yd})^2$, does appear to be adequate to ensure plane strain conditions, however.

The effect of deviating from the standard Charpy specimen notch dimensions was evaluated. Measurable increases in the absorbed energy were obtained with increasing notch angle and decreasing root radius. In general, increasing the specimen thickness from 10 mm to 13.7 mm caused a decrease in all components of the upper shelf energies per unit area, although the lower shelf energy and the transition temperature were not significantly affected.

Crack growth studies confirmed that for general yield failures, crack initiation occurs prior to maximum load; the crack extends to full specimen thickness at maximum load. Estimates of the initiation energy based upon the assumption that a crack initiates at maximum load are therefore nonconservative.

The initiation and propagation components of the total absorbed energy showed transitions with decreasing temperature. This suggests that EI may have particular significance in terms of a transition temperature approach to the fracture initiation event.

A comparison study of the dynamic properties of two acicular ferrite steels clearly demonstrated the usefulness of IIT. The tests revealed that present pipeline toughness specifications may be inadequate for ensuring fracture control. Very low initiation energies were obtained in tests parallel to the rolling direction - a test direction not included in the present toughness test requirements - in one of the AF materials. For precracked specimens, the initiation energy remained at a lower shelf condition even at room temperature. The tests indicate that more stringent pipeline toughness specifications are necessary in all directions in the pipe. It is suggested that the acceptance criterion be based upon the magnitude of the initiation energy obtained from a precracked Charpy specimen. This would ensure a conservative estimate of the initiation energy and be applicable to the most severe in-service defects.

Instrumented impact testing also showed that strain aging the semi-killed acicular ferrite pipeline steel decreased only the propagation energy; the initiation energy was unaffected. This indicates that the potential for crack initiation in this steel is not increased by strain aging.

The total fracture energy as obtained from a standard Charpy test was shown to often mask the fracture toughness value of a material. In some instances, materials of equivalent fracture toughness had dissimilar Charpy energies. In others, similar Charpy values were obtained

with materials of widely different fracture toughness. IIT indicated the initiation energy obtained from testing precracked Charpy specimens accurately denoted the relative magnitude of the fracture toughness; the precracked initiation energy transition temperature also coincided with that of the fracture toughness. Although more work is required to establish the significance of the EI parameter, these tests indicate that it could be a basic parameter for assessing true fracture initiation.

The equation used by the pipeline industry to predict critical defect sizes is based upon a material's Charpy upper shelf energy which is not representative of the fracture toughness, and hence, the critical defect size. In general, the critical crack sizes predicted from fracture toughness data obtained from IIT were more conservative than those obtained from that empirical equation and were responsive to toughness transitions.

Good correlations between the fracture toughness values from IIT and those statically obtained by conventional techniques were observed.

5.2 Suggestions for Future Work

More data is necessary to confirm the effectiveness of the proposed IIT validity criteria. Fracture toughness parameters should

be obtained by conventional test procedure and should be compared with those generated by IIT employing each of the potential plane strain validity criteria.

The significance of the initiation energy as measured by IIT needs to be better defined. A complete fractographic analysis of the specimens tested in this work should provide a better understanding of the conditions necessary to control both the fracture initiation and fracture propagation event. All fractured specimens have been coded and desiccated to permit a future study.

Specific areas of interest to the pipeline industry have been revealed by this study. Additional testing is required to establish the minimum initiation energy needed to protect against crack initiation. More correlations between IIT and Drop Weight Tear Testing are required. An investigation of the usefulness of a precracked full wall specimen is necessary.

The value of IIT in assessing fracture toughness behaviour has also been shown. This approach could be easily applied to a study of the toughness properties in the weld bead and HAZ of the spiral seam welds and girth welds in the pipeline steels, particularly for the AF-1 steel in its low toughness orientations.

All future data from the Department of Metallurgy's instrumented impact machine should be filed in the computer so that correlations may be more efficiently generated and so that sophisticated statistical analyses can be made⁽¹⁵⁷⁾.

The incorporation of a dual-beam oscilloscope would be quite useful for providing both load-time and energy-time data and would relieve the necessity of measuring the energy with a planimeter.

REFERENCES

1. D. Leavitt: Audubon, 1977, vol. 79, No.2, p.145.
2. Instrumented Impact Testing, STP 563, ASTM, Philadelphia, 1974.
3. M.G. Dawes, Ed.: Int. Conf. on Dynamic Fracture Toughness, Welding Inst., London, 1977.
4. R.A. Wullaert, D.R. Ireland, and A.S. Tetelman: Proc. Symp. on Fracture Prevention and Control, p.255, WESTEC, Los Angeles, 1972.
5. A.S. Tetelman and A.J. McEvily: Fracture of Structural Materials, John Wiley and Sons, New York, 1967.
6. G.D. Fearnough: Proc. Conf. on Physical Basis of Yield and Fracture, p.88, Inst. of Physics and Physical Society, Oxford, 1966.
7. D.E. Diesburg: ASME Publication No. 75-Pet-25, ASME, New York 1975.
8. H. Blumenauer, R. Ortmann, and C. Just: Proc. 5th Conf. on Dimensioning and Strength Calculations, 6th Conf. Material Testing, p. I-70, 1974.
9. R.W. Hertzberg: Deformation and Fracture Mechanics of Engineering Materials, John Wiley and Sons, Toronto, 1976.
10. S.T. Rolfe and J.M. Barsom: Fracture and Fatigue Control in Structures, Prentice-Hall, Englewood Cliffs, NJ, 1977.
11. R. Arone: Proc. 4th Int. Conf. on Fracture, p.549, Int. Cong. on Fracture, Waterloo, 1977.
12. C.W.N. Veerling, C.M. Menken, and J. van Duyn: Fracture Toughness of High Strength Materials, ISI Publication 120, p.10, Iron and Steel Inst., London, 1970.
13. Impact Testing of Metals, STP 466, ASTM, Philadelphia, 1970.
14. D.R. Ireland: Effects Technology, Inc., Santa Barbara, CA, private communication, 1977.

15. C.E. Hartbower, Chairman: ASTM Task Group E24.03.03 on Precracked Charpy Standardization.
16. S. Ono: Proc. 1st Japan Cong. for Testing Materials, p.98, 1958.
17. S. Sakui, T. Nakamura, and M. Ohmori: Tetsu-to-Hagane, 1961, vol. 1, p.38.
18. B. Augland: Brit. Weld. J., 1962, vol. 9, p.434.
19. H.P. Tardif and H. Marquis: Can. Met. Q., 1963, vol. 2, p.373.
20. G.D. Fearneough and C.J. Hoy: J. Iron Steel Inst., 1964, vol. 202, p.912.
21. T. Kobayashi, K. Takai, and H. Maniwa: Trans. Iron Steel Inst. Japan, 1967, vol. 7, p.115.
22. J.C. Radon and C.E. Turner: J. Iron Steel Inst., 1966, vol. 204, p.842.
23. G. Ford, J.C. Radon, and C.E. Turner: J. Iron Steel Inst., 1967, vol. 205, p.854.
24. G.D. Fearneough and R.W. Nichols: Int. J. Frac. Mech., 1968, vol. 4, p.245.
25. J.C. Radon and C.E. Turner: Eng. Frac. Mech., 1969, vol. 1, p.411.
26. W.L. Server and A.S. Tetelman: Eng. Frac. Mech., 1972, vol. 4, p.367.
27. W.L. Server: FCC Report 77-2, Fracture Control Corporation, Goleta, CA, 1977.
28. K.E. Stahlkopf, et al: STP 601, p.291, ASTM, 1976.
29. D.R. Ireland: in Reference 3, p.47.
30. J. Man and M. Holzmann: J. Iron Steel Inst., 1970, vol. 208, p.199.
31. S. Venzi, A.H. Priest, and M.J. May: in Reference 13, p.165.
32. P.W.R. Beaumont and W.L. Server: STP 580, p.443, ASTM, 1975.
33. P.K. Mallick and L.J. Broutman: J. Test. Eval., 1977, vol. 5, p.190.

34. D.R. Ireland, W.L. Server, and R.A. Wullaert: ETI Tech. Rpt. 75-43, Effects Technology, Inc., Santa Barbara, CA, 1975.
35. W.L. Server, R.A. Wullaert, and J.W. Sheckherd: ETI Tech. Rpt. 75-42, Effects Technology, Inc., Santa Barbara, CA, 1975.
36. ASTM Standard E604-77, 1977 Annual Book of ASTM Standards, Part 10, ASTM, Philadelphia, 1977.
37. F.J. Loss: NRL Report 7056, U.S. Naval Research Laboratory, Washington, DC, 1970.
38. R.L. Sharkey and D.H. Stone: Trans. ASME, J. Eng. Ind., 1976, vol. 99, p.446.
39. ASTM Standard E436-74, in Reference 36.
40. D.E. Diesburg: Climax Molybdenum Co. of Michigan, Ann Arbor, MI, unpublished research, 1977.
41. Effects Technology, Inc., Santa Barbara, CA, Data Report DR-74-1, 1974.
42. J.E. Miller: Metal Prog., 1975, vol. 108, No.8, p.55.
43. W.L. Server and D.R. Ireland: in Reference 2, p.74.
44. ASTM Standard E23-72, in Reference 36.
45. M. Kostic: R.M. Hardy & Associates, Burnaby, B.C., private communication, 1977.
46. S. Nunomura: Bull. Tokyo Inst. Tech., 1975, No.131, p.59.
47. D.R. Ireland: in Reference 2, p.3.
48. W.L. Server, D.R. Ireland, and R.A. Wullaert: ETI Tech. Rpt. TR74-29R, Effects Technology, Inc., Santa Barbara, CA, 1974.
49. B.Z. Weiss, et al: Weld. J., 1975, vol. 54, p.216-s.
50. W.R. Hoover: in Reference 2, p.203.
51. A.K. Shoemaker, Chairman: ASTM Task Group 24.03.04 on Dynamic Fracture Toughness Standardization.
52. R.A. Wullaert, Chairman: ASTM Committee E10.02, Task Group for Revision of ASTM Method E184.

53. H.J. Saxton, D.R. Ireland, and W.L. Server: in Reference 2, p.50.
54. E.A. Almond and J.D. Embury: Met. Sci. J., 1968, vol. 2, p.194.
55. E.C.J. Buys and A. Cowan: Doc. X-458-68, Int. Inst. Welding, London, 1968.
56. B. Cotterell: Brit. Weld. J., 1962, vol. 9, p.690.
57. M. Grumbach, M. Prudhomme, and G. Sanz: Rev. de Mét., 1969, vol. 66, p.271.
58. D.R. Ireland and W.L. Server: ETI Tech. Rpt. TR 27-16, Effects Technology, Inc., Santa Barbara, CA, 1972.
59. T.J. Koppenaal: in Reference 2, p.92.
60. A. Ewing and L. Raymond: ibid., p.180.
61. J.W. Sheckherd, M. Kangilaski, and A.A. Bauer: ibid., p.118.
62. J. Aleszka: Effects Technology, Inc., Santa Barbara, CA, private communication, 1977.
63. J.D. Lubahn: Weld. J., 1955, vol. 34, p.518-s.
64. R.A. Wullaert: in Reference 13, p.148.
65. W.L. Server and D.R. Ireland: ETI Tech. Rpt. TR 72-19, Effects Technology, Inc., Santa Barbara, CA, 1972.
66. A.P. Green and B.B. Hundy: J. Mech. Phys. Solids, 1956, vol.4, p.128.
67. L.D. Bertholf and C.H. Karnes: Proc. Int. Conf. Mech. Behaviour of Materials, p.936, Soc. of Materials, Japan, Kyoto, 1971.
68. L.P. Trudeau: Research Report R275, Department of Energy, Mines and Resources, Mines Branch, Ottawa, 1974.
69. G.E. Dieter: Mechanical Metallurgy, McGraw-Hill, New York, 1961.
70. F. Ciampi, et al: Met.Ital., 1976, vol. 68, p.251.
71. C. Crussard et al: J. Iron Steel Inst., 1956, vol. 183, p.146.

72. J.R. Low, Chairman: Report of Committee on Rapid Inexpensive Tests for Determining Fracture Toughness, National Academy of Sciences, Washington, 1976.
73. C.E. Hartbower: Weld. J. Res. Supp., 1957, vol. 36, p.494-s.
74. R. Raring: Proc. ASTM, 1952, vol. 52, p.1034.
75. K.R. Lyer and R.B. Miclot: in Reference 2, p.146.
76. P. McIntyre and A.H. Priest: BISRA Report MG/54/71, British Steel Corp., London, 1971.
77. Microalloying 1975, Washington, DC, 1975.
78. Y.E. Smith, A.P. Coldren, and R.L. Cryderman: Toward Improved Ductility and Toughness, Symp., p.119, Climax Molybdenum Co., Kyoto, 1971.
79. R.L. Cryderman, et al: Proc. 14th Mech. Working and Steel Processing Conference, p.114, TMS-AIME, Chicago, 1972.
80. D.B. McCutcheon, T.W. Trumper, and J.D. Embury: Rev. de Mét., 1976, vol. 73, p.143.
81. I.L. Dillamore, R.F. Dewsnap, and M.G. Frost: Met. Tech., 1975, vol. 2, p.294.
82. K.J. Irvine, et al: J. Iron Steel Inst., 1970, vol. 208, p.717.
83. M. Falco, C. Parrini, and A. Pozzi: Met. Ital., 1975, vol. 67, p.361.
84. G. Tither and J.W. Morrow: Met. Eng. Q., 1975, vol. 15, p.42.
85. J.L. Mihelich and R.L. Cryderman: ASME Publication No.72-Pet-36, ASME, New York, 1972.
86. J.L. Mihelich: Proc. 8th Offshore Technology Conf., p.513, AIME, Houston, TX, 1976.
87. M.P. Boussel, M. Miyano, and J.A. Straatmann: X-70, Climax Molybdenum Co., Greenwich, CN, 1976.
88. W.L. Mercer: Rosenhain Centenary Conf., p.41, Metals Soc., National Physical Laboratory and Royal Soc., London, 1975.

89. J. White: Pipeline Engr., 1970, February, p.30.
90. M.J. Bibby and A.B. Rothwell: Noranda Tech. Memorandum No.37, Noranda Research Centre, Pointe Claire, P.Q., 1975.
91. G. Tither and M. Lavite: J. Metals, 1975, vol. 27, No.9, p.15.
92. R.C. Cooke: The Alberta Gas Trunk Line Co., Ltd., Calgary, Alberta, private communication, 1977.
93. D.B. Clay and D.B. McCutcheon: in Reference 88, p.305.
94. F.S. Somerville and T.C. Slimmon: Proc. Conf. Materials Eng. in the Arctic, p.143, ASM, St. Jovite, P.Q., 1976.
95. J.M.E. Wallbridge: ibid., p.149.
96. W.A. Maxey: 5th Symp. on Line Pipe Research, p.J-1, American Gas Association, Catalogue No. L30174, Houston, 1974.
97. W.A. Maxey, et al: STP 514, p.70, ASTM, Philadelphia, 1972.
98. H.C. Cotton and I.M. Macaulay: in Reference 94, p.50.
99. ASTM Standard E112-74, 1976 Annual Book of ASTM Standards, Part II, ASTM, Philadelphia, 1976.
100. ASTM Standard E399-74, in Reference 36.
101. J.H. Gross: in Reference 13, p.21.
102. R.C. McNicol: Weld. J., 1965, vol. 44, p.385-s.
103. G. Green and J.F. Knott: Trans. ASME, J. Eng. Mat. Tech., 1976, vol. 98, p.37.
104. P.W.R. Beaumont, P.G. Riewald, and C. Zweban: Symp. on Foreign Object Impact Behaviour of Composites, p.1, ASTM, Philadelphia, 1973.
105. D.R. Ireland: Technical Report RE-TR-71-75, U.S. Army Weapons Command, Rock Island, IL, 1972.
106. T.R. Wilshaw and P.O. Pratt: Proc. 1st Int. Conf. on Fracture, vol. 2, p.973, Sendai, 1965.
107. M. Civallero and C. Parrini: Proc. 16th Mech. Working and Steel Processing Conf., p.413, TMS-AIME, Dolton, IL, 1974.

108. D.S. Dabkowski, P.J. Konkol, and M.F. Baldy: Met. Eng. Q., 1976, vol. 16, p.22.
109. D.F. Lentz: in Reference 107, p.397.
110. A.J. DeArdo: Met. Trans., 1977, vol. 8A, p.473.
111. R.J. Jesseman and R.C. Smith: ASME Publication No. 74-Pet-9, ASME, New York, 1974.
112. M. Spencer: The Alberta Gas Trunk Line Co., Ltd., Calgary, Alberta, private communication, 1977.
113. H.E. McGannon, Ed.: The Making, Shaping, and Treating of Steel, 8th Edition, U.S. Steel, Pittsburgh, PA, 1964.
114. V.K. Heikkinen and J.D. Boyd: Can. Met. Q., 1976, vol. 15, p.219.
115. J.D. Baird: Metals Mater., 1971, vol. 5, p.1.
116. M.S. Rashid: Met. Trans., 1975, vol. 6A, p.1265.
117. B.J. Brindley: Acta Met., 1970, vol. 18, p.325.
118. J.E. Hood: in Reference 94, p.157.
119. J.M. Sawhill and T. Wada: Doc. IX-885-74, Int. Inst. Welding, London, 1974.
120. M.S. Rashid: Met. Trans., 1976, vol. 7A, p.497.
121. S.T. Rolfe: Int. Met. Rev., 1974, vol. 19, p.183.
122. J.F. Knott: Mat. Sci. Eng., 1971, vol. 7, p.1.
123. J.M. Krafft and G.R. Irwin: STP 381, p.114, ASTM, Philadelphia, 1965.
124. G.R. Irwin: in Reference 3, p.1.
125. A.H. Priest: ibid., p.95.
126. A.R. Rosenfield, E. Votava, and G.T. Hahn: Ductility, p.63, ASM, Metals Park, OH, 1968.
127. J.A. Begley and J.D. Landes, Chairmen: ASTM Task Group E24.01.09 on Elastic Plastic Fracture Criteria.

128. W.F. Brown and E.J. Strawley: STP 410, ASTM, Philadelphia, 1966.
129. A.S. Tetelman, J.N. Robinson, and I. Roman: Prospects of Fracture Mechanics, p.583, Noordhoff International Netherlands, 1974.
130. R.A. Wullaert, W. Oldfield, and W.L. Server: EPRI Report NP-121, vol. 1, Electric Power Research Institute, Palo Alto, CA, 1976.
131. J.R. Rice: J. Appl. Mech., 1968, vol. 35, p.379.
132. R.J. Bucci, et al: in Reference 97, p.40.
133. J.R. Rice, P.C. Paris, and J.G. Merkle: STP 536, p.231, ASTM, Philadelphia, 1973.
134. J.D. Landes and J.A. Begley: STP 560, p.170, ASTM, Philadelphia, 1974.
135. C.G. Chipperfield: in Reference 3, p.169.
136. A.A. Wells: Proc. Symp. on Crack Propagation, p.210, vol. 1, Cranfield, 1961.
137. P.C. Hughes and M.E. de Morton: J. Aust. Inst. Metals, 1971, vol. 16, p.167.
138. D.E. Diesburg: Report L-176-147, Climax Molybdenum Company, Ann Arbor, MI, 1975.
139. T. Ingham et al: Conf. on Practical Application of Fracture Mechanics to Pressure-Vessel Technology, p.200, Inst. of Mechanical Engineers, London, 1971.
140. J.N. Robinson and A.S. Tetelman: STP 559, p.139, ASTM, Philadelphia, 1974.
141. V. Vitek and G.G. Chell: Mat. Sci. Eng., 1977, vol. 27, p.209.
142. F.J. Witt: USAEC Report ORNL-TM-3172, Oak Ridge National Laboratory, Oak Ridge, TN, 1972.
143. J.N. Robinson and A.S. Tetelman: Eng. Frac. Mech., 1976, vol. 8, p.301.

144. P.C. Paris and G.C.M. Sih: in Reference 123, p.30.
145. H. Tada, P.C. Paris, and G.R. Irwin: The Stress Analysis of Cracks Handbook, Del Research, Hellertown, PA, 1973.
146. G.C.M. Sih: Handbook of Stress Intensity Factors, Lehigh University, 1973.
147. J.M. Barsom and S.T. Rolfe: Eng. Frac. Mech., 1971, vol. 2, p.341.
148. R.W. Hertzberg and R. Goodenow: in Reference 77.
149. T.M.F. Ronald: Met. Trans., 1972, vol. 3, p.813.
150. D.E. Diesburg: Report L-176-137, Climax Molybdenum Company, Ann Arbor, MI, 1975.
151. G.T. Hahn, R.G. Hoagland, and A.R. Rosenfield: Met. Trans., 1971, vol. 2, p.537.
152. J.M. Barsom: in Reference 3, p.113.
153. A. Akhtar: British Columbia Hydro and Power Authority, Materials Research Centre, Vancouver, B.C., unpublished research, 1977.
154. F.M. Burdekin, et al: Weld. in the World, 1975, vol. 13, p.29.
155. R.H. Sailors and H.T. Corten: in Reference 97, p.164.
156. S. Ensha and A.S. Tetelman: Report UCLA-ENG-7435, School of Engineering and Applied Science, UCLA, Los Angeles, CA, 1974.
157. R.A. Wullaert, et al: in Reference 3, p.31.

APPENDIX A DYNAMIC CALIBRATION RESULTS

CODE	TEMP	YSS	YSO	PGY	PM	P*1	TGY	TM	ET	EI	EP	A	A/W
	C	ksi			lbs		ms			FT-LBS		IN	
----	----	-----	-----	-----	-----	-----	-----	-----	-----	-----	-----	-----	-----
T10070	-40.	79.0	>229.8	>7627.	7627.	7627.	0.260	0.260	14.0	5.5	8.5	0.079	0.20
T10290	-40.	79.0	>251.1	>8331.	8331.	8331.	0.260	0.260	13.9	4.4	9.5	0.079	0.20
U30242	-40.	79.0	172.3	5710.	6612.	12147.	0.169	0.325	49.5	12.1	37.4	0.079	0.20
U30780	-40.	79.0	169.7	5033.	6642.	10390.	0.217	0.336	46.9	8.7	38.2	0.079	0.20
V70293	-40.	79.0	159.4	5290.	6254.	14304.	0.195	0.527	71.3	16.8	54.5	0.079	0.20
V70963	-40.	79.0	152.7	5069.	6104.	14575.	0.170	0.476	72.3	17.3	54.9	0.079	0.20
CODE	TEMP	CM	INITIATION	NORMALISED		RTR	IER	EO	VO	TR	OSCILLATIONS		
	C	IN/LB*E-6	DEFLECTION	ET	EI								
----	----	-----	IN*E-3	FI-LH/IN*IN	FI			FI-LH	FI/S	MS	MS		
T10070	-40.	2.0	14.61	112.8	44.5	3.56	0.06	201.8	11.3	.0729	.0332		
T10290	-40.	2.4	16.03	111.7	35.3	3.65	0.06	201.8	11.3	.0729	.0332		
U30242	-40.	2.0	29.85	390.8	97.8	2.32	0.08	201.8	11.3	.0729	.0332		
U30780	-40.	3.3	23.13	377.9	70.4	2.98	0.07	201.8	11.3	.0729	.0332		
V70293	-40.	3.0	55.56	574.2	135.0	2.68	0.09	252.2	12.7	.0729	.0332		
V70963	-40.	3.1	51.04	582.4	139.0	2.33	0.09	252.2	12.7	.0729	.0332		
CODE	TEMP	J	CCDH	FRACTURE TOUGHNESS			CCD	SIR					
	C	IN-LH/IN*IN	IN*E-3	PM	P*1	CCDH	J-INT	IN	(KSI-SQRT(IN)/S)*E+5				
----	----	-----	-----	-----	-----	-----	-----	-----	-----				
T10070	-40.	1068.	3.80	143.8	143.8	>174.4	182.6	0.872	5.54				
T10290	-40.	647.	4.23	157.1	157.1	>190.9	162.6	1.040	5.90				
U30242	-40.	2347.	7.86	>124.7	230.0	205.8	270.6	1.785	6.34				
U30780	-40.	1690.	6.11	>125.2	190.0	179.6	229.6	1.363	5.36				
V70293	-40.	3240.	14.67	>117.9	270.8	270.1	317.4	3.075	5.13				
V70963	-40.	3351.	13.63	>116.2	274.8	254.9	323.4	2.739	5.36				
CODE	J-INTEGRAL	CRITERION	PLANE STRAIN	CRITERIA		CCIN	FLOW STRESS						
	IN		PM	P*1		IN	ksi						
----	-----	-----	-----	-----	-----	-----	-----	-----					
T10070	0.116		0.979	0.979		3.616	>229.6						
T10290	0.084		0.979	0.979		3.026	>251.1						
U30242	0.316		1.310	4.456		6.382	185.8						
U30780	0.228		1.361	3.334		6.035	184.9						
V70293	0.406		1.368	7.218		11.570	173.9						
V70963	0.495		1.448	8.094		11.969	169.2						
EXECUTION TERMINATED													

APPENDIX B

DERIVATION OF THE CORRECTED ENERGY (EQUATION 2.9)⁽⁵⁷⁾

Notation:

Subscript o indicates at moment of impact

Subscript f indicates at moment of final rupture

x displacement

t time

a acceleration

v velocity

E_c corrected energy

E_a energy calculated assuming constant
velocity, v_o

E_o available impact energy

m mass of tup assembly

F applied force

From first principles,

$$\begin{aligned} E_c &= \int_{x_o}^{x_f} F dx \\ &= \int_{x_o}^{x_f} (ma) dx \end{aligned}$$

(minus sign due to fact that $a < 0$ during impact)

$$\begin{aligned}
 &= - \int_{t_o}^{t_f} (ma)v dt \\
 &= - \int_{t_o}^{t_f} mv(dv/dt) dt = - \int_{v_o}^{v_f} mv dv \\
 &= - \frac{1}{2} m(v_f^2 - v_o^2)
 \end{aligned}$$

Also,

$$\begin{aligned}
 E_a &= - \int_{t_o}^{t_f} mav_o dt && \text{(Eq. 2.8)} \\
 &= - v_o \int_{t_o}^{t_f} m(dv/dt) dt \\
 &= - v_o \int_{v_o}^{v_f} mdv \\
 &= - mv_o(v_f - v_o)
 \end{aligned}$$

and,

$$E_o = \frac{1}{2} mv_o^2$$

Now,

$$\begin{aligned}
 E_c &= - \int_{t_o}^{t_f} mav dt + \left[\int_{t_o}^{t_f} mav_o dt - \int_{t_o}^{t_f} mav_o dt \right] \\
 &= - \int_{t_o}^{t_f} (mav - mav_o) dt - \int_{t_o}^{t_f} mav_o dt \\
 &= - \int_{t_o}^{t_f} ma(v - v_o) dt - \int_{t_o}^{t_f} mav_o dt
 \end{aligned}$$

So,

$$E_c = - \int_{t_o}^{t_f} ma(v - v_o) dt + E_a$$

and,

$$E_c - E_a = - m \int_{t_o}^{t_f} (v - v_o) a dt$$

Multiplying by $4E_o (= 2mv_o^2)$ gives,

$$\begin{aligned}
 4E_o(E_c - E_a) &= - 2m^2 v_o^2 \int_{t_o}^{t_f} (v - v_o) a dt \\
 &= - 2m^2 v_o^2 \int_{t_o}^{t_f} (v - v_o) (dv/dt) dt
 \end{aligned}$$

$$\begin{aligned}
 &= - 2m^2 v_o^2 \int_{v_o}^{v_f} (v - v_o) dv \\
 &= - 2m^2 v_o^2 \int_{v_o}^{v_f} (v - v_o) d(v - v_o)
 \end{aligned}$$

$$(v_o = \text{constant, so } dv_o = 0)$$

So,

$$4E_o(E_c - E_a) = - 2m^2 v_o^2 \left[\frac{(v_f - v_o)^2}{2} \right]$$

$$4E_o(E_c - E_a) = - m^2 v_o^2 (v_f - v_o)^2 = - E_a^2$$

and, therefore,

$$E_c = E_a - E_a^2/4E_o$$

$$E_c = E_a (1 - E_a/4E_o) \quad (\text{Eq. 2.9})$$

APPENDIX C

LISTING OF FORTRAN PROGRAM "ENERGY"
FOR IIT DATA REDUCTION

```
C THIS PROGRAM CALCULATES VALUES FROM DATA OBTAINED WITH AN INSTRUMENTED
C CHARPY IMPACT MACHINE. A LOAD-TIME PHOTOGRAPH OF THE IMPACT EVENT IS
C FIRST ANALYZED TO OBTAIN THE AREA UNDER THIS CURVE FROM WHICH THE
C ENERGY ABSORBED IN FRACTURING THE SPECIMEN CAN BE OBTAINED. OTHER
C DATA IS SUPPLIED TO MAKE OTHER STRENGTH AND TOUGHNESS CALCULATIONS.
  DIMENSION TEMP(99),YSS(99),YSD(99),EO(99),VO(99),TR(99),OSCIL(99)
  DIMENSION PGY(99),PM(99),PSI(99),TGY(99),TM(99),ET(99),EI(99)
  DIMENSION FP(99),A(99),R(99),CM(99),DI(99),ETN(99),EIN(99),RTR(99)
  DIMENSION RIER(99),RJ(99),CODM(99),RKPM(99),RKPSID(99),RJIC(99)
  DIMENSION RKCODM(99),CCD(99),SIR(99),CCTW(99),RKJ(99),SFLOW(99)
  REAL*8 CODE(99)
  LOGICAL*1 BL,GT,SWA(99),SWB(99),SWC(99),SWD(99)
  DATA BL,GT/' ','>'/
  DIMENSION S1(100),SIGMA1(99),A1(99),B1(99),P1(100)
  DIMENSION PSCPM(99),PSCPSI(99),PSCCOD(99)
  DIMENSION S2(100),SIGMA2(99),A2(99),B2(99),P2(100)
  LOGICAL LK
  READ(5,5) LJ
5  FORMAT(I2)
  DO 990 I=1,99
    SWA(I)=BL
    SWB(I)=BL
    SWC(I)=BL
    SWD(I)=BL
  990 CONTINUE
  DO 9999 J=1,LJ
C FI IS THE AREA UNDER THE LOAD-TIME PHOTOGRAPH, UP TO THE POINT OF
C MAXIMUM LOAD, IN SQ-IN.
C FP IS THE AREA UNDER THE LOAD-TIME PHOTOGRAPH, FROM THE POINT OF
C MAXIMUM LOAD, IN SQ-IN.
C PMD,PGYD,TMD,TGYD ARE THE LOAD & TIME MEASUREMENTS ON THE PHOTO TO MAXIMUM
C LOAD & ELASTIC LIMIT, RESPECTIVELY, IN INCHES
C DH=DROP HEIGHT OF TUP, IN FEET
C A=CRACK LENGTH, IN
C YSS=STATIC YIELD STRENGTH, PSI
C E=ELASTIC MODULUS, PSI
C PR=POISON'S RATIO
C S=SUPPORT SPAN, IN
C W=SPECIMEN WIDTH, IN
C B=SPECIMEN THICKNESS, IN
C RR=ROTATIONAL RATIO, FOR COD CALCULATIONS
C RLCF & TCF ARE FACTORS TO CONVERT THE MEASUREMENTS FROM THE PHOTO TO
C LOAD & TIME ANALOGS (LB/IN & SEC/IN)
C EO=IMPACT ENERGY      VO=IMPACT VELOCITY
  READ(5,99) CODE(J)
99  FORMAT(A8)
  READ(5,10) TR(J), DH,PMD,PGYD,
1TMD,TGYD,FI,FP
10  FORMAT(F20.8)
  E=31200000.
  PR=0.30
  A(J)=0.079
  S=1.574
  W=0.394
  B=0.394
  TEMP(J)=20.
  RR=0.33
  YSS(J)=77300.
  RLCF=2985.1
  TCF=0.000597
```

```

CP=RLCF*TCF
EO(J)=100.875*12.*DH
VO(J)=((9266.11*DH)**0.5)
C AI AND AP ARE THE VALUES UNDER THE LOAD-TIME CURVE, UP TO AND FROM
C THE POINT OF MAXIMUM LOAD, IN LB-SEC.
WRITE(6,880) FI,FP
880 FORMAT(1X, 2F10.3)
AI=FI*CF
AP=FP*CF
AT=AI+AP
C WT AND WI REPRESENT THE UNCORRECTED TOTAL ABSORBED ENERGY AND THE
C ENERGY REQUIRED TO INITIATE A CRACK (CRACK INITIATION IS ASSUMED
C TO OCCUR AT THE POINT OF MAXIMUM LOAD).
WT=(AT)*(VO(J))
WI=(AI)*(VO(J))
C THE SOURCE OF MOST OF THE FOLLOWING EQUATIONS IS: SERVER, IRELAND,
C AND WULLAERT, "STRENGTH AND TOUGHNESS EVALUATIONS FROM AN INSTRUMENTED
C IMPACT TEST", DYNATUP TECHNICAL REPORT TR 74-29R, EFFECTS TECHNOL-
C OGY, INC., SANTA BARBARA, CA, 1974.
C PM= MAXIMUM LOAD DURING IMPACT EVENT (ASSUMED TO BE POINT OF CRACK
C INITIATION)
C PGY=GENERAL YIELD LOAD
C P*I="EQUIVALENT ENERGY" FRACTURE LOAD
C TM=ELAPSED TIME TO MAXIMUM LOAD
C TGY=ELAPSED TIME TO GENERAL YIELD LOAD
C YSD=DYNAMIC YIELD STRENGTH
C SFLOW=FLOW STRESS
PM(J)=(RLCF)*(PMD)
PGY(J)=(RLCF)*(PGYD)
TM(J)=(TCF)*(TMD)
TGY(J)=(TCF)*(TGYD)
C A/W=CRACK DEPTH TO SAMPLE WIDTH RATIO
R(J)=A(J)/W
C CM=MACHINE COMPLIANCE (REF.: IRELAND, INSTRUMENTED IMPACT TESTING,
C ASTM STP 563, 1974, PP. 3-29) CALCULATED FROM: TOTAL COMPLIANCE
C MINUS SPECIMEN COMPLIANCE
CM(J)=((VO(J))*(TGY(J))/(PGY(J)))-
1((72.*(1.8625*(R(J)*R(J))-3.95*(R(J)**3)+16.3777*
1(R(J)**4)-37.2277*(R(J)**5)+77.554*(R(J)**6)-126.8727*(R(J)**7)
1+172.5325*
2(R(J)**8)-143.964*(R(J)**9)+66.564*(R(J)**10))+20.)/(E*B))
C OSCIL=PERIOD OF SPECIMEN OSCILLATIONS. TGY AND TM SHOULD BE >3 (OSCIL)
C FOR A VALID TEST IN WHICH INERTIAL EFFECTS ARE AVOIDED.
OSCIL(J)=1.68*S*((W/S)**0.5)*((72.*(1.8625*(R(J)*R(J))-3.95*
1(R(J)**3)+16.3777*(R(J)**4)-37.2277*(R(J)**5)+77.554*(R(J)**6)
1-126.8727*(R(J)**7)+172.5325*(R(J)**8)-143.964*(R(J)**9)+
166.564*(R(J)**10))+20.))**0.5)/196850.
C ET, EI, AND EP ARE THE CORRECTED TOTAL, INITIATION, AND PROPAGATION
C ENERGIES OF THE IMPACT EVENT (REF.: GRUMBACH, ET AL., REVUE DE METAL-
C LURGIE, APRIL, 1969, P. 271)
ET(J)=((WT)*(1.-(WT)/((4.)*(EO(J)))))/12.
EI(J)=((WI)*(1.-(WI)/((4.)*(EO(J)))))-(PM(J)**2)*(CM(J))/(2.))/12.
EP(J)=ET(J)-EI(J)
C ET AND EI ARE NORMALIZED BY DIVIDING BY THE SPECIMEN LIGAMENT AREA
ETN(J)=(ET(J))/((B)*(W-A(J)))
EIN(J)=(EI(J))/(B*(W-A(J)))
C DI= SAMPLE DEFLECTION AT CRACK INITIATION
DI(J)=(TM(J))*(VO(J))*(1.-(WI)/((4.)*(EO(J))))-(PM(J))*(CM(J))
IF(PM(J).EQ.PGY(J)) GO TO 999
TAN=((PGY(J))/((TGY(J))*(VO(J))*(1.-(PGY(J))*(TGY(J))*(VO(J)))/

```

```

YSD(J)=YSD(J)*0.001
YSS(J)=YSS(J)*0.001
SFLOW(J)=SFLOW(J)*0.001
RKPM(D(J)=RKPM(D(J)*0.001
RKPSID(J)=RKPSID(J)*0.001
RKC(D(J)=RKC(D(J)*0.001
RKJ(J)=RKJ(J)*0.001
SIR(J)=SIR(J)*(1.E-8)
CODM(J)=CODM(J)*1000.
IF(PMD.EQ.PGYD) SWB(J)=GT
IF(PM(J).EQ.PGY(J)) SWA(J)=GT
IF(PM(J).GT.PGY(J)) SWD(J)=GT
IF(PM(J).EQ.PGY(J)) SWC(J)=GT
9999 CONTINUE
WRITE(6,100)
100 FORMAT('1',4X,'CODE',4X,'TEMP',4X,'YSS',6X,'YSD',6X,'PGY',5X,'PM',
16X,'P*I',7X,'TGY',6X,'TM',6X,'ET',5X,'EI',4X,'EP',5X,'A',6X,'A/W')
WRITE(6,200)
200 FORMAT(15X,'C',10X,'KSI',18X,'LBS',20X,'MS',14X,'FT-LBS',10X,'IN')
WRITE(6,300)
300 FORMAT(5X,'-----',4X,'-----',4X,'-----',6X,'-----'
1---',6X,'-----',6X,'-----',2X,'-----',4X,'-----')
DO 42 J=1,LJ
WRITE(6,700) CODE(J),TEMP(J),YSS(J),SWA(J),YSD(J),SWB(J),PGY(J),PM(
1J),PSI(J),TGY(J),TM(J),ET(J),EI(J),EP(J),A(J),R(J)
42 CONTINUE
700 FORMAT(3X,A8,1X,F5.0,3X,F5.1,2X,A1,F5.1,5X,A1,F5.0,2X,F5.0,1X,F6.
10,6X,F5.3,2X,F5.3,5X,F5.1,1X,F5.1,1X,F5.1,2X,F5.3,3X,F5.2)
WRITE(6,400)
400 FORMAT('0',4X,'CODE',4X,'TEMP',7X,'CM',5X,'INITIATION',7X,'NORMALI
1SED',6X,'RTR',4X,'IER',4X,'EO',6X,'VO',5X,'TR',5X,
1'OSCILLATIONS')
WRITE(6,500)
500 FORMAT(31X,'DEFLECTION',4X,'ET',11X,'EI')
WRITE(6,550)
550 FORMAT(15X,'C',4X,'IN/LB*E-6',4X,'IN*E-3',8X,'FT-LB/IN*IN',
119X,'FT-LB',3X,'FT/S',4X,'MS',10X,'MS')
WRITE(6,570)
570 FORMAT(5X,'-----',4X,'-----',3X,'-----',2X,'-----',4X,'-----'
1-----',3X,'-----',3X,'-----',3X,'-----',3X,'-----',3X,'-----',
16X,'-----')
DO 52 J=1,LJ
WRITE(6,800) CODE(J),TEMP(J),CM(J),DI(J),ETN(J),EIN(J),RTR(J),RIER(
1J),EO(J),VO(J),TR(J),OSCIL(J)
52 CONTINUE
800 FORMAT(3X,A8,1X,F5.0,5X,F4.1,7X,F6.2,6X,F6.1,4X,F5.1,3X,F4.2,3X,F
14.2,3X,F5.1,3X,F4.1,3X,F5.4,6X,F5.4)
WRITE(6,580)
580 FORMAT('0',4X,'CODE',4X,'TEMP',6X,'J',6X,'CODM',8X,'FRACTURE TOUGH
1NESS',8X,'CCD',11X,'SIR')
WRITE(6,590)
590 FORMAT(20X,'INTEGRAL',10X,'PM',5X,'P*I',4X,'CODM',4X,'J-INT')
WRITE(6,525)
525 FORMAT(15X,'C',1X,'IN-LB/IN*IN',1X,'IN*E-3',10X,'KSI-SQRT(IN)',
111X,'IN',4X,'(KSI-SQRT(IN)/S)*E+5')
WRITE(6,600)
600 FORMAT(5X,'-----',4X,'-----',3X,'-----',2X,'-----',2X,'-----'
1-----',2X,'-----',2X,'-----')
DO 62 J=1,LJ
WRITE(6,900) CODE(J),TEMP(J),RJ(J),CODM(J),SWD(J),RKPM(D(J),RKPSID(J)

```

```

1 ((8.)*(EO(J))))-(PGY(J)*(CM(J))))
PSI(J)=(TAN)*((12.*2.*EI(J)/TAN)**0.5)
GO TO 1000
999 PSI(J)=PM(J)
1000 YSD(J)=(2.99*PGY(J)*W)/(B*((W-A(J))**2))
C RTR=RESPONSE TIME RATIO (SHOULD BE >1.11 FOR A VALID TEST IN WHICH
C THE EFFECT OF SIGNAL ATTENUATION IS MINIMIZED)
C IER=INITIATION ENERGY RATIO (SHOULD BE <.33 FOR A VALID TEST)
RTR(J)=TGY(J)/TR(J)
RIER(J)=WI/EO(J)
SFLOW(J)=(2.99*(PGY(J)+PM(J))*W)/(2.*B*((W-A(J))**2))
C STRESS INTENSITY PARAMETERS (RKPMID,RKPSID,RKCODM,RKJ)
RKPMID(J)=((1.5)*S*(PM(J))*(A(J)**0.5)/((B)*(W**2)))*(1.93-
13.07*R(J)+14.53*
1(R(J)*R(J))-25.11*(R(J)**3)+25.8*(R(J)**4))
PSCPM(J)=(2.5)*(((RKPMID(J))/(YSD(J))**2)
RKPSID(J)=((1.5)*S*(PSI(J))*(A(J)**0.5)/((B)*(W**2)))*(1.93-3.07*
1R(J)+14.53*
1(R(J)*R(J))-25.11*(R(J)**3)+25.8*(R(J)**4))
PSCPSI(J)=(2.5)*(((RKPSID(J))/(YSD(J))**2)
C J=J-INTEGRAL
RJ(J)=24.*EI(J)/(B*(W-A(J)))
RKJ(J)=((E*RJ(J))**0.5)
YSG=YSS(J)
IF(YSD(J).GT.YSS(J)) YSG=YSD(J)
C RJIC=J-INTEGRAL VALIDITY CRITERION
RJIC(J)=25.*RJ(J)/SFLOW(J)
C CODM=CRACK-TIP-OPENING-DISPLACEMENT AT MAXIMUM LOAD
C VALUE OF CODM IS VERY MUCH DEPENDENT UPON THE ROTATIONAL
C RATIO (RR), THE VALUE OF WHICH IS IN DEBATE.
CODM(J)=(2.54)*(W-A(J))*(DI(J))*(RR)
IF(PM(J).EQ.PGY(J)) RKCODM(J)=((CODM(J))*(YSG)*(E/(1.-
1(PR**2))))**0.5
IF(PM(J).GT.PGY(J)) RKCODM(J)=((CODM(J))*(YSD(J))*E)**0.5
RKL=RKCODM(J)
ZZ=RKPSID(J)
IF(RKCODM(J).LT.RKPSID(J)) ZZ=RKCODM(J)
IF(ZZ.LT.RKJ(J)) RKL=ZZ
IF(RKJ(J).LT.ZZ) RKL=RKJ(J)
C CCD=CRITICAL CRACK DEPTH (REPRESENTS CRITICAL SIZE OF A
C HYPOTHETICAL ELLIPTICAL SURFACE FLAW SUBJECTED TO THE STATIC
C YIELD STRENGTH WHICH WILL PROPAGATE. STRESS INTENSITY IS ASSUMED
C TO BE THE MINIMUM VALUE CALCULATED).LENGTH/DEPTH=6/1.
IF(PM(J).EQ.PGY(J)) CCD(J)=(RKPMID(J)**2)/((1.21)*3.1416*(YSS(J)**2))
IF(PM(J).GT.PGY(J)) CCD(J)=(RKL**2)/((1.21)*(3.1416)*(YSS(J)**2))
C CCTW=LENGTH OF CRACK EXTENDING THRU-WALL THAT WILL PROPAGATE WHEN
C SUBJECTED TO STATIC YIELD STRENGTH.STRESS INTENSITY FACTOR USED IS
C THAT CALCULATED BY J-INTEGRAL TECHNIQUE.
CCTW(J)=(0.7144*(RKJ(J)**2))/(YSS(J)**2)
C SIR=STRESS INTENSITY RATE
IF(PM(J).EQ.PGY(J)) SIR(J)=RKPMID(J)/TM(J)
IF(PM(J).GT.PGY(J)) SIR(J)=RKL/TM(J)
TM(J)=TM(J)*1000.
TGY(J)=TGY(J)*1000.
CM(J)=CM(J)*(1.E+6)
DI(J)=DI(J)*1000.
EO(J)=EO(J)/12.
VO(J)=VO(J)/12.
TR(J)=TR(J)*1000.
OSCIL(J)=OSCIL(J)*1000.

```

```
1),SWC(J),RKCDM(J), RKJ(J),CCD(J),SIR(J)
62  CONTINUE
900  FORMAT(3X,A8,1X,F5.0,4X,F5.0,4X,F5.2,2X,A1,F5.1,2X,F5.1,1X,A1,F5.
11,2X,F5.1,3X,F5.3,9X,F5.2)
WRITE(6,505)
505  FORMAT('0',4X,'CODE',4X,'J-INTEGRAL CRITERION',3X,'PLANE STRAIN
1CRITERIA', 9X,'CCTW',7X,'FLOW STRESS')
WRITE(6,510)
510  FORMAT(39X,'PM',12X,'P*I')
WRITE(6,515)
515  FORMAT(22X,'IN',24X,'IN',19X,'IN',12X,'KSI')
WRITE(6,520)
520  FORMAT(5X,'-----',4X,'-----',3X,'-----'
1,3X,'-----',8X,'-----', 6X,'-----')
DO 72 J=1,LJ
WRITE(6,555) CODE(J),RJIC(J),PSCPM(J),PSCPSI(J),CCTW(J),SFLOW(J)
72  CONTINUE
555  FORMAT(3X,A8,10X,F6.3,12X,F6.3,6X,F6.3,10X,F6.3,9X,F5.1)
STOP
END
```


APPENDIX D

INSTRUMENTED IMPACT TEST RECORD

<u>(CODE)</u> Specimen	<u>(TEMP)</u> Temperature °C	<u>Load</u> Scale mV/div	<u>Time</u> Scale mS/div	<u>(TR)</u> Response Time, μ s	<u>(VO)</u> Impact Velocity in/s	<u>(EO)</u> Impact Energy in/lb
						<u>(DH)</u> Drop Height, Ft
↓		↓				
<u>(RLCF)</u> Load Conversion Factor, lb/in	<u>(TCF)</u> Time Conversion Factor, s/in	<u>(CF)</u> Area Conversion Factor, $\frac{\text{lb-s}}{\text{in}^2}$				
		X		=		
Impact Photo Measurements						
<u>(FI)</u> Area to Max Load, in^2				<u>(FP)</u> Area from Max Load, in^2		
<u>(PMD)</u> Max. Load, in	<u>(PGYD)</u> Gen'l Yield Load, in	<u>(TMD)</u> Time to Max. Load, in	<u>(TGYP)</u> Time to Gen'l Yield Load, in			
<u>(S)</u> Span, in	<u>(B)</u> Thickness, in	<u>(W)</u> Width, in	<u>Crack Length</u>			
			Center, mm () - () =			
			$\frac{1}{4}$ point, mm () - () =			
			$\frac{3}{4}$ point, mm () - () =			
<u>(A)</u> Crack Length, in			()			
			÷ 3			
←			x (0.03937 in/mm) ()			
			Shorter surface, mm () - () =			
<u>(YSS)</u> Static Yield Strength, lb/in^2		<u>(E)</u> Elastic Modulus, lb/in^2		<u>(PR)</u> Poisson's Ratio		
Precracking Data:						
<u>Max. Applied Torque, in-lb</u>		<u>K_f(max.), psi-in$^{\frac{1}{2}}$</u>		<u>Fatigue Cycles</u>		

APPENDIX E

STRAIN-AGE STUDY: CALCULATIONS

AF-1 Pipe Seam Welding Parameters:

welding speed: 12.7 mm/s voltage: 31.5 volts
amperage: 787.5 amps
2-pass weld

Calculation of Heat Transfer Efficiency, f_1 :

From: C.M. Adams, Welding Handbook, 7th Ed., Vol. 1,
pp.80-98, AWS, Miami, 1976.

$$\frac{1}{T_p - T_o} = \frac{4.13\rho CtY}{H_{net}} + \frac{1}{T_m - T_o} \quad (\text{Eq. E.1})$$

where, T_p = peak temperature ($^{\circ}\text{C}$) at distance, $Y(\text{mm})$,
from weld fusion boundary

T_o = initial temperature ($\approx 25^{\circ}\text{C}$)

T_m = liquidus temperature ($\approx 1510^{\circ}\text{C}$)

H_{net} = net energy input = $f_1 EI/V$

E = volts I = amperage

f_1 = heat transfer efficiency

V = travel speed (mm/s)

$$\begin{aligned}\rho C &= \text{volumetric specific heat} \\ &(\approx 0.0044 \text{ J/mm}^3 \cdot ^\circ\text{C}) \\ t &= \text{thickness of pipe (mm)}\end{aligned}$$

By macroetching, heat-affected zone boundary determined to be 4.5 mm = Y_{HAZ}

The peak temperature T_p , for the visible HAZ boundary in low alloy steels is approximately 730°C.

So, from Equation E.1:

$$\begin{aligned}\frac{1}{730 - 25} &= \frac{4.13(.0044)(13.7)(4.5)}{[(f_1)(31.5)(787.5)/12.7]} + \frac{1}{1510 - 25} \\ f_1 &= 0.77 \quad \text{for AF-1 pipe}\end{aligned}$$

Calculation of Peak Temperature at Various Distance from Seam Weld:

for $Y = 0.6\text{-in}(15.2 \text{ mm})$, using Equation E.1:

$$\begin{aligned}\frac{1}{T_p - 25} &= \frac{4.13(.0044)(13.7)(15.2)}{[(.77)(31.5)(787.5)/12.7]} + \frac{1}{1510 - 25} \\ T_p &= 337^\circ\text{C}\end{aligned}$$

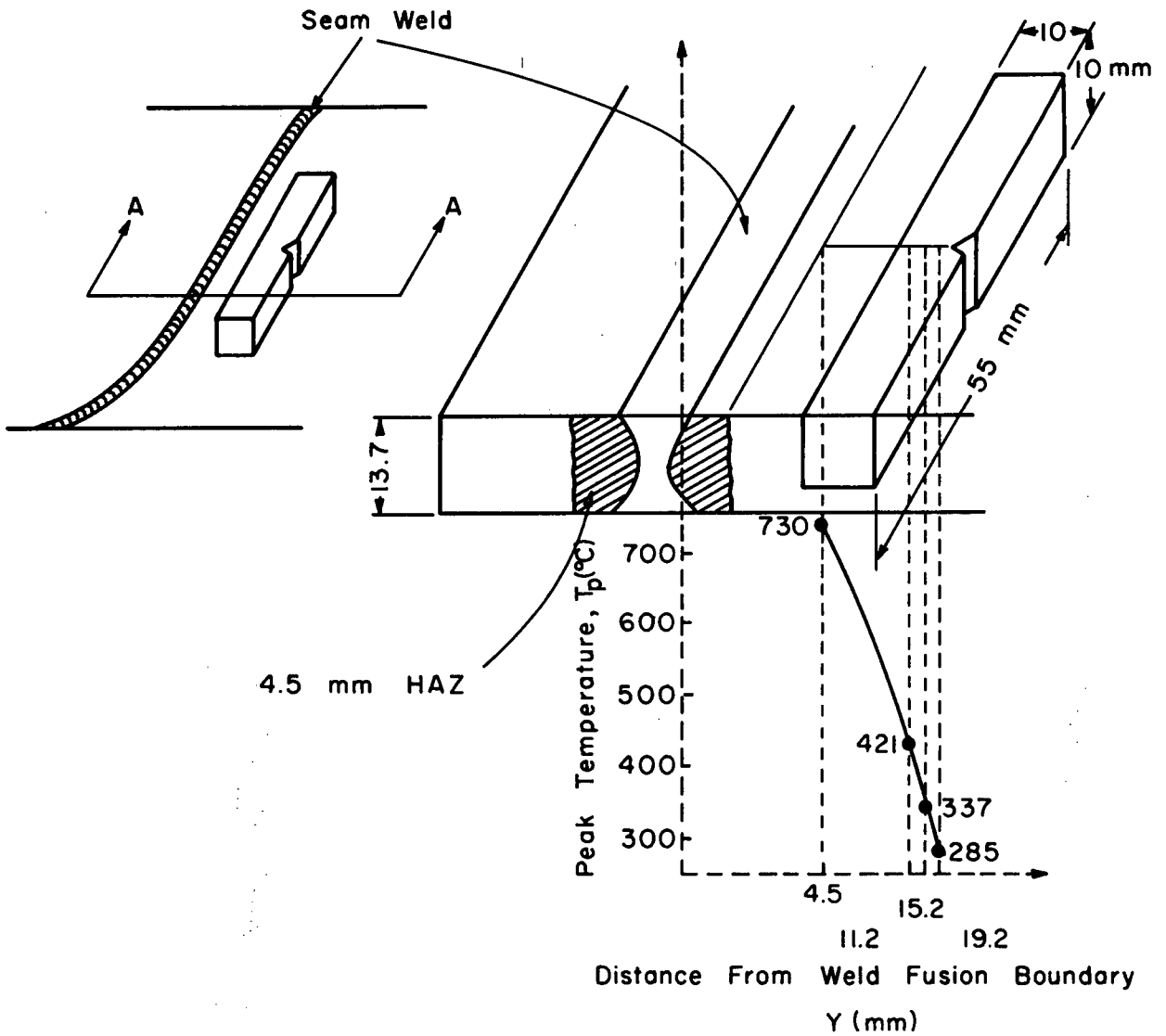


Figure E.1 Temperature gradient in Charpy specimens from near seam weld.

Similarly, for the Charpy specimen shown above,

for $Y = 19.2$ mm (distance to notch)

$$T_p = 285^\circ\text{C}$$

and for $Y = 11.2$ mm (distance to bottom of specimen)

$$T_p = 421^\circ\text{C}$$

Calculation of Cooling Rate:

for relatively thin plates:

$$R = 2\pi k \rho C (t/H_{\text{net}})^2 (T_c - T_o)^3 \quad (\text{Eq. E.2})$$

where, R = cooling rate ($^{\circ}\text{C/s}$)

k = thermal conductivity ($\approx 0.051 \text{ J/m}\cdot\text{s}^{\circ}\text{C}$ for steel at 300°C)*

T_c = temperature ($^{\circ}\text{C}$) at instant at which cooling rate applies

Approximation of the cooling rate at a point 15.3 mm from the weld fusion boundary, when $T_c = 337^{\circ}\text{C}$, can therefore be calculated:

$$R = 2\pi (.051) (.0044) \left[\frac{13.7}{(.77)(31.5)(787.5)/12.7} \right]^2 (337 - 25)^3$$

$$R = 3.5^{\circ}\text{C/s}$$

It is recognized that $R, k = f(T)$ and that R is strictly valid only for the weld center line.

Temperature for optimum strain-age effect is approximately $285^{\circ}\text{C}^{(113)}$:

Material below Charpy specimen in Figure E.1 goes from 337°C to 285°C in:

$$(337 - 285)^{\circ}\text{C}/3.5^{\circ}\text{C/s} \approx 15 \text{ s}$$

* From: BISRA Report "Physical Constants of Some Commercial Steels at Elevated Temperatures," BISRA, London, 1953.

Pipe is welded in two-passes, so a given point near the seam weld experiences temperatures optimum for strain-aging for $2(15 \text{ s}) \approx 30 \text{ seconds}$.

N.B. Time between welding passes is 132 s; so weld bead cools to ambient temperatures between passes.

Calculation of Times and Temperatures to Approximate Strain-Age Conditions near Seam Weld:

Assuming that the effective aging time and temperature near the seam weld was 1 minute at 316°C ($Y = 16.7 \text{ mm}$), the times/temperatures required to artificially age Charpy specimens an equivalent amount may be calculated from⁽¹²⁰⁾:

$$\log t_1/t_2 = 7500[1/T_1 - 1/T_2] \quad (\text{Eq. 3.7})$$

where, $T_1 < T_2$ ($^\circ\text{K}$)

Table E.1 lists equivalent aging conditions.

Table E.1

<u>Time(minutes)</u>	<u>Temperature($^\circ\text{C}$)</u>
60	244 $^\circ$
15	266 $^\circ$
5	285 $^\circ$
1	316 $^\circ$
0.5	330 $^\circ$